THE UNIVERSITY *of* EDINBURGH

Study of Construction Methodology and Structural Behaviour of Fabric-formed Form-efficient Reinforced Concrete Beam

Daniel Sang-Hoon Lee

A thesis submitted for the degree of

Doctor of Philosophy

The University of Edinburgh
2011

Declaration

This thesis is the result of research work for the degree of Doctor of Philosophy undertaken in the Department of Architecture, University of Edinburgh.

It is declared that all the work and results in this thesis have been carried out and achieved by the author himself and the thesis has been composed by him under the supervision of Professor Remo F. Pedreschi and Fiona McLachlan, unless otherwise stated.

Edinburgh, June 2011

Daniel Sang-Hoon Lee

Acknowledgements

I would like to express my gratitude to Professor Remo and Fiona for the guidance, Alistair, Alan, and Malcolm for their technical support in the workshop, and to my talented Masters students; Michael, Rebecca, Hamish, and Eoin, and Tom.

Above all, I thank my God for giving me the strength to complete this work.

Symbols and Notations

The followings are the definitions of the symbols used in this thesis, unless noticed otherwise:

A = Area of section

A_{cc} = Area of flange concrete in compression

A_{cw} = Area of web concrete in compression

A_i = Area of a strip in the section

A_{ns}' = Compression reinforcement area

A_{ps} = Prestressed steel

A_t (A_s) = Area of steel

a = Distance between the adjacent flexural cracks

α_e = Modular ratio

α_{vx} = the ratio M_{ax}/V_{ax}

b = Width of the section

be = Effective width of flange

b_w = Width of the web

b_1 = Effective width

C= Compression force

d = Effective depth

dA = Elemental area

d_{max} = Maximum aggregate size

dT = Temperature difference between the surface and the bulk fluid

E = Modulus of elasticity

Ec = Modulus of elasticity of concrete

E_T = Modulus of elasticity of steel

e_{cr} = Concrete cracking strain

e_t = Concrete tensile strain

ε_c = Concrete strain

F_c = Corresponding concrete stress for the given strain

F_y = Standard ultimate strength of steel

F_y' = Actual ultimate strength of steel

f_{ck} = Cracking strength of concrete

f_{cu} = Concrete cube strength

f_c' = Concrete cylinder strength

f_{cm} = Mean compressive strength

f_{ctm} = Mean axial tensile strength

f_s (f_y) = Characteristic strength of the tension steel

G_F = Fracture energy

G_{FO} = Base value of fracture energy

h_f = Flange height

I = Second moment of area

I_{eff} = Effective second moment of area

I_x = Second moment of area about x-x axis

l_s = Shear span

M_a (M_{ax}) = Applied moment

M_{cx} = Moment corresponding to shear failure

M_l = Moment capacity per unit inch width

M_u (M_{fx}) = Ultimate moment of resistance (Flexural capacity)

Q = First moment of area

q = Heat transfer per unit time

r = Radius of curvature

σ_t = Tension stress of concrete

ρ = Area of tensile reinforcement / Area of concrete to effective depth

ρ_w = Area of tensile reinforcement/ Web area of concrete to effective depth

T = Tension force

v = Vertical shear stress

v_c = Concrete shear strength

V_{ax} (V) = Applied shear force (Vertical shear force)

$\bar{y}$ = Neutral axis

$\bar{y}_i$ = Perpendicular distance from the given axis to a strip in the section

z = Lever arm

Abstract

The nature of this research is in advancing conventional structures and their methods of construction by exploring new technology.

The formwork construction of the modern concrete structure involves the use of rigid materials such as steel and timber. This type of formwork often produces structures of forms with limited flexibility which would also hinder the even distribution of the induced stresses. To construct concrete structures with more organic forms; ones that responds to a more natural flow of the induced stresses, it is thought to be more logical to use flexible mould such as the fabric formwork. In such form-active shape the materials' utilization can be maximized and the degree of material waste can be reduced. For example, when the form responds to the externally applied loads in the way that the internally incurred stresses at any point of the body closely match the capacity of the material, then the form is material-efficient and said to be in its optimal form. The use of fabric formwork, due to its permeability can also improve the quality of concrete by eliminating any air holes on the surface, and also there are reports showing the increase in concrete's compression strength due to the reduction in water-cement ratio when cast in a fabric mould. This research concentrates on finding such material-efficient form (thus more sustainable) for reinforced concrete beam of improved material quality, through the development of the more efficient construction system of flexible fabric formwork.

For this research 11 different types of beams have been built and tested in total, and their construction methods are illustrated and discussed also (Chapter 7 and Chapter 4 respectively). The designs of the beams are developed through consecutive experiment, analysis, evaluation, and modification process (Chapter 6). For the structural analysis of the beams, the most widely accepted analysis methods are reviewed and adapted (Chapter 8). Based on the evaluations of the analytical results the following variables of the beams are modified through the development of the beam designs:

- The effect of Compression Steel Mesh in Flange
- Stress Distribution Around Anchorage;
- Vertical and Horizontal Web Geometry
- Varying Depth of Flange
- Steel Content

Also it is a part of the current research's aim to look at the possible application of the current design methods for the design of the fabric formed beams that are discussed in this research. Thus the experimental results are compared with the results which are calculated from the standard design methods suggested by the British Standard Code of Practice (BS8110) (Chapter 9).

Computational finite element (FE) analysis is carried out where more intensive analysis is required (Chapter 10). The results of the FE analysis are also compared with the theoretical and experimental results for the verification purpose.

The material efficiency of the beam in its final form is assessed through the embodied energy analysis, which compares the total embodied energy consumed through the construction of the beam with a virtual beam that is designed in accordance with the BS8110 (Chapter 11). The analysis indicates that the total embodied energy of the fabric formed beam is about 20~40% less in comparison with the beam designed in accordance with the BS8110.

This thesis has the purpose to illustrate and provide the practical information on the design and the construction process of the fabric formed beams, which can be used as a reference to the future research and construction.

Contents

Chapter 1: Introduction

1.1 Concrete and Form

The use of concrete as a construction material could be dated back to the early civilizations; Egyptians used lime and gypsum mortar for pyramids construction, and the Romans used quicklime and pozzolana which react with water to harden (hydraulic cement). The dome of the Pantheon in Rome (Figure 1-1) spanning 43.4 metres is constructed by unreinforced concrete which varies in thickness from 6.4 metres at the base to 1.2 metres at the top (ROTH, L. M., 1998). Nowadays Portland cement is commonly used for concrete which consists of about 60% to 65% of lime and the rest includes silica (18 – 25%), alumina (3 – 8%), iron oxide (0.5 – 5%).

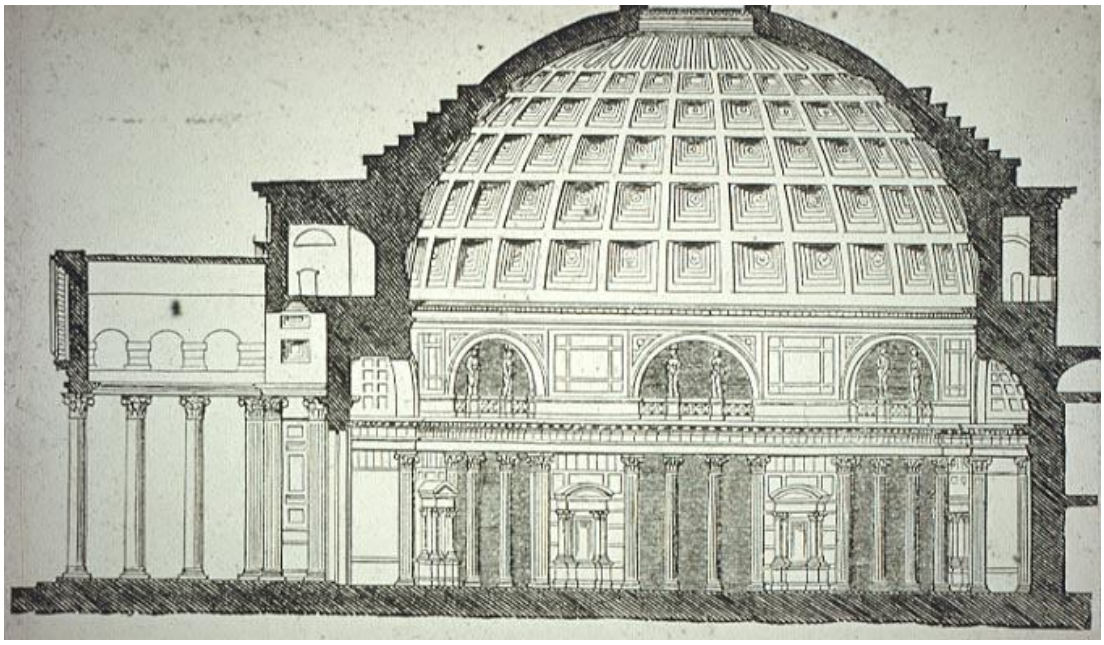

Figure 1.1: Pantheon, Rome (SULLIVAN, Mary Ann)

Our knowledge of the modern concrete technology has had a steady development since the more commercial introduction of the reinforcement for concrete in the nineteenth century (ADDIS, B., 2007); William B. Wilkinson (1819-1902) had patented the floor system in 1854 that reflects of modern reinforced concrete under the title "Improvements in the Construction of Fireproof Dwellings, Warehouses, and other Buildings" (Figure 1-2 top image). His reinforced concrete system was used for a cottage in Newcastle, and iron cables were placed in the lower tensioning part of concrete slab. In Europe the wider acceptance of reinforced concrete system grew with the success of two contracting companies founded by Gustav Wayss (1851-1917) and François Hennebique (1842-1921). Behind their successes there was

professional development of their expertise of their own and also in collaboration with university research teams (ADDIS, B., 2007).

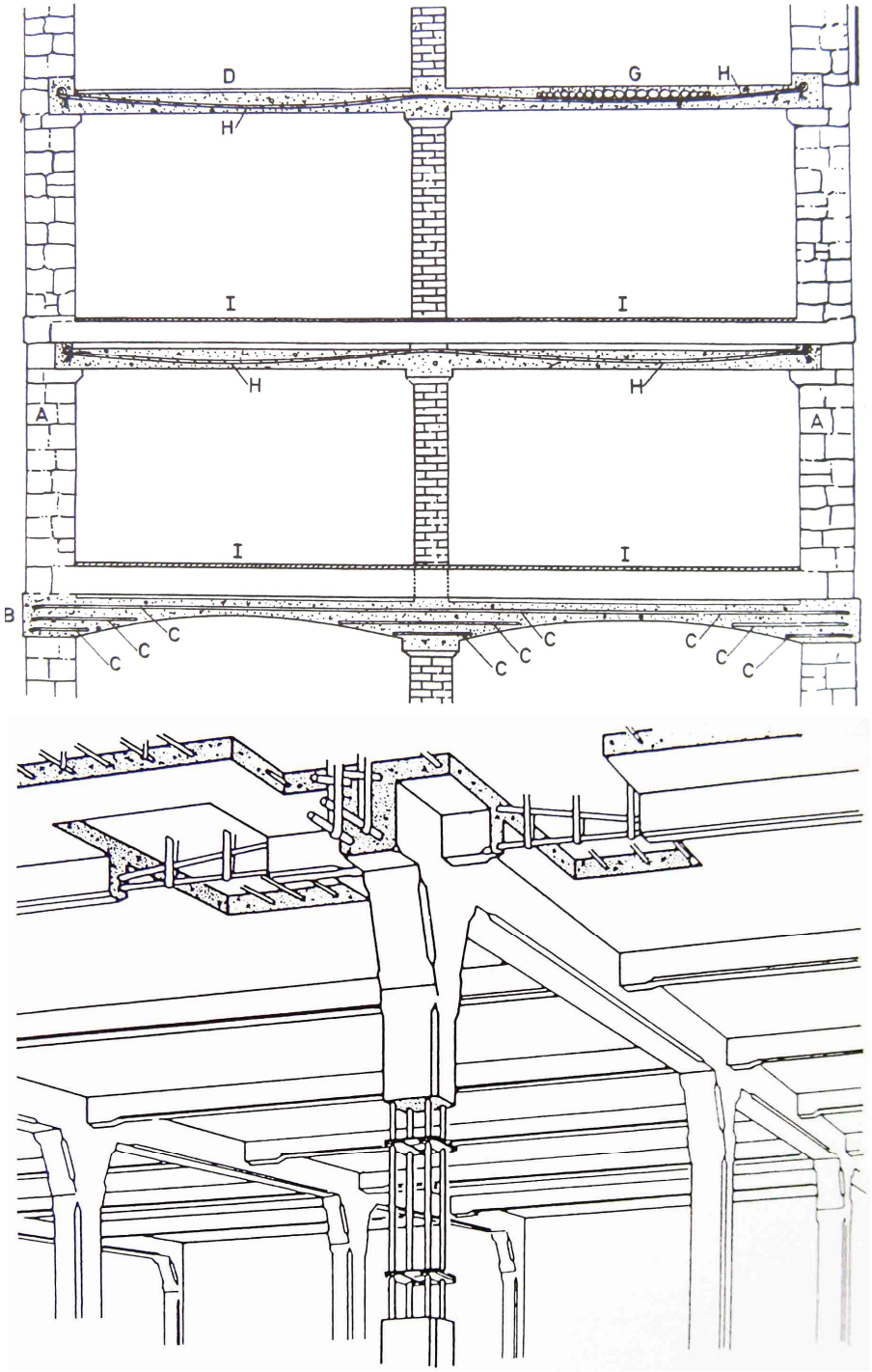

Figure 1-2: Drawing from patent by William B. Wilkins for "Improvement in the Construction of Fireproof Dwellings, Warehouse and other Buildings", 1854 (top) and Drawing of reinforcement in a Hennebique Building, c. 1910 (bottom) (ADDIS, B., 2007)

In the broader scope of concrete's development, there have been engineers, specialists and architects attracted to the material with their individual interests and they have been developing its quality and use; the strength of concrete has improved compared with early 20th century (Figure 1-3), and the analysis and design methods

for concrete structure have been changed from the Modular ratio method (; a design method which assumes that the concrete and steel behaves only elastically that the modular ratio between steel and concrete can be applied to find the stresses in them) to the Euro Code 2 (introduced in 2004, the code uses limit state design criteria with the representative load method) (WHITTLE, R., 2008).

The language of concrete structure/architecture has developed far more since the early 1800's buildings. Concrete structures becoming slenderer through the time with more definitive characteristics shows the professions' establishments and confidence in their knowledge of the material. In the recent years many scientists and engineers in concrete industry have been putting efforts into producing more sustainable concrete.

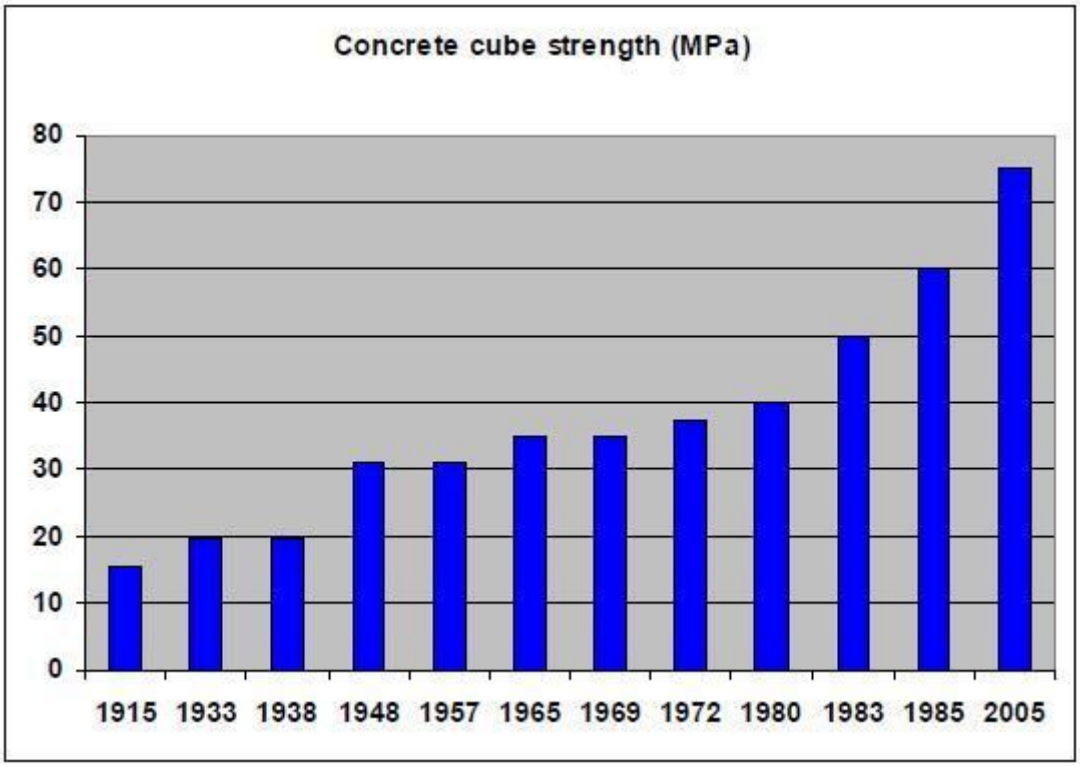

Figure 1-3: Increase of concrete strength during the 20th century (WHITTLE, R., 2008)

According to the Concrete Industry Sustainability Performance Report (2009) (The 1st Concrete Industry Sustainability Performance Report) published by the Concrete Centre, it is estimated that five out of eighty tonnes of aggregates used in concrete production is recycled and secondary materials[1] in year 2007. The entire production of reinforcement bar produced in UK is made from recycled scrap (refer footnote

1 Recycled materials are sourced from the demolition of buildings and structures, and the secondary materials are by-products of iron and steel making process and other extractive processes.

number 1). The amount of cement used is reduced by using the alternative cementitious material such as ground granulated blastfurnace slag and fly ash.

At the centre of these achievements, there has been the industry's demand to build more cost-efficient and more sustainable structures. In future structures should be built at a faster pace using more efficient construction solutions and using the less amount of material, and thus they are lighter and more sustainable. Lighter structures can be achieved from two ways. Firstly, a structure can become lighter simply using lighter materials with the equal strength, though it is often found that such material comes with high cost. Secondly, a structure becomes light through the efficient shape or form. The idea of efficient form is related to the utilisation of the material; in a structure of an efficient form the induced stress closely matches the material's capacity. As it can be observed from the natural world efficient forms are often consists of sophisticated structural system. For instance, our bones are designed to provide structural support to our body. When each bone is studied in detail it is made of a very complex system. For structural types of bone, there are Cortical (compact) bone; which resists in bending, and Cancellous (spongy or trabecular) bone; which resists in compression. Within the Cancellous bone there are number of interconnecting layers of bone called trabeculae, and interestingly the thickest and strongest layers (trabeculae) are placed in the in the direction where the greatest stress could occur (NATHER, A., 2005). In such structures it can be seen that materials are used for their best abilities, and they are designed to sustain mainly only one type of stress; either compressive stress or tensile stress. In composite structures two materials can be used together to give greater strength, and in such cases both materials will work together at their best ability while compensating for each other's weaknesses.

This is also the case for the reinforced concrete system. Concrete sustains the compression stress and steel sustains the tension stress. Thus reinforced concrete structure can perform well both in compression and tension, and this gives freedom to adapt more complex forms, especially with the fluidity of fresh concrete that enables it to be moulded into limitless forms. Yet this privilege cannot be fully experienced due to the restraints coming from the formwork construction.

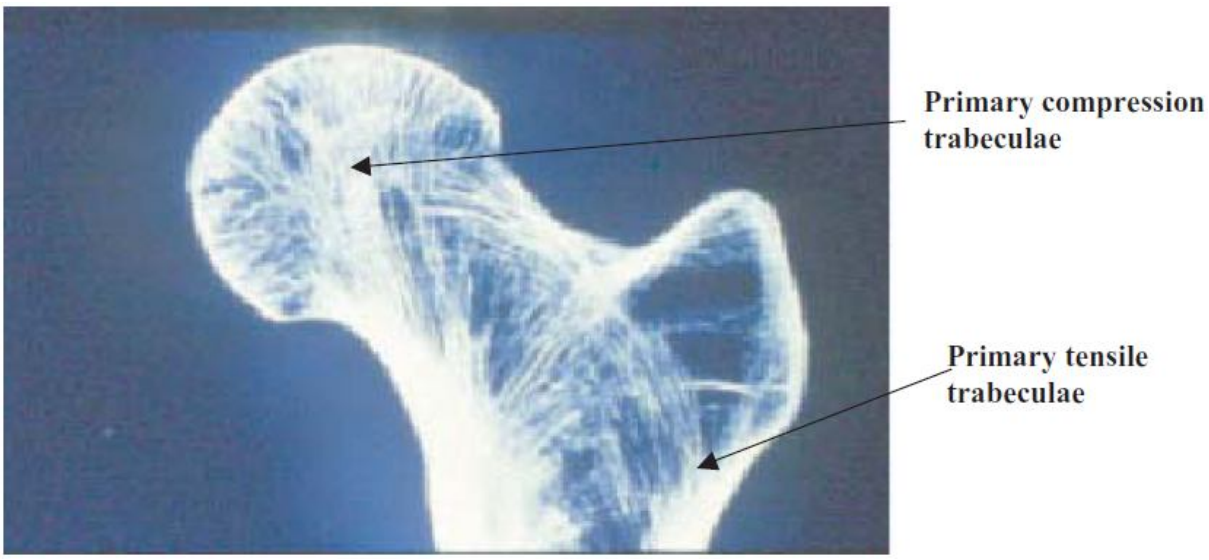

Figure 1-4: Primary compression trabeculae appear in the direction the femur is subjected to most loading. Tensile trabeculae occur in the outer part subjected to most bending forces: image and descriptions are directly extracted from the reference. (NATHER, A., 2005)

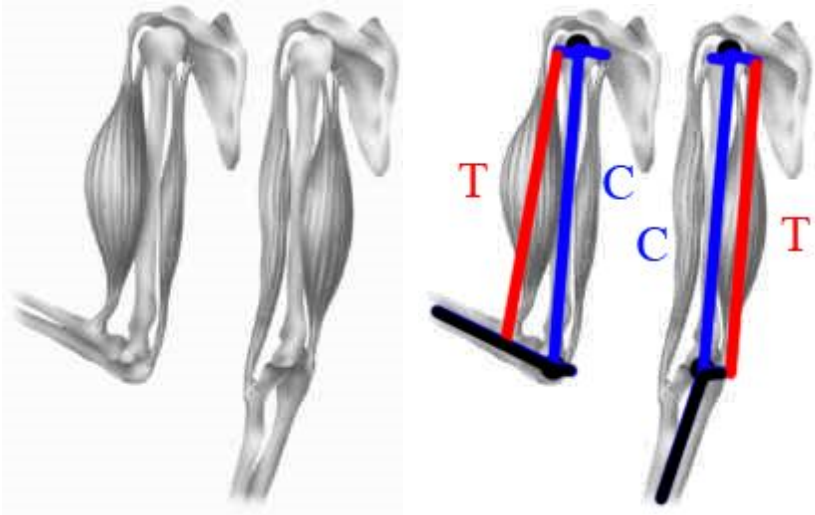

Figure1-5: Showing how the muscles in tension and the bones in compression are used in a single system. Two different components are in couple for the system.

"*It may be noted that although reinforced concrete has been used for over a hundred years and with increasing interest during the last few decades few of its properties and potentialities have been fully exploited so far.....the main cause of this is a trivial technicality: the need to prepare wooden forms*" (NERVI, P. L., 1956)

This is rarely felt for the simple rectilinear constructions but when the form becomes complex the designer must examine initially whether the specific formwork (which is generally made of rigid materials such as steel and timber) for the design can be built, not only in the technical aspects but also within the given budget and time. For this

reason the formwork technology is closely linked with the development history of concrete forms, and their correlation has been a big interest to designers.

Figure 1-6: Formwork construction for Auditorium of Tenerife in Santa Cruz, Tenerife by Santiago Calatrava (PERI Ltd. UK, Formwork, Scaffolding, Engineering); Concrete can be used to define any complex forms yet the formwork must be carefully devised to meet the time and budget limit. The picture shows one of the limited examples where the complex forms could be achieved using innovative formwork technology. The cost for preparing such formwork could be a lot greater in comparison with for the simple forms.

Despite these restraints of the formwork construction there have been engineers like Heinz Isler, Eduardo Torroja, and Felix Candela who have successfully managed to explore the possible ingenious structural forms which can be built using reinforced concrete. Most of their structures are monolithic and consist of relatively thin elements (as thin as 20mm in case of Cosmic Rays Pavilion in Mexico City by Felix Candela; Figure 1-8), and it is this thinness of the structure that overwhelms the viewers. The thin cross-section speaks about the small induced stress in the structure not because the external loads are small, but because of the structural efficient form. Thus the particular forms of structure save the additional materials, which could have been required in the case where other structural forms are considered.

"..., shape is cheaper than material." (BEUKERS, A. and van Hinte, E., 2005)

As an example, Heinz Isler's thin shell structures demonstrate such forms. The forms are directly transferred from the physical models, which are normally made

from a hanging cloth or membrane sagging under its own weight (Figure 1-7).

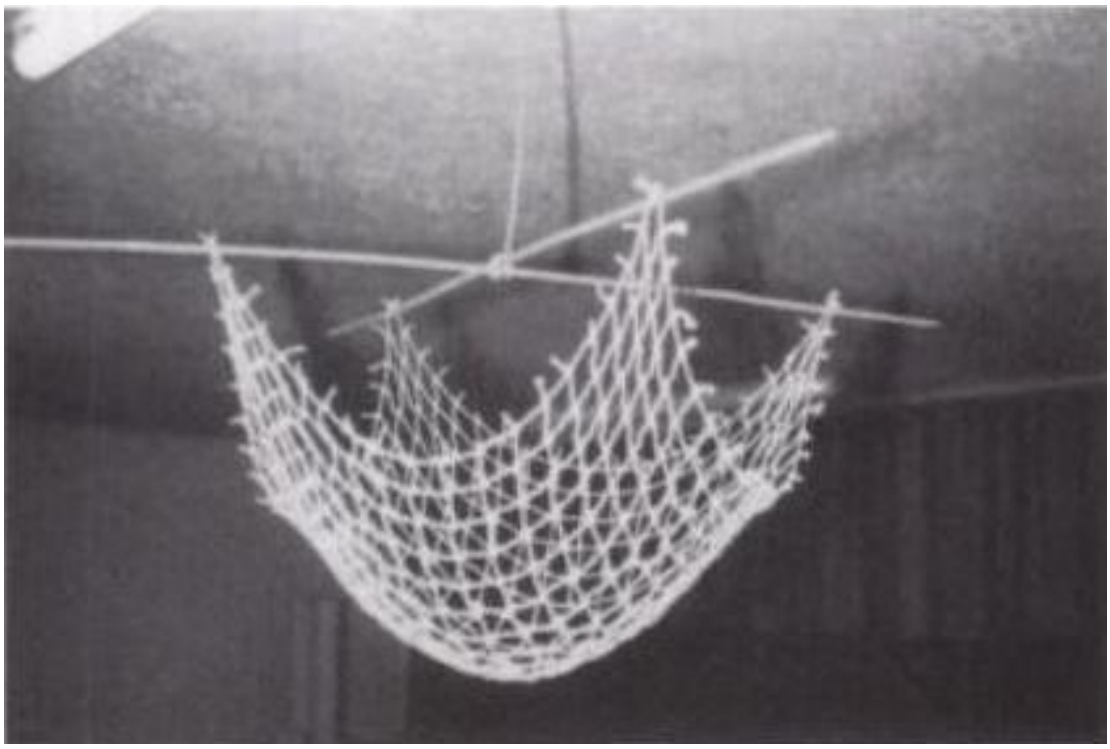

Figure 1-7: Hanging membrane model with unstiffened free edges (CHILTON, J., 2000)

As the cloth is hanged it is free to deform in the way the natural forces determine. Among the many forms that it can hold a static form is captured into a solid and thus it can no longer deform. As the hanging cloth was in pure tension, when the form is put upside down it becomes in pure compression. The geometry of the form is then measured by coordinates, and the coordinates are transferred to real structure on site. The concrete naturally performs well in compression but it is very weak in tension, and thus constructing such form with concrete gives the ideal condition for the material. The structures of Felix Candela are also good examples of reinforced concrete structures built in efficient forms, and it is often stated that he always thought through the construction aspects of the structural forms that he designed. The structures of Felix Candela are well known for their hyperbolic paraboloid (hypar) forms. The hypar is a doubly ruled surface and hence the surface is formed from straight lines; and the lines automatically indicate the positions of the formwork timber beams. Felix Candela stated that,

"of all the shapes we can give to the shell, the easiest and most practical to build is the hyperbolic paraboloid."

(HOLZER, C. E., Garlock, M. E. M., and Prevost, J. H., 2008)

Figure 1-8: Cosmic Rays Pavilion by Felix Candela (ISONO, Yoshito)

For an example of his structures there is the famous Los Manantiales restaurant at Xochimilco, Mexico City (Figure 1-9). It is formed by arranging the hypars of curved edges in polar direction (Figure 1-9 and 1-10).

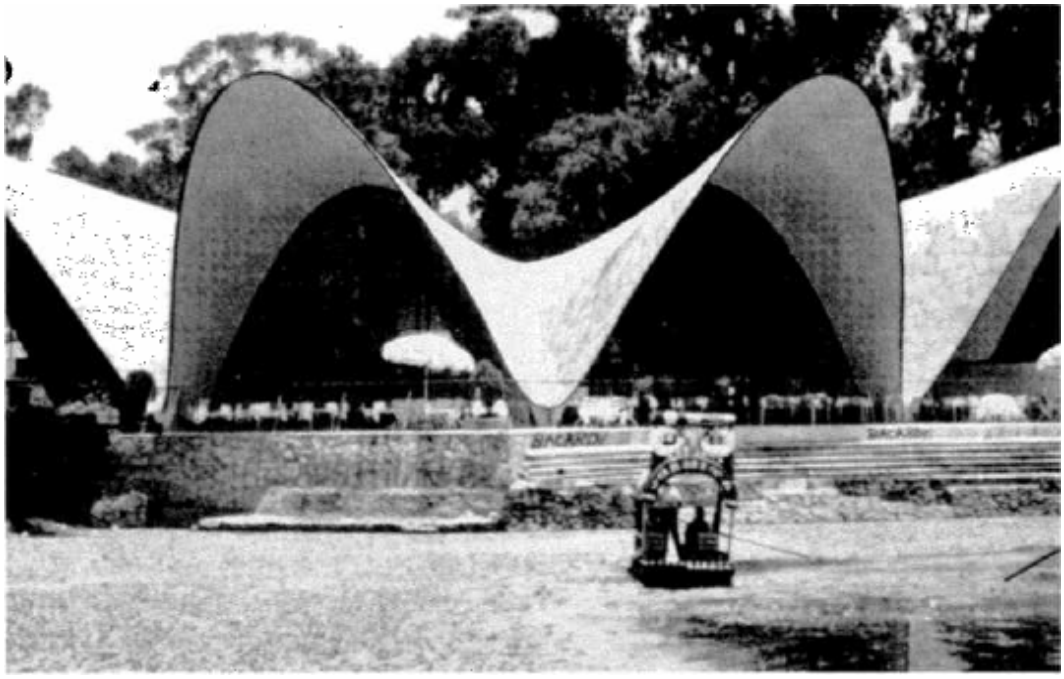

Figure 1-9: Los Manantiales Restaurant, Xochimilco, Mexico City, by Felix Candela (NORDENSON, G. (edited by), 2008)

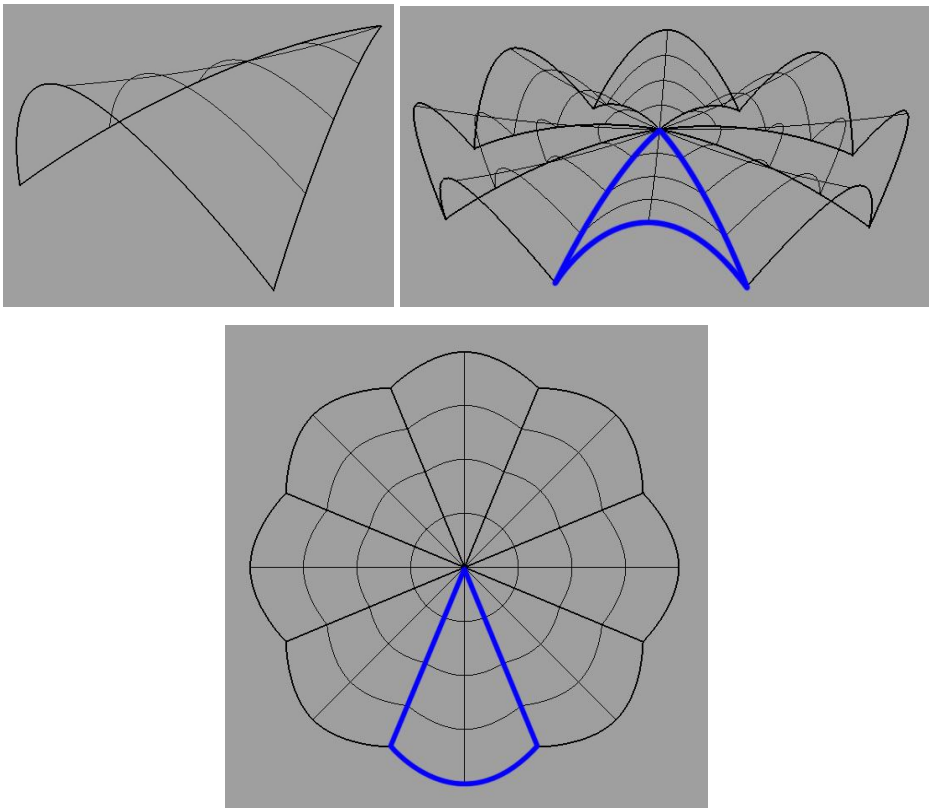

Figure 1-10: A design element extracted from a hypar form used for Los Manantiales restaurant in Mexico City.

The downside of building such the structure is the construction of the formwork. Despite the structural efficiency and delightfulness of the forms, their multi-dimensional geometry requires high cost and labour-intense construction of formwork and falsework. This aspect has prevented the wide acceptances of such structures.

Figure 1-11: View of scaffolding for Los Manantiales restaurant, Xochimilco, Mexico City (PRINCETON UNIVERSITY ART MUSEUM)

Figure 1-12: Labourers placing the concrete for Los Manantiiales restaurant, Xochimilco, Mexico City (PRINCETON UNIVERSITY ART MUSEUM)

1.2 Problems of Conventional Concrete Construction Methods

Constructing complicated forms using conventional rigid materials requires large finance and resources, and for this reason it has become more common to build structures in the simple rectilinear shapes. However the concrete structures in such simple forms embody more materials than they are structurally required. For structural members to be efficient the forming materials need to be placed only where it is required with the right amount, but as the form becomes simpler the efficiency has to be compromised. The structure taking up additional material increases its deadweight, and this causes a chain reaction of increasing the size of the other supporting structures. Since more materials are consumed, overall it results in a negative effect on means of sustainable development as more CO_2 is produced for the production of the materials.

In case of a simply supported beam, the effective depth at the mid-span is designed according to the applied bending moment. The shear capacity of the beam is then checked with the pre-determined effective depth, and when the shear capacity of the section is not sufficient the appropriate amount of shear reinforcement is added. For the conventional method the cross-section profile of the beam is designed to be uniform throughout the length as it is more practical to build. Thus the beam ends up having the cross-sectional depth over the entire span that is required only at the mid-

span. This means, while the concrete at the mid-span of the beam is fully utilized as the stress reach the ultimate collapse level, the materials near the ends of the beam might have not been used to its full capacity. It is true that the effective depth of the mid-span might be also required near the supports for shear resistance. However, the combined shear and bending behavior of reinforced concrete beam near supports is very complex and, thus it is also true that the conventional form does not reflect the beam's behavior in shear; this is why additional shear reinforcement is designed where required rather than changing the form of the beam. Also many research papers (there is a lot of research publications covering the shear aspect of reinforced concrete and it is very difficult to list all but only few are included here; (ARSLAN, G., 2008) (REBEIZ, K. S., 1999) (SCHLAICH, J. and Schafer, K., 1991) (VECCHIO, F. J., and Collins, M. P., 1988)) published on the shear behaviour of reinforced concrete beams show, that the research interest has been concentrated on the understanding of the behaviour with either further development of the present equations or with more sophisticated analysis methods rather than avoiding the problem by design. Thus this concludes that the form of conventionally constructed reinforced concrete beam might not be at its optimum level, and there is a requirement to develop the form to higher efficient level. In the sustainability point of view, production of structural element that is not fully efficient can be seen as both act of energy and material wasting.

1.3 Exploring New Formwork Technology

The minimum practical requirements for concrete formwork are the sufficient strength to sustain the structure during the curing time and the sufficient stiffness to resist against the deformation. For this reason more rigid materials such as steel or timber with the required thickness are commonly used in the industry. In the occasions when the labour and cost can be saved by having lighter formwork materials such as aluminum also could be used. Although the good durability of the conventional materials allows for multiple uses, this is not always the case due to the following reasons:

- Unless the building structure is relatively large or the geometry is relatively repetitive, the shape of a formwork unit that is suitable for a particular section might not be suitable for other parts of the structure.
- Generally the formwork units designed for a particular project are not perfectly transferable to other projects, mainly due to the requested sizes and

shapes between projects can vary. In this case either the prebuilt formworks are reshaped and reassembled to suit the new project's requirements.

- In case of timber, during the assembly and dismantling process of the material can be damaged and the number of times that they can be reused is limited between five and ten times (CHILTON, J., 2000).
- In small to medium scale construction projects the contractors simply prefer formwork built from newly ordered materials.
- There is a problem of storing the old formworks. The cost and the room must be considered.
- There are extra costs involved in re-using the old formworks. Before the re-use they need to be re-sanded and re-varnished for good quality of concrete finishing.

Larger companies overcome the above obstacles by having uniquely developed formwork construction system with wider range of unit sizes and types, however, again as the companies take on projects requiring more complex structures it is still inevitable to come up with new system and specifically tailored units. It would be fair to state that behind the development of formwork technology there is a competition to meet the designers' demand for the realisation of evermore sophisticated forms and visual qualities.

Though steel and timber have been the most commonly used formwork materials, there are construction cases in which different types of formwork material are used for casting concrete. Fabric (Woven or non-woven textiles) has been used since the mid-1960s to form concrete on the ground and under water for erosion control, cooling pond liners, and pile jackets. In architectural context Miguel Fisac used non-permeable flexible formwork for his wall panels (Figure 1-13), Felix Candela used fabric formwork for a school building project (Figure 1-14) and for one of the most recent projects San Francisco based architect Andrew Kudless constructed so called P-Wall (2009) using 150 plaster panels cast from nylon fabric formwork (Figure 1-13). P-wall was exhibited at the Museum of Modern Art (MoMA) in San Francisco. More examples will be discussed in the following Chapter 2. The three primary benefits of using fabric formwork have been fabric's flexibility, ease of working, and permeability. The P-wall example alone can show the use of flexibility of fabric in casting concrete in complex forms. Recent research results show that using

permeable formwork can produce better concrete quality regarding its appearance and its physical performances owing to its permeability (AL AWWADI GHAIB, M., Gorski, J., 2001), (MALONE, P. G., 1999). Fabric formwork allows any trapped air bubbles immediately behind the formwork surface to escape through. Also any excess water can be filtered out through the fabric which results in lower water/cement ratio at the surface of the concrete.

> *"This material frees our structural imaginations almost completely, and it is sad to realize that so far its potentialities have been little explored and even less used."*
>
> (NERVI, P. L., 1956)

The US Army Corps of Engineers technical report (MALONE, P. G., 1999) discusses the advantages of use of permeable formwork, and the key points are extracted below:

- Increased resistance to freezing and thawing: the extent of the damage to concrete cast in permeable formwork should be less than one fifth the damage to concrete cast with conventional formwork
- A reduced rate of surface carbonation: The smoother surface that permeable formwork imparts to the concrete reduces the area in contact with the atmosphere; the increase in density can reduce the rate of diffusion of carbon dioxide into the concrete; and the increased amount of cement in the surface layer can make additional calcium hydroxide available to maintain alkalinity at the surface. The extent of carbonation in concrete cast in permeable formwork should be generally less than 50 percent of that observed in concrete cast with conventional formwork and exposed to identical conditions of weathering.
- A reduced rate of chloride-ion infiltration: Resistance to chloride ion infiltration is extremely important to the service life of steel-reinforced concrete because the chloride ion greatly accelerates the rate of corrosion of the steel reinforcement. The extent of chloride-ion infiltration in concrete cast in permeable formwork should be less than 67 percent and generally less than 60 percent of that observed in concrete cast with conventional formwork.
- Increased surface strength. Surface strength measurement methods,

such as rebound hammers and pin penetration tests, have typically been useful in estimating the change in the overall strength of concrete as it cures. The rebound hammer readings in concrete cast in permeable formwork should be over 10 percent higher and possibly as much as 18 percent higher than those observed in concrete cast with conventional formwork. Marosszeky et al. (1993) reported an increase of approximately 20 percent in surface strength in concrete cast against permeable formwork at opposed to conventional formwork.

Fabric is a light, low cost material and readily available worldwide. Because of its lightweight nature, it allows significant savings for storage and transportation. Particularly, when the fabric formwork needs to be manufactured abroad and shipped to the site, the material's flexibility allows it to be compacted into very small volume, which can easily be shipped by air.

The above advantages of fabric show that with extensive research and development it has the potential to become the formwork material, which can be used more commonly as an alternative to steel, timber and others. Thus this current research looks into the development of fabric formwork system for the alternative construction method for reinforced concrete beam.

The thesis addresses that with fabric as formwork material reinforced concrete beam could be cast into more material-efficient form, and it aims at developing such form of reinforced concrete beam from studying the structural behaviour with physical tests, in conjunction with the development of construction method for fabric formwork. Thus, it demonstrates the development of reinforced concrete beam's form through the performance optimization process. In other words, the form is improved through consecutive load testing, structural analysis, evaluation of results, and modification.

In total eleven types of beams have been tested and analysed for three design criteria; Bending, Shear, and Deflection. The thesis describes the test methods for material properties, which are used in the structural analysis, and it also describes the experiment procedure including the illustrations of the equipments used. As part of the structural analysis where more comprehensive understanding is sought, the finite element analysis is used. For example, a number of finite element models are used to understand the types of stress induced around the anchorage area, and also the

distribution of the stress.

The thesis also illustrates the construction method of the formwork. In the beginning of the research it describes how the fabric is incorporated with other components as part of the formwork. As the form of the beam develops the formwork also evolves and it shows how the fabric becomes more dominant part of the formwork.

At the end of the thesis it discusses the improvement of construction efficiency as a result of the above developments of beam's form and formwork.

Figure 1-13: Wall panels of Casa En La Moraleza De Madrid in Madrid by Miguel Fisac (Arquitectura de casas: Casa en La Moraleja - Madrid)

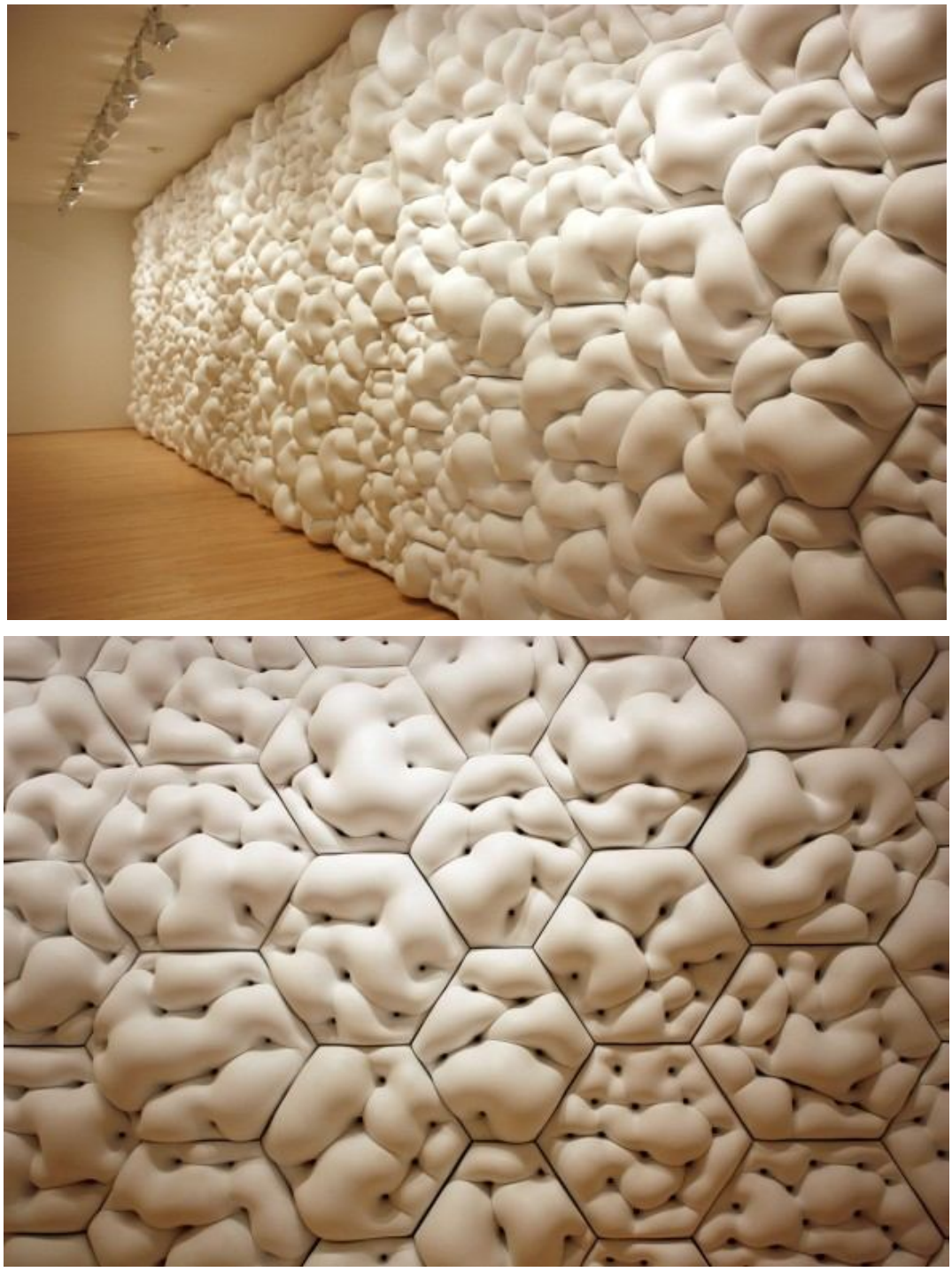

Figure 1-14: P-Wall at MoMA in San Francisco by Andrew Kudless (P_Wall (2009))

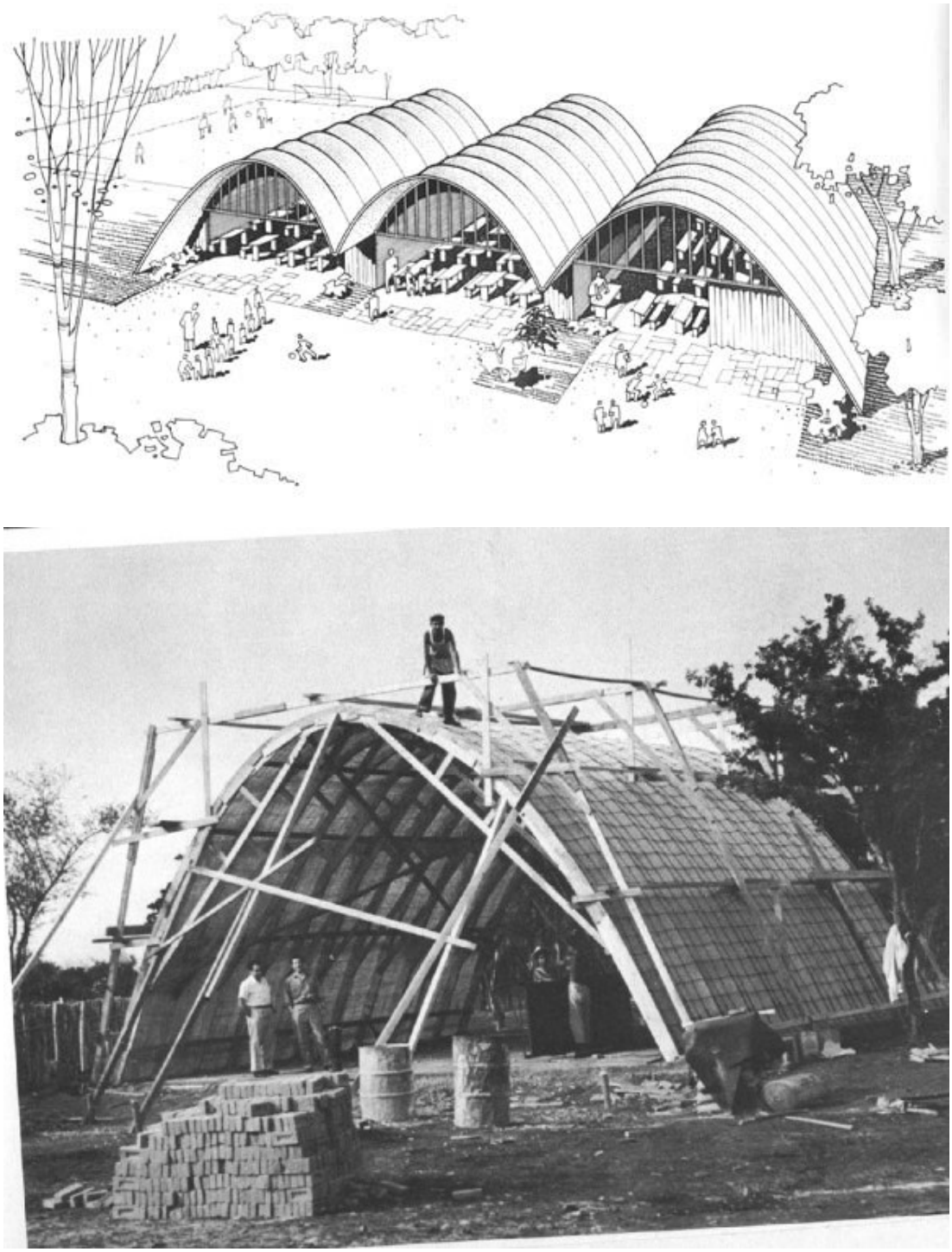

Figure 1-15: Felix Candela's Fabric Formed School (FABER, Colin, 1963)

Chapter 2: Literature Review

2.1 Introduction

The aim of this chapter is to review the existing research and practice in fabric formwork construction and their applications for constructing form-efficient reinforced concrete structures. From the review the following aspects are discussed:

- Using flexibility of fabric formwork to find concrete forms
- Using permeability of fabric formwork to cast mechanically improved concrete
- Exploring practical development of fabric formwork

This chapter also reviews briefly the relevant research describing the structural behaviour of reinforced concrete beams. However, there is vast number of works present on the topic, and thus only the selected works, which are directly applicable for the development of the form of fabric formed reinforced concrete beam, are discussed in this section.

2.2 Fabric Formwork Technology

2.2.1 Work of Construction Techniques Incorporated: Fabriform (Construction Techniques Fabriform Fabric Formed Concrete System, all images are extracted from the company's website)

Construction Techniques is an American company based in Ohio, and the company has been using woven fabric for casting concrete in numerous civil engineering projects for many years. The company obtained patent for the 'Fabriform System' in mid-1960 and the products are used for construction of revetments, pile-jackets, retaining walls, and etc. The strength of the products comes from economical construction, easy installation process, and the production of highly durable concrete due to lower water/cement ratio owing to the fabric's ability to filter out the excess water in the fresh concrete. In the paper by Bruce A. Lamberton, President of Construction Techniques Inc. (LAMBERTON, B., PRESIDENT, CONSTRUCTION TECHNIQUES INC., 1980), it is stated that the concrete cast in fabric forms increased compressive strength in comparison with the concrete cast in conventional water-tight moulds:

"A refinement of the fabric forming technique uses a highly water permeable fabric which is designed to serve as a filter as well as a form. This fabric is woven of high-strength industrial nylon which has been textured to provide improved filtering as well as adhesion to the mortar. The mortar is pumped into the form and pressure is maintained on the mortar after the form is full. Excess mixing water is squeezed through the fabric causing a pronounced reduction in the water-cement ratio for a distance up to 6 inches or more from the surface of the fabric." (LAMBERTON, B., PRESIDENT, CONSTRUCTION TECHNIQUES INC., 1980)

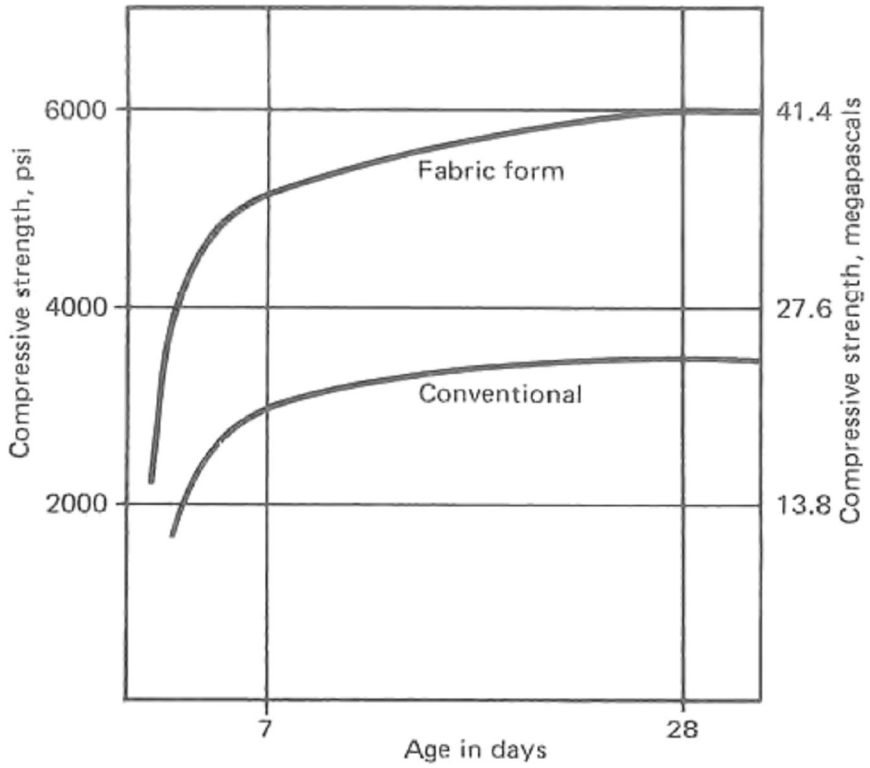

Figure 2-1: A comparison of strength of concrete cast on conventional watertight molds and in fabric forms of nylon fiber. The fabric forms increase strength by permitting a lower water-cement ratio as excess mix water is squeezed through the fabric (LAMBERTON, B., PRESIDENT, CONSTRUCTION TECHNIQUES INC., 1980).

The fabriform products adapt the merits of fabric material in the most practical way, and the company has been successful in promoting the use of fabric in concrete construction. Their products have been recognized and used by many clients including U.S. Army Corps of Engineers.

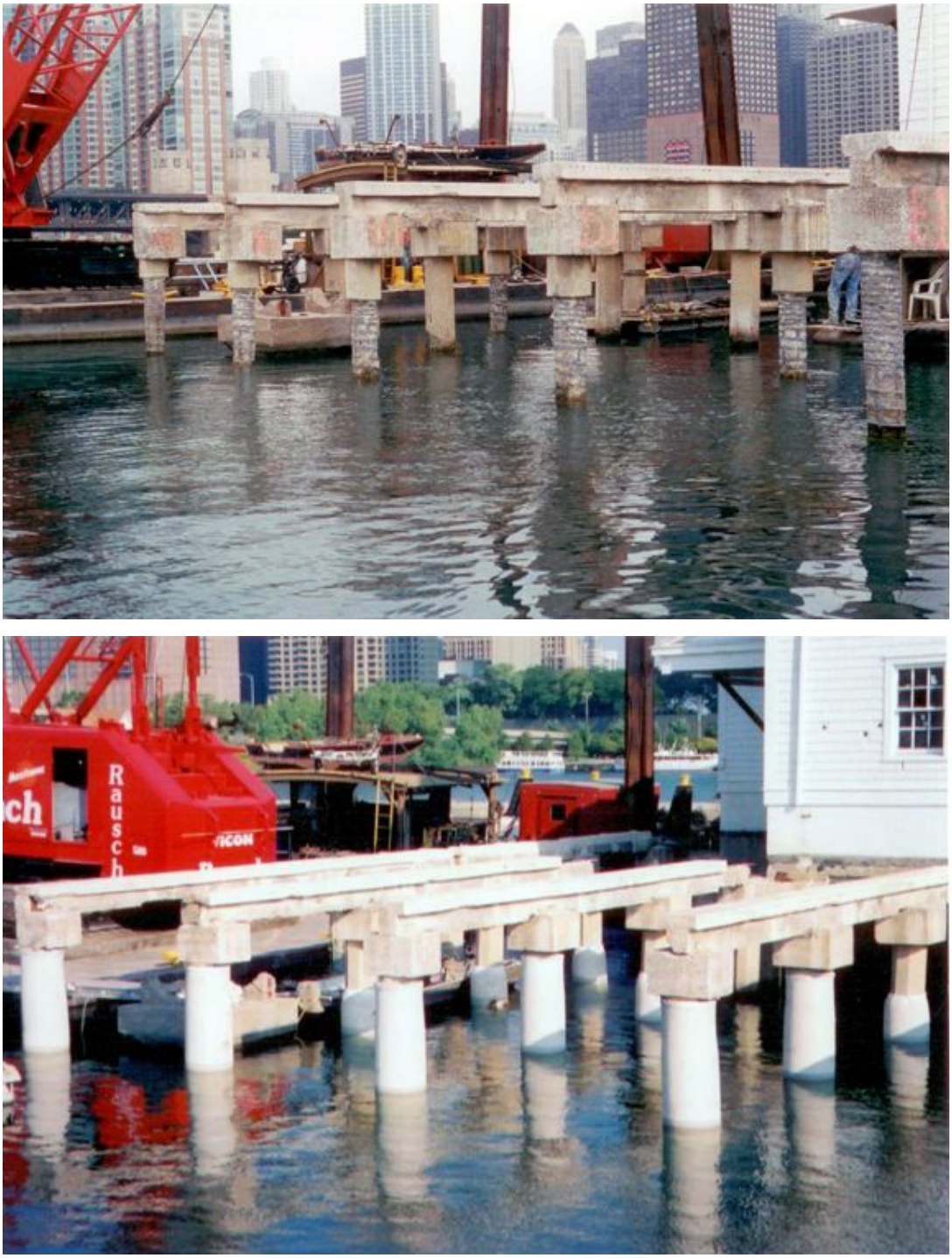

Figure 2-2: Chicago Marine Safety Station before (above) and after (below) pile jacket installations

Figure 2-3: Fabriform installed in 1967 on the Kinzua Reservoir, New York

2.2.2 Work of Fab-Form Indutries Ltd (Fab-Form Fabric-Formed Concrete)

Richard Fearn is the President, CEO and Founder of Fab-Form Industries Ltd., a manufacturer of fabric forming products. The company's products adapt the advantages of fabric (which in this case is made of non-permeable Polyethylene), which are widely available, cheap, light weight, compact, easy to cut into sizes, strong in tension, and weatherproof.

As an example, Fast-tube is one of the company's products, and it is a mould to form concrete column tube.

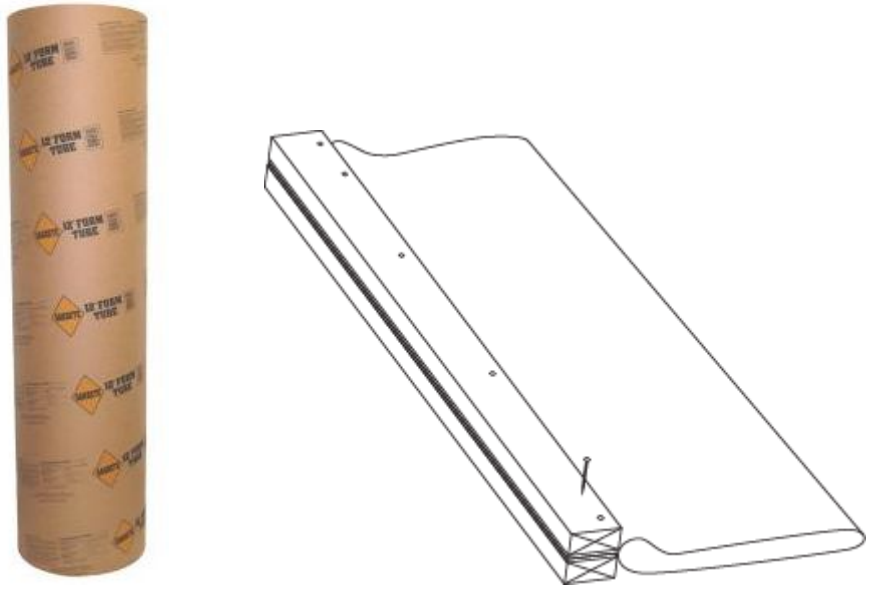

Figure 2-4: Cardboard tube mould (left) and Fast-Tube mould (Right) (Fab-Form Fabric-Formed Concrete)

In comparison with the cardboard formwork, Fast-tube is weatherproof and thus it can be conveniently stored on site without any extra care for wet damage, however, cardboard mould significantly loses its strength when it is wet, and it can be tear off very easily. Fast-tube can be compacted into much smaller volume than cardboard mould so it saves the storage space, and also it is easy to handle and to move it around the site with its light weight and compact volume. When the concrete has set, the stripping Fast-tube is a lot quicker and simpler by just peeling it off the concrete, and also the removed fabric can be used as a vapour barrier placed under the floor slab. This demonstrates the good durability of the fabric which can be reused repeatedly, and its flexible use as other component of construction.

The following pictures (Figure 2-5) are prepared as an example to show the installation process of the Fast-tube (Fab-Form Fabric-Formed Concrete).

Figure2-5: The installation process of the Fast Tube

1. Lay the tube on the ground, and nail the tab to the 2x4. Then sandwich the tab by nailing a second 2x4 to the first.
2. Stand up and brace the 2x4s in position. The Fast-Tube will align itself across from the 2x4s when filled with concrete.
3. At the start of the pour place the left foot at 8:00 o'clock and the right foot at 4:00 o'clock around the perimeter to position the base. Once there is 6" of concrete in the column, fabric tension will position the tube and prevent concrete leakage.
4. Stripping the Fast-Tube™ is fast – pull the welded seam apart.

2.2.3 Work of Miguel Fisac, Spanish Architect (1913-2006)

Miguel Fisac is one of the pioneers along with Felix Candela who adopted flexible formwork for casting concrete. Although he did not use permeable fabric for any of his projects, his applications have been inspirations and eye-opener to the use of fabric as a formwork material. He mainly used impermeable plastic sheet to cast concrete panels, and his intention was to express the fluidity of concrete's initial physical state in the final set form. He used steel mesh or wires to mark patterns to the liquid concrete, and this gave more soft and life quality to the set concrete.

Figure 2-6: Examples of Miguel Fisac's Works: Centro de Rehabilitación para la Mutualidad del Papel in Mupag (Left), Centro social de las Hermanas Hospitalarias in Madrid (Right) (Betonu Biçimlendirmek)

Figure 2-7: Examples of Miguel Fisac's Works: Casa de Miguel Fisac in Almagro (Betonu Biçimlendirmek)

2.2.4 Work of Kenzo Unno: Architect, Tokyo, Japan

Kenzo Unno is an architect in Tokyo, Japan, and he works at the Umi Architectural Atelier. Kenzo Unno has invented and developed methods of forming cast-in-place concrete walls using fabric moulds. This method is known as URC ("Unno Reinforced Concrete"). His works show good example of fabric formed concrete that is economical to build and visually satisfying. In his projects he used two methods to build so call URC walls;

1. Frame method: Fabric is placed inside a braced stud wall, and concrete is poured in between these walls. The poured concrete is vibrated by poking the fabric.

Figure 2-8: The fabric-formed wall construction of the Frame method for the Mitsushi Turu residence in Kawasaki City, Kanagawa in 1997. Photo 1 by Kenzo Uno (Tokyo, Japan) and Photo 2 by Mark West (Manitoba, Canada).

2. Quilt point method: Standard form-ties with washers fix the fabric onto the wall formwork. The ties then form 'quilt-points' when concrete is poured. Again the vibration can be done by poking the wet concrete behind the fabric.

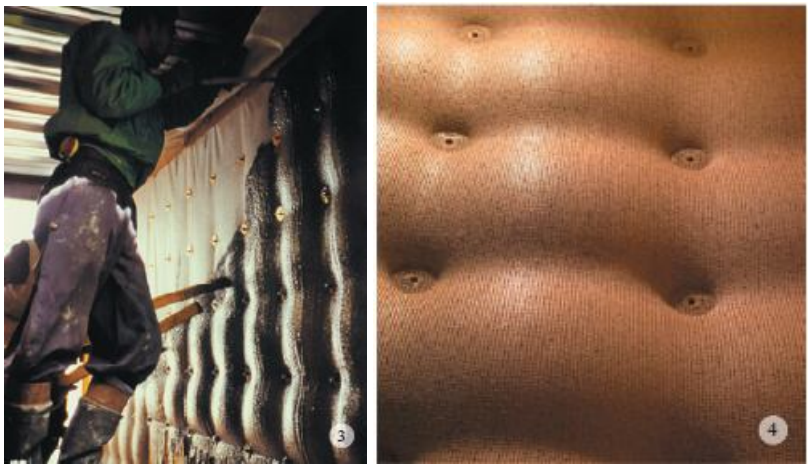

Figure 2-9: The fabric-formed wall construction of the Quilt point method. Photo 3 by Tsunenori Yamashita (Tokyo, Japan) and Photo 4 by Mark West (Manitoba Canada).

Kenzo Unno's development of Zero-Waste formwork provides a complete solution for fabric-formed wall construction.

Figure 2-10: Kenzo Unno's Zero-Waste formwork system (CHANDLER, A.)

Zero-Waste formwork consists of the fabric, the reinforcing steel that supports the fabric, the rigid polystyrene insulation, and the form ties and the furring studs to support the insulation. The concrete is poured in the space between the fabric and the insulation. When the concrete is set this cast-in-place formwork then becomes part of the wall and only part that comes off the system is the fabric.

The above construction method makes the fabric formwork construction more adaptable to the practitioners. The system is also complete and can be bought ready for the construction. This saves a lot of work for the builders to set up the formwork.

2.2.5 Work of Mark West, the University of Manitoba, Canada (The Centre for Architectural Structures and Technology, all images from C.A.S.T. website unless noticed otherwise)

Mark West is the director of C.A.S.T. (Centre for Architectural Structures and Technology) at the University of Manitoba, and he has been involved in a number fabric formed concrete projects scaling from concrete panels to structural columns and beams. The projects at C.A.S.T demonstrate applications of fabric formwork in casting various types of concrete elements including beams, columns, slabs, trusses, and thin-shell panels. Mark West has also written many papers on the works at C.A.S.T. Among the many works of C.A.S.T only the selected works are illustrated in this section.

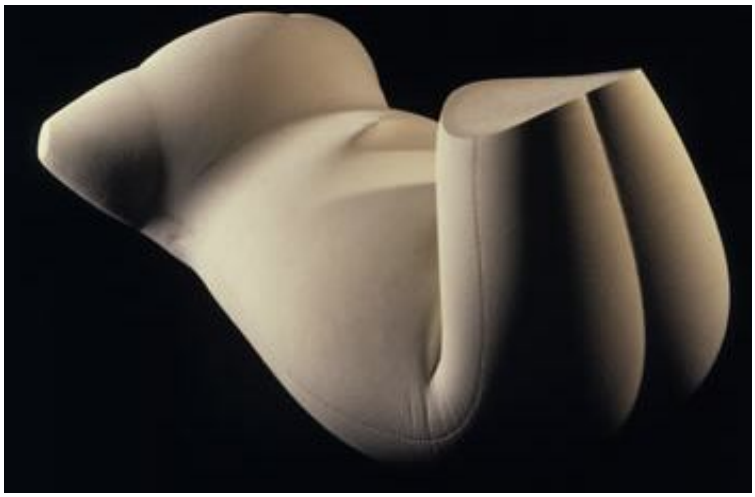

Figure 2-11: Fabric formed concrete sculpture at C.A.S.T.

Fabric Formed Panels

The concrete panels which designed by C.A.S.T. are good examples of showing the use of fabric formwork in conjuring the concrete's aesthetical quality. Through the form of the panels the viewer can see the compression and tension points in the fabric, and the shapes of any materials the panel is cast against is imprinted in the most direct way. The forms of the panels have the magical ability to tell the viewer more about the characteristics of the mould in which they were cast than the concrete material itself. In this sense the material becomes an artistic medium for the formwork. Another point is that the panels can be 'inversely' duplicated using the 'invert cast' method. This method uses a fabric formed panel (the original panel) as a mould, and a panel cast onto this original panel will have the invert geometry. This is an ingenious solution in the consideration that any form cast on fabric formwork will be in tension geometry due to the sagging of fabric under the concrete dead load. However using the invert cast method the tension geometry could be easily converted to the compression geometry.

Figure 2-12: Fabric formed panels built at C.A.S.T; Direct and Indirect Cast Panels

Figure 2-13: Fabric formed panels built at C.A.S.T; Direct and Indirect Cast Panels

Fabric Formed High-Efficiency Reinforced Concrete Beam

The picture below is 12m long reinforced concrete beam developed in C.A.S.T. in the spring of 2003. The shape of the beam follows the bending moment diagram of the specific load condition, in other words the shape reflects the required bending capacity of the beam sections. This beam demonstrates the most interesting ability of fabric formwork that is, using fabric formwork high material efficient concrete beams can be cast by putting only the required amount of materials at where is necessary.

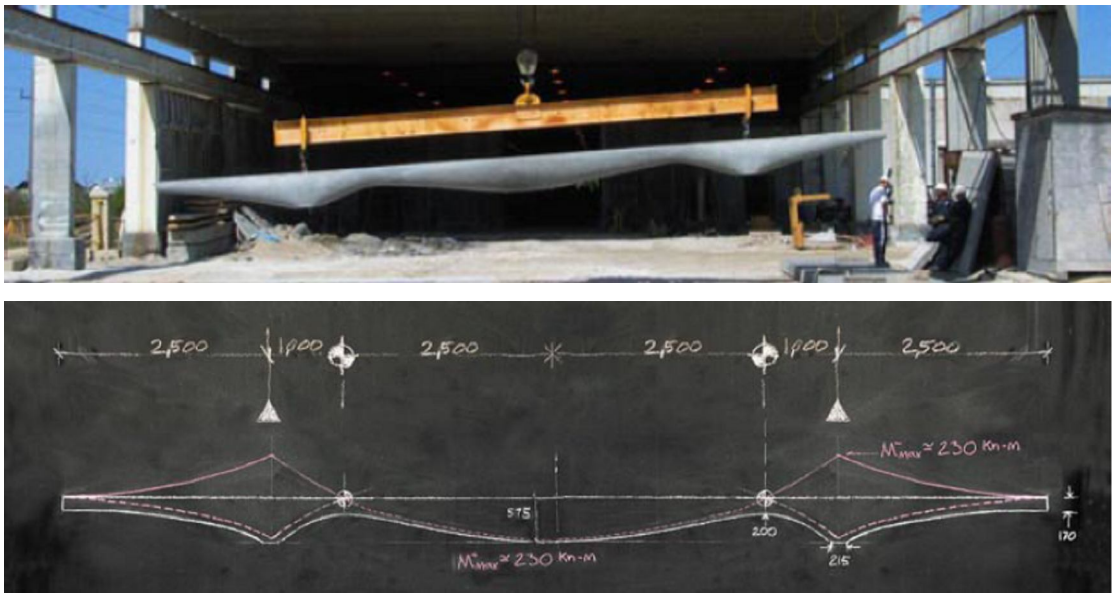

Figure 2-14: 12m long fabric formed beams cast at C.A.S.T

The pictures below briefly illustrate the construction method of the above prototype beam.

Figure 2-15: Construction of fabric formwork for the beam at C.A.S.T

The main process is to drape down the fabric between tables of timber sheets, and the concrete is poured onto the sagging fabric. The fabric is stretched accordingly to the predetermined shape by adjusting the sagging length between the timber sheets.

Fabric Formed Trusses

The application of fabric formwork for building more material efficient concrete structure is further developed and demonstrated through the construction of the 4 metres long fabric formed trusses.

Figure 2-16: Fabric formed truss at C.A.S.T. in the University of Manitoba

The formwork consists of three timber frames; two clamping pieces and one the central piece. The fabric is initially stretch and fixed on to the clamping pieces, which are pressed against each other to form the complete formwork.

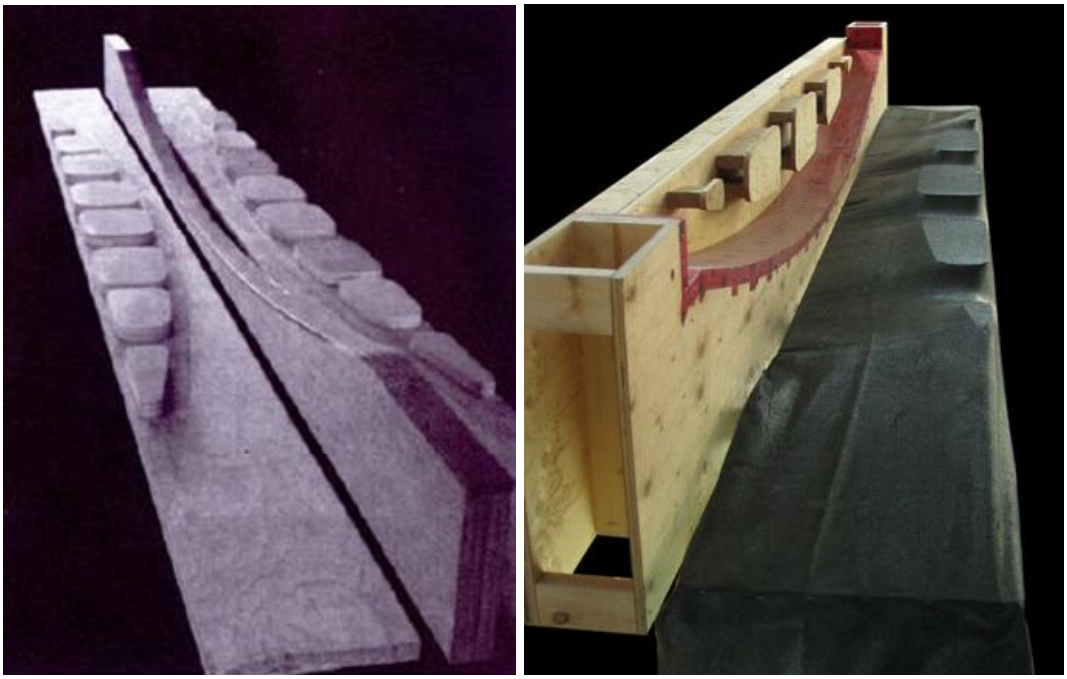

Figure 2-17: Truss mould

Figure 2-18: Completed formwork (left), and concrete pouring process (right)

The reinforcement bars are placed at the bottom curve of the truss and the fresh concrete is poured through the void formed between the clamped pieces.

The truss beam is also structurally tested as a part of PhD engineering research. The following pictures show that the vertical bending cracks are rather uniformly distributed over the full span of the beam, and there is no sign of diagonal shear crack in the beam.

Figure 2-19: Four metres long fabric formed truss after structural test

2.2.6 Work of Remo Pedreschi, University of Edinburgh, U.K. (Fabric Formed Concrete at Department of Architecture, the University of Edinburgh)

Pedreschi has been actively involved in research and live construction projects which explore the structural, constructional, and architectural opportunities of fabric formed concrete. The live construction projects include the Whitburn Project in West Lothian, Scotland with E & F McLachlan Architects, Castleview Primary School in Craigmillar, Scotland, and the Fenchurch Garden Project for the Chelsea Flower Show 2009 in London (MCLACHLAN, F., Pedreschi, R., Lee, S-H, Dhir et al, 2008). For the above projects he demonstrated the efficient way of finding forms with using different types of fabric and the practical applications of the technology in the real projects. The skills and knowledge of fabric formed concrete that Pedreschi gained through his past projects is well demonstrated in a refined way especially in the Chelsea Flower Show Project (constructed at the University of East London in collaboration with Alan Chandler) (Figure 2-20) and the Fabric Formed Concrete Rain-Screen Cladding Project (Figure 2-24).

Pedreschi and Chandler also edited the book *Fabric Formwork* (CHANDLER, A., Pedreschi, R. (editied by), 2007) which consists of essays contributed by six authors, and it presents the different views on the new concrete forming method in context of practice and theory, and aesthetics and the pragmatic. The book is the first major text in this area.

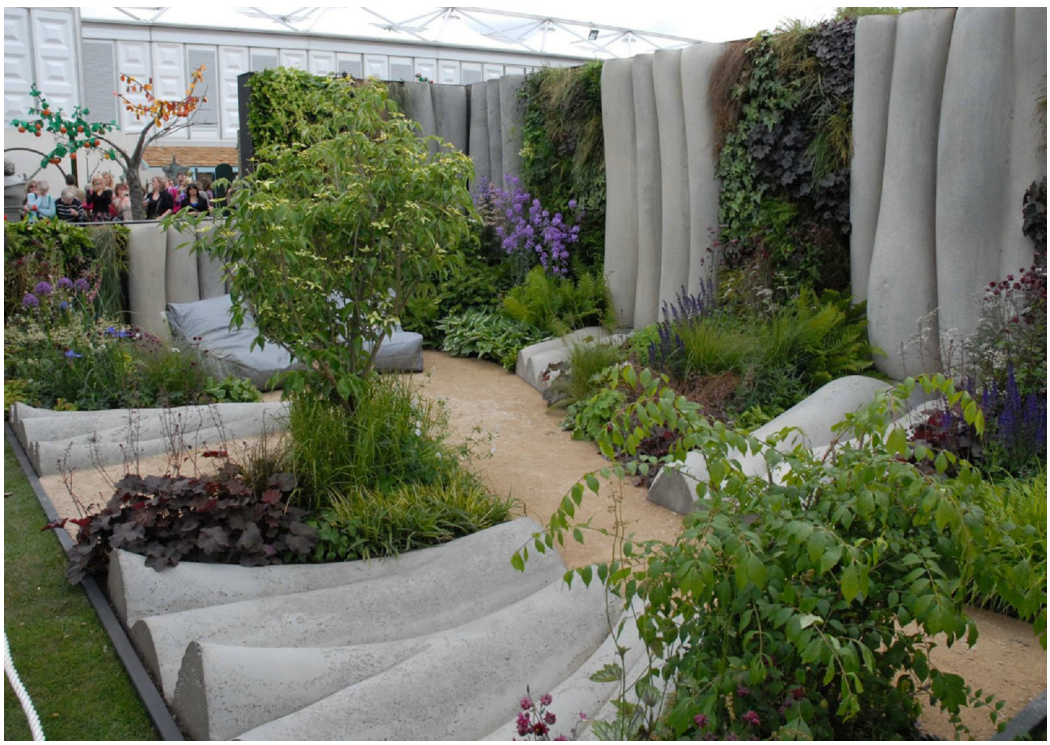

Figure 2-20: the Fenchurch Garden in Chelsea Flower Show 2009

For the Chelsea Flower Show in total 19 fabric formed concrete pieces are cast (largest was 2.5 by 0.75 m), and each panel has a different overall geometry and forms. Each piece is generally made by pouring fresh concrete into a fabric draped onto a rectangular wooden frame, and thin timber fins cut into different wave forms are placed under the fabric. The fins push up the fabric and results the horizontal curves of concrete.

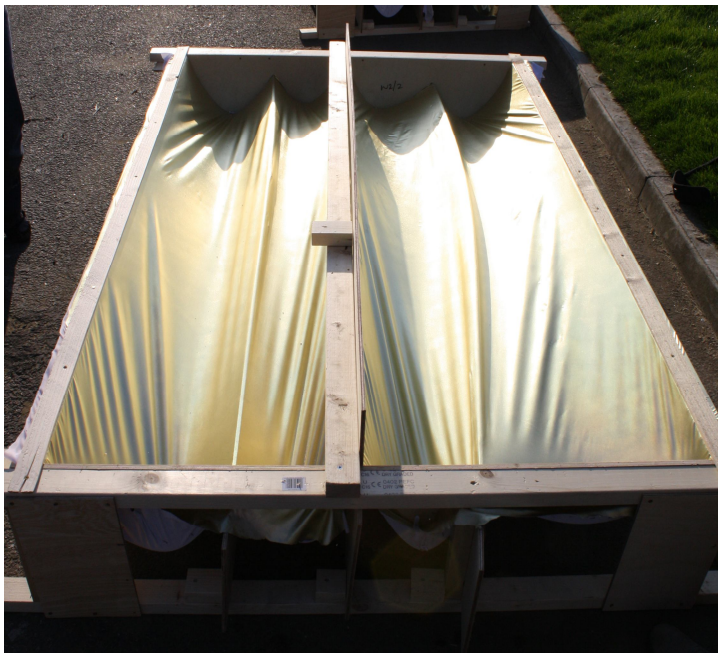

Figure 2-21: A formwork of the panels for the Chelsea Flower Show

Figure 2-22: Construction of the fabric formed concrete panels of the Fenchurch Garden

The allocated time for the project was only five weeks from design of the formwork to the installation. Considering the scope of the project this was a tight time schedule, and this shows the efficiency of fabric formwork construction method and the quality of the outcome as it was presented to the public and selected by the judges for the most creative design award.

Pedreschi's in-house research has been carried out through student projects. Typical element such as beams, columns, walls and shells have been developed, with particular reference to construction accuracy, repeatability and simplicity of construction.

Figure 2-23: Fabric formed concrete elements at the University of Edinburgh workshop; wall/screen elements (Top and bottom left) and column construction using modular elements (Right)

Further studies explored the ideas of Heinz Isler and Eladio Dieste, in a doubly curved Gaussian vault using fabric as the formwork. (Figure 2-23).

Figure 2-24: Fabric formed concrete doubly curved vault at the University of Edinburgh workshop

The above vault is formed by pouring concrete over a fabric draped between two catenary curves of different heights defined by separate timber profiles. If the formwork was only made with timber then obviously a lot more materials would have been required and it could have taken a lot more time to build. The fabric's flexibility has formed a further catenary under the dead-weight of the fresh concrete without any extra effort. This example demonstrates the fast, simple, and cheap concrete construction using fabric formwork.

The following picture shows the fabric formed concrete panel cladding system (Figure 2-24). This diversity has been achieved very effectively by simply changing the type of fabric or by varying the way the fabric is pressed to form different textures. It could have been a time consuming process to cast all the panels in such different designs using other materials. The use of permeable fabric also made the surface of the concrete more durable for external weathering condition. The work is a good example to see the use of fabric formwork in producing fully functioning aesthetic building element, which is also technically sound and practical to build. The surface finish quality of the panels has been very appealing to the viewers and people are naturally drawn to touch and feel their texture.

Figure 2-25: Fabric formed rain screen panels by Professor Remo Pedreschi and Keith Milne

2.2.7 Work of Alan Chandler: the University of East London, U.K.

At the University of East London Alan Chandler has been researching fabric formwork for both concrete and rammed earth. His works (fabric formed elements) demonstrate the relationship between the materials and the fabric moulds in finding elements in unprecedented forms.

Figure2-26: Photos of some of the fabric formed elements at the University of East London.

The pictures below (Figure 2-26) show one of the projects called 'Wall One' which was took place at the University of East London called in collaboration with Remo Pedreschi from the University of Edinburgh. The 2m x 3m concrete wall is cast in a fabric formwork. An engineered geotextile fabric has been hung from the upper deck and comes down to the bottom plate.

The upper deck and the bottom plate are vertically held apart using acroprops. The bulging of the wall is controlled throughout the pouring process, and it has been done using metal rods which are put through the wall and changing the local width using the wooden washers. There are no predeterminations of the widths and they have been adjusted as the concrete is being poured. This 'play as you make' aspect of

construction method seems very tactile and thus very attractive. The above picture of the final form shows that the colour of the concrete varies vertically as the concrete pouring procedure was divided into a number of steps. Thus the mix from different batches gave different colours, and this effect gives additional attractiveness to the final form. This project mainly demonstrates the use of the flexible characteristic of fabric and physical properties of fresh concrete in finding concrete forms.

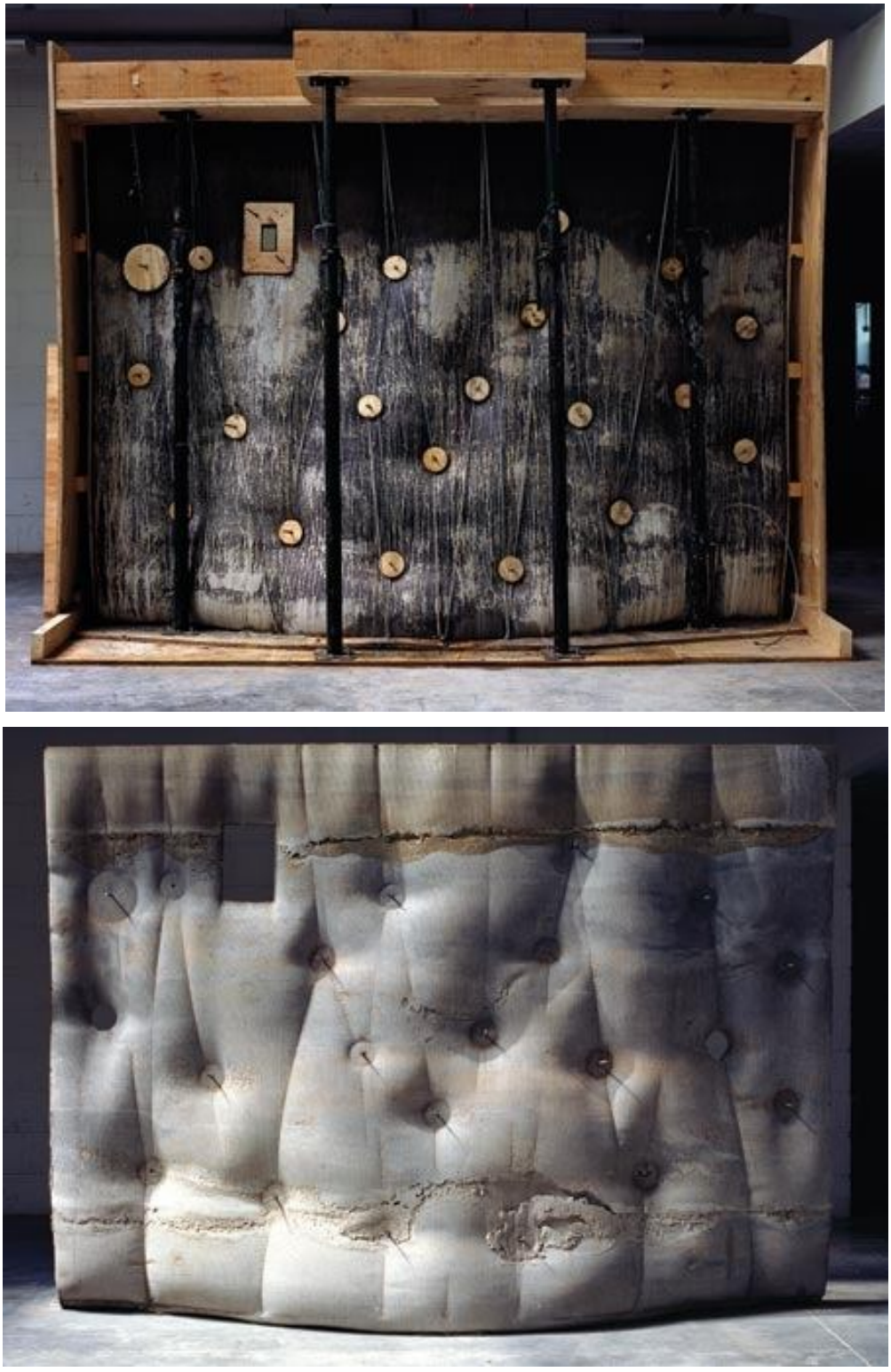

Figure 2-27: Fabric formed concrete wall at the University of East London

Figure 2-28: Wall Two (Top) and Rammed Earth Wall (Bottom) at the University of East London

Wall One shows some similarities to the Quilt Point walls of Kenzo Unno, yet it is more complex in its shape and there is also more freedom to the form.

Figure 2-27 shows other wall construction projects at the university. The two walls

are constructed in similar mould, and their forms express more control on the designer in comparison with Wall One. Wall Two also expresses more even distribution of the material. The rammed earth wall clearly shows the roughness on the surface as more coarse aggregates are visible, in contrast with Wall One and Wall Two which show more dense surface quality owning to the nature of fabric that allows the excess water to escapes while keeping fine aggregate and cement at the outermost layer.

2.2.8 Work of Daniel S-H Lee and Tom Dowdall, the University of Edinburgh

Lee and Dowdall carried out a research project for their undergraduate final year thesis on the construction methodology and structural behaviour of fabric formed form-active reinforced concrete beam. This project initiated the current research that informs the core of this thesis. The work started with a structural experiment of a prototype beam, which was constructed at the work shop by Remo Pedreschi, for the purpose to examine the practical construction methods for concrete beam using fabric formwork. The prototype beam (which is discussed in more detail in Chapter 6) was further developed by Lee and Dowdall through the process of design, construction, experiments, analysis and modification.

Figure 2-29: Fabric formwork construction for form-active beam at the University of Edinburgh

The beams consist of flange and web, and the formwork was developed with the particular aim of achieving repeatable dimensional accuracy. The fabric formwork was mainly used to form the complex geometry of the web, and the plywood soffit formwork is used to form the flange. The vertical geometry of the web was defined

by plywood pieces cut into the parabolic shape, which are then clamped to the fabric from both sides.

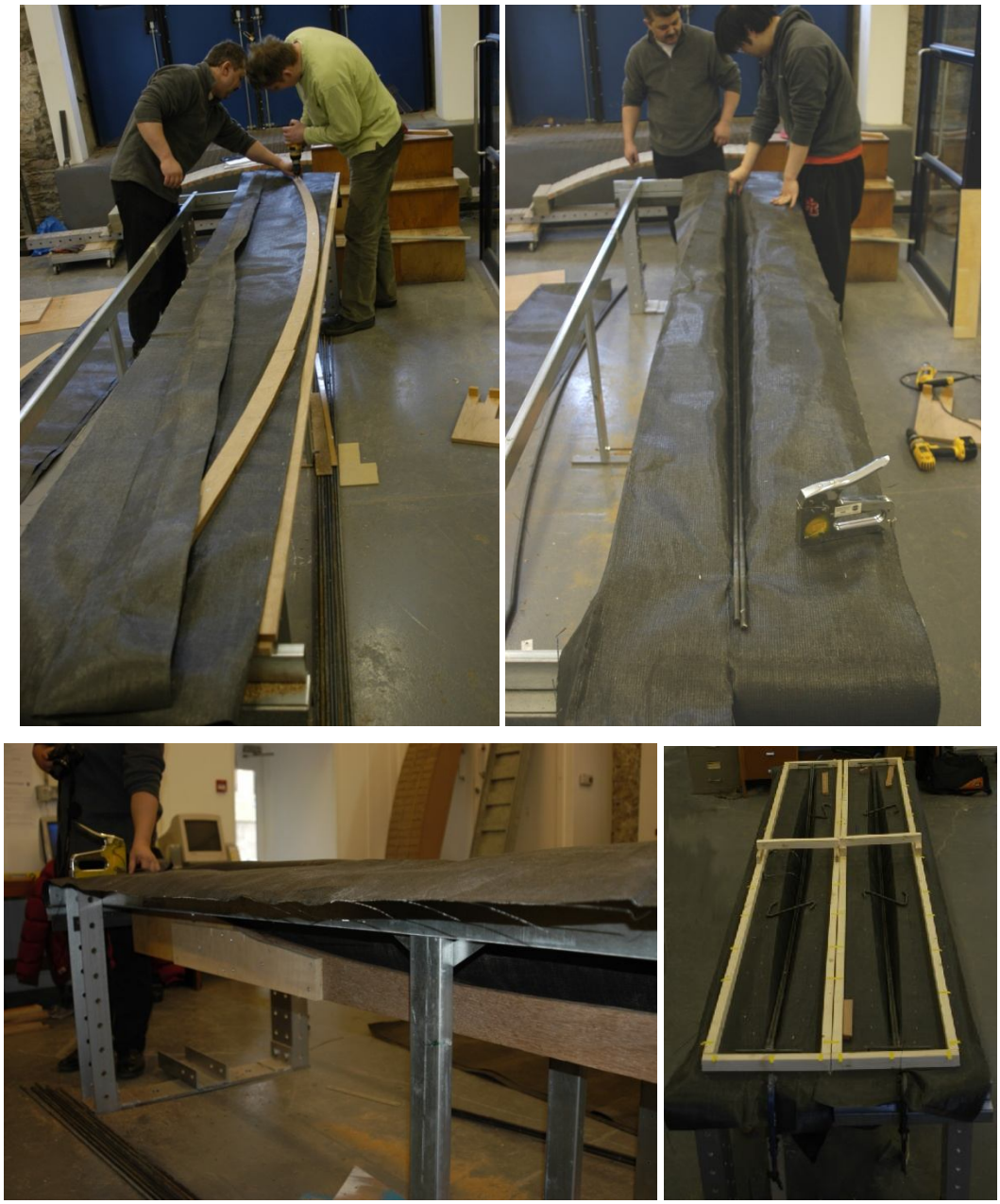

Figure 2-30: Fabric formwork construction for form-active beam at the University of Edinburgh

Figure 2-31: A fabric formed beam by Lee and Dowdall at the University of Edinburgh

In comparison with conventional rectangular and T-beams, the mass of the cast beams appears lighter, slender and elegant. Also, the end geometry of beams is simple flat slab which is good for bearing and simplifies the installation of the beam; however in contrast conventional T-beam requires extra work to fill the void formed by the web of the adjacent beams. For their work in total three beams are constructed and tested. The first beam adopts the form-active catenary curve, but the subsequent beams adopted a parabolic curve. Also in the first beam the area of rebar changes with the length; there is twice the steel near the mid-span than the adjacent to the supports.

However, the test shows that the beam fails at the exact section where the amount of steel decreases. The two other beams failed due to the axial compression stress exerted by end anchorage which leads to compression failure of the adjacent concrete (Figure 2-30 and Figure 2-31). In fact the third beam has higher steel ratio than the second beam, but both beams fail at the same load since the cause of failure is related to the anchorage compression stress. A strut-and-tie model was used to analyse the compression force of the anchorage (Figure 2-32).

Figure 2-32: Failure of the beam: concrete crushed by the pulled in anchorage

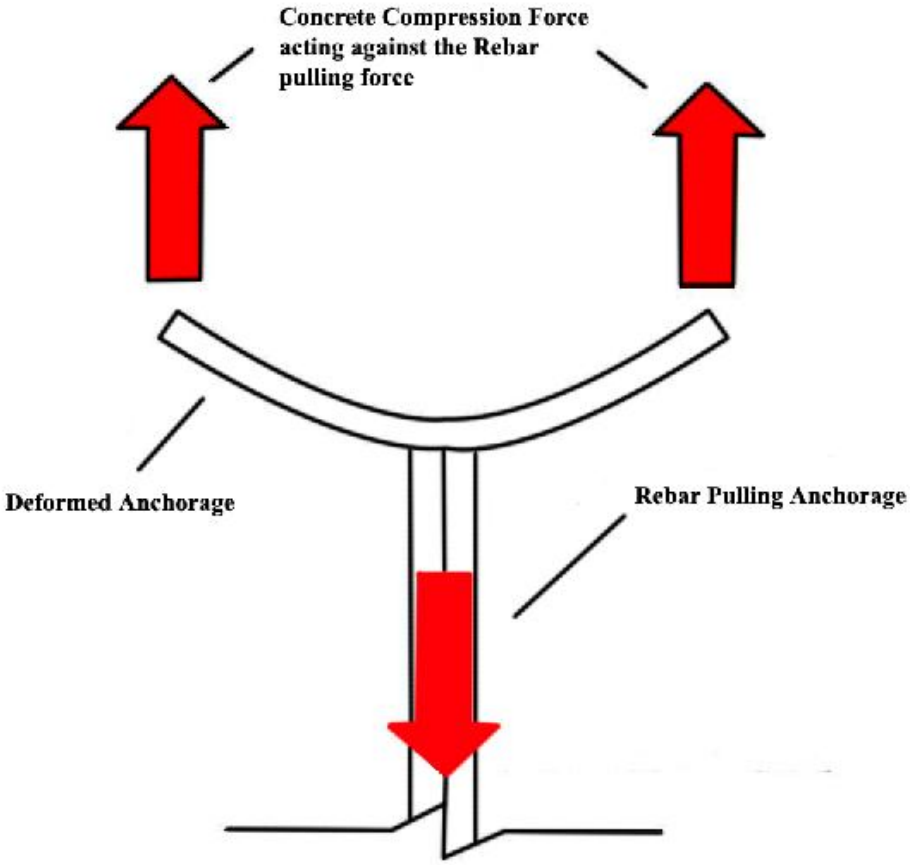

Figure 2-33: The failure mechanism of the beam

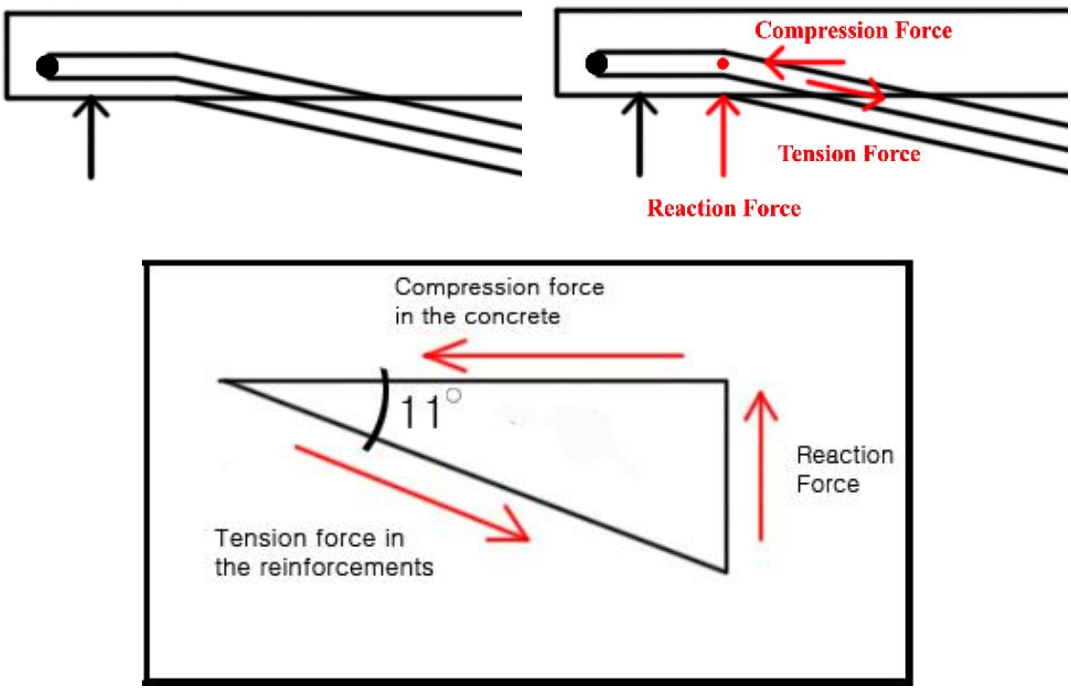

Figure 2-34: The strut-tie model of the failed section

It was proposed that the following modifications were made to eliminate the stress problems around the anchorage area;

a. Increase the number of anchorage points to disperse the compressive stress over larger area of concrete.

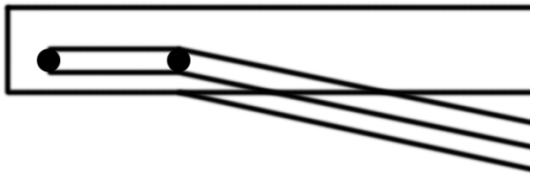

Figure 2-35: Showing the double anchorages

b. Increase the angle of reinforcement bar that goes into web. This will also reduce the total horizontal stress transferred to the concrete.

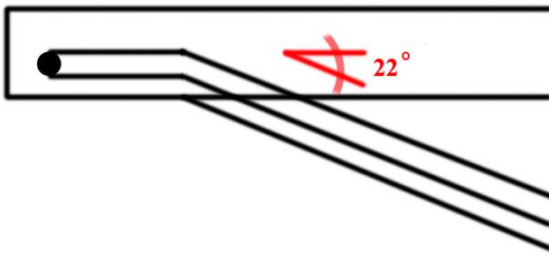

Figure 2-36: Showing the increased rebar angle

2.2.9 Work of Bailiss, the University of Bath: 'Fabric-Formed Concrete Beams Design and Analysis' (BAILISS, J.)

Bailiss' working under the supervision of Prof Ibell studied the structural behaviour of fabric formed beams, and also he carried out small scale tests to see the variation of geometry of fabric defined by the hydrostatic pressure the liquid concrete. In total four beams are built and tested. All beams are 2 metres long and with the design capacity of 15kN determined by the flexural criteria. Beam 1 is designed to follow the bending moment diagram of three point load condition. The beam failed by yielding of rebar at the location where strain gauge is attached. The steel is filed at the position to secure a flat surface for the strain gauge, and this caused reduction in cross-sectional area which results increase of stress.

Figure 2-37: Beam 1 on the test rig

Beam 2 is designed to follow a parabola. The beam fails by bending at the applied load of 9kN near the load jack.

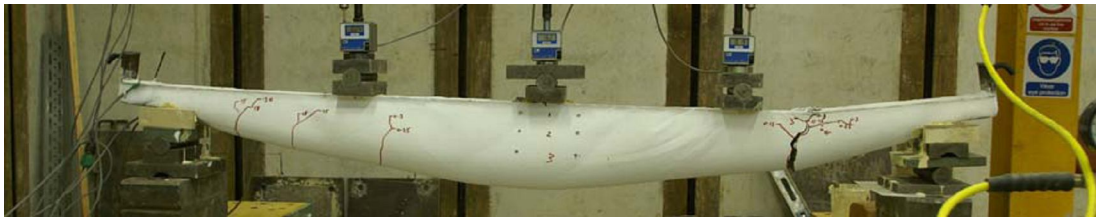

Figure 2-38: Beam 2 at failure

Beam 3, which is inspired by the beam designed by Professor Mark West, has wider top face near the mid-span. Hessian fabric is used for to allow the specific design modification. The beam failed at 13.5kN due to the shallow design depth of reinforcement near the supports.

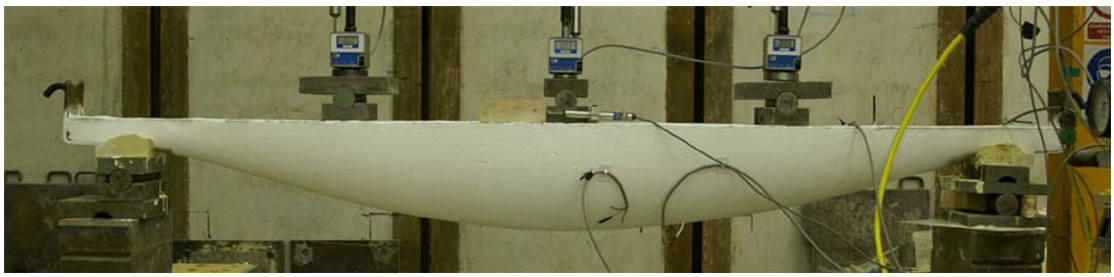

Figure 2-39: Beam 3 on the test rig

Beam 4 is designed to follow the asymmetric bending moment diagram for a concentrated loading condition. The beam failed at 12.9kN due to bending near the support on the side of the concentrated loads.

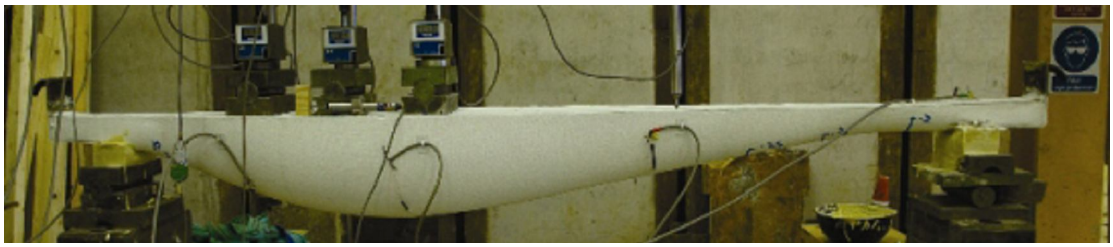

Figure 2-40: Beam 4 on the test rig

2.2.10 Work of Ibell, Darby, Denton: 'Fabric formwork for Innovative Concrete Structures' (IBELL, T., Darby, A., Denton, S., 2009)

The paper presents the structural behaviour of reinforced concrete beams developed to the optimized forms. The paper states that 55% of the relative materials were saved in the optimized beam (beam on the right in Figure 2-39) in comparison with a traditional rectangular form. Beam 2 in the figure is developed from Beam 1, and

further material saving is made by removing ineffective material below the neutral axis (around web area). The paper states that in Beam 2 40% of materials were saved over Beam 1.

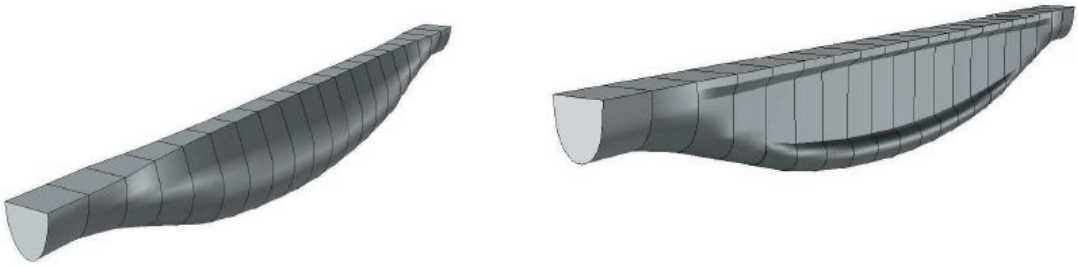

Figure 2-41: Optimized beams: Beam 1 (Left) and Beam 2 (Right) (image and description extracted from the reference)

The two metres long optimized beams were tested on simple supports under five point loading condition. During the experiments showed evenly distributed vertical cracks throughout the span of the beam indicating the efficient forms of the beams, at the ultimate loads both beams failed by shear.

Figure 2-42: Loading Sequence: Beam 1 (Left) and Beam 2 (Right)

2.2.11 International Society of Fabric Forming (ISOFF) (Research Papers in Fabric Forming, 2008)

The first international conference of Fabric Formwork for Architectural Structures was held in 2008 at the University of Manitoba in Canada. It was the first ever conference of the fabric forming industry and the speakers came from different parts of the world including the U.K., Canada, Holland, Japan, and the U.S.A. Among the speakers there were Remo Pedreschi, Alan Chandler, Mark West, Kenzo Unno, and

Richard Fearn, whose works are already discussed in this chapter. The other speakers include Sandy Lawton (founder of ArroDesign), who is an Architect/Builder and he presented the 'Tree House Project' for which the fabric formwork is used for the construction of the house in Vermont, U.S.A.; David South (U.S.A.) and Arno Pronk (Holland) presented the projects where concrete shell structures are built using inflatable fabric forms.

Just over 100 people were participated in the conference including researchers, engineers, architects, students, and construction companies. Also, the International Society of Fabric Forming (ISOFF) was formed at the conference, with the vision to provide the platform for the effective communication and knowledge sharing between the researchers and practitioners.

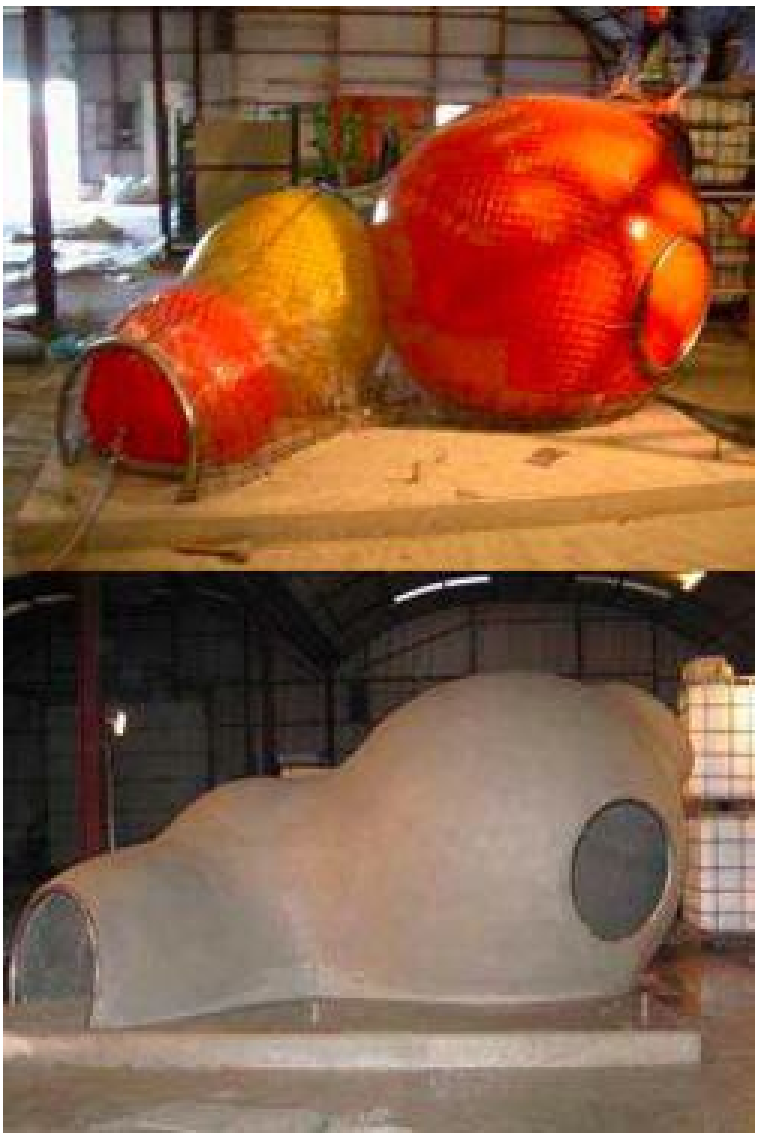

Figure 2-43: Thin shell concrete structure - Arno Pronk (Research Papers in Fabric Forming, 2008)

Figure 2-44: Concrete Tree House – Sandy Lawton (Research Papers in Fabric Forming, 2008)

2.3 Structural Behaviour of RC beam (Rectangular and T-Section)

There are comprehensive research reports on the structural behaviour of reinforced concrete beam and the structural behaviour of reinforced concrete beam in bending and the deflection can be relatively comfortably explained and predicted with the existing structural theory. However, in the matter of shear or more precisely diagonal tension stress in beam many researchers present different theories for the prediction of shear strength and the precise mechanisms of failure. The published literature is on shear is very extensive. An aspect of this work is the behaviour of the beams at the support and the followings are research works that discuss the shear (diagonal tension) failure mechanism of RC beam and suggest the relevant useful analytical methods. Again to note that only a very small selection of the work are presented which are particularly relevant to the form of beams explored in this thesis. Thus the following information discusses the shear behaviour of reinforced concrete beam, and they are selected for their possible application in developing the structural form of fabric formed beam.

2.3.1 Work of M. D. Kotsovos, J. Bobrowski, and Prof. J. Eibl: *'Behaviour of Reinforced Concrete T-beams in Shear'*

The paper states that aim of the research is to provide experimental evidence to the view that the shear resistance of RC beams is provided by region of the compressive force path rather that the region below the neutral axis. Regarding the concept of compressive force path it states that, 'shear' failure is associated with the presence of tensile stresses developing in the region of the path along which the compressive force is transmitted to the supports' (KOTSOVOS, M. D., 1983). Following this statement the paper describes four mains reasons for development of the tensile stresses. They are restated below with the relevant diagrams, which are extracted from the paper:

(a) *Changes in the path direction.* A tensile stress resultant (T in figure 2-41) develops for equilibrium purposes at locations where the path changes direction.

(b) *Varying intensity of the compressive stress field along the path.* The compressive stress will reach a critical level at the smallest cross-section of the path, where the stress intensity is the highest, before this level is reached in adjacent cross-sections. This level marks the start of an abrupt and large material dilation which induces tensile stresses **(**t_1 in Figure 2-41**)** in the surrounding concrete (KOTSOVOS, M. D., 1982).

(a) *Tip of inclined cracks.* It is well known from fracture mechanics that large tensile stresses **(**t_2 in Figure 2-41**)** develop perpendicular to the direction of the maximum principal compressive stress in the region of the crack tip (KOTSOVOS, M. D., 1979) ,(KOTSOVOS, M. D., and Newman, J. B., 1981).

(d) *Bond failure.* Bond failure at the level of the tension reinforcement between two consecutive flexural cracks changes the stress conditions in the compressive zone of the beam element between these cracks, as indicated in Figure 2-42. From the figure it can be seen that the loss of the bond force results in an extension of the right-hand side flexural crack sufficient to cause an increase Δz of the lever arm z, such that $C^* \Delta z = V^* a$. The extension of the flexural crack reduces the depth of the neutral axis is and thus increases locally the intensity of the compressive stress block. This change in the stress intensity should give rise to tensile stresses in the manner described in (b).

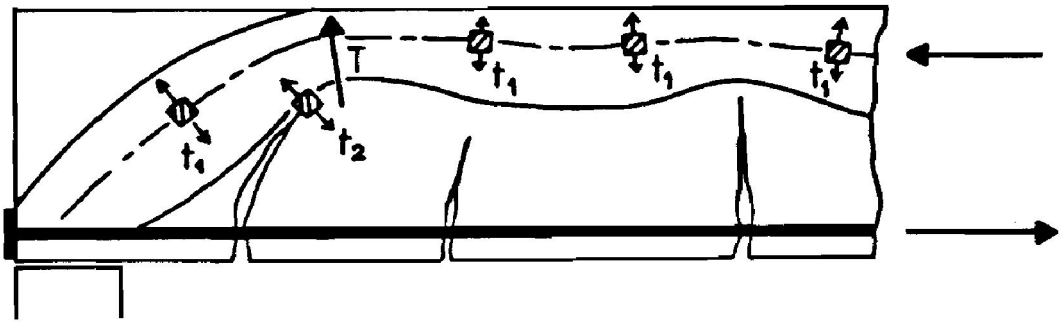

Figure 2-45: Path of compressive force indicating locations of tensile stresses

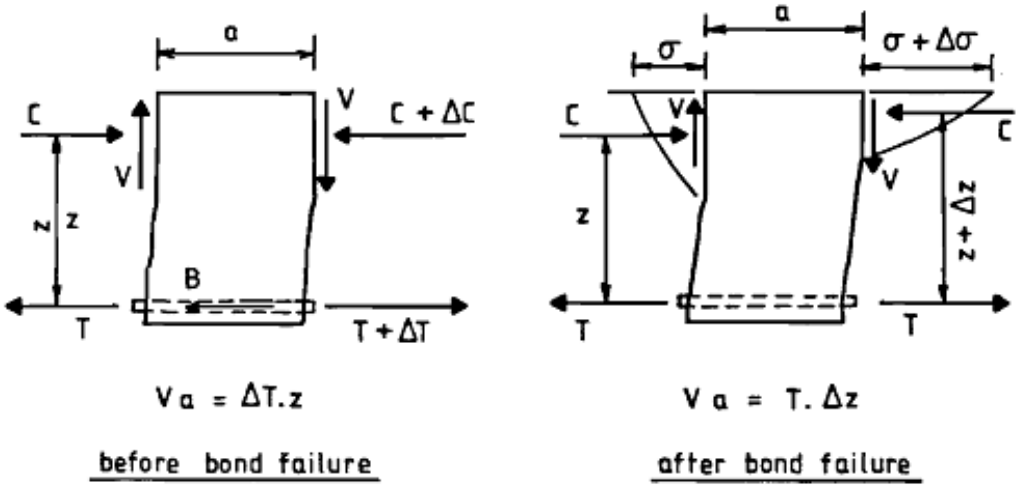

Figure 2-46: Effect of bond failure on stress conditions in compressive zone

There are three types of T-beams constructed for the paper and their specifications are illustrated below:

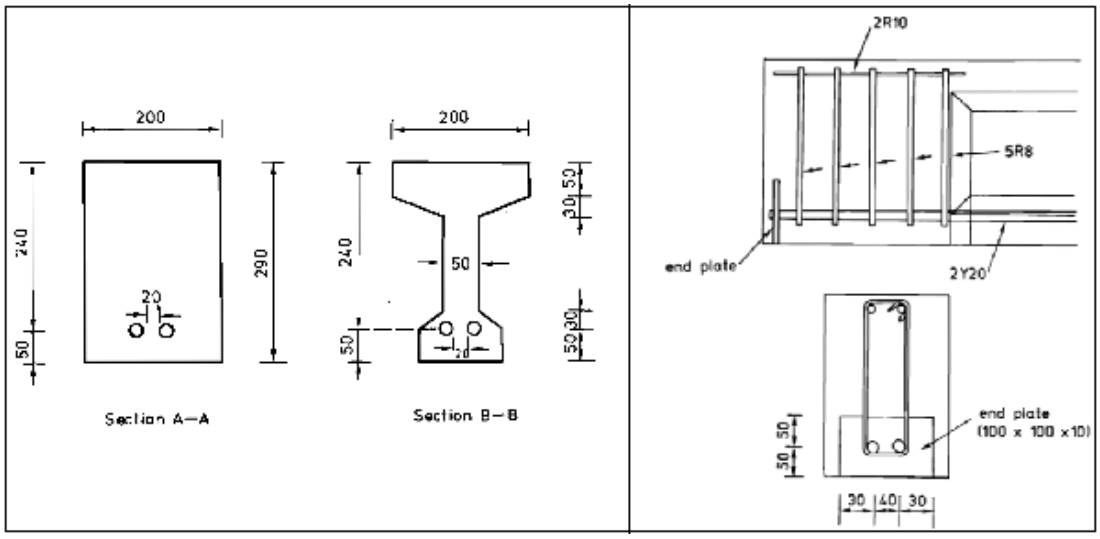

Figure 2-47: Cross-sectional characteristics of beams tested in the programme (left), Reinforcement details of beams tested in the programme (right)

The summarizes six conclusions that are drawn from the experiments of the above beam types, and they are restated below:

(l) A comparison of the behaviour of RC T-beams with that of beams with a rectangular cross-section has indicated that shear resistance is provided by the flange and ***not,*** as widely considered, the web.

(2) Inclined cracking is found to cause debonding of the tension reinforcement in the region between the inclined cracking and the support, and because of this the beam appears to behave as a *tied arch.*

(3) The above experimental evidence supports the concept that the shear capacity of reinforced concrete beam is associated with the region of the path along which the compressive force is transmitted to the supports rather than the region of the beam below the neutral axis.

(4) It is shown that the compressive zone is capable of sustaining very high stresses because of the triaxial stress conditions that exist there.

(5) It is found that, although Code predictions can underestimate shear capacity considerably, Code provisions may lead to unsafe solutions since shear failure frequently occurs in regions not classified as critical by the Code.

(6) Unlike Code provisions, an already published empirical formula, which is compatible with the concept described in item (3), appears to provide realistic predictions of both shear capacity and location of shear failure.

2.3.2 Work of J. Bobrowski, and B. K. Bardhan-Roy: 'A method of calculating the ultimate strength of reinforced and prestressed concrete beams in combined flexure and shear'

In this paper the authors present an equation which can be used to predict the failure load on a reinforced concrete beam. The equation is modified based on the Charles Whitney's (WHITNEY, Charles S., 1957) empirical formula (Equation 2-1) that defines the moment capacity of a beam in correlation with the shear strength of the beam:

$$M_l = 0.875 d l_s (50 * 0.3 M_u / d^2 * \sqrt{(C/l_s)}) \quad \text{.....Equation 2-1}$$

Where,

M_l = Moment capacity per inch width = M/width (lb in)

d = effective depth (in)

l_s = Shear Span (defined as ratio of bending moment to shear at a given section) (in)

M_u = Ultimate moment of resistance of a given section where shear influence is negligible (lb in)

C = Lever Arm (in)

The authors point out that the above Whitney's formula (Equation 2-1) is aimed for beams with rectangular sections, and it does not take account of the effect of steel stresses. Thus the authors modify the formula based on assumptions and rewrite it as below:

$$M = 0.875\, d l_s (50 b_1 + 0.3 M_u / d^2 * \sqrt{(C/l_s)}) * \sqrt[4]{(0.0108 f_y / \rho f'y)} \quad \text{.....Equation 2-2}$$

Where,

f_y = Standard ultimate strength of steel (224 000 lb/in^2)

f_y' = Actual ultimate strength of steel used (lb/in^2)

ρ = Area of tensile reinforcement (A_t)/ Area of concrete to effective depth (in^2)

The values calculated with this modified formula are compared with the test results of five different types of beams in the later section, and the both seem to be in close range. In the work of Kotsovos, Bobrowski, and Eibl this formula is also mentioned but in more familiar SI base units:

$$M_{cx} = 0.875 a_{vx} d\{0.342 b_1 + 0.3(M_{fx}/d^2) * \sqrt{(z/a_{vx})}\} * \sqrt[4]{(16.66/\rho_w f_y)} \quad \text{....Equation 2-3}$$

Where,

M_{cx} = the moment corresponding to 'shear' failure (Nmm)

M_{fx} = the flexural capacity (Nmm)

a_{vx} = the ratio M_{ax}/V_{ax} (mm)

M_{ax} = the applied moment (Nmm)

V_{ax} = the applied shear force (N)

z = lever arm (mm)

d = the effective depth (mm)

ρ_w = area of tension steel/web area of concrete to effective depth

f_y = the characteristic strength of the tension steel (N/mm2)

b_1 = the effective width (mm) given by the lesser of $b_o + 2b_s$, $b_o + 2d_s$, b_o, b_s, d_s, are shown below, which is extracted from the paper;

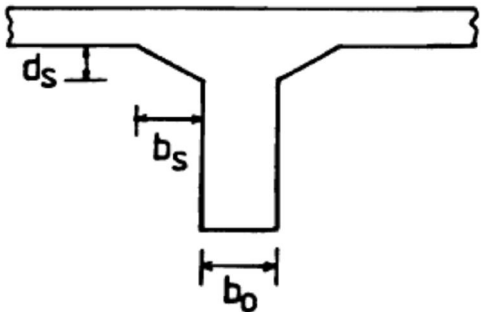

Figure 2-48: Definition of b_o, b_s, d_s

2.3.3 Possible failure modes of anchorage zone in pre-stressed concrete

In pre-stressed concrete the anchorages on both ends of steel reinforcement provide the resistance against the induced tension force inside the reinforcement; they hold the reinforcement so that it does not get pulled in by the incurred tension force. The resistance is provided by the bearing stress of concrete on where the anchorage is pressing. Therefore, if the concrete fails to provide the resistance against the anchorage as a result the reinforcement will become slack and the overall structural system is compromised. Thus in the design stage the capacity of concrete should be checked in consideration with possible failure modes.

In the thesis by Burdet (BURDET, O. L., 1990) the possible failure modes are described:

1. The first type of failure is related to the local compression failure of concrete either due to the concrete insufficient strength or due to the lack of confining reinforcement.

Figure 2-49: Photo included in Burdet's thesis showing the 'compression failure in the local zone with cone of concrete characteristic of the first mode of failure' (BURDET, O. L., 1990)

2. The second mode of failure is related to the transverse tensile stress formed perpendicular to the direction of steel tendon (reinforcement). The line of crack due

to the stress is thus in parallel to the steel tendon.

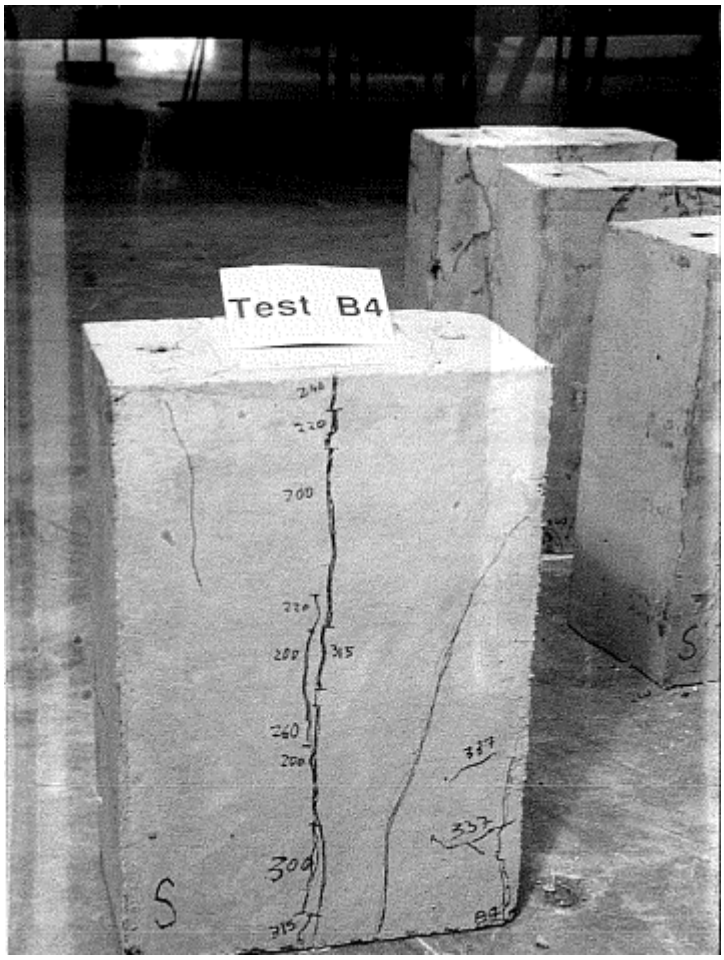

Figure 2-50: Photo included in Burdet's thesis showing the 'large cracks along the tendon path characteristic of the second mode of failure (tension failure)' (BURDET, O. L., 1990)

3. The third mode is due to compression failure of concrete (as described in Burdet's thesis), and it is different to the first mode. Third failure mode is due to the separation of concrete section confined by the anchorage and the unconfined concrete section which is outside the zone affected by the anchorage. It seems it is a type of spalling failure. The main difference with the first mode of failure is it occurs over larger distance from the anchorage, and the unconfined concrete zone is bulging out from the confined concrete.

Figure 2-51: Photo included in Burdet's thesis showing the 'compression failure at the interface between confined and unconfined concrete, characteristic of the third mode of failure' (BURDET, O. L., 1990)

Burdet states that regarding the first failure mode the local compressive strength of concrete could be increased by either providing confining reinforcement or surrounding concrete; both are to provide lateral confining stress to restrain the lateral volumetric expansion which will increase the compressive strength of the concrete. The second mode of failure would occur immediately after the sufficient tensile crack is formed without any transverse reinforcement, and in case the reinforcement is present the failure would occur after the reinforcement yields. The third mode of failure occurs mainly due to the interaction between the concrete section that is in great confinement due to the anchorage and the other concrete section that is outside the confinement of anchorage. Generally, the failure depends on the dimensions of the two concrete sections; when the dimension (or the thickness) of the concrete section that is outside the confinement of anchorage is smaller than the dimension of the concrete section that is under the anchorage confinement, the third mode of failure could occur.

The book by Gilbert and Nickleborough, 'Design of Pre-stressed Concrete' (GILBER, R. I., and Nickleborough, N. C., 2002) describes the stress condition of the pre-stressed concrete with useful diagrams and they are included below to aid the understanding of the above failure modes.

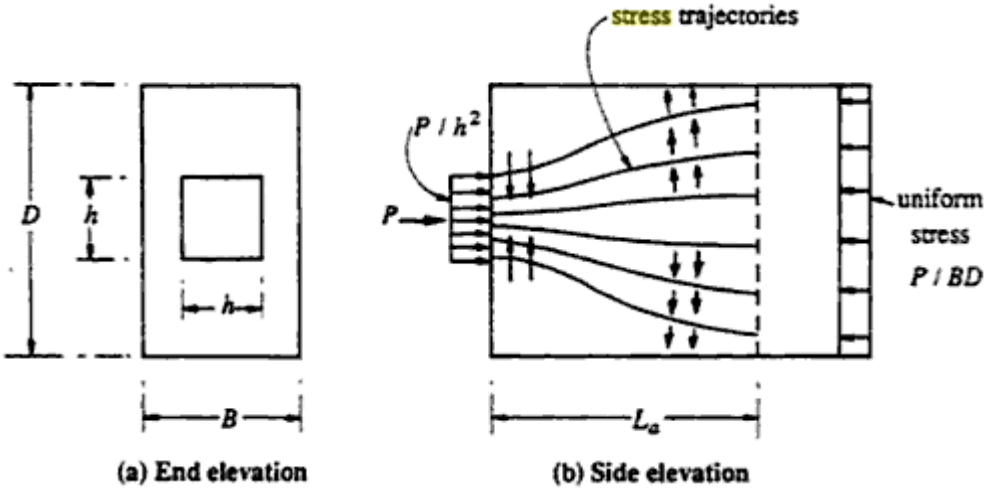

Figure 2-52: : Diagrammatic stress trajectories for a centrally placed anchorage (GILBER, R. I., and Nickleborough, N. C., 2002)

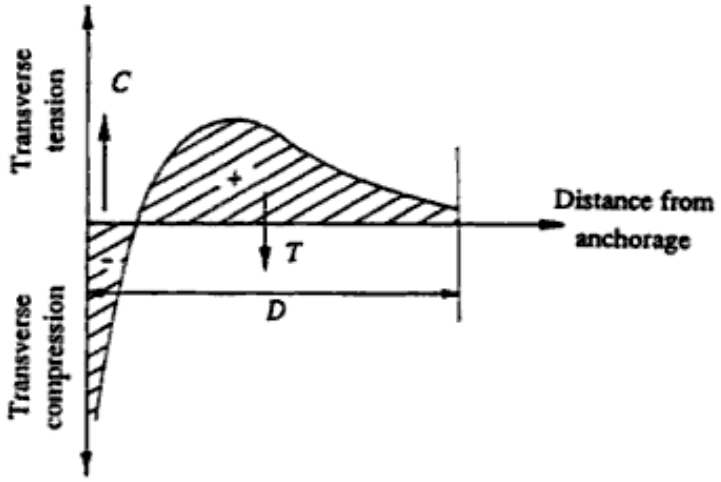

Figure 2-53: Distribution of transverse stress behind single central anchorage (GILBER, R. I., and Nickleborough, N. C., 2002)

Figure 2-48 (b) Side elevation describes that immediately behind the anchorage there exits compression stress and as the distance moves away from the point the stress turns into tension stress. Figure 2-49 describes the variation of stress intensity with the distance from anchorage. There is greatest compression strength immediately behind the anchorage and without sufficient compressive strength of concrete the first mode of failure can occur. In the zone where the tension stress exists the second mode of failure can take place. And depends on the value of D and h the third mode of failure can occur.

2.4 Summary and Conclusion

Over the past 50 years the possible use of fabric in concrete construction has been explored by people from various professional fields, and the above reviews show good examples of the material's adaptations in numerous commercial and non-commercial projects. However it is evident that the use of fabric formwork is still very limited, and there have only been very few research studies on fabric formed beams; there is an issue about finding the efficient geometry which adapts the complex stress conditions (combination of bending, shear, support force, and interaction between concrete and steel) in a beam.

People's interests in fabric formwork have grown rapidly in recent years and a number of institutional research works have begun and some promising works have been published. In 2008, the first international fabric formed concrete conference was held in Manitoba University in Canada, and people from various places over the world came to take part in the event. In the three day long conference, the leaders in the field presented their works including university based research projects to commercial projects. There also have been workshop opportunities for the visitors to learn and experience the actual construction process of fabric formed concrete.

As the recognition of fabric formwork is starting to grow, the industry's demand for more advanced yet practical applications of the technology would also increase. Thus now is for the construction professions to develop more scientific and engineering based research projects, which study the following aspects of fabric formed concrete.

- Economics
- Flexible forms
- Ease of construction
- Durability and Surface Quality
- Sustainability

The flexibility of fabric allows more complex concrete forms to be cast, and in case of load bearing structures the behaviour of the forms must be studied and understood to the sufficient level before they can be used on site. This would involve properly arranged structural experiments in a controlled environment followed by series of careful analysis using both the traditional and state of the art analytical methods. It is also important to provide simple and clear design methods at the end of the research which would encourage more practitioners to design and construct the fabric formed

structure by their own.

The studies on form-efficient beams to date have been limited in extent but do indicate the potential benefits of the technology. The works show that the developed forms have become more economical and sustainable through the construction of fabric formwork instead of timber or steel formwork. The work (Lee and Dowdall) also address technical issues occurring in the process of constructing the formwork including the tensioning of fabric and defining more precise geometry using timber forms and braces.

There is the need for further study into the development of the structural form and structural behaviour of beams made using fabric formwork. Particular aspects include:

- More practical and efficient construction solutions which can be easily taught and adapted by the practitioners. This will be one of the key aspects to promote the use of fabric formwork in the future generation.
- Determine the most efficient form of fabric beams by studying their structural behaviour experimentally.
- The practical design methods should be established which can be easily understood and adapted by the practitioners.
- Analyse the sustainability of the technology. This would also provide the future directions of research.

Based on the above points the aims of the thesis are:

- Research and develop the most efficient form of reinforced concrete beam using fabric formwork. It involves understanding the structural behaviour of the forms experimentally and theoretically, with the additional use of high end finite element analysis tools.
- Develop more practical and efficient construction methods of fabric formwork, in consideration of material consumption, labour, and time.
- Overall more sustainable construction of reinforced concrete beam by reducing the amount of the total embodied energy.

Chapter 3: Scope of the Present Investigation

A total of eleven variations of beams were designed and tested for the thesis. The development of geometry of the beams has been by progressive testing, evaluation, and modifications to optimize the form and improve structural performance. Through the development of the form, the following aspects have been developed. It must be noted that each is varied one at a time to assess the change in the result is caused by the specific modification.

1. Number of Anchorages
2. Geometry of the web as it meets the flange
3. Flange Thickness where the maximum shear occurs
4. The Horizontal Interface between the flange and the web
5. Percentage of Steel Reinforcement

Each modification was made following an evaluation of the preceding experiment. Thus there was progressive modification of the form and detail of the beam to improve performance. This thesis also considers the development of formwork in detail (Chapter 7). The design of fabric formwork was also modified as the design of the beam developed. Any high efficient formwork would use the least material and it must require the least effort to assemble and disassemble for the fast and efficient construction. Thus constant attempts were made to reduce the amount of materials involved in the formwork. Also the formwork divided into more components of smaller sizes. The reason behind this was that as the components become smaller there were less chance of them being damaged during the assembly and dismantling process, and also the shape of the smaller components become more 'neutral' which make them more possible to be components for different types of construction. For the current research three different types of formwork have been constructed and with each successive development less timber materials were used.

In the structural analysis of the beams (Chapter 8), a number of structural theories are adopted. The analysis has been categorized largely into three fields:

1. Ultimate Moment
2. Ultimate Shear
3. Deflection at the Service Load

For the bending analysis the most widely accepted reinforced concrete theories are

used, and the results are coherent.

The shear capacity of beam was checked against 1) the British Standard Code of Practice BS8110 criterion and 2) the equation stated in the work by Kotsovos and Pavlovic (KOTSOVOS, M. D. and Pavlovic, M. N., 1999).

The central deflections are calculated using the 'Moment-Curvature' method based on the theoretically calculated neutral axis, and the theoretical values are then compared with the experimental results.

The above methods are then reviewed for their possible applications in designing fabric formed concrete beam.

In addition to the above theoretical analysis finite element (FE) analysis is used where a more detailed analysis of the stresses is needed (Chapter 10). For example the FE analysis is used to look into the stress distribution inside the concrete around the anchorage zone. In total nine finite element models have been analysed and the output data are compared with the experimental results as well as the theoretical results. They include the tensile stress in the reinforcement, compression stress/strain in the concrete, deformation of anchorage, and the central deflections of the beams. The models take the nonlinear behaviour of the materials into account through the manually defined stress-strain curve of the materials.

In order to see the overall sustainability of the fabric formed concrete beam, the embodied energy is calculated based on the Inventory of Carbon and Energy (ICE) (HAMMOND, G., and Jones, C.), (Chapter 11). The calculation is carried out independently for the beam and for the formwork. Thus the beam's embodied energy could be compared with a reinforced concrete T- beam in accordance with the BS 8110. This comparison gives guidance to the structural efficiency of the fabric formed beam. For the overall sustainability, the embodied energy value of the formwork is added to that of the beam and compared.

Chapter 4: Material Property

4.1 Introduction

This chapter includes the information on the material properties of concrete and steel used for this research. The properties of steel are obtained using the Instron Universal testing machine; which is a loading machine that is generally used to test the elastic behavior and the yield of steel and it produces a stress-strain table at the end of each test. For concrete a mix design is carried out to determine that appropriate proportions of the constituents. The same mix was used throughout the programme for consistency. However, even if all the beams are cast with the same given mix ratio the concrete strength would still vary based on a number of factors including the temperature and moisture condition of the laboratory, initial water content of the aggregates. Therefore in each beam construction concrete cubes are made in accordance with the British Standard method (THE BRITISH STANDARD BS 1881: Testing Concrete), and the cubes are tested at the close to the time of the testing of the beam. Cylinders are also made concurrently with the concrete cubes and used to determine the elastic modulus of the concrete.

4.2 Concrete Mix Design

As stated in the above paragraph, the purpose of concrete mix design is to ensure the consistency of the concrete material property for all the beams; thus the same concrete mix ratio will be used for the all beams. Using the same mix of the concrete for all beams would reduce any discrepancies in test results which may rise from using different mix of concrete between the beams.

The constituents of concrete are kept as simple and straightforward in-keeping the general desire to adopt a relatively low technology approach as possible, no additives in the mix which would either enhance the properties of concrete, or speed up the curing process.

4.2.1 Concrete Constituents

Cement: Ordinary Portland cement

Coarse Aggregate: 10mm Round Aggregates

Fine Aggregate: Sharp Sand

Water: Tap Water

4.2.2 Equipment

The following equipment was used in the mix design process:

- 9 steel cylinder moulds
- Lubrication
- Tamper
- Scale (Aggregate Grading, Measuring aggregate and cement per the boxes)
- Slump test equipment

4.2.3 Aggregate Preparation

The aggregates were air-dried in the laboratory for 2 days to remove any excess water on the surface of the aggregates. The purpose behind this was to prepare the aggregates to the Saturated Surface Dry (SSD) condition. In this condition the aggregate will not absorb water, thus the free water content of the mix could be accurately determined.

4.2.4 Mix Design

The mix design is carried out with the reference to "Design of Normal Concrete Mixes", published in 1975 by the UK Department of Environment (DOE), also known as the Building Research Establishment (BRE) and the Transport and Road Research Laboratory (TEYCHENNE, D. C., Franklin, R. E., and Erntory, H. C., 1975).

Mix Design Calculation

- Characteristic cube strength of 35 N/mm^2 at 28 days.
  Proportion defective 5%.
  Standard deviation = 8 N/mm^2 (figure 3 of Building Research Establishment, BRE)
  Margin = 1.64 * 8 = 13.12N/ mm^2
  Target Mean Strength at 28 days = 35 + 13.12 = 48.12 N/ mm^2
- For W/C = 0.5 approximate compressive strength at 28 days = 42 (Table 2 of BRE). From figure 4 of BRE, W/C = 0.46 is obtained for 48.12N/ mm^2
- Slump height (mm) = 25 ~ 100mm; this initial value is taken from the book, *Concrete Technology* by Neville, p85, (NEVILLE, A. M., Brooks, J. J., 1987) regarding the beam constructions as 'Normal reinforced concrete manually compacted'. Thus, for mix design, 30~60mm is the target.

- From Table 2.7 – 3, p57 of Kong and Evans (also table 3 of the BRE document), for 10mm of Max. size aggregate and Uncrushed of Type of aggregate, the approximate free water content = 205 kg/m^3

  (Note: the water to be added to the mix is equal to the free water less the moisture content of the aggregates.)

  Thus, cement content = 205/0.46 = 455.65 kg/m^3; this value is checked with the minimum cement content, 400 kg/m^3 given from Table 2.5-7, p39 of Kong and Evans.

- Aggregate content is then calculated using the below equation,

  Total aggregate content = D – C – W

  Where D = the wet density of concrete (kg/m^3)

  C = the cement content (kg/m^3)

  W = the free-water content (kg/m^3)

  (Note: The following calculation is based on the assumption that the aggregates surface condition is saturated surface dry, SSD condition)

  Assumed relative density of uncrushed aggregate (SSD) = 2.6

  From figure 5 on page 14 of BRE, with the free-water content of 205kg/m^3, the wet density of concrete mix = 2340 kg/m^3

  Thus, the total aggregate content = 2340 – 205 – 455.65 = 1643.35 kg/m^3

  To determine the % of fine aggregate the grading is required.

  Grading of aggregate; Percentage passing 0.600mm sieve = 38.03% (=270g/710g)

  Proportion of fine aggregate (figure 6 of BRE) = 48%

  Thus, the fine aggregate content = 0.48 * 1643.35 = 788.81 kg/m^3

  And the coarse aggregate content = 1643.35 – 788.81 = 854.54 kg/m^3

  This gives,

  Coarse aggregate content = 854.54 kg/m^3

  Fine aggregate content = 788.81 kg/m^3

  Water content = 205 kg/m^3

  Cement content = 455.65 kg/m^3

  Cement: Sand: Shingles = 1: 1.73: 1.87 = 2: 3.46: 3.74 with w/c = 0.46

A trial mix was prepared based on the above ratio;

- Total mix of volume 0.05m^3 is prepared.
- Coarse : Fine : Cement : Water = 42.72kg : 39.44kg : 22.78kg : 10.25kg

- Extra 2.5 litre of water is added because the mix was too thick to work with when only the designated amount of water was added. The amount of water seems to be either absorbed by the aggregate or used to wet the surface of the mixer.
- Slump height was measured and it was 77mm.

There was a consideration that the mix should have high workability in order to place the concrete around reinforcement, since the placing area is very narrow and the highly tensioned fabric is making is more difficult to place the concrete.

According to the publication, "*Concrete Constituents and Mix Proportions*" by Cement and Concrete Association (SHACKLOCK, B. W., 1974), a mix with high workability should have a slump height in the range of 25~100mm. Thus the workability of the mix seems satisfactory.

The following table (Table 4.1) shows the compressive strength test result of the trial mix. The 28 days strength was lower than the anticipated characteristic strength of 35N/mm^2, and the main cause of thus is 2.5 litres of additional water added during the mixing process.

Curing Duration	Average Equivalent Cube Strength (MPa)
7 Days	25.18
14 Days	27.22
28 Days	28.95

Table 4.1: Compressive Test result of the trial mix

Thus for the actual concrete mix of the beams, in order to achieve the characteristic strength (though there is not a specific rule to meet the characteristic strength), it is decided not to add the extra water than as it was initially suggested by the calculation. Instead, the aggregates will not be air-dried before the mixing and the will be used straight from the pack. The aggregates in the pack already include little bit of moist and thus it will increase the workability of the mix without adding the extra water.

4.3 Concrete Compressive Strength Tests

Concrete cubes were made concurrently with the beams. The concrete batch from which the cubes are made is the same as the batch used for the flange of the beam. Thus the compressive strength of the beam (which is of the flange) is directly

reflected by the cube strengths. The actual in-situ concrete strength of the web of the beam is expected to be greater than the strength measured by the cubes as it is cast against the fabric, which will allow the excess water to escape from the mix, and lowers the water/cement ratio of the concrete.

The cubes were made in accordance with the British Standard BS1881 – 108 in 100mm by 100mm steel mould. The cast cubes are taken out of the mould after 1 or 2 days, and tested for the strength on the day of beam test. An Avery machine is used for the cube testing (Figure 4-2).

Figure 4-1: Concrete cubes in steel moulds

Figure 4-2: Cube testing using Avery machine

4.3.1 Summary of Cube Strengths for the Beams

For each of the beams a minimum six concrete samples were tested; the samples are made from the same batch for the flange of the beam. The water-cement ratios given in the table below are the actual amount of water added during the mixing process. In most cases less amount of water is added than initially suggested by the

calculation. The reason behind this is because the aggregates already have some water with them which is not included in the initial calculation. Thus the amount of water added was reduced based on the workability of the mix. The table below (Table 4-2) shows the concrete compressive strengths of the beams.

Beam Reference	The Average Cube Strength (N/mm^2)	W/C Ratio	Curing Days
11DA-WS10mm without Mesh	43.40	0.61	28+
11DA10mm with Mesh	39.60	0.50	28+
22SA10mm – 1	38.63	0.58	28+
22SADF 10mm – 2	25.23	0.45	14
22SADF 10mm	27.45	0.40	13
22SADF 12mm	26.78	0.42	14
11DADF 10mm	32.70	0.31	28+
22SADF 3No. 10mm	32.70	0.31	28+
11DADF 12mm	28.94	0.31	28+
22SADF 3No. 12mm	28.94	0.31	28+
11DADFWW 12mm	39.70	0.34	28+
22SADFWW 3No. 12mm	41.30	0.33	28+

Table 4-2: Summary Table of Cube Compression Tests

Concrete compression capacity of the beam would be slightly different to the cube strength. The actual compression strength could be assumed between 67% ~ 80% of the measured cube strength (KONG, F. K. and Evans, R. H., 2001). This is due to the lateral restraint caused by frictional resistance incurred between the top and bottom plates and the concrete surfaces. Thus it is accepted to apply 0.8 to the measured value to get more realistic value. However, the local compression capacity of concrete inside a beam may be higher than the test value, because the compression capacity of the concrete cube is measured from uni-axial stress but the actual concrete in a beam is in tri-axial stress condition. These differences in the stress condition results some discrepancies in the compression strength value.

4.4 Elastic Modulus of Concrete

The Young's Modulus was measured from the tests on the cylinder samples cast from the representative mix. In total twelve concrete cylinders of 100mm diameter aged minimum of 28 days from casting date were tested. It must be noted here that the elastic modulus of concrete varies with age and water/cement ratio of the concrete (J. M. Illston, 2004). The general relationships are, that the modulus increases with the age and decreases with the water content. Thus the modulus values of the above cylinders cannot be considered as the same for the beams tested in this research, because the beams' ages are all different and the water content also varies beam to beam based on the permeability of the fabric.

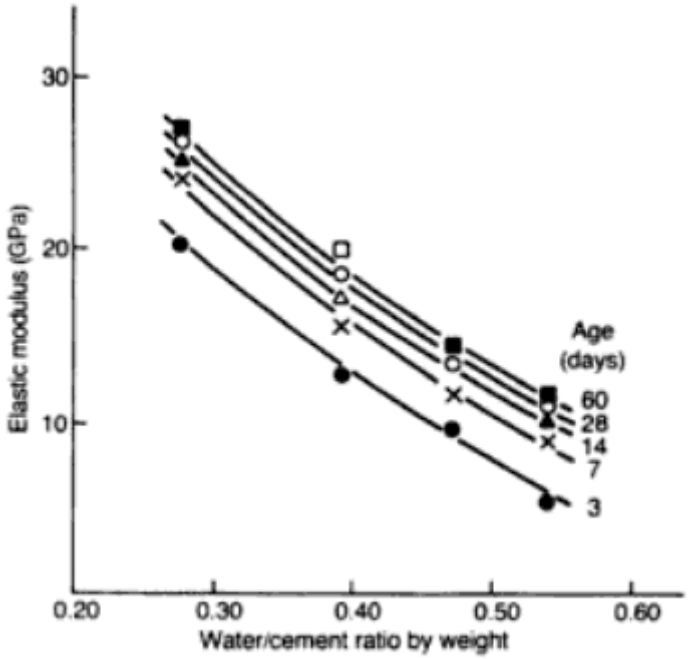

Figure 4-3: Effect of water/cement ratio and age on the elastic modulus of hardened cement paste (Hirsch, 1962) (HIRSCH, T. J., 1962); figure and description extracted from the reference (ILLSTON, J. M. and Domone, P. L. J. (edited by), 2001)

The applied stress is converted from the applied load by dividing by the cross sectional area, and the compression strain of the cylinders is calculated from the measured displacements at the certain load intervals divided by the height of the sample. The displacement is measured using a dial gauge. Initially a Demec gauge was going to be used for measuring displacement but for safety reasons a dial gauge attached to the cylinder using a steel ring was used. Electrical strain gauges were also considered however the concrete surface is not ideal for effective attachement. Later the stress-strain graphs are plotted and the elastic modulus, E_c of concrete is obtained from these graphs.

After each test the rings of gauge are deformed and damaged. They are reshaped

after each test for the next cylinder.

4.4.1 Summary of Test Results

- Water-cement ratio of both batches based on the water added: 0.31.
  *Please note that the actual water-cement ratio in the mix is higher, because the aggregates come wet in the package.
- Curing ages of both batches: The samples have been cured almost 40 days.

Sample	Batch 1: kN/mm2	Batch 2: kN/mm2
1	8.59	11.05
2	25.44	12.74
3	18.95	14.96
4	19.61	11.54
5	17.35	12.89
6	15.79	12.88
Average	**17.62**	**12.68**

Table 4-3: Summary Table of Young's Modulus of the Concrete Sample Mixes

For the stress-strain graphs of the each group please refer to the Figure 4-4 and 4-5. The modulus values of the first batch vary significantly from 8.59kN/mm^2 to 25.44kN/mm^2, and in average it is about 17.62kN/mm^2. Though the two extreme values (8.59kN/mm^2 to 25.44kN/mm^2) are neglected in the calculation, the average value still comes to 17.93kN/mm^2. The values from the second batch are more uniform and the average value comes to 12.68kN/mm2. Thus overall average value is 15.15kN/mm^2. These values are quite low considering that the typical value for concrete is 24kN/mm^2.

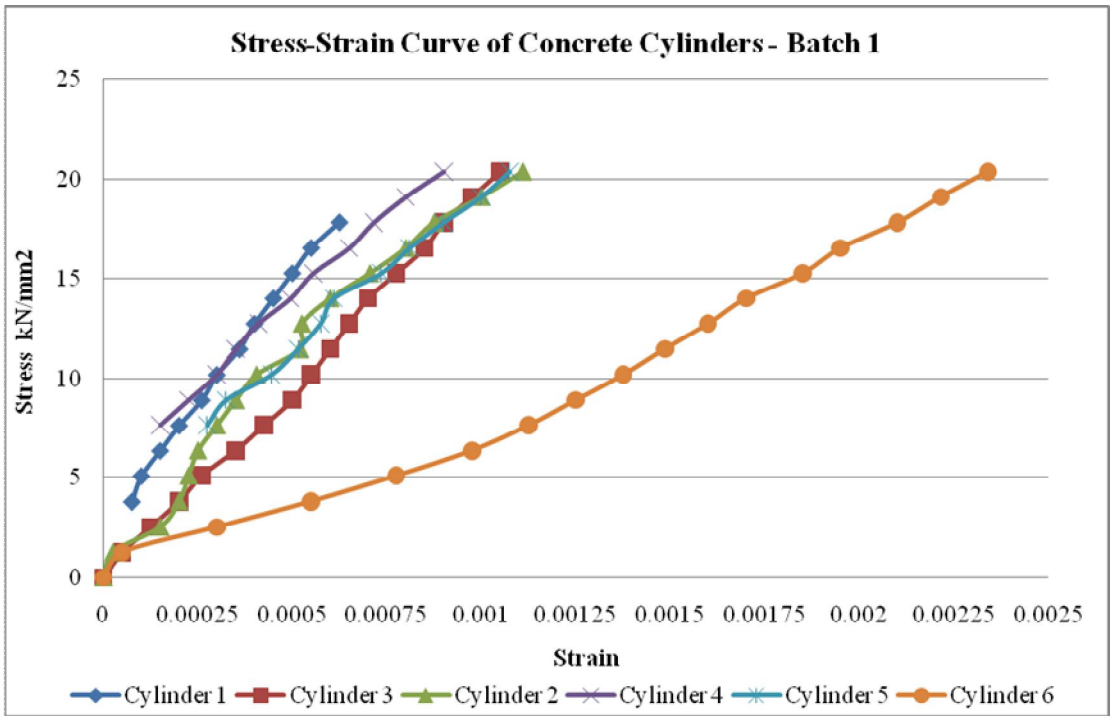

Figure 4-4: Cylinder samples test results: Batch 1

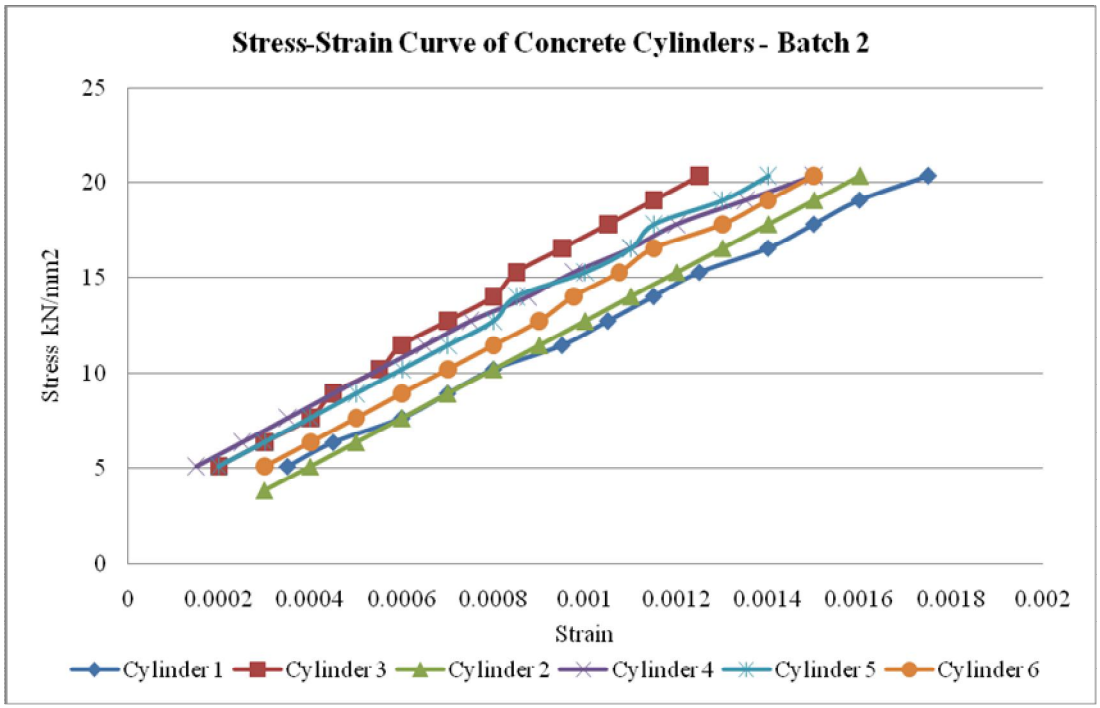

Figure 4-5: Cylinder samples test results: Batch 2

However the values show some consistency between the cylinders and thus the overall average value seems valid and can be used for analytical purposes, and in some cases it still gives room for estimation as long as it is in the range of 8.59kN/mm^2 to 25.44kN/mm^2. Another thing to note about the values is that there is some discrepancy between the average modulus value of the first batch and the

second batch. The main reason behind these differences between the batches seems to be caused by the change in water content in the mixes. During the mixing of concrete it is clearly noticed that the amount of water added to the mix has to be varied due to the already existing water in the coarse aggregate. The water content is adjusted visually, and in total much less amount of water has been added to the mix than initially calculated.

4.5 Properties of the Steel

200mm long samples of the steel reinforcement were tested (Figure 5-5). When the sample is in the grips of the Instron the actual length of the sample between the grips is 160mm. The strains were measured using electrical resistance strain gauges. The modulus of elasticity was calculated from the results.

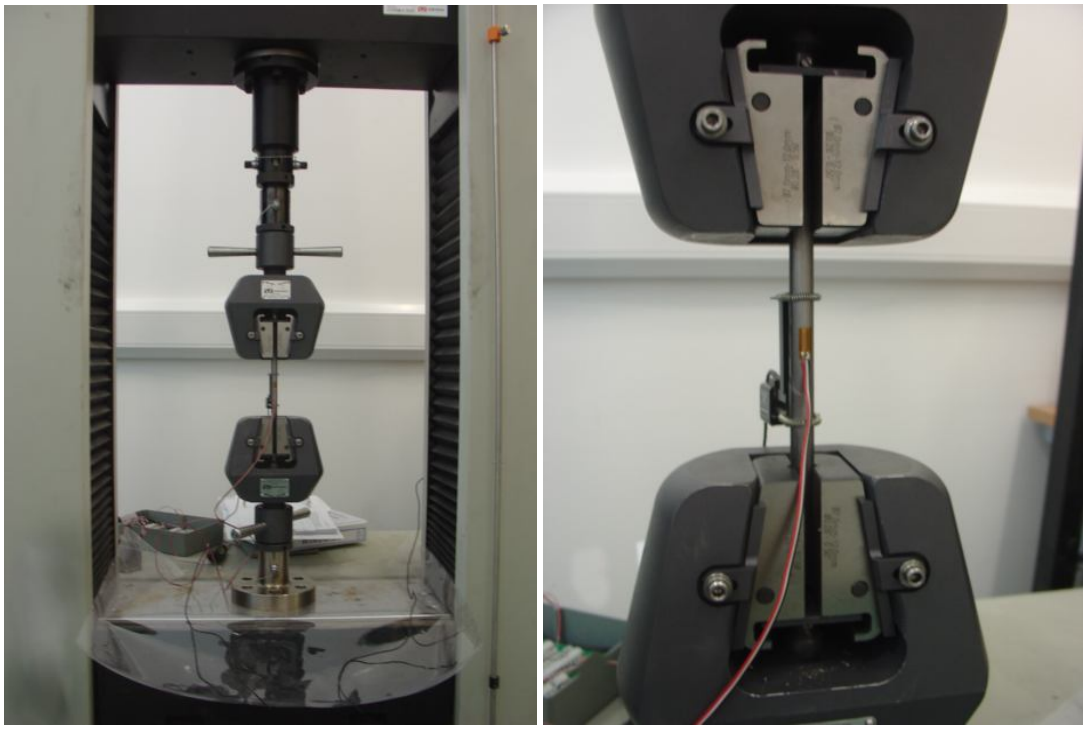

Figure 4-6: Steel sample on the Instron machine with electrical strain attached

4.5.1 Summary of Test Results

Please note that even though the samples are cut from the same steel bar with the length of approximately 3m long, the diameter of the bars vary with the locations and this makes the ultimate strength of the samples vary. Though the diameters are measured before the tests were carried out it is hard to predict exactly where of the sample would yield.

10 mm	Test 1	Test 2	Test 4	Test 5	Average
E kN/mm2	218.31	214.87	185.89	200.01	204.77
Yield Strength N/mm2	354.10	352.82	344.09	353.22	351.06
Yield Strain	0.00162	0.00164	0.00185	0.00177	0.00172
12 mm	Test 1	Test 2	Test 3	Test 5	Average
E kN/mm2	231.55	201.20	207.46	175.25	203.87
Yield Strength N/mm2	368.40	365.79	364.50	352.78	362.87
Yield Strain	0.00159	0.00182	0.00176	0.00201	0.00179

Table 4-4: Summary of Steel Tension Strengths

4.6 Technical Information of the Fabric (Don & Low Woven and Nonwoven polypropylene industrial textiles)

The fabric used for the research is type 50R manufactured by Don & Low Limited. 50R is a woven polypropylene geotextile fabric that is often used for highway construction for coastal protection as a reinforcement fabric. The following is the technical data provided by the company. This particular fabric is chosen due to its low cost and high tensile strength, and so the fabric will sustain the beam weight and also will not be damaged during the construction process. It is durable and thus it is ideal for repeatable use for fabric formwork construction.

It is worth noting that there is not a permeable woven fabric specially developed for the purpose of concrete beam construction. It is considered that a more specific fabric material could be developed and become more available for the better acceptance of fabric formwork in future applications.

For detailed technical specification of type 50R please refer to Table 4-5.

Technical Data	
Tensile Strength (EN 10319)	Warp 52kN/m Weft 52kN/m
Tensile Strength at 5% Extension (EN10319)	Warp 27kN/m Weft 40kN/m
Elongation at maximum load (EN 10319)	Warp 12% Weft 7%
CBR Puncture Resistance (EN ISO 12236)	6000N
Cone Drop Penetration (EN 918)	8mm
Pore Size 90% finer than (EN ISO 12956)	200 microns
Water Permeability (EN ISO 11058)	$14 * 10^{-3}$ m/sec
Mass per unit area	$240g/m^2$

Table 4-5: Technical Specification of Lotrak 50R

Chapter 5: Experiment Procedure and Instrumentation

5.1 Introduction

This chapter provides detailed information about the procedure programme and includes,

- The test rig set up; loading element, type of loading, support conditions, and the equipment used for taking measurements such as strains and displacements.
- Equipments for data acquisition: load cell for measuring applied load, dial gauges for displacement measurement and Demec gauge and electrical gauge for strain measurement. Also the information includes about the calibration method for the equipments used.
- The experimental procedure

5.2 Test rig

General Diagram of the Test Rig Arrangement

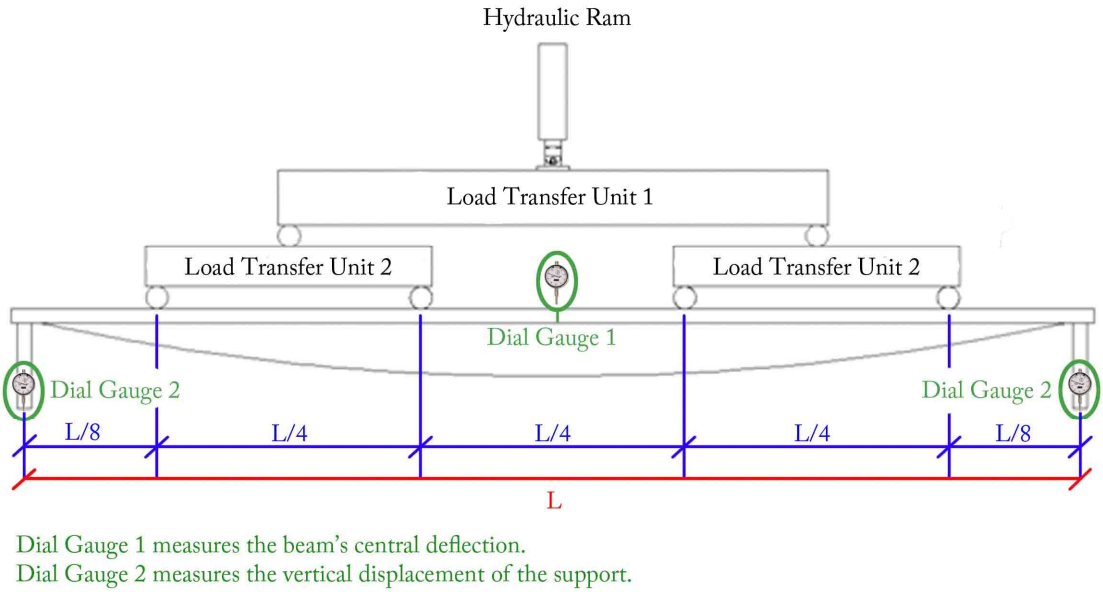

Figure 5-1: Showing the general arrangement of the test rig

The test rig is designed to apply four point loads on the test beam. The original design of the beam has a web curved in a parabolic shape to be adaptive of uniformly distributed loading. Thus the test was designed to test the efficiency of the parabolic shape in resisting the load. However, considering the practicality of the experimentation the application of the load was not ideal. Thus it was decided to arrange a number of point loads in symmetry over the span of the beam to give the

same bending moment profile as of the uniformly distributed load. Also there was an aspect of measuring the central deflection and compression strains from the top face of the beam. Thus there should be sufficient workable space between the point loads to take the measurements. Thus with the consideration of the total span is 3020mm, it was initially decided to have four points loads equally spaced at 604mm. Then another aspect was considered in regarding with the distance of the first point load from a support, the shear span, a_v. The purpose of the test is to examine the efficiency of the beam, which requires devising the experiment in anticipation of the possible shear failure of the beam. Reinforced concrete beam tends to fail by a brittle mode which is associated with the formation of inclined crack within the shear span when the value of a_v/d (shear span/effective depth ratio) is in range of 1 to 5. The effective depth at the position of the first point load was around 95mm and thus with the shear span value of 604mm the ratio becomes 6.37, which is higher than the upper range value, 5. Thus the position of the first point load was adjusted closer to the support and now the point loads were re-arranged to the positions as shown in the above diagram; the distance between the point loads are now L/8, L/4, L/4, L/4, L/8. L is the span of the beam and it is 3020mm. The following diagram compares the bending moment curves of four-point load and uniformly distributed load.

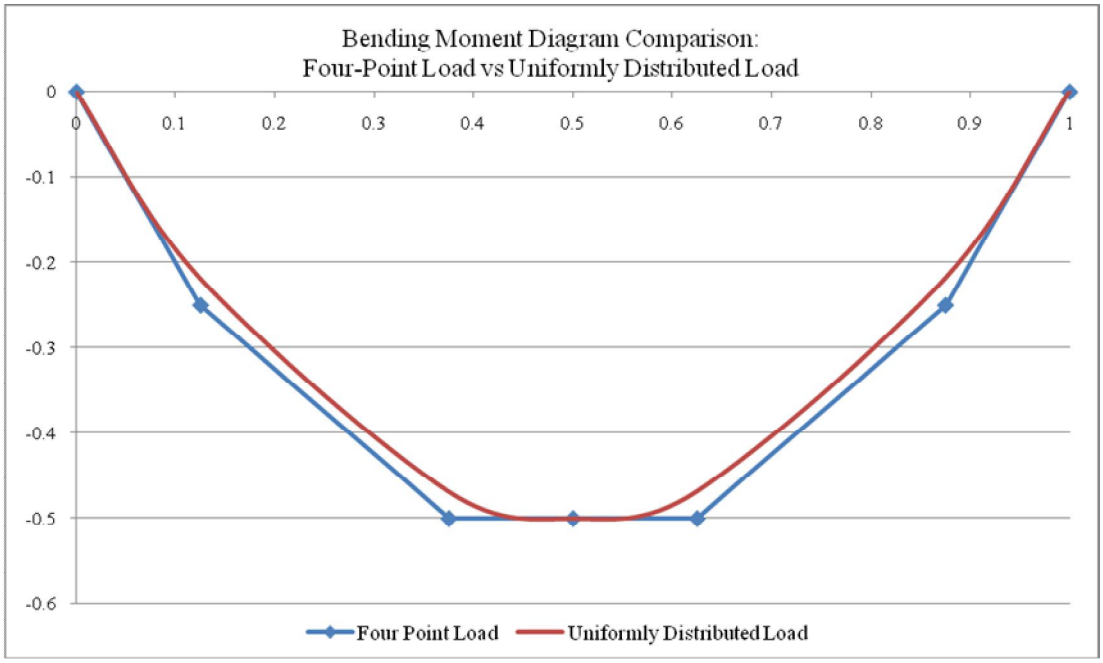

Figure 5-2: Diagram comparing the bending moment curve of four-point load and uniformly distributed load.

The shear span/effective depth criteria is generally for reinforced concrete beams

with uniform effective depth throughout the span, and it might not be fully applicable in case of the fabric formed beams with varying depth. However the above estimation to find the appropriate a_v value for the experiments was considered as the minimum preparation for future possible outcomes.

The load is applied by the hydraulic ram attached to a single hydraulic pump, and transferred onto the beam through spreader beams (Figure 5-2).

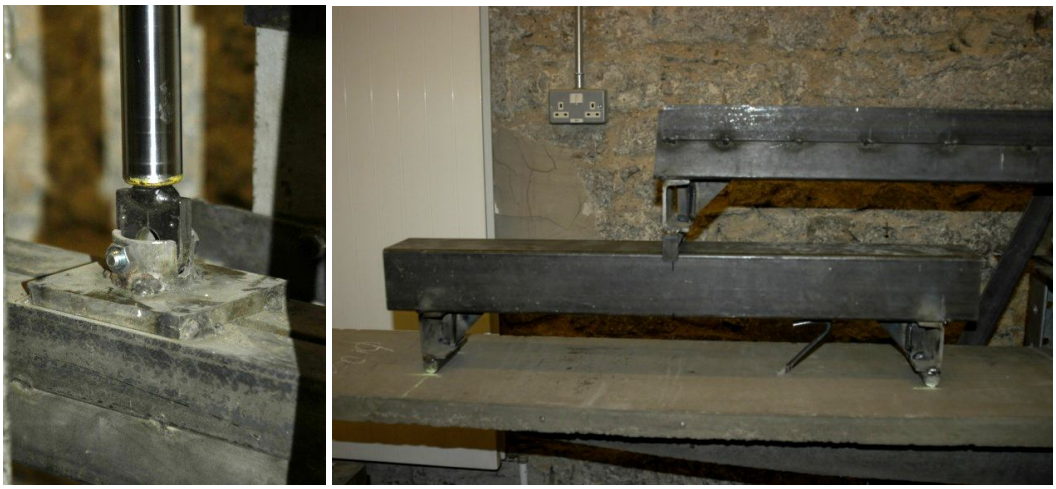

Figure 5-3: The bolt connection at the primary loading element (left),
and the secondary loading element in contact with the primary loading element (right)

At the bottom of the secondary loading element, additional steel bars are welded with the bracings to increase the accuracy of the point loads, and the same detail is applied to the connection between the beam and the simple supports.

Figure 5-4: The steel bar connection between the support and the beam to increase the accuracy of the support reaction

5.3 Instrumentation

5.3.1 Load Measurement

Load is applied to the beams using a hydraulic double acting hollow plunger cylinder (Enerpac) and a pump (Enerpac) (Figure 5-4). The load is measured using a compression load cell type CLP-NB (Tokyo Sokki Kenkyujo CO.) (Figure 5-5).

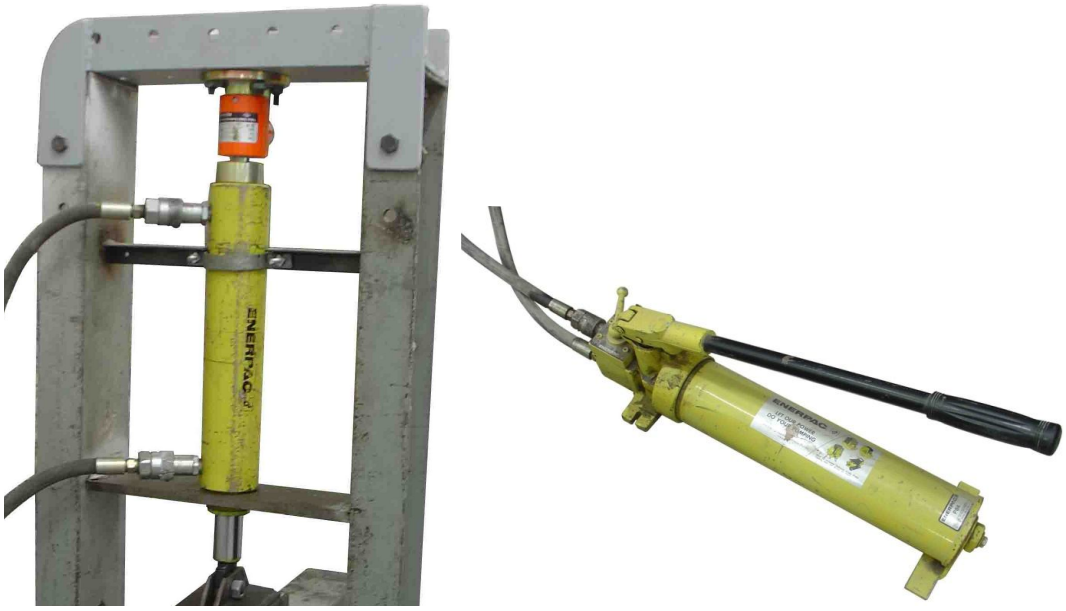

Figure 5-5: The central tower with the load cell at the top of the hydraulic ram

Figure 5-6: Load cell

5.3.2 Strain Measurement

Concrete strain is measured using the electrical Demec gauge (Mayes Group) (Figure 5-6), and steel strain is measured using electrical strain gauge CEA-06-240UZ-120 (Vishays) (Figure 5-7).

Figure 5-7: Demec Strain Gauge

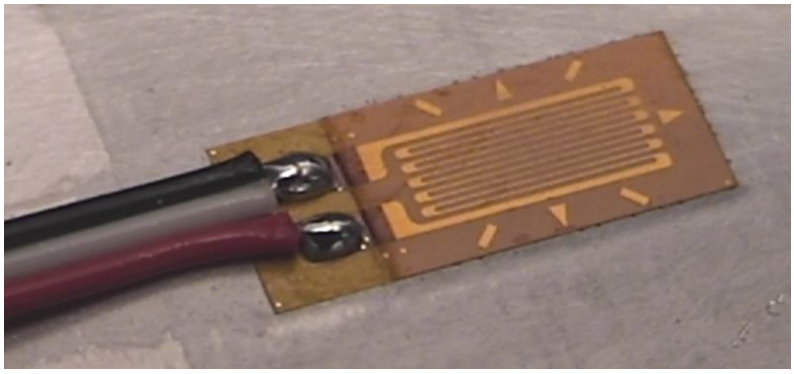

Figure 5-8: Electrical Strain Gauge

5.3.3 Electrical Strain Gauge Calibration

Electrical strain gauge measures deformation of reinforcement as a change in voltage to to a change in resistance in the circuit which is recorder by the data loggers. These are then converted to strains. However the interpreted strain readings must be verified before the gauge set can be put to use, just to make sure that the readings are coherent with the actual strain of the rebar. Therefore, Instron[2] (Figure 5-8) is used and steel samples are tested for the verification purpose. Stress-strain graphs are plotted based on the data provided by the data logger and Instron, and by overlapping the two graphs it would be able to see how accurately the gauge reads strain of rebar in tension. The verification process is as follows:

1. A sample of rebar (approximately 200mm long) is prepared.

2 Instron is a universal material testing machine capable of tension, compression, flexure, bend, peel, shear and friction testing.

2. An electrical strain gauge is carefully attached onto the sample following the application procedure provided by Vishay Measurements Group and the British Society for Strain Measurement (BSSM).
3. The sample with electrical strain gauge is then connected to the data logger.
4. An extensometer [3] is then attached onto the sample, and the attached extensometer is plugged into the Instron.
5. The rebar sample with the electrical strain gauge and the extensometer is then placed in the Instron.
6. Instron is also connected to the data logger to send the data of applied loads.
7. Load is applied to the sample.
8. Data logger records the strain readings from the electrical strain gauge, and the applied loads from the Instron. The Instron individually records the strain readings from the extensometer and the applied loads.
9. Stress-strain graphs are plotted from these two sets of data, and the two graphs are compared.
10. 1~9 is repeated with other samples to see consistency in the results.

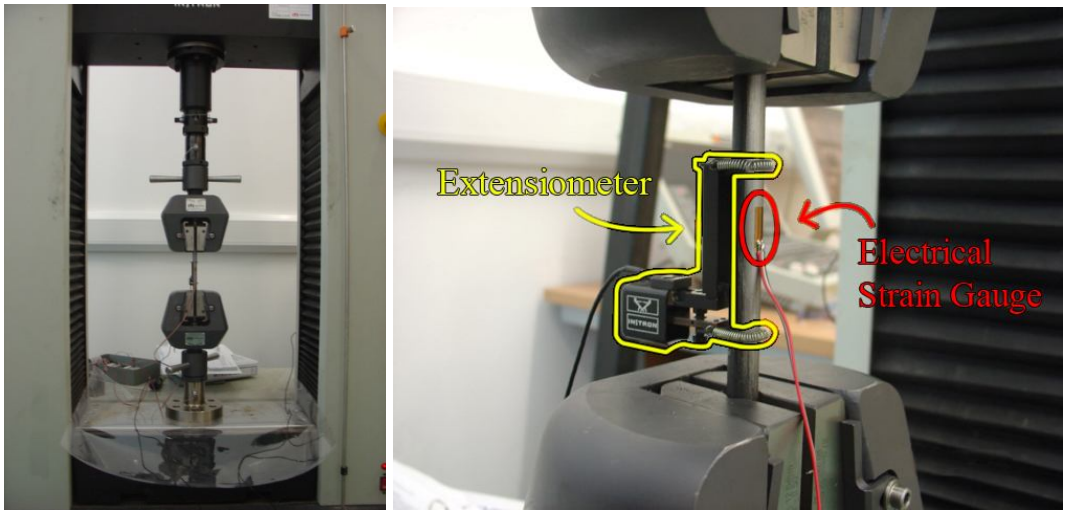

Figure 5-9: Steel sample in the Instron with the extensiometre and electrical strain gauge attached

When the results of the first set of samples were compared the stress-strain curve of the electrical strain gauge values did not match with the curve of the Instron values (Figure 5-9 and 5-10). Thus the enquiry was brought to the manufacturer, but even then the deviation of the values between the electrical strain gauge and the Instron could not be explained. However, with further investigation it was found that the variation was consistent. It is also found that the degree of variation between the

3 Instrument for measuring changes in linear dimensions.

strain gauge and the extensomenter varied with the diameter of the sample tested (or the curvature of the surface on where the electrical strain gauge is attached varies).

The graphs of the Instron were verified by comparing Young's modulus. The typical young's modulus of steel is known to be around 205 kN/mm^2 (COBB, Fiona, 2004). When the values are calculated from the graphs it could be confirmed that the values of the Instron are closer to the actual stress-strain relationship of the steel bars (Figure 5-9 and 5-10). Thus it is concluded that the stress-strain readings of the electrical gauge is affected by the curvature of the steel bar, and the discrepancy increases as the diameter reduces and hence the curvature gets greater.

In order to confirm the above conclusion a number of flat samples were tested with the electrical gauges attached. The graphs show that the curves of the data logger and the Instron are in a good agreement (Figure 5-11). Thus this investigation confirms that the electrical strain gauge gives correct strain readings and there was a fault in the equipment itself, however, when the surface curvature of the sample increases (as the diameter increases) the difference between the gauge readings and the actual strains of the sample also increases.

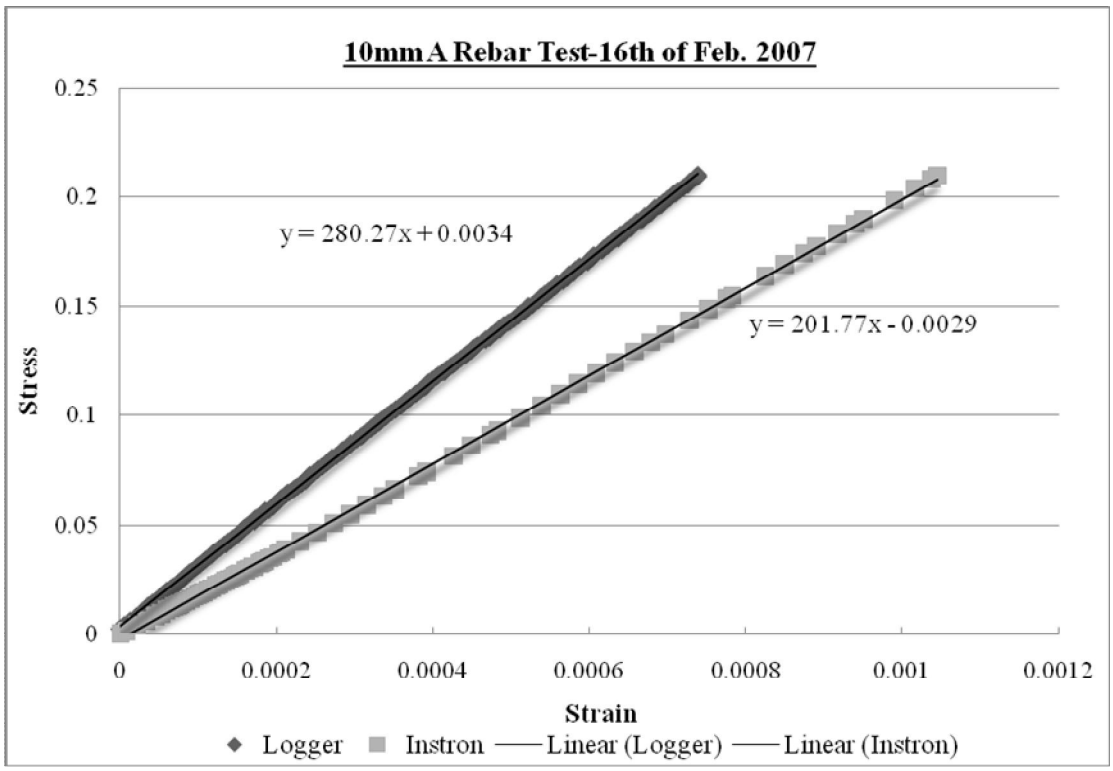

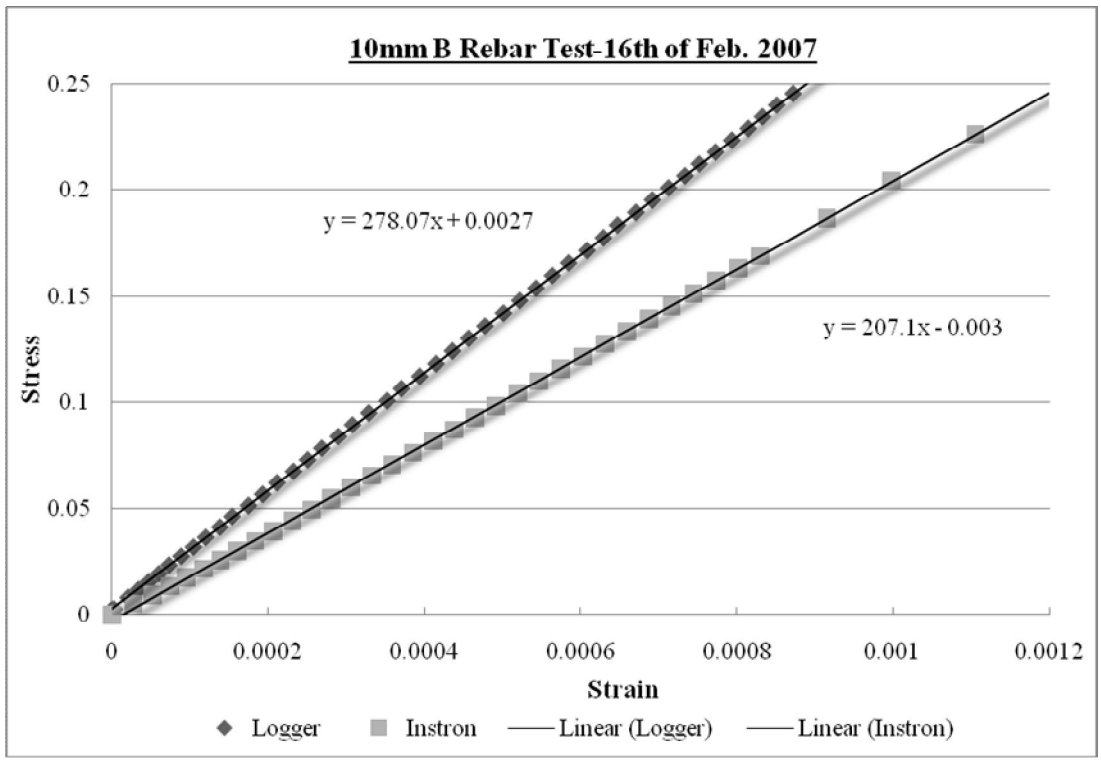

Figure 5-10: Comparing the Stress-Strain relationships of 10mm steel bar measured by the Instron and the logger.

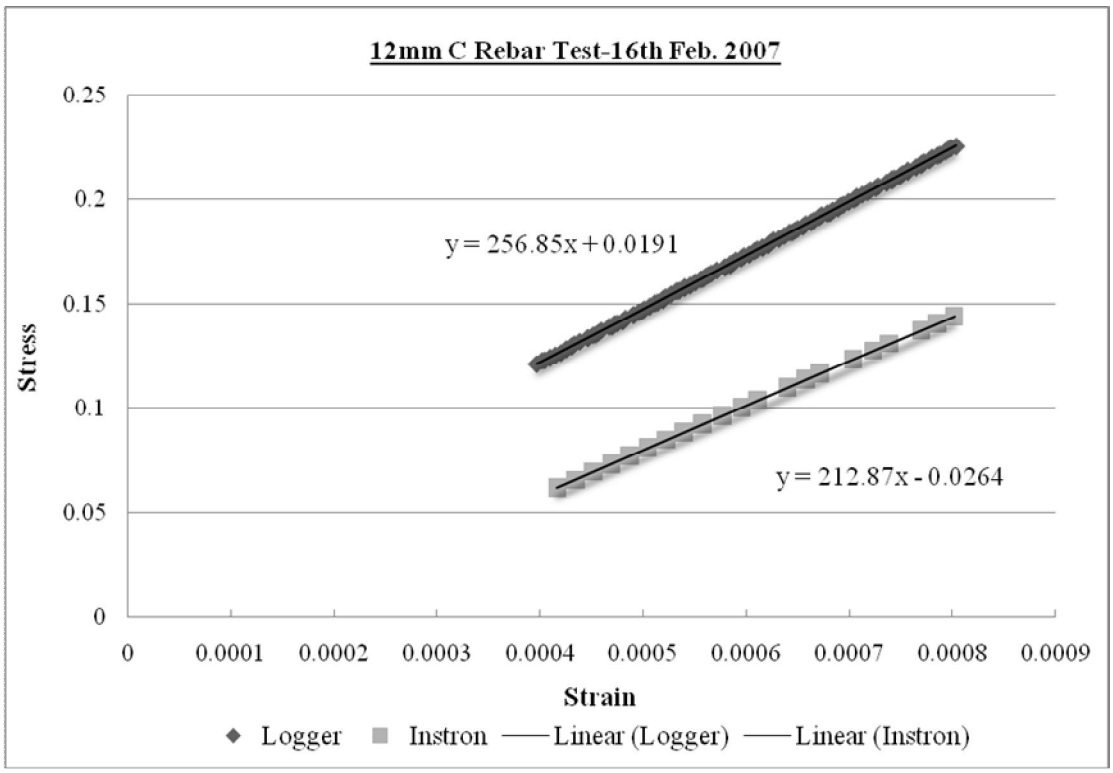

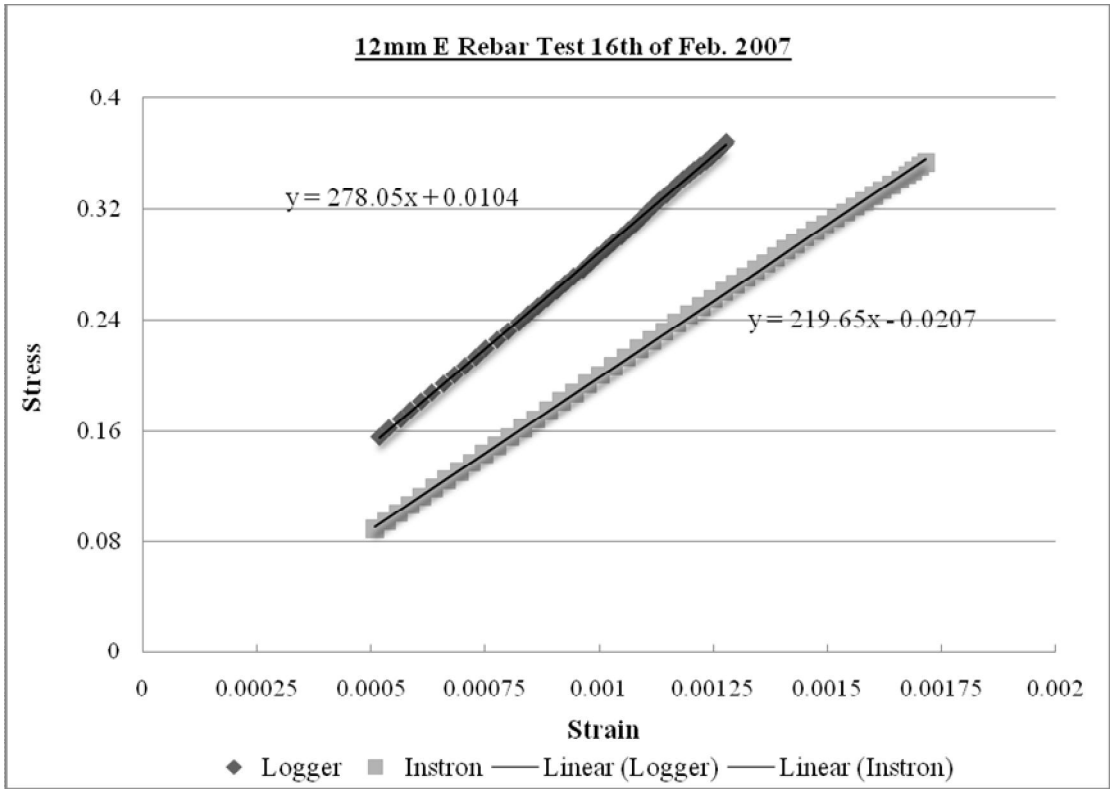

Figure 5-11: Comparing the Stress-Strain relationships of 12mm steel bar measured by the Instron and the logger.

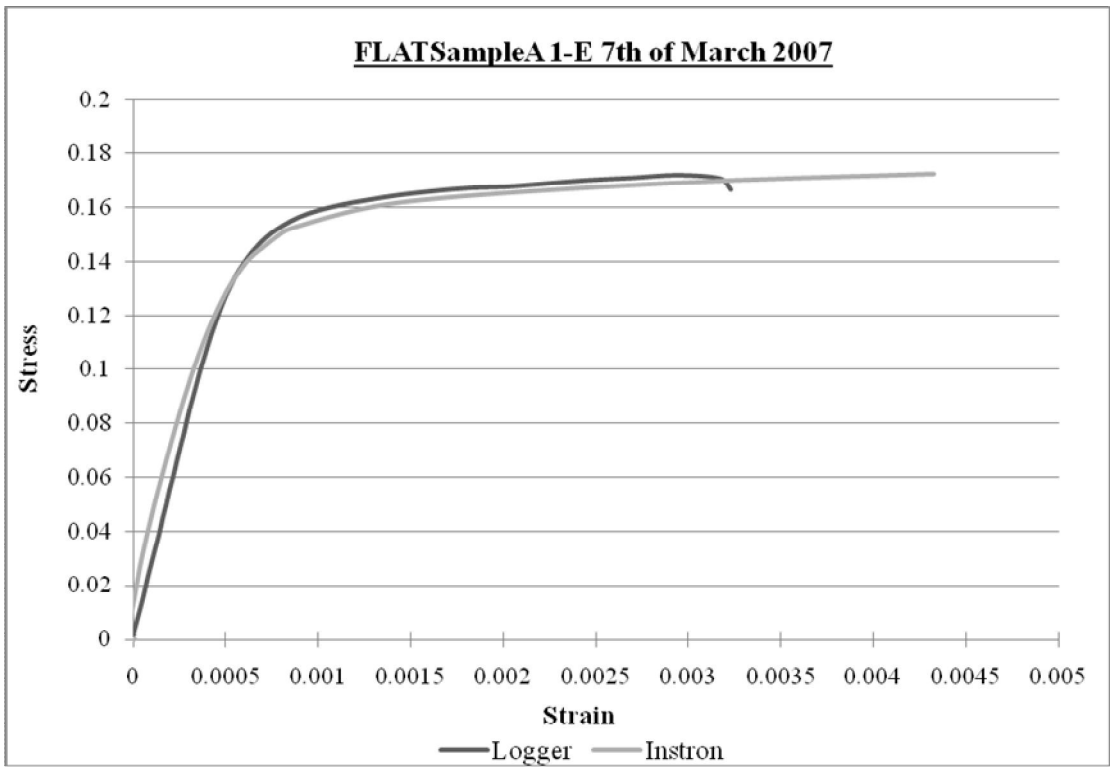

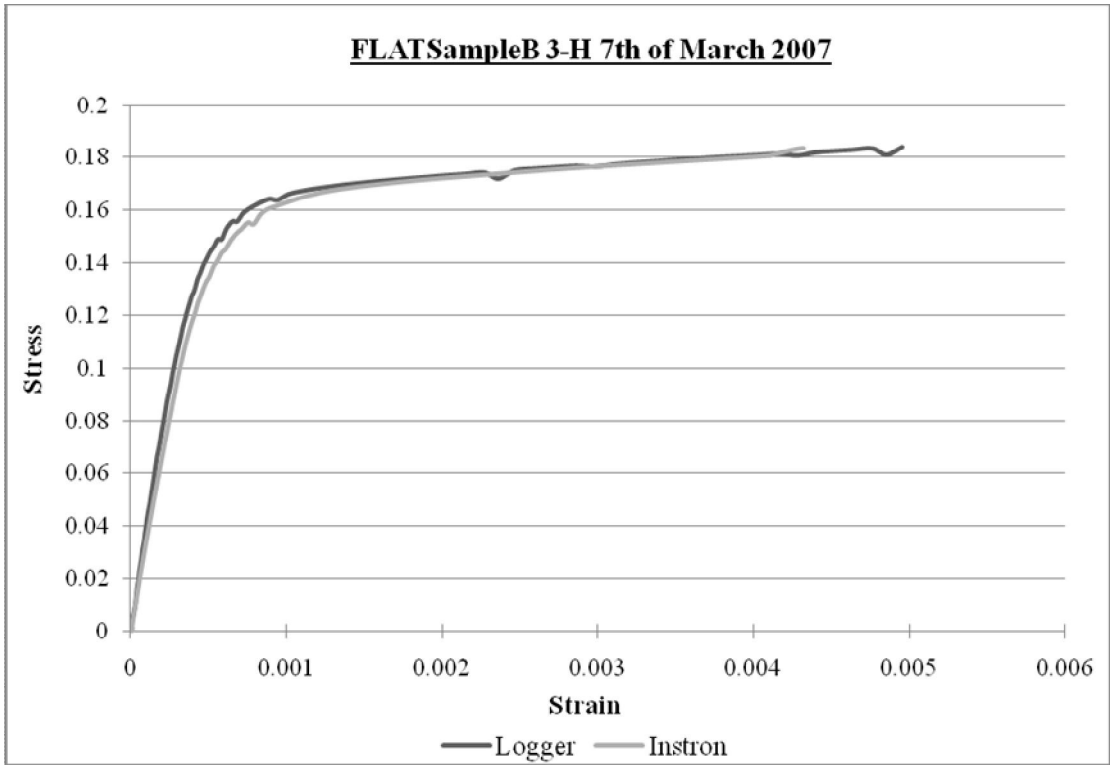

Figure 5-12: Comparing the Stress-Strain relationships of Flat Sample measured by the Instron and the logger.

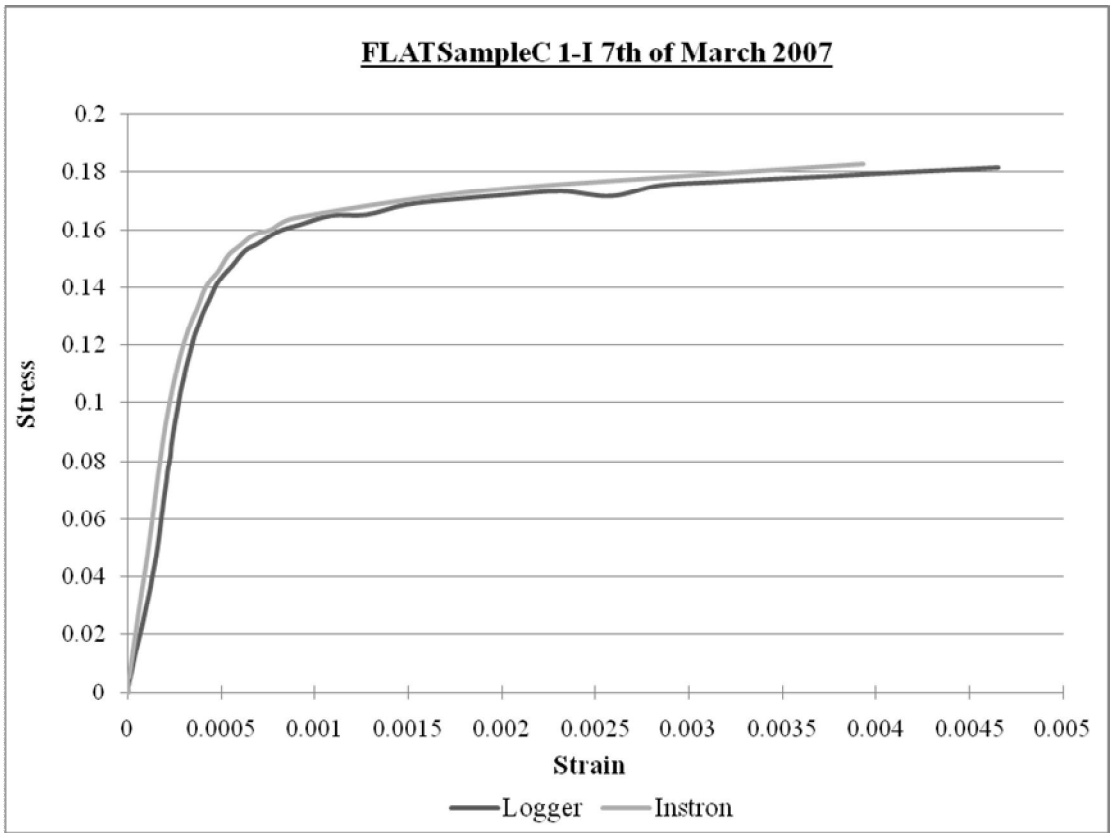

Figure 5-13: Comparing the Stress-Strain relationships of Flat Sample measured by the Instron and the logger.

In order to find the discrepancy factor between the logger values and the actual strain of the rebar, the graph of the logger values versus the Instron values are plotted (Figure 5-12 and 5-13). From the graphs the following relationships are found for 10mm and 12mm diameter steel bars.

	Equation	Average
10mm	1.389x + 3e-5	1.366x + 3e-5
	1.342x + 3e-5	
12mm	1.221x + 2.14e-4	1.244x + 1.57e-4
	1.266x + 1.00e-4	

Table 5-1: Table of conversion factors for the electrical strain gauge readings for 10mm and 12mm diameter rebar

Thus the above expressions will be used to convert the gauge strain readings to the actual rebar strain readings. For example when a strain reading of the rebar with 10mm diameter from the logger is 100, the actual strain of the rebar is $1.37*(100*1.0e^{-6}) + 3e^{-5} = 0.000167$. Please note that the logger reading 100 is multiplied by $1.0e^{-6}$ because the reading is in microstrain.

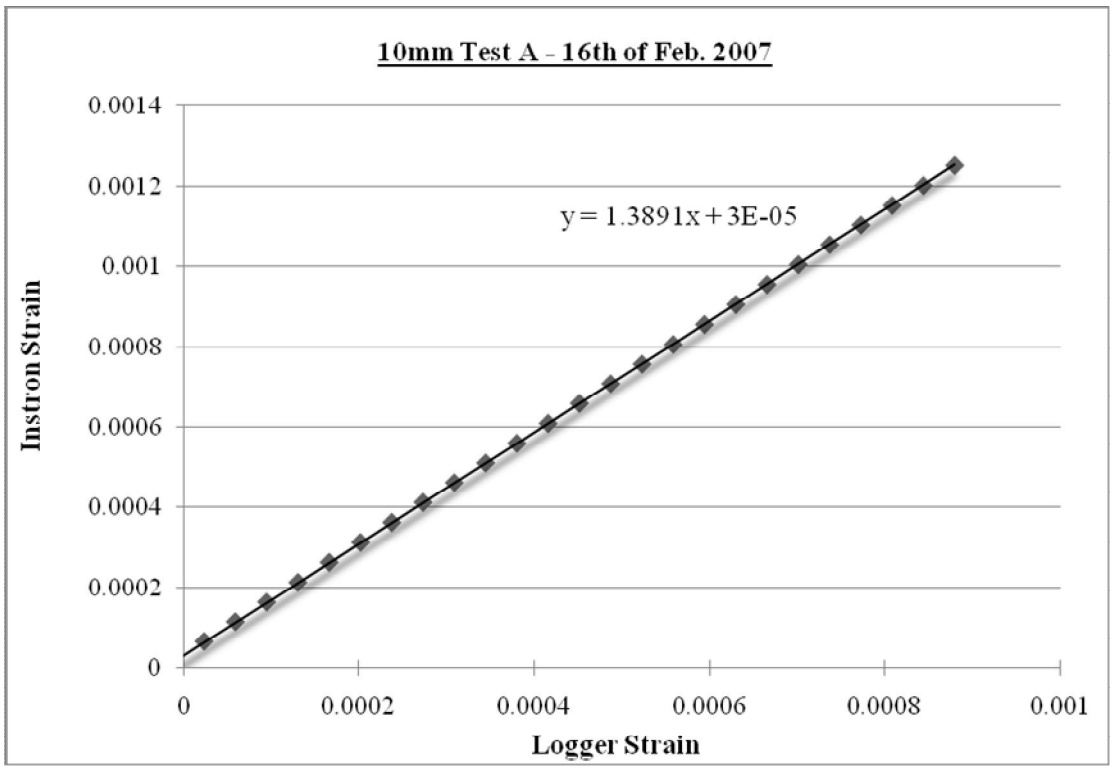

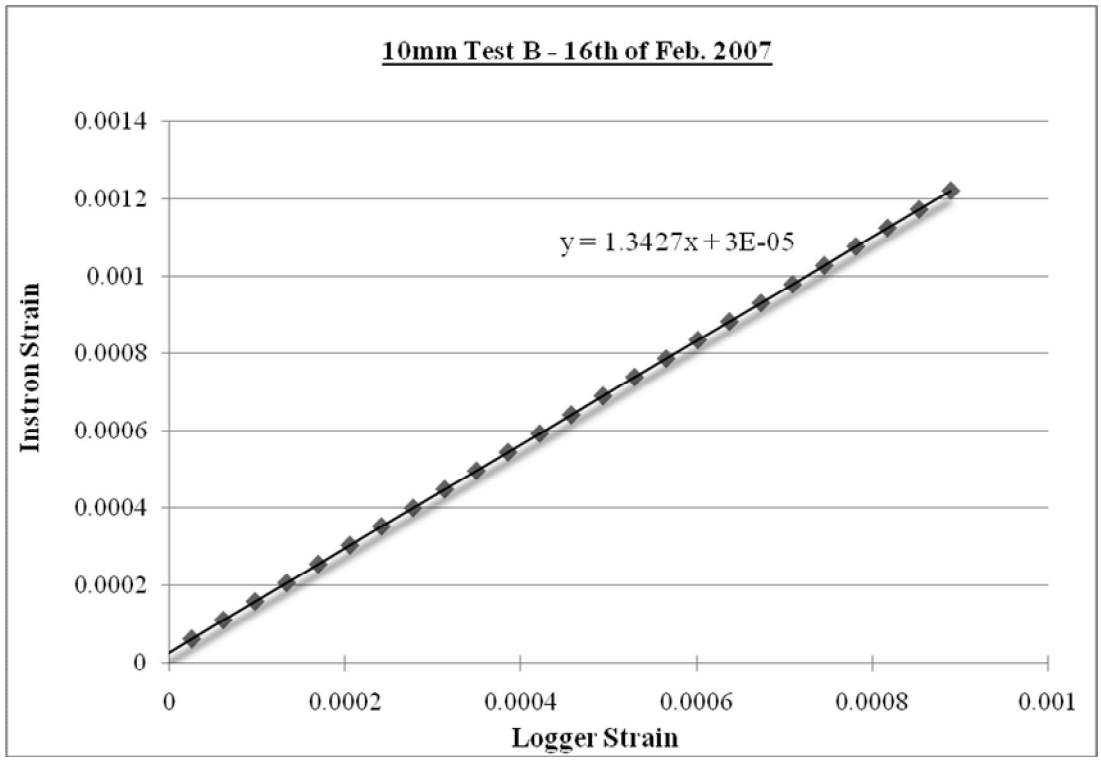

Figure 5-14: Graphs showing the relationship between the Instron strain readings and electrical gauge strain readings for 10mm diameter steel bar

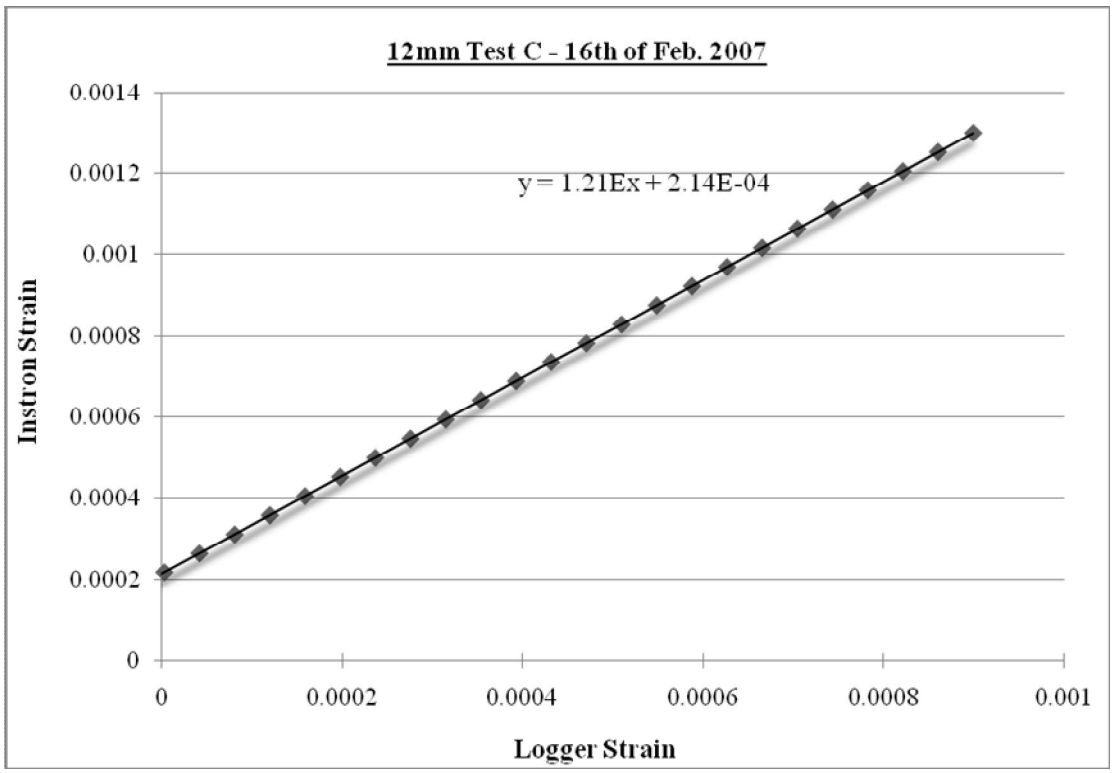

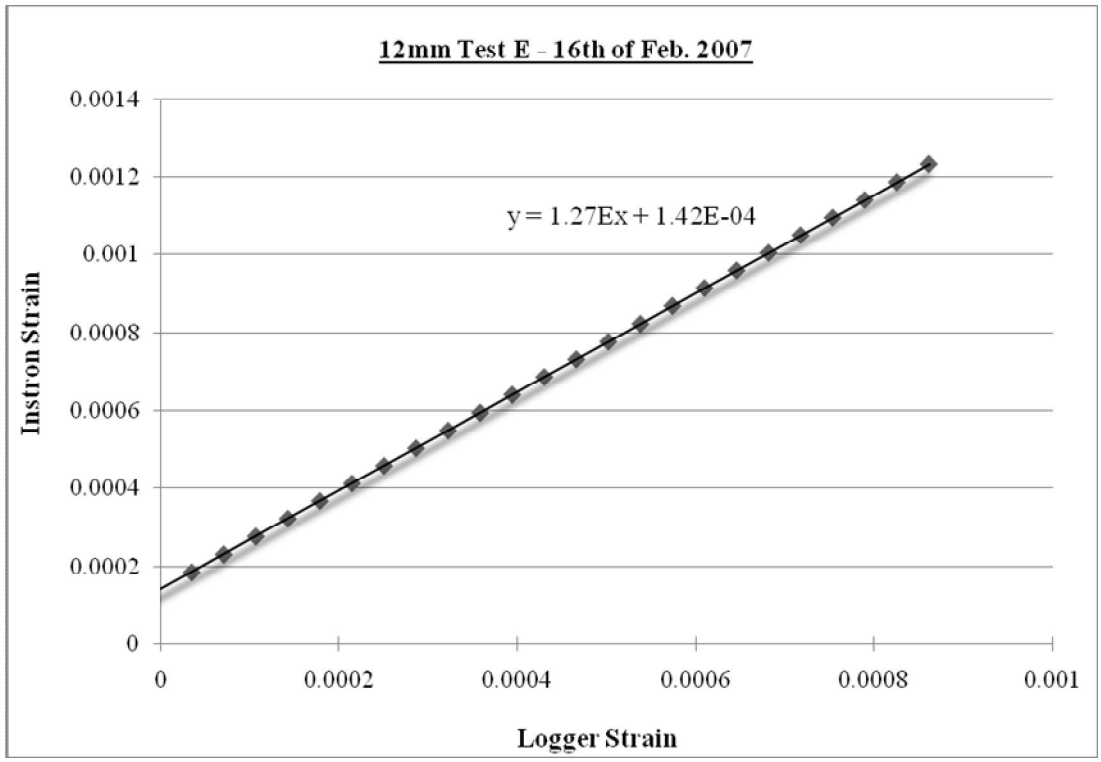

Figure 5-15: Graphs showing the relationship between the Instron strain readings and electrical gauge strain readings for 12mm diameter steel bar

Please note that the application of electrical strain gauge was reviewed and adapted only after first few beams were tested. Thus for the following beams only the Demec gauge was used to measure the tension strain of reinforcement bar.

- 11DA-WS10mm
- 11DA10mm
- 22SA10mm

5.3.4 Deflection Measurement

The central deflection of the beams was measured using the mechanical dial gauges. At the centre of the beam a dial gauge reading to 0.01mm is placed to measure the central deflection of the beam. However, the supports of the beam are placed on top of a large steel beam, which is part of the test rig, and there has been a concern that this beam will also deflect by the load in the supports. Therefore, the two additional dial gauges are placed on the steel beam at directly below the simple supports to measure any vertical displacements. Thus in order to obtain the actual deflection of the beam the following calculation is used:

Actual Central Deflection of the Beam
= Central Deflection Reading – Average of the Support Displacement Reading

Later on the test results show that the deflection of the steel beam is in between 1%~5% of the actual central deflection of the beam.

Figure 5-16: Showing the dial gauge measuring the vertical deflection of the supporting beam

5.3.5 Data Acquisition

Data from the load cell the electrical strain gauges are saved to a computer file using a logger called Microlink 751 (Figure 5-15). The logger receives the strain reading from a bridge unit Microlink 594 (Figure 5-15) which the electrical strain gauges and the dummy gauges are connected to. The load cell is connected to a digital indicator TD-91M (Tokyo Sokki Kenkyujo CO.) (Figure 5-16), which then connected to the logger. Windmill Measurement & Control Software is used to record and generate the data files (Figure 5-16).

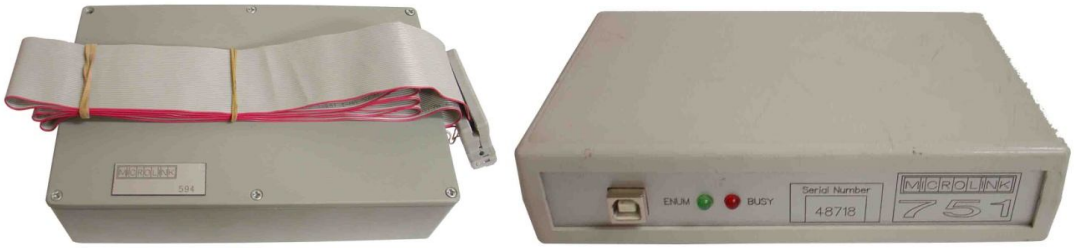

Figure 5-17: Microlink 594 (left) and Microlink 751 (right)

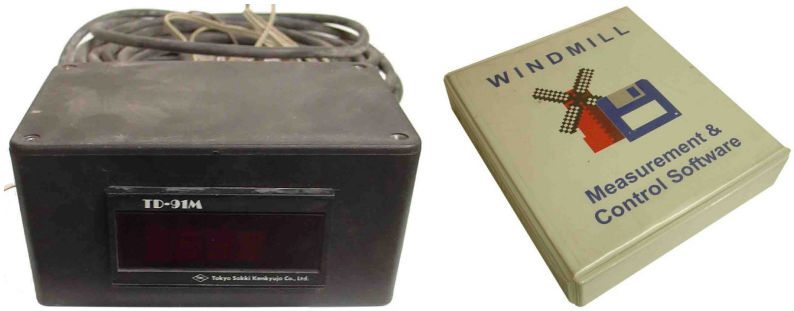

Figure 5-18: Digital indicator (left) and Windmill software package (right)

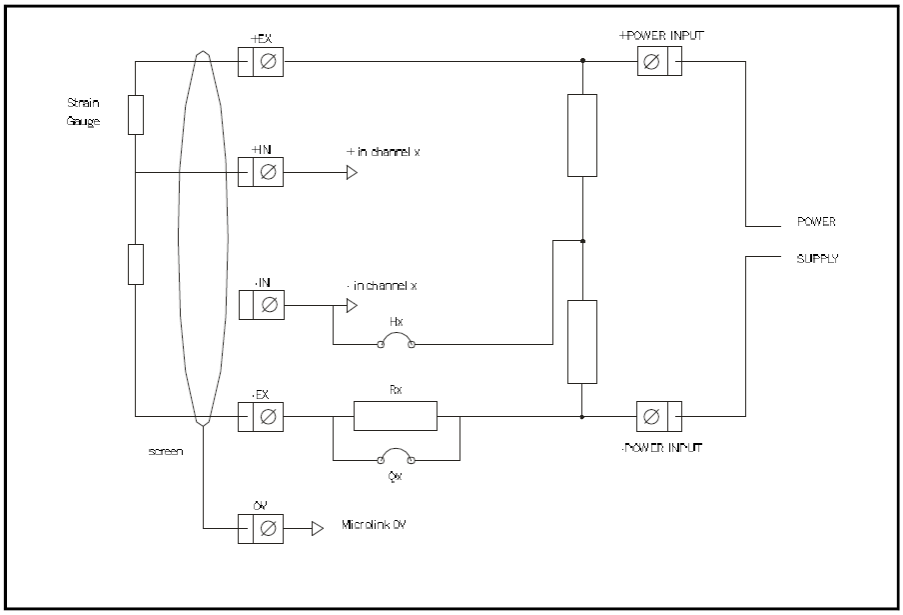

Figure 5-19: Half bridge connection in Microlink 594 for electrical strain gauge

5.4 Experimental Procedures

The beams were loaded initially in three cycles up to first crack is formed. Then the beam is test to its ultimate limit in the fourth cycle.

The following procedure is carried out for the beams:

1. The dial gauges readings and the Demec gauge readings are recorded before the loading.
2. The beam is loaded up to the point when the first crack is formed. The dial gauges and the Demec gauges are read at the given load intervals until the first crack.
3. The beam is unloaded.
4. After a minute the dial gauge readings and the Demec gauge reading are taken.
5. Step 2 to Step 4 is repeated two more times.
6. Up to this point is the initial three cycles. This process is necessary for any loose joints of the test rig to adjust and settle into the positions.
7. Now the beam is given a recovery time of minimum 10 minutes.
8. After the recovery time, the dial gauges and the Demec readings are recorded.
9. Now in this load cycle (4^{th}) the beam is loaded until it collapses. The dial gauge and the demec gauge readings are recorded at the given load intervals.
10. The locations and patterns of cracks are marked on the beam as they appear and develop.

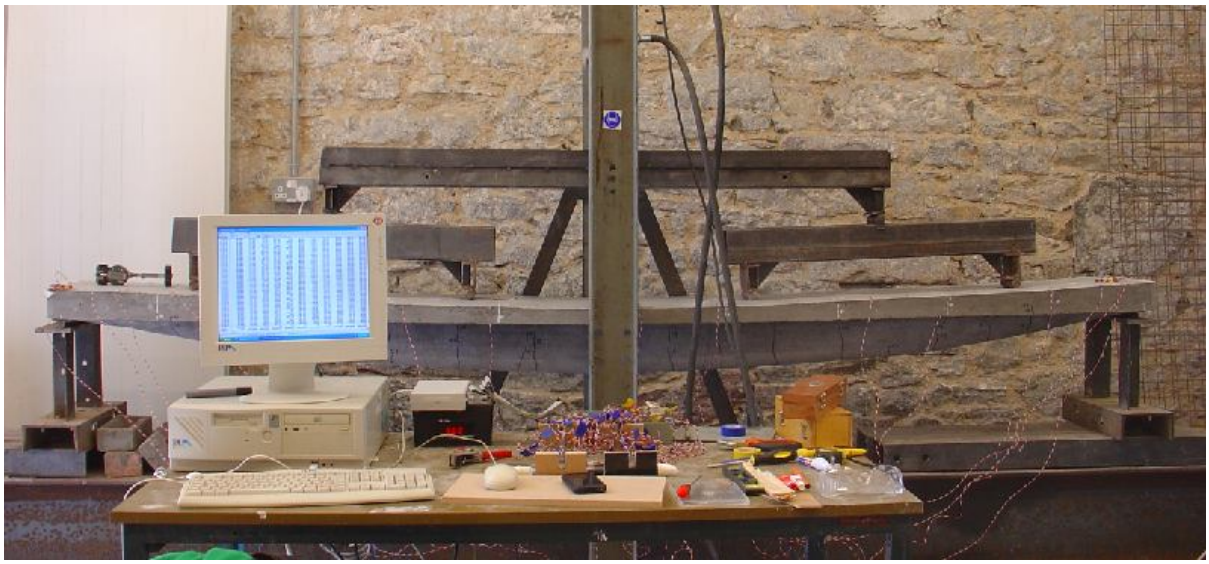

Figure 5-20: Showing a typical experiment set up

Chapter 6: Design and Development of the Fabric Formed Beams

6.1 Introduction

This chapter presents detailed information on the development of the geometry and structural form of the fabric formed reinforced concrete beams. The very first fabric formed beam (called the prototype beam, Figure 6-1) designed and constructed at the laboratory was by Remo Pedreschi. This prototype beam consists of flange and web, which adapted the catenary curve to reflect the form-active shape.

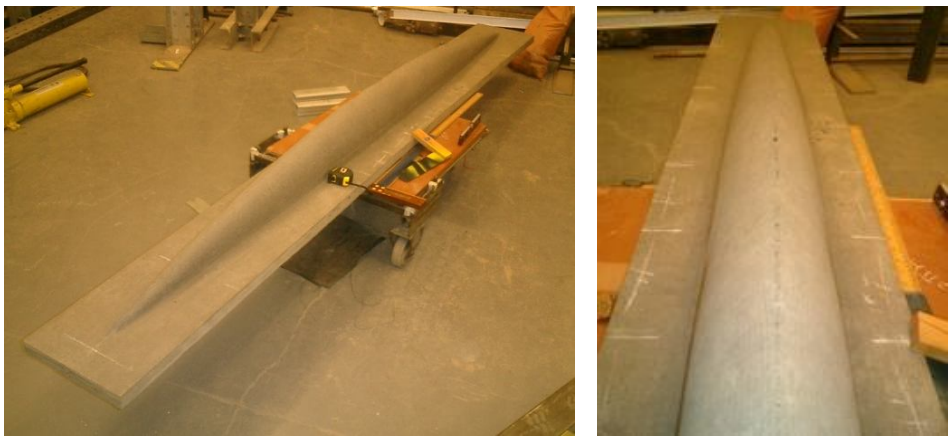

Figure 6-1: Prototype Beam

The dimensions of the prototype beam were determined based on a number of factors:

1. Initial span length of the web was decided to be 3000mm.
2. Total length of the beam was decided to be 3160mm, leaving 80mm of flange at each end for the bearing purpose.
3. The width of the flange was decided to be 1/10 of the total length of the beam. Thus, 3160/10 = 316mm, which was then rounded up to 320mm. The size was taken also because it was suitable size for the test rig.
4. The depth of flange was 40mm just to give enough cover for the reinforcement (10mm diameter) and steel compression mesh (about 3mm diameter).
5. According to the concrete design code BS 8110 (reference p116 of code) that the span/effective depth ratio of simply supported flanged beams is 16.0, the mid-span depth of the suspended string was calculated to be 187.5mm. However, the initial profile of the beam did not exactly suit the conditions of a flanged beam. Therefore it was decided to take the average value of the

span/ effective depth ratio of the rectangular beam (20.0) and the flanged beam (16.0). Therefore, the mid-span depth was calculated as following: (16+20)/2 = 18 = span/depth ratio. So, 3000/18 = 167mm

6. To draw the catenary curve for the web, a string was pulled horizontally to have the horizontal length of 3000mm and the mid-span depth of 167mm, and the shape was copied onto a board.
7. The width of the web at the mid-span was 120mm giving 100mm space on each side of the flange, and the width gradually reduces in a catenary curve and eventually comes to a closing point.

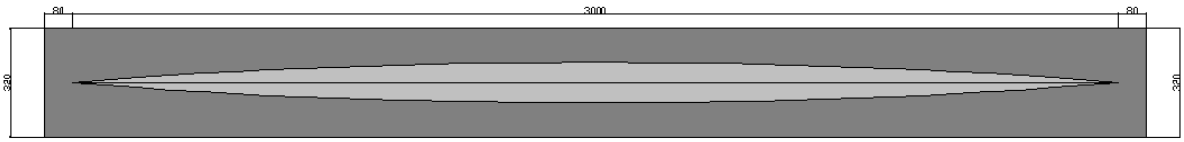

Figure 6-2: Plan drawing of web

The main purpose of constructing the above beam was to explore the practicality of fabric formwork construction for casting concrete beam. The beam was not designed with the consideration of its specific structural performance. The following pictures (Figure 6-3) show the first formwork built at the research laboratory for the construction of the prototype beam.

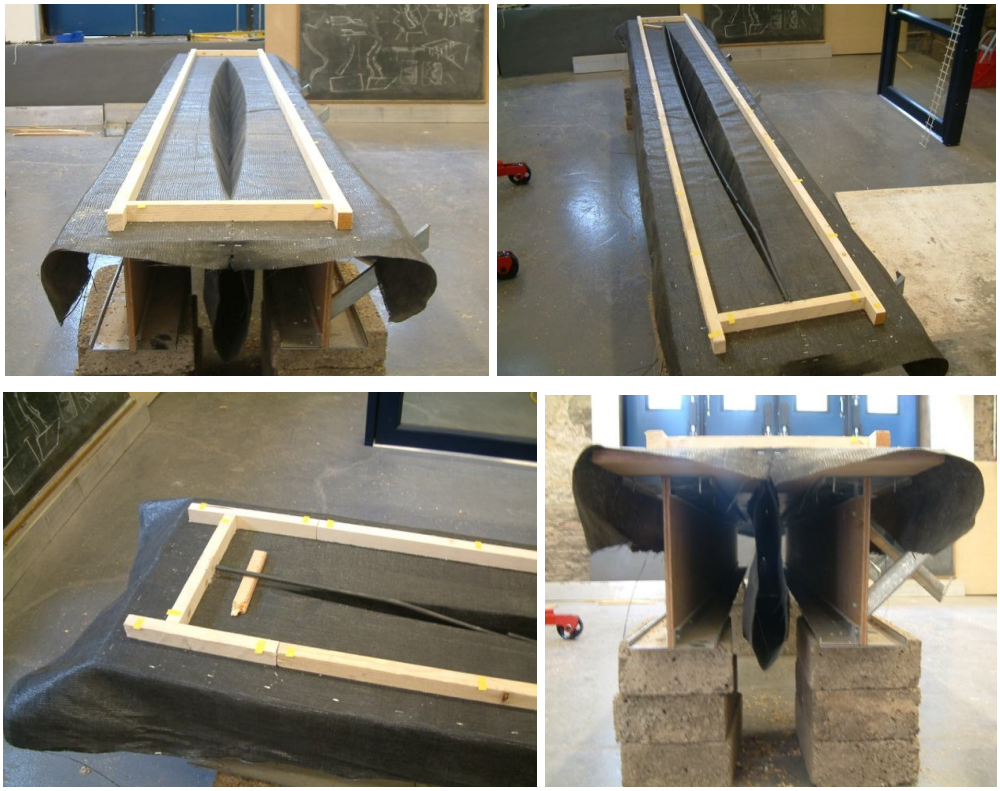

Figure 6-3: Formwork for the prototype beam

The tension reinforcement of the beam also follows the catenary curve (Figure 6-4). Two steel bars of 10mm diameter are used the reinforcement around the mid-section and only one of the bars runs through the whole span. The reason behind the steel bar not running the entire span is solely because it was the only available length at the time of construction. Logically both bars should span the whole length. Please refer to the following picture for the reinforcement arrangement.

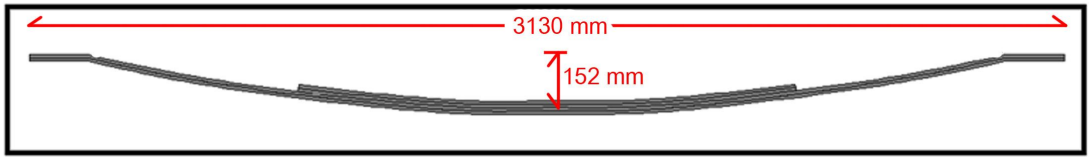

Figure 6-4: Reinforcement Arrangement

At the later structural test of the beam shows that this arrangement of reinforcement had caused the failure of the beam. The beam failed by the bending where the two steel bar changes to one steel bar only (Figure 6-5 and Figure 6-6).

Figure 6-5: Prototype beam's crack at the failed section

Figure 6-6: Showing the reinforcements at the failed section of Prototype beam

After the prototype beam's test further two beams were constructed with the main intention to explore the structural behaviour of the beams. The next beams were

modified based on the bending failure of the prototype beam and the summary of the modifications are stated below:

1. The reinforcement arrangement is modified to have two rebar running the full span.
2. One anchorage is added at each end of the reinforcement bars to act against the slippage of the bars inside concrete. The overall depth of the flange is too shallow to have bent-up bars, and it is a lot practical to have a simple bar attached perpendicular to both ends of the reinforcement.
3. Shear reinforcement is not considered at this stage and its requirement is discussed based on the result of structural testing. However the attempts are made to eliminate the use of shear reinforcement in the beam design, through the modification of the overall form of the beam.
4. The design of the web is changed from the catenary curve to a parabolic curve. The catenary curve is in respect of the dead load of the structure that is not uniformly distributed, and more loads are distributed near the supports (please refer to the diagram below). In respect of a uniformly distributed load, for which a beam would be designed, it is more sensible to adapt a parabolic curve.

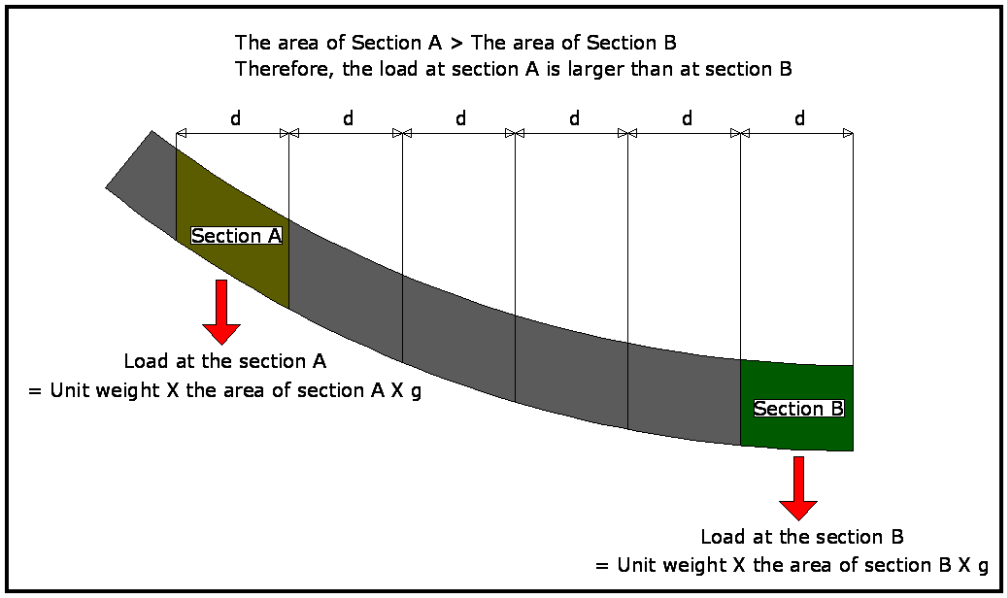

Figure 6-7: Load distribution of a cable in a catenary form.

5. The size of the reinforcement bars was varied between the beams to see the effect of steel content on the behaviour of the beam. In one beam, the same 10mm diameter steel bars are used (total cross-sectional area is 157.08 mm^2),

and in the other beam 12mm diameter steel bars are used (total cross-sectional area is 226.19 mm^2).

The test results of the two beams have been already discussed in the literature review section. However, to briefly recall, for both beams the failure occurred around the concrete, where the anchorage was embedded (Figure 6-9). The failure was due to the crushing of concrete by the compressive stress exerted by the anchorage, which was initially pulled in due to the tensile force in the reinforcement. Due to this premature failure of the anchorage zone the effect of steel content could not be seen.

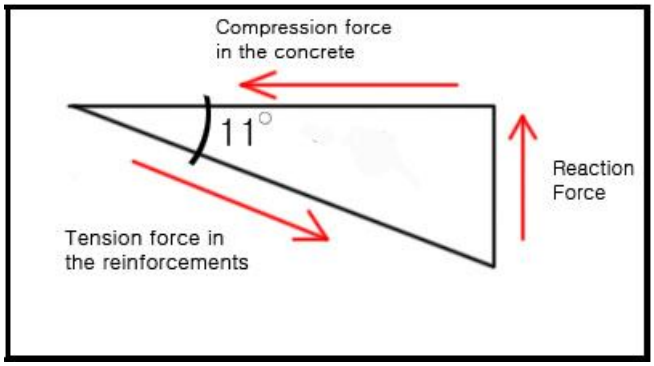

Figure 6-8: Strut-Tie model illustrating the equilibrium condition at the anchorage the failure zone (LEE, 2005)

Figure 6-9: Concrete failure due to the compressive stress of anchorage

The following sections of this chapter discuss how the above two beams are further

developed into more structurally efficient form since the above experiments. The evolution of the beams takes place over five Design and Development stages, and in total eleven types of beams have been built and tested. Each Design and Development stage takes the following path:

1. For the first step, the results of the initial beam are reviewed. Based on this review the beam's design is modified for increased structural performance. The concept design is drawn for the construction.
2. The beam is constructed according to the concept design.
3. The cast beam is tested to failure.
4. The tested beam is first examined visually, and it is further analysed using the structural theory and computer based modelling analysis.
5. All the results are summarized and evaluated. The evaluation draws conclusions on the cause of beam's failure.
6. Based on the evaluation the next concept design is developed.

Throughout the developments of the beam the effects of the following variables are studied:

- Flange Thickness
- Web Geometry
- Percentage of Tension Reinforcement (Steel Ratio)
- Type of Anchorage
- The Effect of Compression Steel Mesh

Development of beam's form continued until the beam failed by yielding of the rebar around the mid-span. This failure mode occurs in a ductile manner by forming large visible cracks which gives sufficient warning prior to the ultimate collapse, and it is the desired failure mode for a reinforced concrete beam. Also the ultimate load of the final beam (the beam in its latest developed form) exceeded the capacity of the load cell (50kN).

6.1.1 Beam Nomenclature

The names of the beams are coded on basis of their physical design specifications. Thus by looking at the names the reader should be able to tell about their detail specifications without constantly referring back to the list and check. The following information has been prepared to help the reader to easily identify the beam in any

part of the thesis.

The numbers 11 and 22 at the beginning of the names identifies the end angles of the reinforcement as it enters the flange at the reaction points. The two letters coming after the numbers indicate type of anchorage. SA (Single Anchorage) means there is only one anchorage at the end of rebar, and DA (Double Anchorage) means there are two anchorages (An anchorage comprises steel bar welded at right angle to the primary reinforcement). If there are the letters DF (Deeper Flange) after the letters SA or DA; this means the beam has thicker flange towards the supports. In other words, the flange depth is 40mm at the mid-span and gradually increases and becomes 80mm towards the supports. The beams without the letters have constant flange depth of 40mm the entire span. The beam names with WW (Wide Web) after the letters, DF; this means the beam has the web profile which horizontally diverges towards the supports. The beams which do not have WW in their names have the web profile that horizontally converges towards the supports.

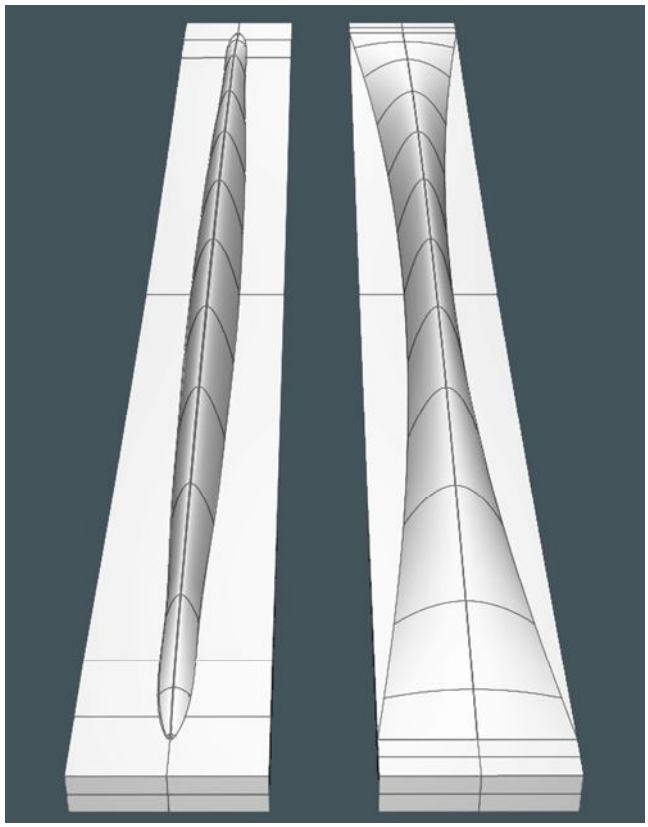

Figure 6-10: Showing the two types of web profile. The beam with the web profile that horizontally diverges towards the supports as shown on the right has the letters WW in their names.

All beams have a minimum of two steel bars as the tension reinforcement. If the beams have three steel bars '3 no.' has been included in their names. Finally the names end by specifying the diameter of the steel bars in the beam; whether it is

10mm diameter or 12mm diameter steel bars.

The figures on the following pages show the evolution of the beam designs (Figure 6-11), the brief test summary sheet (Figure 6-12) with the diagrams of the beams showing the failure mode, failure location, the ultimate load, and the central deflection at the ultimate load. The figure (Figure 6-13) coming after the test summary sheet illustrates the overall dimensions of the beams with the effective depths of the mid-span sections.

The first two beams, (11SA10mm and 11SA12mm) at the beginning of Figure 6-11 have already been discussed at the beginning of this chapter.

The following sections of this chapter will illustrate how the geometry and the structural form of the beams are developed from the two beams, starting by adding more anchorage (11DA10mm), and by increasing the end angle of the reinforcement (22SA10mm).

Figure 6-11: THE EVOLUTION OF THE BEAMS

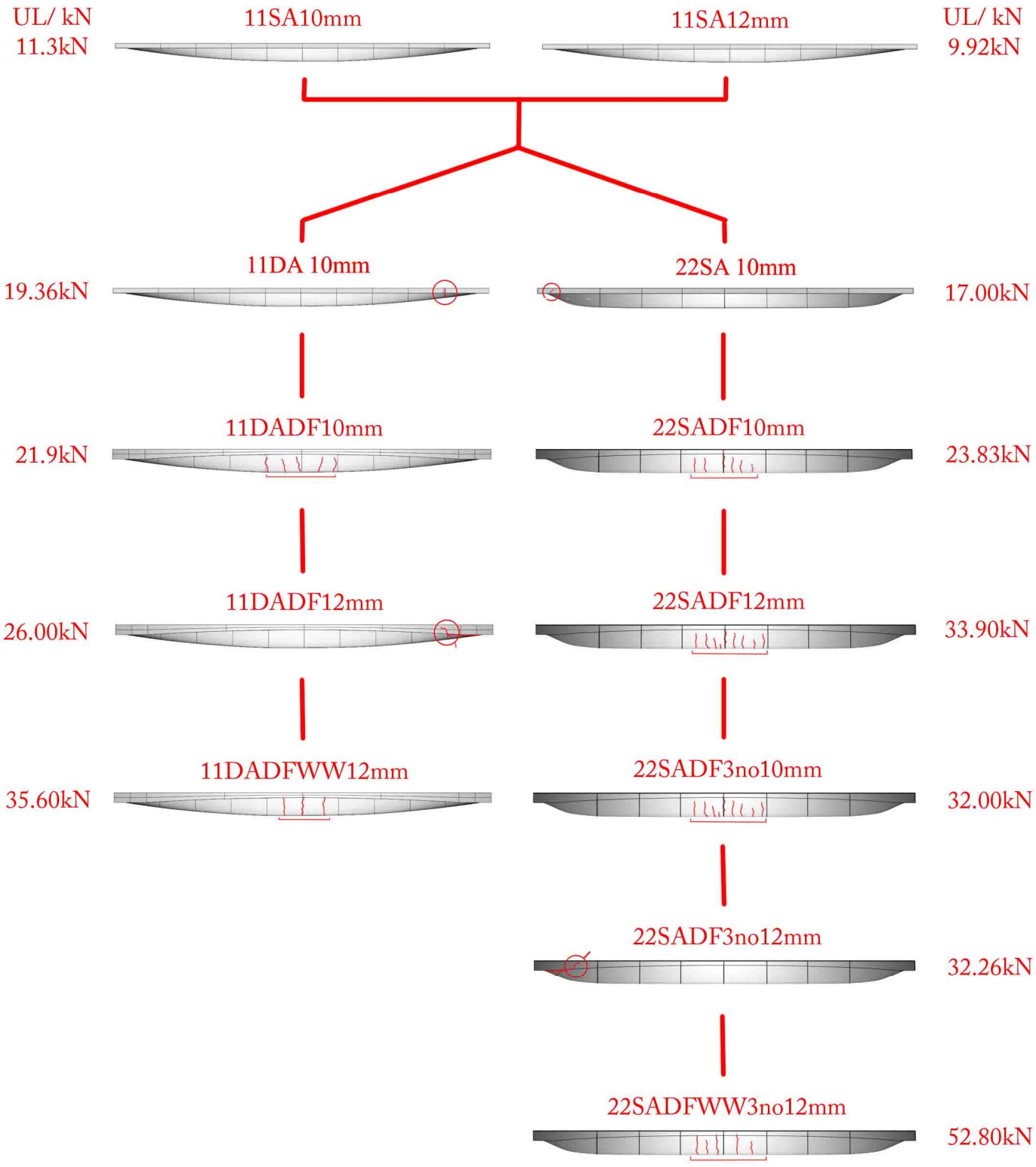

Figure 6-12: SUMMARY OF THE TEST RESULTS

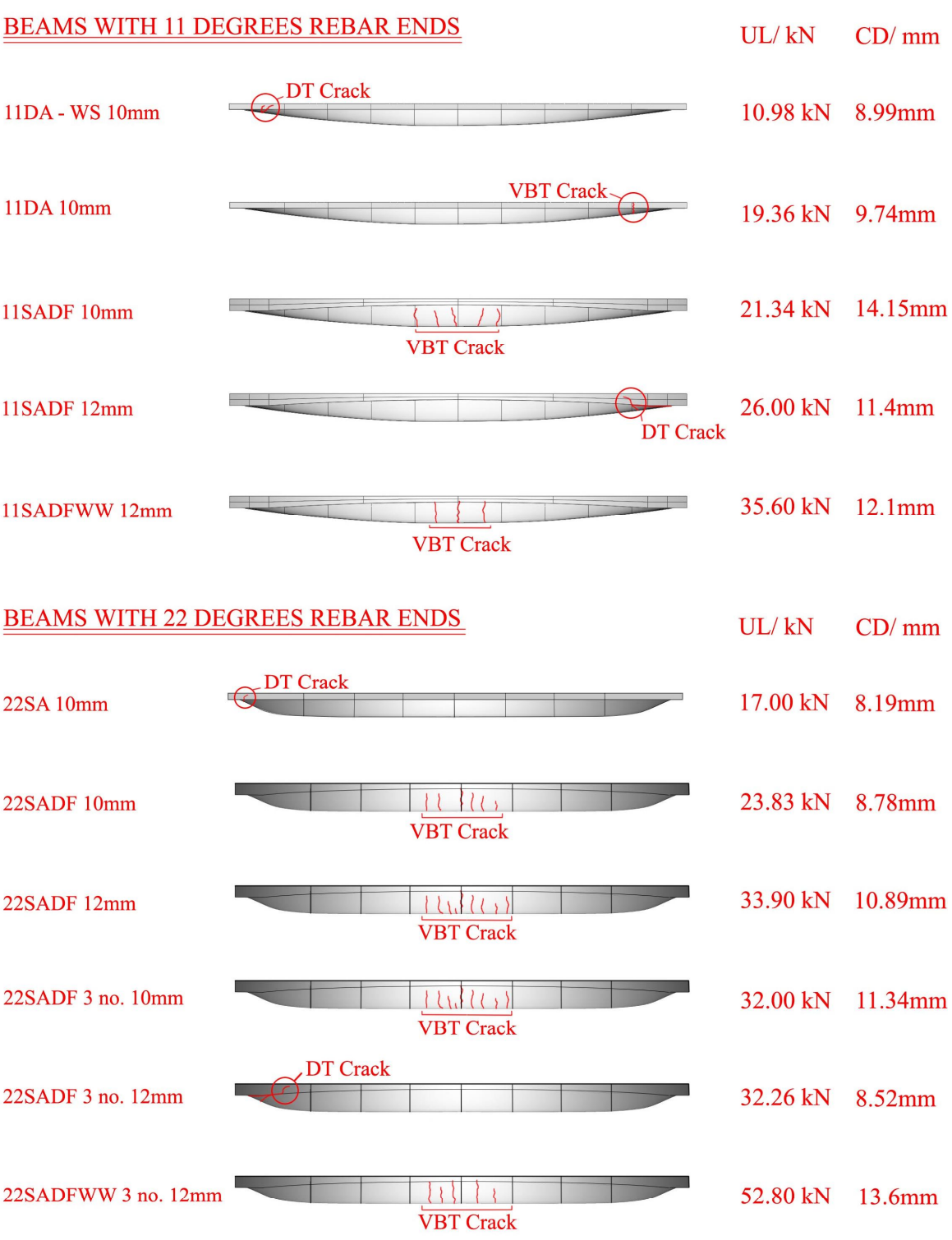

*DT = Diagonal Tension Crack
*VBT = Vertical Bending Tension Crack
*UL = Ultimate Load
*CD = Central Deflection at Service Load

Figure 6-13: BEAMS' OVERALL DIMENSIONS WITH THE MID-SPAN EFFECTIVE DEPTH

Beam Drawings - 11 degrees Type

11DA 10mm
11DA-WS 10mm

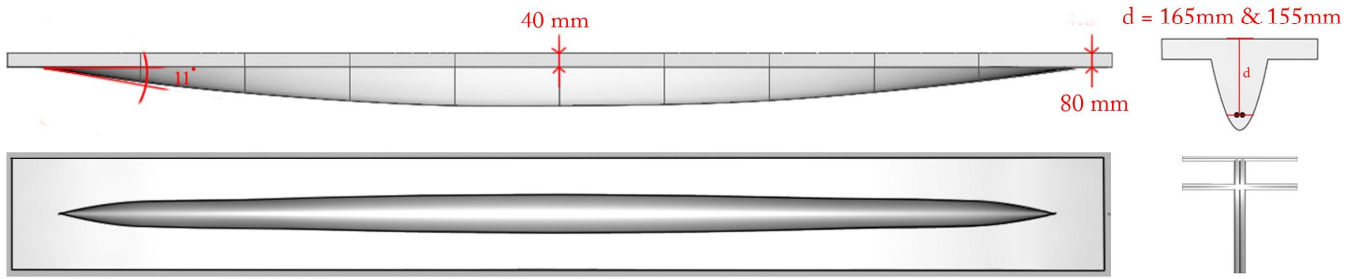

11DADF 10mm

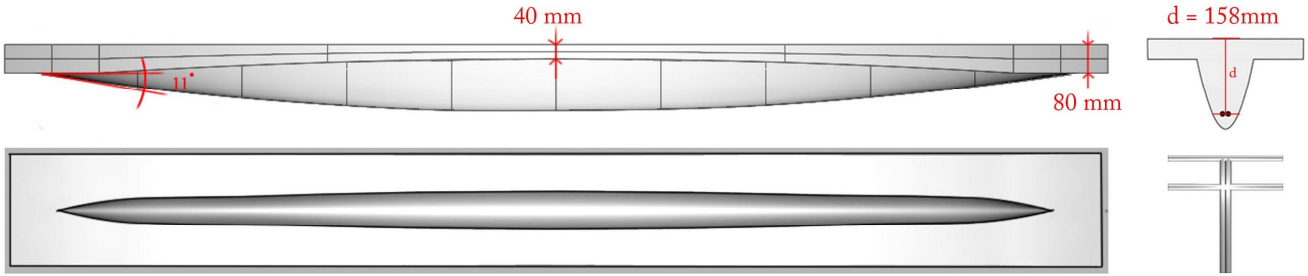

11DADF 12mm

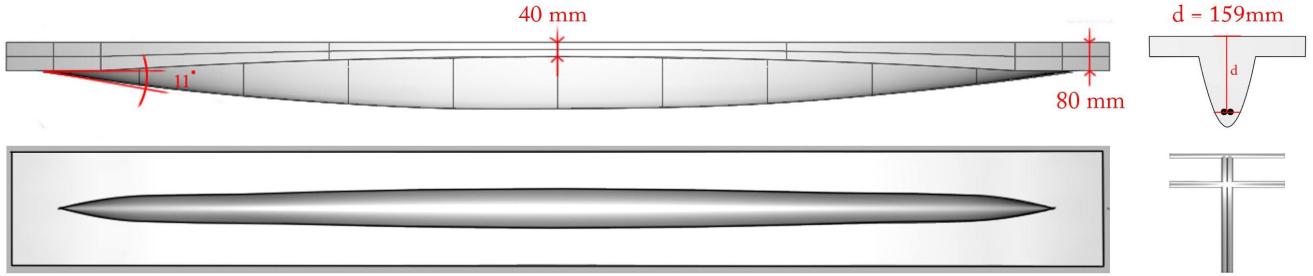

Beam Drawings - 11 degrees Type

11DADFWW 12mm

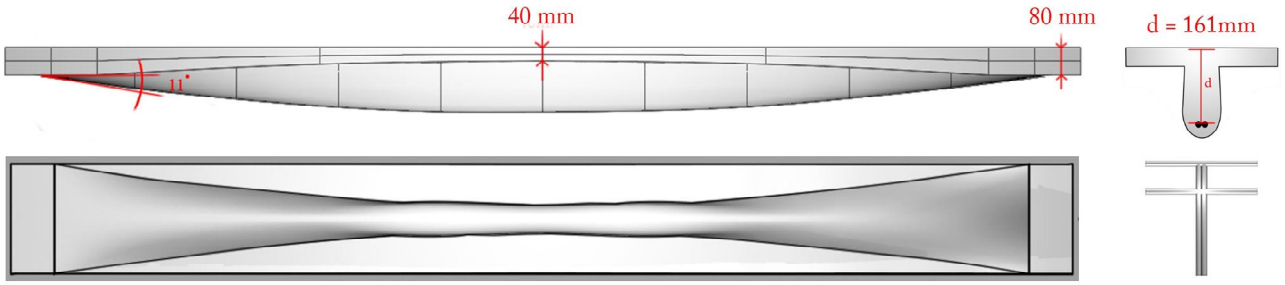

Beam Drawings - 22 degrees Type

22DA 10mm

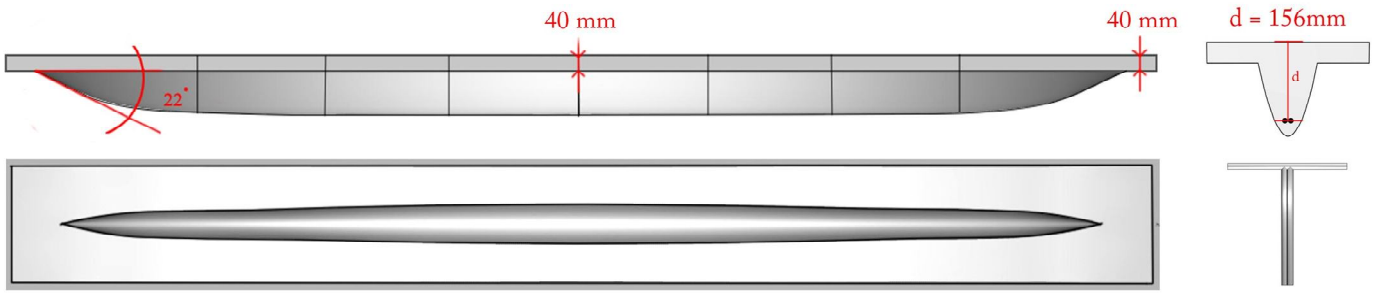

22SADF 10mm

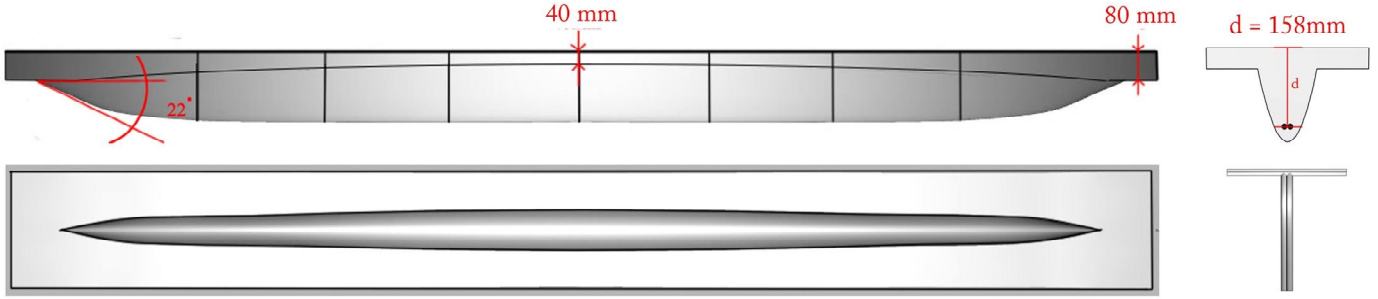

22SADF 12mm

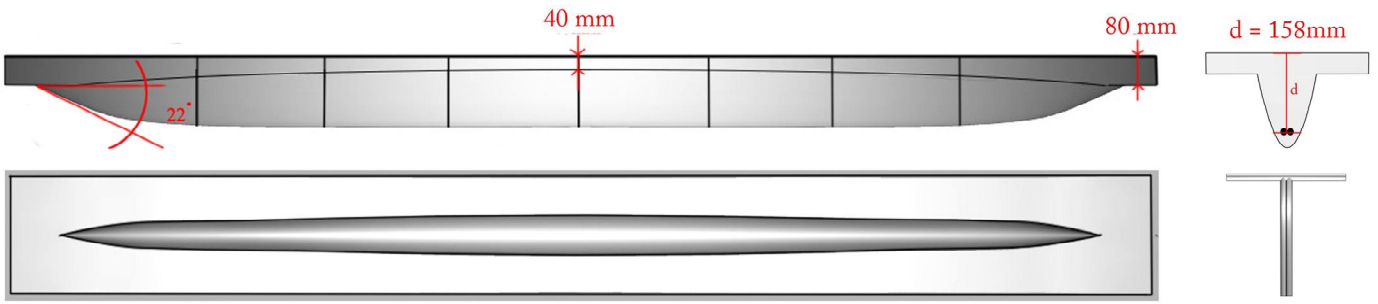

Beam Drawings - 22 degrees Type

22SADF 3 no. 10mm

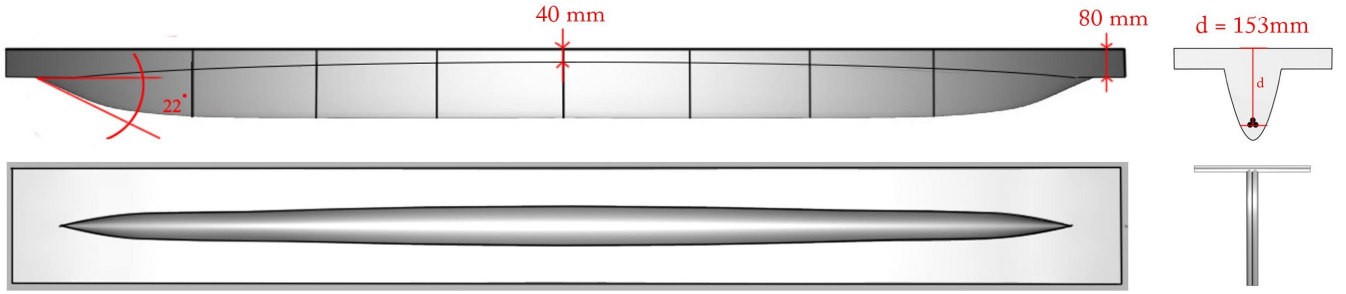

22SADF 3 no. 12mm

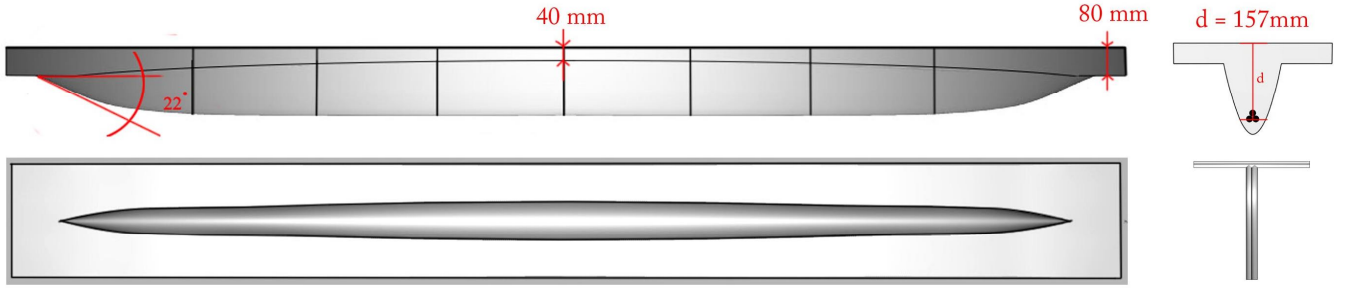

22SADFWW 3 no. 12mm

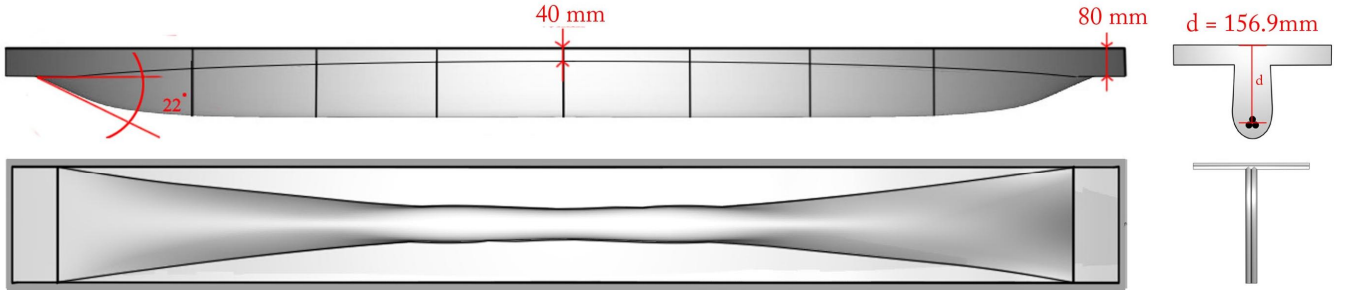

6.2 Design and Development 1: Anchorage and Steel Mesh

6.2.1 Concept Design

The problem behind the structural failure of the beams, 11SA10mm and 11SA12mm was the high compression forces applied by the anchorage which eventually crushed the concrete in the flange. To overcome this problem the following modifications are proposed;

- 11DA10mm: Increase the number of anchorages at the end of the reinforcement bar. More anchorages would transfer the tensile force in the reinforcement over greater area of the concrete, and this would reduce the compression stress exerted on the adjacent concrete.

Figure 6-14: 11DA10mm showing the double anchroage

- 22SA10mm: The end angle of the reinforcement is increased from 11º to 22º. This modification is based on the strut-and-tie model (Figure 6-8), and the reason was to reduce the horizontal force applied to the concrete increasing the angle. By studying the resolution of the forces at the reactions it can be seen that the compressive force reduces as the angle of the reinforcement increases. Please note that the effective depth at the mid-span should be kept the same at 163mm, and this means the geometry of the web should be redrawn to adopt these two conditions.

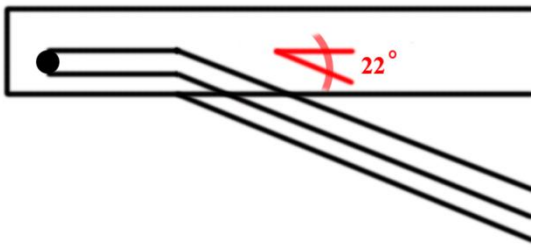

Figure 6-15: 22SA10mm showing the increased web angle

- 11DA-WS10mm: The form is identical to 11DA10mm but the steel mesh in the flange is omitted. In addition to the above proposals another design is proposed here and the purpose of this design is to see the effect of steel mesh

over the behaviour of the beam. In the prototype beam the steel mesh was included without any attention to its contribution to the structural performance of the beam, but it was included as merely accepted practice. However considering the shallow depth of section near the support the effect of the steel mesh seems worth investigating. If the results show that the beam's performance is not affected by the steel mesh, and then it could be omitted from the future constructions to further reduce the material consumption. In addition the anchorage zone is relatively thin and there is a tendency to cause congestion of the reinforcement at the support points.

6.2.2 Discussion of Results

6.2.2.1 General Discussion

Design Development Number	Beam	Ultimate Load (kN)	Load increase from the initial design (%)	Failure Mode	Location
-	11SA10mm	10.73	-	Anchorage Compression	Anchorage zone
	11SA12mm	9.32	-	Anchorage Compression	Anchorage zone
1	11DA10mm	19.36	80.43	Rebar Yielding	360mm from the support
	22SA10mm	17.00	58.43	Shear Compression	Close to the support
	11DA-WS10mm	10.98	2.33	Shear Compression	Close to the support

Table: 6-1 Summary of Test Results

Table 6-1 shows that both 11DA10mm with the additional anchorage and 22SA10mm with the increased angle of rebar resulted in an increase the ultimate load of 11SA10mm, by 80.43% and 58.43% respectively. Thus the results show that the increasing number of anchorage spreads the force over wider compression zone, and increasing the reinforcement angle can reduce the horizontal compression stress.

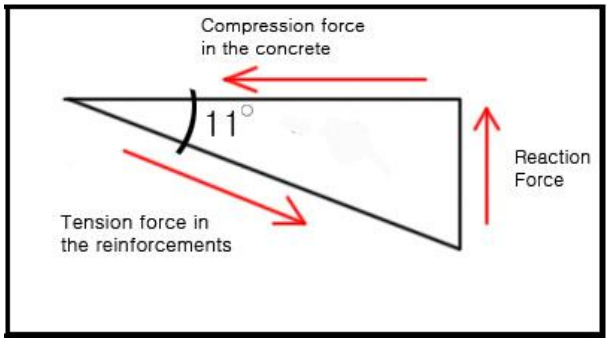

Figure 6-16: Strut and Tie model of failure zone

At the ultimate load both beams did not show any concrete compression failure around the anchorage. Thus it is considered that both beams managed to sustain the anchorage compression force. The following calculation is carried out to quickly check the compression stress in concrete adjacent to the anchorage. Again the simple strut-tie model is used;

The compressive stress due to the act of Anchorages:

The reaction force R1 = ((20000N + 351.69N + (125.37N*2))/2 = 10.3kN

The load 351.69N and 125.37N are the weights of the load transfer unit 1 and 2 (please refer to figure 5-1 in chapter 5.)

The angle, a = 11 degrees

Therefore, the total compressive force applied by the pulled in anchorages to the concrete (thus the total resistance force applied by concrete) at the failure load is,

10.3/ tan 11 = 53.0 kN

Total surface area of anchorages of which the concrete is compressed by is,

((200-20)*10) = 1800 mm^2

Thus, the total axial compressive stress applied to concrete by the anchorages is,

53.0 /1800 = 29.4 N/mm^2; divided over two anchorages = 14.7 N/mm^2

The compressive strength of concrete is;

f_{cu} = 39.6N/mm^2 * 0.8

= 31.7N/mm^2, which is the equivalent cylinder strength > 14.7 N/mm^2

The above calculation shows that the applied compressive stress by anchorage does not exceed the concrete capacity, and thus it can be said that the failure is not caused by the anchorage stress. It also must be stated that the compressive stress calculated this way is very approximate and it is used purely as an indication. Additionally, the cylinder strength does not reflect the true strength of concrete in the beam. However, it is still a good indication since the uni-axial compression strength of the concrete in the beam tends to be greater than the cylinder strength, owning to the concrete's tri-axial stress state[4]. Thus when the applied stress is less than the cylinder strength it

4 When concrete is compressed the mass would try to expand laterally. In a structure this expansion is resisted by the surrounding concrete and steel mesh by providing the confining stresses to the expanding concrete. With this laterally acting confining stress the concrete is said to be in the tri-axial stress state. The tri-axial effect in the concrete will be discussed in more detail in Chapter 9.

also satisfies that the applied stress is less than the actual concrete strength inside the beam.

6.2.2.2 Bending Tension Failure (rebar yielding) of 11DA10mm

From the following pictures (Figure 6-17) a clearly defined crack crossing the entire flange width can be observed indicating a rotational axis of bending. There is a clear vertical bending crack which moves all the way up to the top of the flange. The large width and rotation in the compression zone indicate that the section has failed by bending. Also the ductile behaviour of the failed section indicates the yielding of rebar.

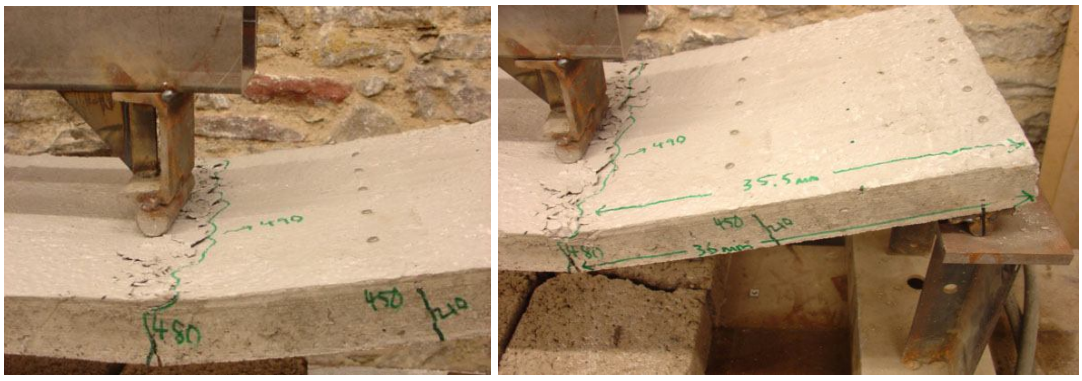

Figure 6-17: 11DA10mm at failure; Flexure Cracks

Figure 6-18: 11DA10mm at failure; Flexure Cracks

The following graph (Figure 6-19) has been plotted to compare the bending capacity, M_c of the beam sections and the applied bending moment. The bending capacities of the sections are calculated from the following equation. For more detail information of the calculation, please refer to the 'Chapter 9' under the subheading '9.3Ultimate

Limit State Bending':

$$M_c \text{ (or } M_u) = F_T * z \text{.....Equation 6-1}$$

where,

Mc = the moment capacity based on the tensile strength of the steel (Nmm or kNm)

F_T = the ultimate tension force the reinforcement (N or kN)

z = the lever arm (mm or m)

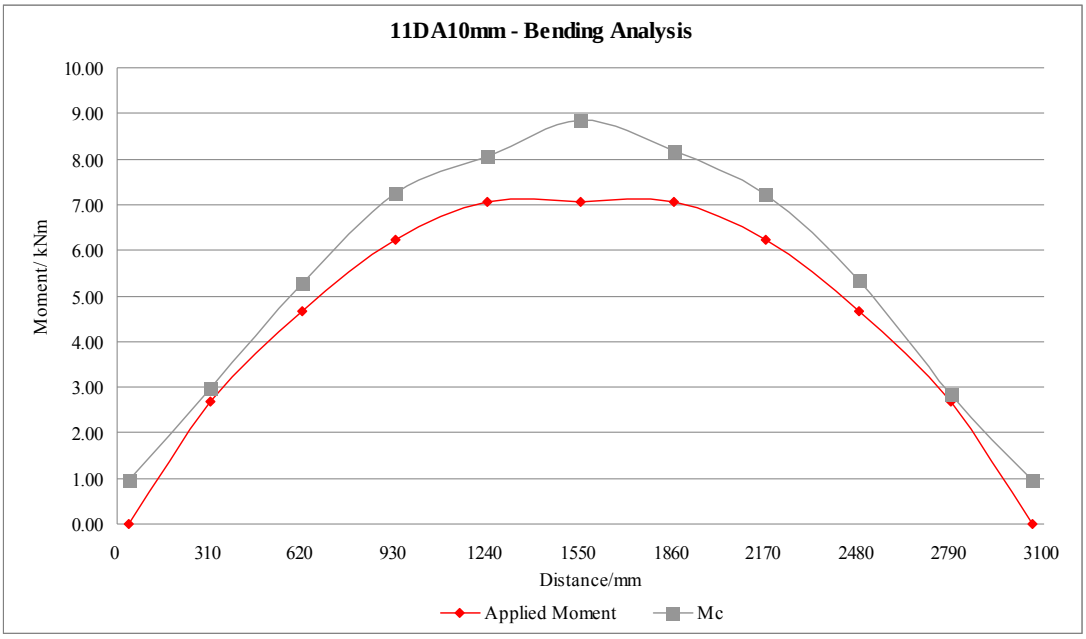

Figure 6-19 Bending Moment Graph for 11DA10mm

At 310mm and 2790mm from the left hand reactions the applied moments are very close to the moment capacities of the sections. The applied moment is 2.7 kNm and the capacity of the section is 2.8 kNm. Thus the applied moment is about 95% of the capacity of the section. The actual failure occurred at 2745mm point from the right hand side support (please refer to the x-axis of the graph) and thus it is considered that the section has failed by the rebar yielding at the section. This result confirms that the additional anchorage has successfully prevented the crushing of concrete around the anchorage zone, and increased the ultimate load of the beam, which later failed by rebar yielding due to the bending.

6.2.2.3 Shear Compression Failure of 22SA10mm

Figure 6-20 shows the failed section of 22SA10mm. Again, vertical bending cracks are present at the front elevation of the beam which turns into diagonal shear crack

about the location of rebar. Another diagonal shear crack is seen on the rear elevation. The picture of top of the beam shows crushed concrete parts from the shear failure.

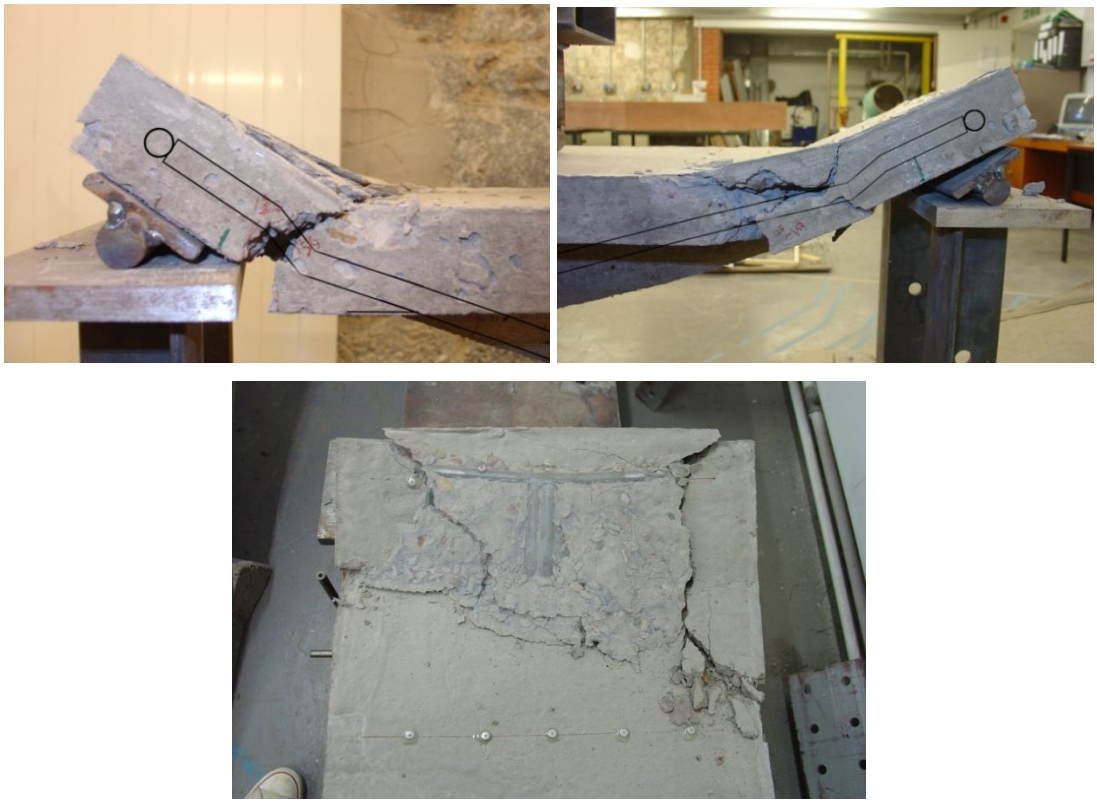

Figure 6-20: Beam 22SA10mm at failure; top surface (bottom), front side (left) and rear side (right)

Despite the obvious shear cracks, the bending capacity of the failed section also low due to its shallow effective depth. The following bending moment diagram (Figure 6-21) indicates that the beam is close to bending failure.

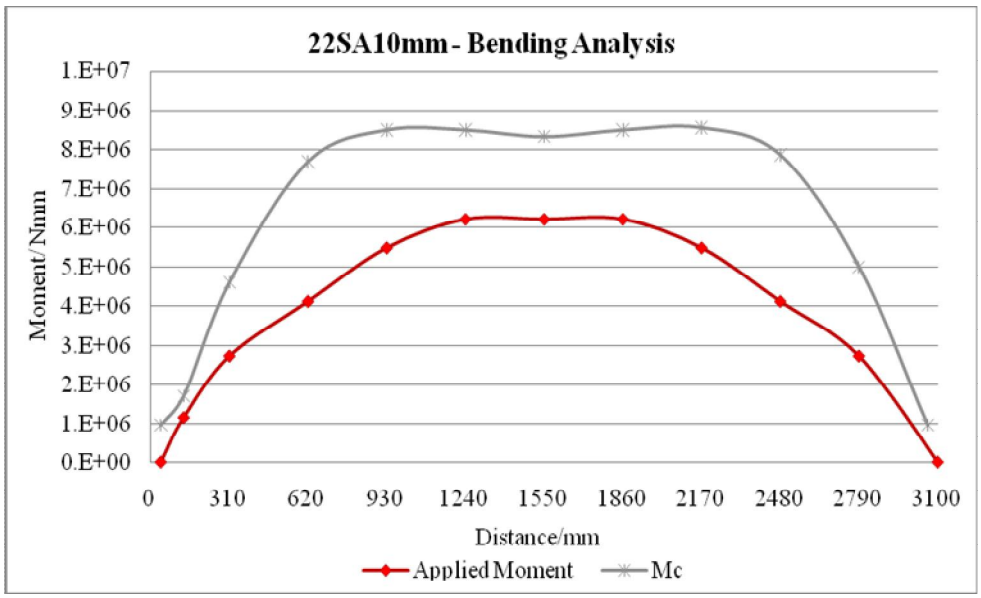

Figure 6-21: Bending Moment Graph for 22SA10mm

The moment capacity of the failed section is 1.7kNm and the applied moment is 1.14kNm; this is 67% of the section capacity. Thus it is unlikely that the beam had failed in bending.

After the test the crushed concrete fragments are removed for closer investigation (Figure 6-22). When the concrete was crushed and lost its compression capacity, the beam was separated into two parts.

Figure 6-22: Showing the crushed concrete around the rotated rebar

Part A was sitting on the support and Part B was held up by the rebar which connected to Part A. The weight of Part B (which is the most part of the beam) caused the rebar to bend (Figure 6-23).

Figure 6-23: Showing the deformation of reinforcements due to the bending

It is initially suspected that the section has a shear contribution by the dowel action of the rebar; however, this is considered unlikely based on the fact that the section is too shallow to see such a large dowel deformation of the steel without the prior crushing of concrete. Also it is considered that such deformation of the rebar is caused after the crushing of concrete.

The above observations show that 11DA10mm and 22SA10mm are likely to be failed by the rebar yielding and shear compression respectively.

To recall, 11DA-WS10mm is the same design as 11DA10mm except it does not include the compression steel mesh.

11DA-WS10mm failed at 10.98kN, which is 43.29% less than the ultimate load of 11DA10mm, and the failure mode was shear compression. Please refer to the following pictures (Figure 6-24 and 6-25) of the failed section of 11DA-WS10mm.

Figure 6-24: 11DA-WS10mm at failure: Front (left) and Rear (right)

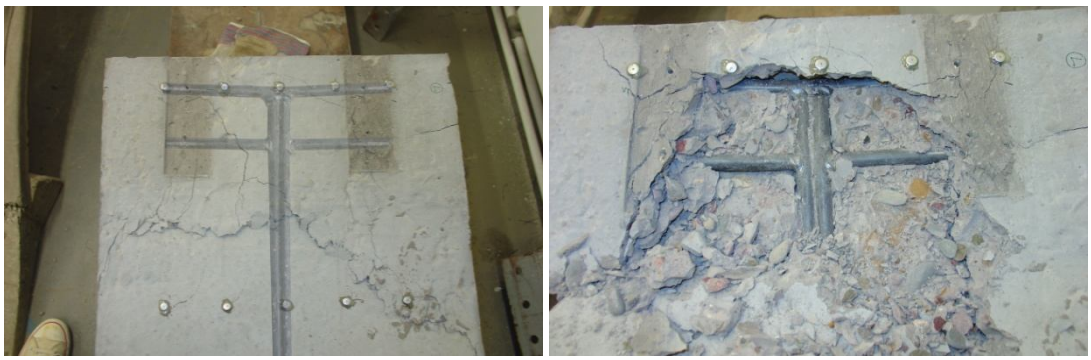

Figure 6-25: Beam 11DA-WS10mm at failure (left) and after the concrete layer is removed (right)

This result proves that the absence of the compression steel mesh caused the early shear compression failure of the beam. In other words, 11DA10mm resist greater shear load as its compression capacity has increased with the presence of the steel mesh. Thus the shear capacity of the section increases with the capacity of the concrete in compression. A similar conclusion is stated in the paper 'Behaviour of reinforced concrete T-beams in shear' by M. D. Kotsovos, J. Bobrowski, and Prof. J. Eibl (KOTSOVOS, M. D., Babrowski, J., Prof. Eibl, J., 1987),

> *'…the shear capacity of reinforced concrete beams is associated with the region of the path along which the compressive force is transmitted to the supports rather than the region of the beam below the neutral axis…'.*

6.2.3 Design Proposal – based on the results of 22SA10mm and 11DA10mm

11DA10mm failed due to rebar yielding at a section close to the support, and there

was an excess of bending capacity at the mid-span (Figure 6-19). The intention is to make the rebar to yield at the mid-span, and thus the effective depth at the failed section should be increased. Initially it was considered to increase the depth of the web as to increase the effective depth. However the modified geometry of the web will be similar to that of 22SA10mm. Thus it is decided to increase the flange depth instead.

22SA10mm failed due to compression shear stress at a section close to the support. Since the rebar capacity of the section is related to the compression capacity of the section above the neutral axis, it is decided to increase the thickness of the flange.

It must be remembered that the other design specification of the beams should remain unchanged. Thus it can be known that any different results are specifically due to the design modifications.

6.3 Design and Development 2: The Parabolic Flange

6.3.1 Concept Design

Two designs have been prepared based on the above proposals. The main modification made to the designs is the depth of the flange.

With respect to the bending failure of 11DA10mm, the effective depth at the failed section was 65mm at 360mm from the supports. To increase the bending capacity twice the effective depth would be 130mm and thus the resultant flange depth becomes 105mm.

With respect to the shear failure of 22SA10mm, the effective depth at the failed section was measured as 35mm at 127.5mm from the support, which is close to the actual depth of the flange, 40mm. Thus it was decided to double the depth of flange and increase the shear capacity.

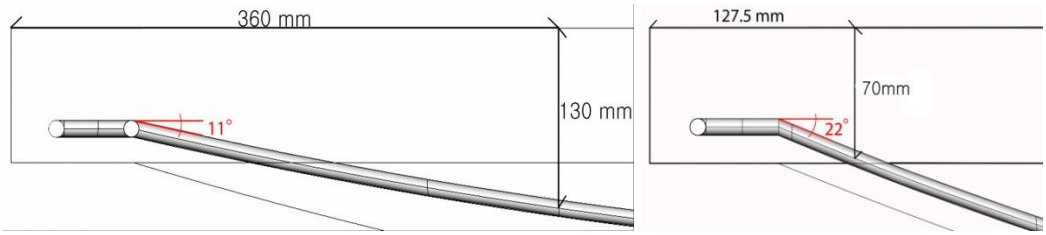

Figure 6-26: Reinforcement Type A: Reinforcements angle at 22°, single anchorage, and cover length below the anchorage is kept constant.

Eventually it was decided to change the flange depth of 11DA10mm also to 80mm for the following reasons:

- Having the same depth between two beams, the same formwork can be used for the construction of the other beam type. Again less material and less time are consumed in the formwork construction.
- Increasing the depth of flange to 80mm will increase the effective depth to 105mm at the failed location. This is about 62% increase from the initial 65mm effective depth. The section of 11DA10mm failed because the ultimate moment of the section had been reached and the reinforcement yielded. Moment capacity is proportional to the effective depth of the section. Thus the 62% increase of the effective depth will theoretically increase the moment capacity of the section by the same amount, and this increase is sufficient enough to prevent the section from early bending failure.
- 105mm deep flange requires more concrete than 80mm deep flange.

Thus both designs have the flange that has 80mm thickness near the supports, which has been doubled from 40mm, and at the mid-span the flange depth has been kept the same as before at 40mm. These designs have been named as 11DADF10mm and 22SADF10mm.

The next design consideration is in regard to the location where the 80mm thick flange starts to curve up towards the 40mm thick flange at the mid-span. For 22SA10mm the 80mm thickness should be maintained at least to the location where the initial failure occurred, and the location coincides with where the rebar in the flange enters the web. Thus it is decided that for both beams the 80mm thickness of the flange will continue to the point that the rebar enters the web. Also, in order to make the flange more form-efficient, the curve is designed to be a parabola.

The beam developed from 11DA10mm is named 11DADF10mm and the beam developed from 22SA10mm is named 22SADF10mm.

The following diagram shows the concept design of the beams (Figure 6-27). The first beam is 11DADF10mm and the second beam is 22SADF10mm.

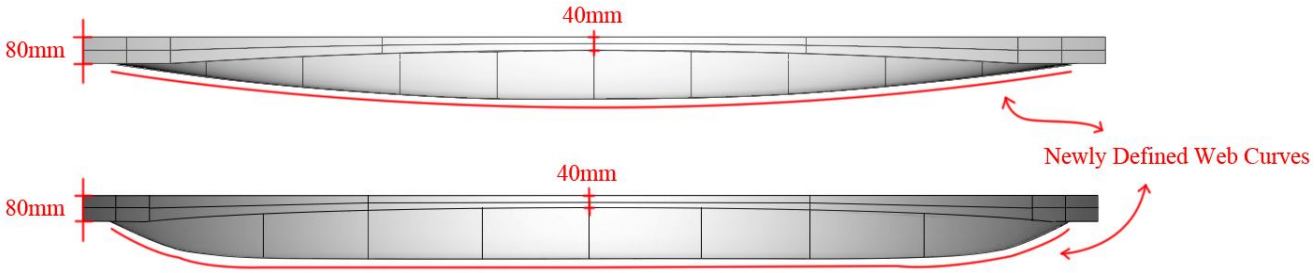

Figure 6-27: Concept Design of the Beams, 11DADF10mm and 22SADF10mm

6.3.2 Discussion of Experiment Result

6.3.2.1 General Discussions

Design Development Number	Beam	Ultimate Load/ kN	Failure Mode	Location/ mm
1	11DA10mm	19.36	Rebar Yielding	360mm from the support
	22SA10mm	17.00	Shear Compression	Near the support
	11DA-WS10mm	10.98	Shear Compression	Near the support
2	11DADF10mm	21.34	Rebar Yielding	Mid-Span
	22SADF10mm	23.83	Rebar Yielding	Mid-Span

Table 6-2: Summary of Test Results

Table 6-2 shows that the ultimate capacity of both beams increased; 11DADF10mm failed at 21.34kN, which is increased by 10.2%, and 22SADF10mm failed at 23.83kN, which is increased by 40.2%. The most interesting thing is that both beams failed by rebar yielding at the mid-span. It has already been mentioned in the earlier chapter that such type of failure is the most preferred for reinforced concrete beam. The following picture shows the bending crack distribution of the beams.

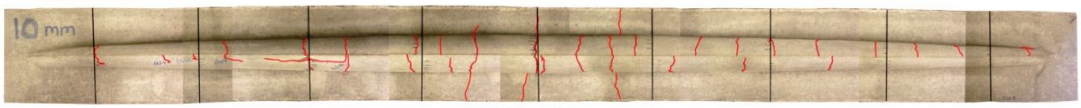

22SADF 10mm

11DADF 10mm

Figure 6-28: The Crack Distribution of the Tested Beams

For 11DADF10mm the last cracks located at each end of the beams are diagonal shear cracks, and it is likely that the beam would have failed by shear if the rebar yielding at the mid-span had not occurred at the ultimate load.

6.3.2.2 Bending Tension (rebar yielding) Failure of 11DADF10mm and 22SADF10mm

Figure 6-29 and 6-30 compare the moment capacity of the beams with the applied moment. Both graph show that the moment capacities of the sections near the mid-span have been reached by the applied moments.

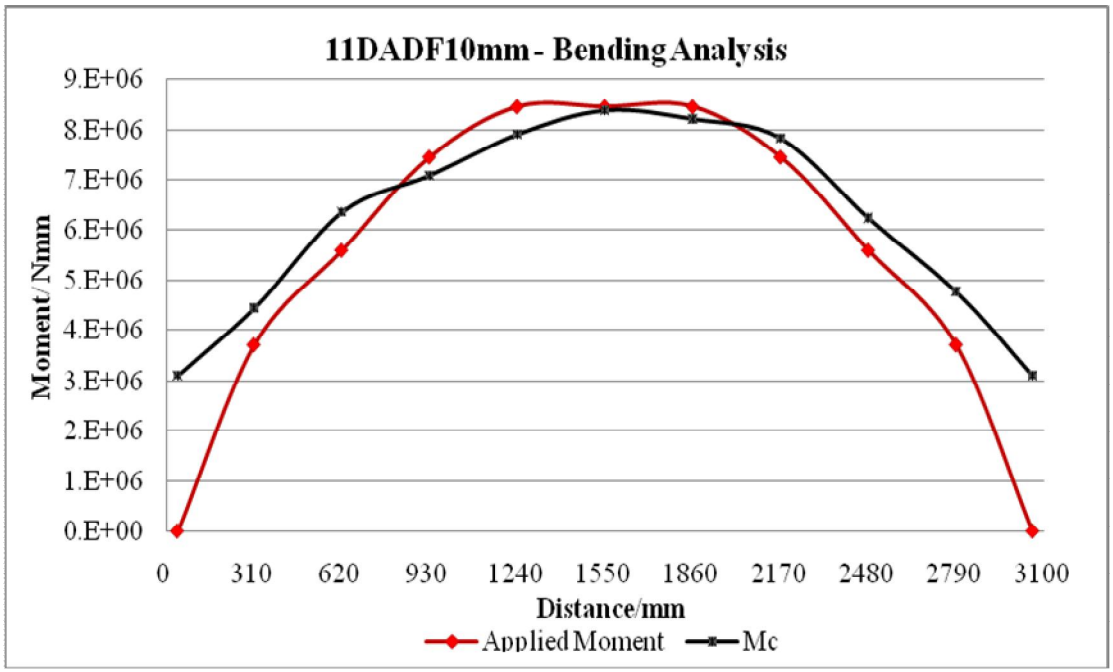

Figure 6-29: Bending Graph of 11DADF10mm

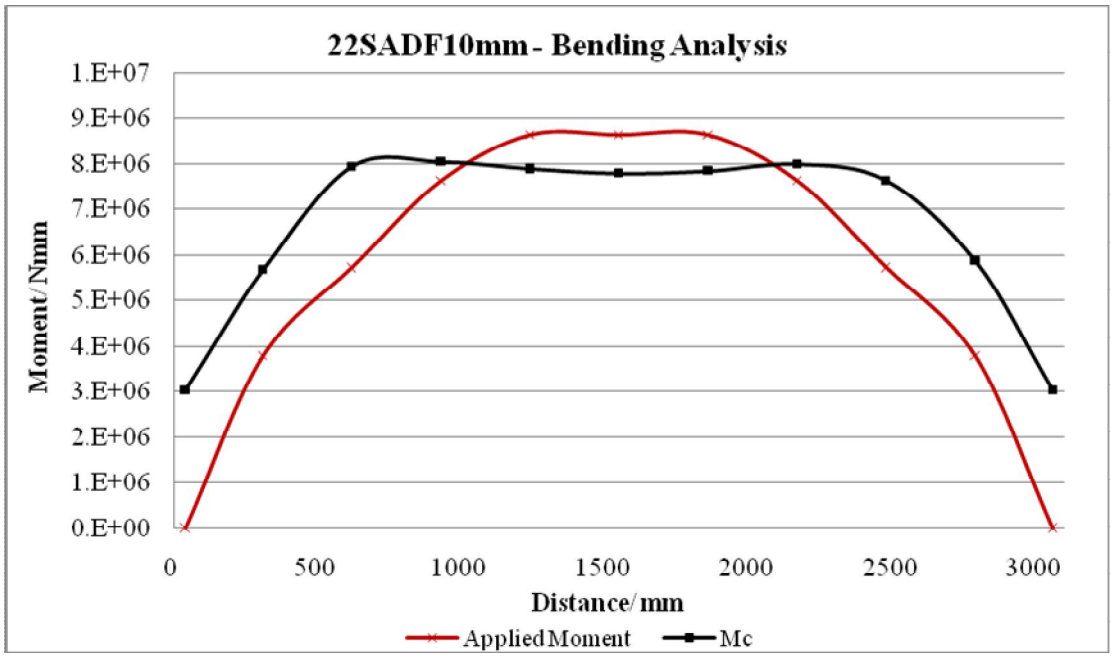

Figure 6-30: Bending Graph of 22SADF10mm

The following graph (Figure 6-31) shows the tensile strain readings of the rebar measured with electrical strain gauges.

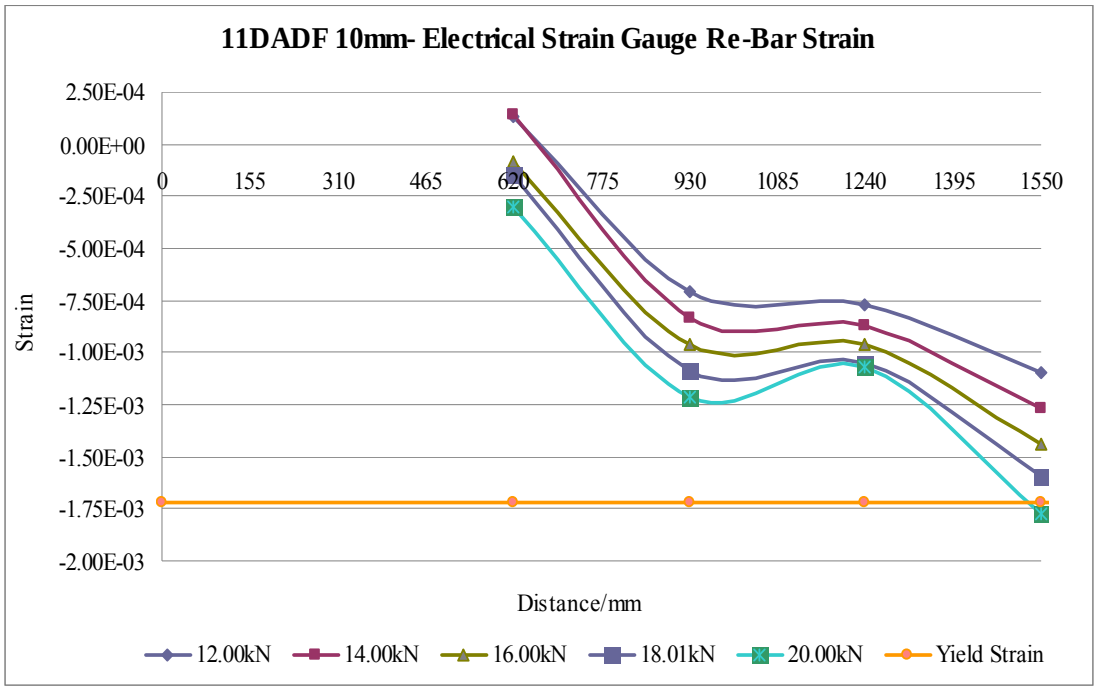

Figure 6-31: Tension Strain of Rebar

The above graph clearly shows that at the mid-span the rebar strain has reached its yield strain, 0.00172 (please refer to the Table 4-4). Thus these results confirm that 11DADF10mm failed by mid-span rebar yielding.

The above beams did not show any signs of concrete failure in the anchorage zone. Again the Strut-and-Tie model is used to examine the compressive stress;

The reaction force R1 for 11DADF10mm = (21340N + 351.69N + (125.37N*2))/2 = 10971.17N

*Please note that 351.69N and 125.37*2N are the weight of the load transfer units. Please refer to the figure 5-1 of the test rig set up

The reaction force R2 for 22SADF10mm = (23830N + 351.69N + (125.37N*2))/2 = 12216.22N

The angles for 11DADF10mm = 11 degree,

and for 22SADF10mm= 22 degrees

Therefore, the total compressive force applied at the anchorages at the failure load is,

10971.17/ tan 11 = 56441.78 N for 11DADF10mm and,

12216.22/tan 22 = 30236.19 N for 22SADF10mm

Total surface area of anchorages of which the concrete is compressed by is,

((200-20)*10) * 2= 3600 mm^2 for 11DADF10mm and,

((200-20)*10) = 1800 mm^2 for 22SADF10mm

Thus, the total axial compressive stress applied to concrete by the anchorages is,

56441.78/3600 = 15.68 N/mm^2 for 11DADF10mm and,

30236.19/1800 = 16.80 N/mm^2 for 22SADF10mm

From the concrete cube test results, the average compressive strength of concrete is obtained;

The ultimate compressive strength of concrete is,

32.70N/mm^2 * 0.8= 26.16N/mm^2; which is the equivalent cylinder strength for 11DADF10mm and,

27.45N/mm^2 * 0.8= 21.96N/mm^2; which is the equivalent cylinder strength for 22SADF10mm.

Thus the compression strengths of concrete are greater than the applied compressive stresses from the anchorage and the bending.

It is to state again that the cylinder strength does not reflect the true strength of concrete in the beam. However, it is still a good indication to use since the actual uni-axial compression strength of the concrete inside the beam tends to be greater than the cylinder strength, owning to its tri-axial stress state of the concrete inside the beam. Thus when the applied stress is less than the cylinder strength it also satisfies that the applied stress is less than the actual concrete strength inside the beam.

6.3.3 Design Proposal – based on the results of 11DADF10mm and 22SADF10mm

Based on the results the above forms have proven its capability of having the mid-span bending tension failure, though signs of imminent shear failure were evident.

This is the first time to see the fabric formed beams failed at the mid-span. However it is interesting to consider further improvements in the efficiency of the form. Thus, for the next investigation the efficiency of form will be further tested with increased steel area.

6.4 Design and Development 3: Steel Ratio – 1

6.4.1 Concept Design

Two beams were constructed. Their forms are identical with 11DADF10mm and 22SADF10mm; however the percentage of steel has been increased. The beams now

have two steel bars of 12mm diameter. Thus the amount of steel has been increased by 44% for both beams. They are named as 11DADF12mm and 22SADF12mm.

6.4.2 Discussion of Experiment Result

6.4.2.1 General Discussions

Design Development Number	Beam	Ultimate Load (kN)	Load increase from the initial design (%)	Failure Mode	Location (mm)
2	11DADF10mm	21.34	-	Rebar Yielding	Mid-Span
	22SADF10mm	23.83	-	Rebar Yielding	Mid-Span
3	11DADF12mm	26.00	21.84	Shear Tension	310mm~400mm from support
	22SADF12mm	33.94	42.26	Rebar Yielding	Mid-Span

Table 6-3: Summary of Test Results

The ultimate load of both beams has been increased. The experiment result shows that the ultimate load of 11DADF12mm is 26kN which is 21.8% increase from 11DADF10mm, and for 22SADF12mm the ultimate load is 33.9kN which is 42.3% (, which is almost proportional to the increase in the reinforcement area, 44%) increase from 22SADF10mm. According to these results 22SADF12mm sustained about 30% more load than 11DADF12mm. This is due to the early shear tension failure of 11DADF12mm which shows the limit of the form's efficiency. In contrast, 22SADF12mm again fails at the mid-span by the rebar yielding. However, it is interesting to note that the shear failure of 11DADF12mm occurred in a ductile manner without sudden failure. After the ultimate load, the load is applied further which only caused the steel to elongate further in a ductile manner. Typically in shear failure the beam is no longer able to sustain load.

6.4.2.2. Shear Tension Failure of 11DADF12mm

Figure 6-32 below shows the failed section of 11DADF12mm. There is a clear diagonal shear crack starting at the bottom of the web and inclining towards the top of the flange. Also the longitudinal bond failure crack (due to the dowel shear stress) is found along the line of the rebar (please refer to Figure D3-2). The bond crack continues until the anchorage location. Such shear and bond failure cracks are often seen in rectangular section beams.

Figure 6-32: Showing the crack pattern of 11DADF12mm at the failure load

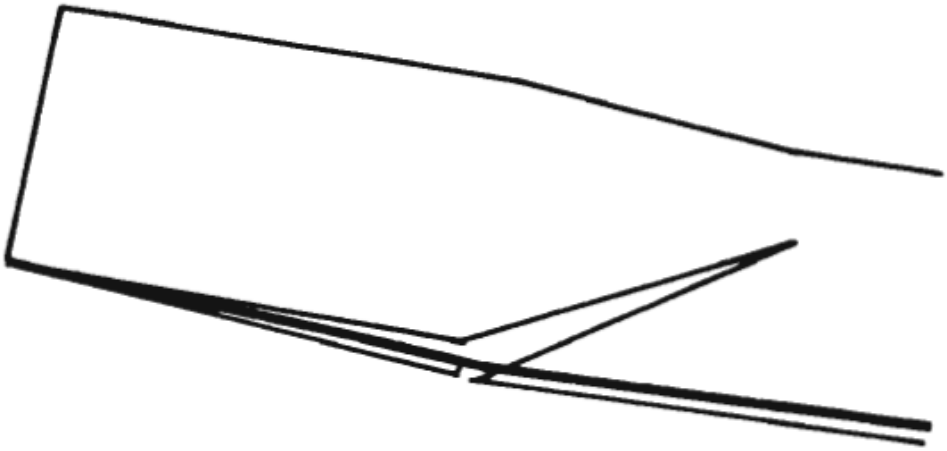

Figure 6-33: Schematic representation of bond failure due to opening of inclined crack (KOTSOVOS, M. D., Babrowski, J., Prof. Eibl, J., 1987)

When the bond failure crack is formed the part of the flange above the crack is prone to move away from the web. After the crack is fully developed the rotation of the flange is only resisted by the concrete in compression and the rebar in tension. As the applied load increases the rotation of the flange about the un-cracked section becomes greater, and thus the tension stress in the rebar also increases. Eventually the rebar yields and ductile shear tension failure takes place.

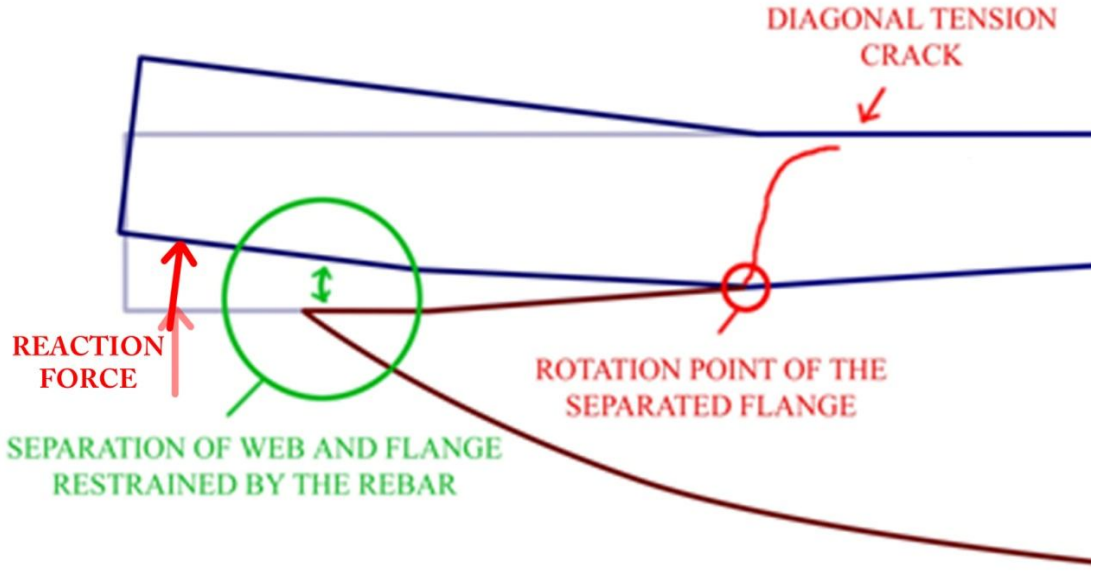

Figure 6-34: The behaviour of flange after the separation from web

The following pictures (Figure 6-35 and 6-36) shows the crack formed at the bottom of the flange due to tension stress of rebar which pulls out anchorage embedded in the flange.

Figure 6-35: Crack formed due to the pull of force by the rebar

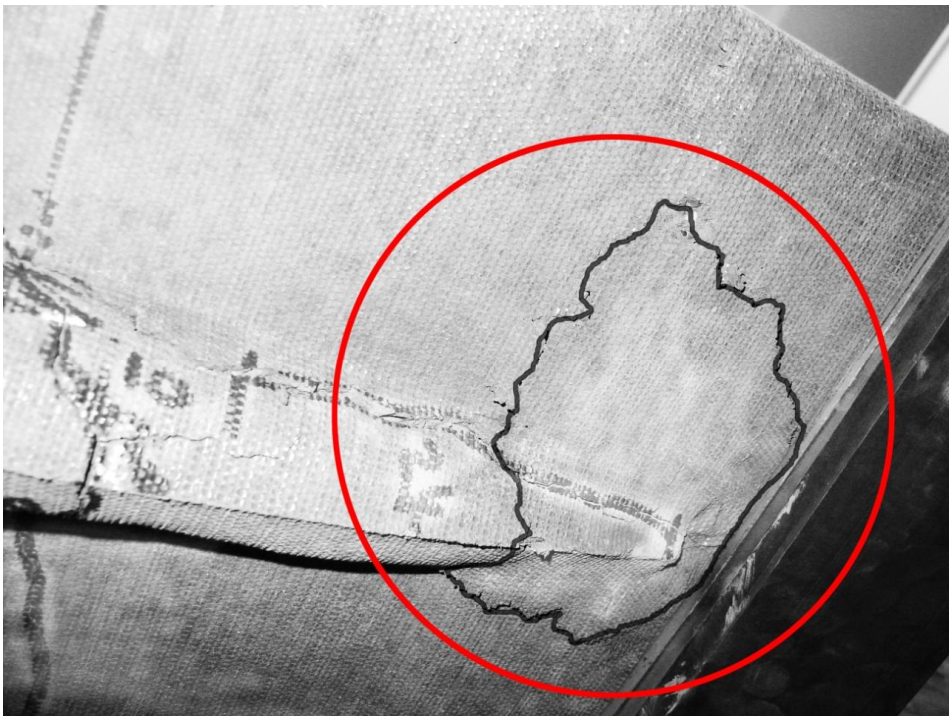

Figure 6-36: Crack formed due to the pull of force by the rebar

After the experiment the concrete fragments around the anchorage are partly taken off for further exploration. It is found that the inner anchorage has been disconnected from the rebar and thus only one of the two anchorages was solely the tensile force in the reinforcement.

Figure 6-37: Showing the bent anchorage and crushed concrete near support

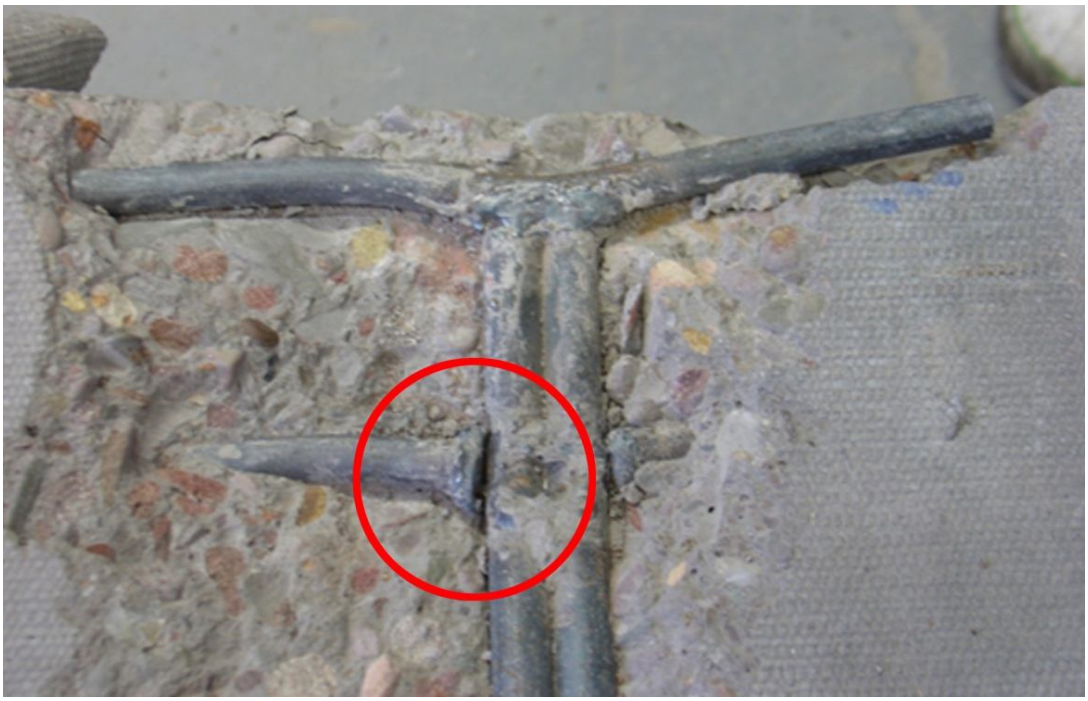

Figure 6-38: Disconnection of inner anchorage

To check the anchorage compression stress the following calculation has been carried out:

The reaction force R1 = (13000N + 351.69N + (125.37N*2))/2 = 6800N

The angle, a = 11 degrees

Therefore, the total compressive force applied by the pulled in anchorages to the concrete (thus the total resistance force applied by concrete) at the failure load is,

6800/ tan 11 = 35000 N

Total surface area of anchorages of which the concrete is compressed by is,

((200-20)*10) = 1800 mm^2

Thus, the total axial compressive stress applied to concrete by the anchorages is,

35000/1800 = <u>19 N/mm^2</u>

From the concrete cube test results, average compression strength of concrete is obtained;

The ultimate compressive strength of concrete is,

28.94N/mm^2 * 0.8 = <u>23N/mm^2</u>; which is the equivalent cylinder strength.

This value is 21% larger than the anchorage compressive stress.

6.4.2.3 Bending Failure of 22SADF12mm

To recall the ultimate load of 22SADF12mm is 33.94kN; this is about 42% more than the ultimate load of 22SADF10mm. 22SADF12mm has about 44% more steel than 22SADF10mm and thus the ultimate load is directly proportional to the area of steel. This implies that the cause of the failure may be yielding of steel at mid-span. The beam experienced a lot of vertical cracks near the mid-span, and at the failure load these cracks opened widely. Based on this observation it is considered that the beam failed due to the rebar yielding at the mid-span. The following graph is plotted to compare the bending capacities with the applied moments. Figure 6-39 shows that the applied moment exceeds the capacities of the section about the mid-span.

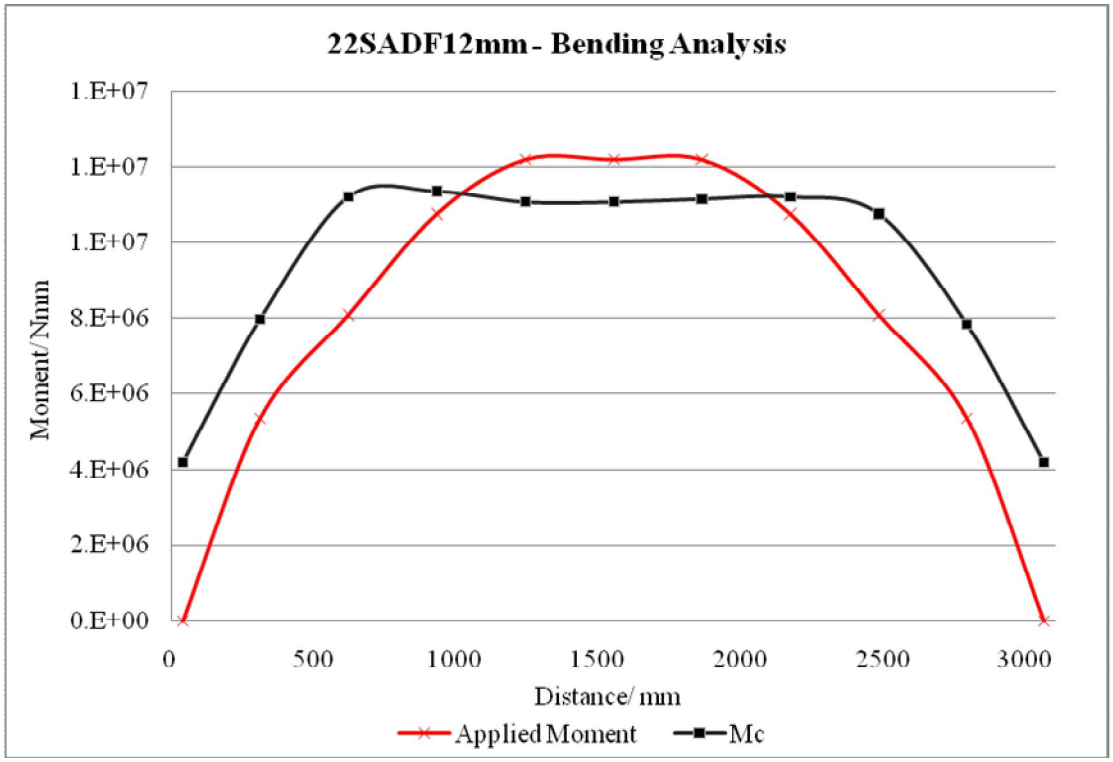

Figure 6-39: Bending Graph of 22SADF12mm

Figure 6-40 shows 22SADF10mm and 22SADF12mm after the tests. More vertical bending cracks are present in 22SADF12mm as the beam sustained greater bending stress than 22SADF10mm. The crack spacing in 22SADF12mm is closer than 22SADF10mm due to higher steel content. Also to note that the beams are exactly the same in form but due to the high load of 22SADF12mm the diagonal shear cracks started to form near the supports.

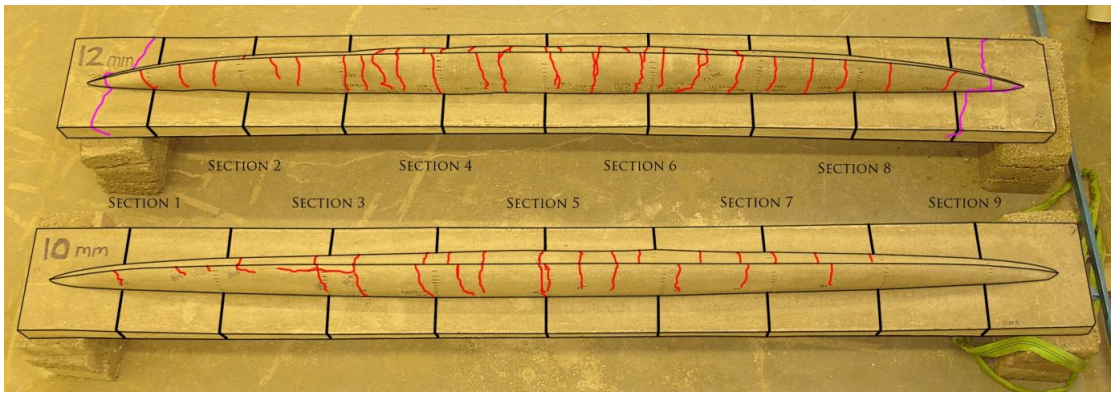

Figure 6-40: Comparing the cracks of 22SADF10mm and 22SADF12mm

Again beyond the ultimate load the central deflection increased rapidly and the vertical cracks near the mid span were opening up in excess. Near the ultimate load the shear cracks reached very close to the top of the flange.

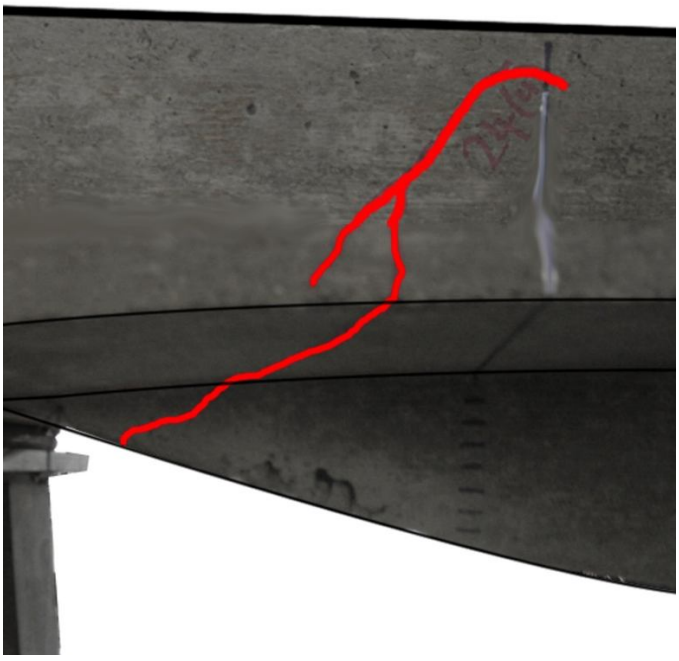

Figure 6-41: Diagonal Shear Crack near the support of 22SADF12mm

It is suspected that 22SADF12mm may have been closer to shear failure at where the diagonal tension cracks have been located; however, there was sufficient strength to ensure that bending failure at mid-span occurred. Again the beam did not show any signs of concrete crushing near the anchorage area. The following calculation is carried out to check the compressive stress incurred by the anchorage based on the strut-tie model.

The reaction force R1 = (33900N + 351.69N + (125.37N*2))/2 = 17251.22N

The angle, a = 22 degrees

Therefore, the total compressive force applied by the pulled in anchorages to the concrete (thus the total resistance force applied by concrete) at the failure load is,

17251.22/ tan 22 = 42698.27 N

Total surface area of anchorages of which the concrete is compressed by is,

((200-20)*10) = 1800 mm^2

Thus, the total axial compressive stress applied to concrete by the anchorages is,

42698.27/1800 = <u>23.72 N/mm^2</u>

From the concrete cube test results, average compression strength of concrete is obtained;

The ultimate compressive strength of concrete is,

26.78N/mm^2 * 0.8 = <u>21.42N/mm^2</u>; which is the equivalent cylinder strength. This value is less than the applied compression stress of the anchorage.

According to the above analysis the concrete adjacent to the anchorage the stresses in compression under the anchorage are greater than the uni-axial compressive strength although crushing did not occur. One reason for such results is that the capacity of the concrete is measured in uni-axial stress condition; however the actual concrete inside the beam is in tri-axial stress condition. Thus the actual compression capacity of the concrete in the beam is higher than the measured capacity. Later a more detailed stress analysis is carried out using the finite element models (please refer to chapter 10) of the anchorage zone, and it is found that the induced compression is not the sole reason to cause the failure of the concrete, but it is also to do with the transverse tension stress generated at perpendicular to the direction of the anchorage stress. In the finite element analysis, the two beams which failed by the anchorage stress (11SA10mm and 11SA12mm) are analysed and compared with the beams of two anchorages and increased rebar angle. It is found that, in the models of the beams that failed by the anchorage compression stress the transverse tension stress spreads over the large area of the flange's top surface. However, in models with two anchorages or of the rebar with increased angle the transverse tension stress does not reach to the top of the flange. Anchorage in 80mm thick flange is also analysed and again the transverse tension stress does not reach to the top of the flange due to the excess concrete around it. Thus as long as the anchorage compression stress is

smaller than the tri-axial compression capacity of concrete, or the flange is thick enough so that the transverse tension stress does not spread over the entire depth then, the section would not crush to failure.

6.4.3 Design Proposal – based on the results of 11DADF 12mm and 22SADF 12mm

Though 11DADF12mm failed prematurely by shear 22SADF12mm successfully sustained the full load and failed by the rebar yielding. Thus the next step is to further test the form of 22SADF12mm with higher steel content as to apply greater load.

6.5 Design and Development 4: Steel Ratio – 2

6.5.1 Concept Design

22SADF12mm experienced diagonal shear cracks near the supports and it is suspected that 22SADF12mm was not far from failing by shear, and it is considered worthwhile to find the point where the beam is on the state where it is likely to fail either by either bending or shear. Thus it was decided to increase the steel ratio by only a very slight amount (three of 10mm diameter rebars, which will give only 4.3% increase) to see the possible shear failure.

Beam 22SADF3no12mm was also constructed increasing the steel area by 50% over 22SADF 12mm.

6.5.2 Discussion of Experiment Result

6.5.2.1. General Discussions

Design Development Number	Beam	Ultimate Load (kN)	Load increase from the initial design (%)	Failure Mode	Location (mm)
3	11DADF12mm	26.00	-	Shear Tension	310mm~400mm from support
	22SADF12mm	33.90	-	Rebar Yielding	Mid-Span
4	22SADF3no10mm	32.00	None	Rebar Yielding	Mid-Span
	22SADF3no12mm	32.26	None	Shear Tension	310mm~400mm from support

Table 6-4: Summary of Test Results for 22SADF3no10mm and 22SADF3no12mm

The ultimate loads of the two tested beams have not increased at all, and both failed around the same load as of 22SADF12mm.

22SADF3no10mm did not fail by shear as predicted and failed by the mid-span rebar yielding. However the predicted shear (tension) failure incurred for 22SADF3no12mm near a support, at about the same load as for 22SADF12mm. Again the failure occurred in a very ductile manner, and there was not sudden movement of the section during the failure.

The above results can draw very interesting point about the form of the following beams:

- 22SADF12mm
- 22SADF3no10mm
- 22SADF3no12mm

Please refer to the following summary notes:

- The beams have the identical form.
- The only difference of the beams is the amount of steel
- The beams with less steel (22SADF12mm and 22SADF3no10mm) failed by bending
- The beams with more steel (22SADF3no12mm) failed by shear, however still at the same load as the other beams with less steel

Based on the above key points the following conclusions are drawn:

1. Increase of the steel content did not increase the shear capacity. Otherwise 22SADF3no12mm would have not failed by shear at the same load as the other two beams of less steel.
2. The three beams have identical form, and the amount of steel has little effect on the shear capacity of the beam. This means that the shear capacity of the three beams is similar.
3. Thus, in fact, the induced shear stress and bending stress in 22SADF3no10mm and 22SADF12mm were both very close to the sections' capacities. However, in the particular cases the stress in the rebar reached the yield point prior to the possible shear failure near a support.
4. Another point to add is in regard with the effect of compressive capacity of the concrete on the shear tension failure of the beam. Based on the Compressive Force Path theory, which states that the compressive zone is the main contributor to the shear capacity of the beam, it is thought that there might be a relationship between the compressive strength of the concrete and the shear tension failure mode. Table 6.5 is presented for comparison.

Beam	Failure Mode	Ultimate Load (kN)	Cube Strength (N/mm^2)
22SADF12mm	Mid Span Rebar Yielding	33.94	26.78
22SADF3no10mm	Mid Span Rebar Yielding	32.00	32.7
22SADF3no12mm	Shear Tension	32.26	28.94

Table 6-5: Comparing the ultimate loads and the cube strengths

The table shows that 22SADF3no12mm failed by shear and it had a lower compressive strength than 22SADF3no10mm, which failed by the mid-span

rebar yielding. However, the compression strength of 22SADF3no12mm is still higher than of 22SADF12mm, which failed by the mid-span rebar yielding. Thus based on the above observation at this point no particular relationship is found between the compression strength of the concrete and the failure mode of the beams.

6.5.2.2 Bending Tension (rebar yielding) Failure of 22SADF3no10mm

Figure 6-42: 22SADF3no10mm at failure load

The following graph (Figure 6-43) compares the applied moments with the capacties of the sections. The curves touch at the mid-span, indicating rebar yield failure of the beam.

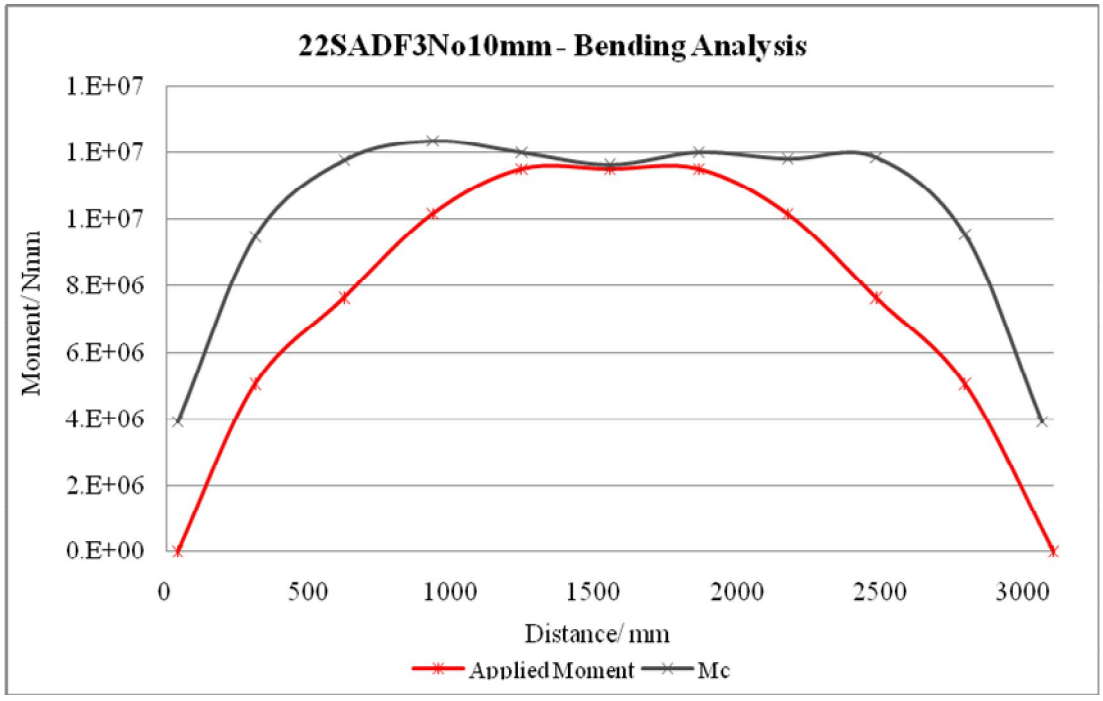

Figure 6-43: Bending Graph of 22SADF3no10mm

Near the ultimate load, the vertical bending crack close to the support has become a diagonal shear crack. Again the crack has moved far up, and the crack is turning into a diagonal shear crack (Figure 6-44).

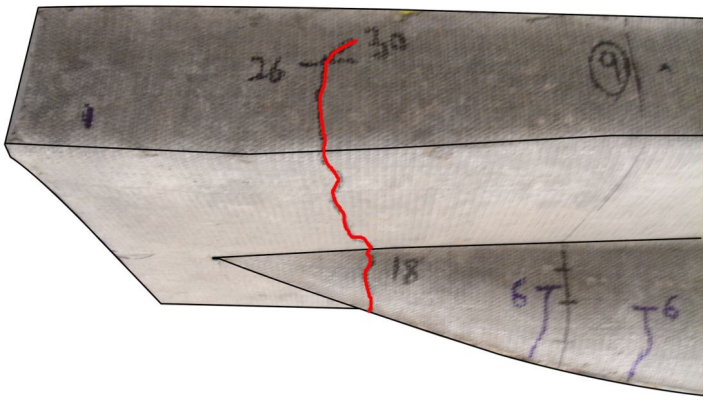

Figure 6-44: Showing vertical bending crack becoming diagonal shear crack-22SADF3no10mm

6.5.2.3 Shear Tension Failure of 22SADF3no12mm

The following pictures (Figure 6-45) show the failed section of the beam. The diagonal tension crack indicates incipient shear failure the section has failed by shear. Again the crack pattern close to the anchorage indicates the pull out stress applied by rebar. Such crack pattern was also noted from the test result of 11DADF12mm.

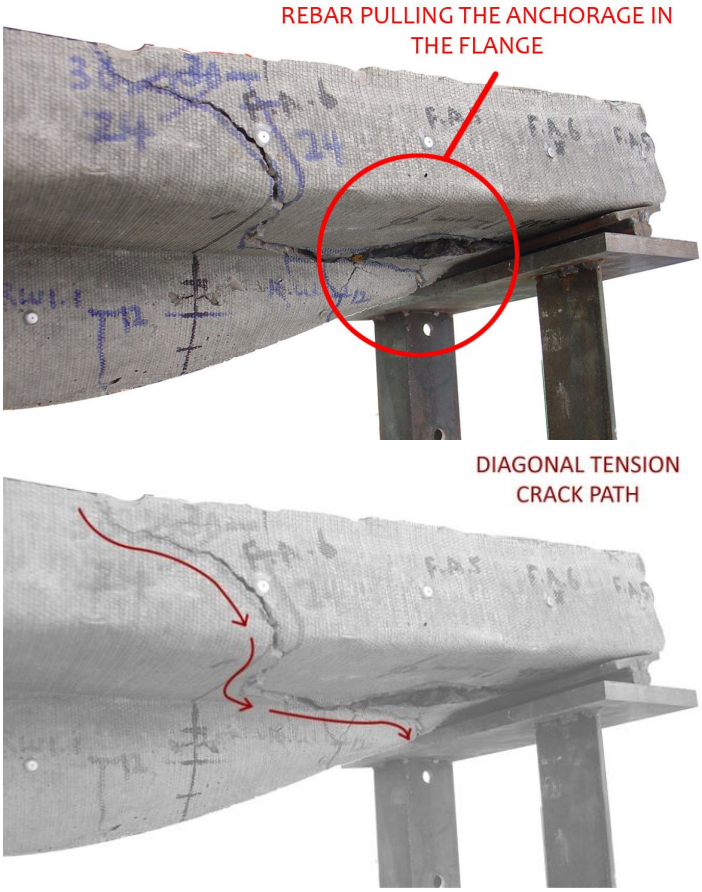

Figure 6-45: Showing the diagonal tension crack of 22SADF-3no-12mm

The following pictures (Figure 6-46) show the cracks about the failed section.

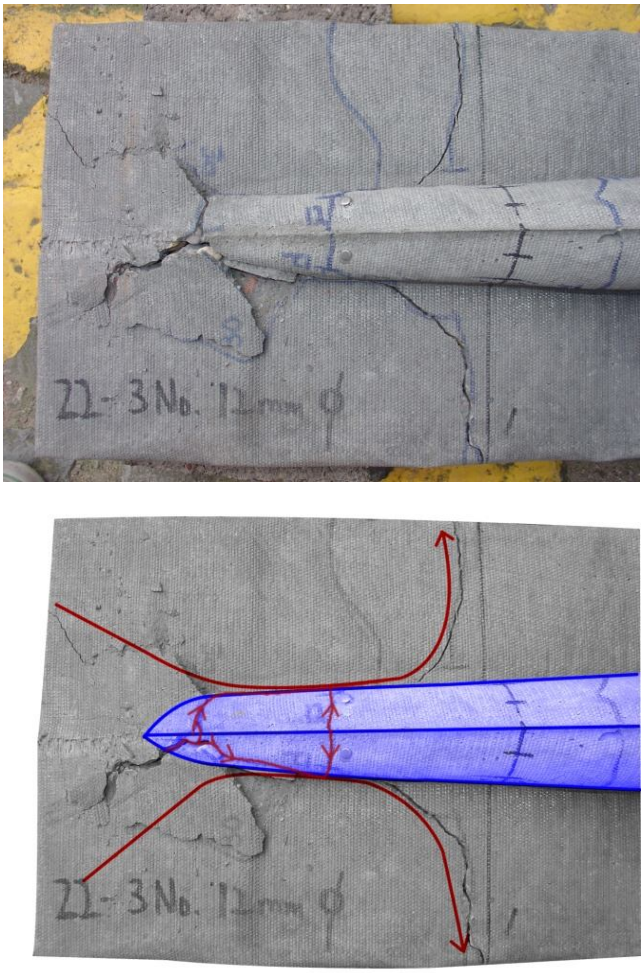

Figure 6-46: Showing the crack pattern near the end of web of 22SADF-3no-12mm

The picture shows the shear crack moving along the outline of the web, and gradually curving into the flange. It is considered that the crack describes the existence of the horizontal shear stress existing at the interface of flange and web (Figure 6-47).

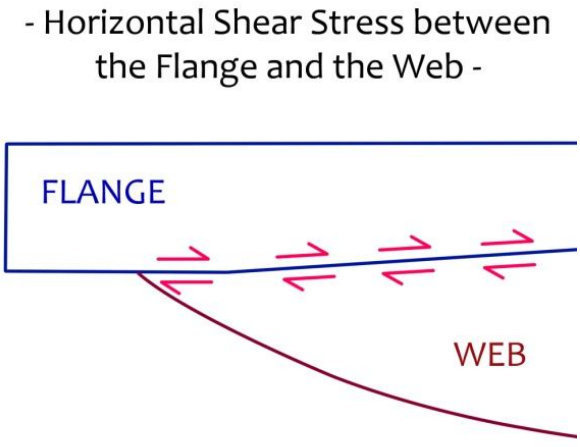

Figure 6-47: Horizontal Shear Stress at the interface of the Flange and the Web

Due to the specific profile of the beam the horizontal shear stress is relatively hight towards the support as the interface surface between the flange and the web decreases. Later this horizontal stress is accompanied with the dowel action (, which results the bond failure crack as mentioned for 11DADF12mm) and causes the separation of flange and web. After the separation the section's stiffness is reduced significantly and becomes more prone to fail by the shear (Figure 6-48 and Figure 6-49).

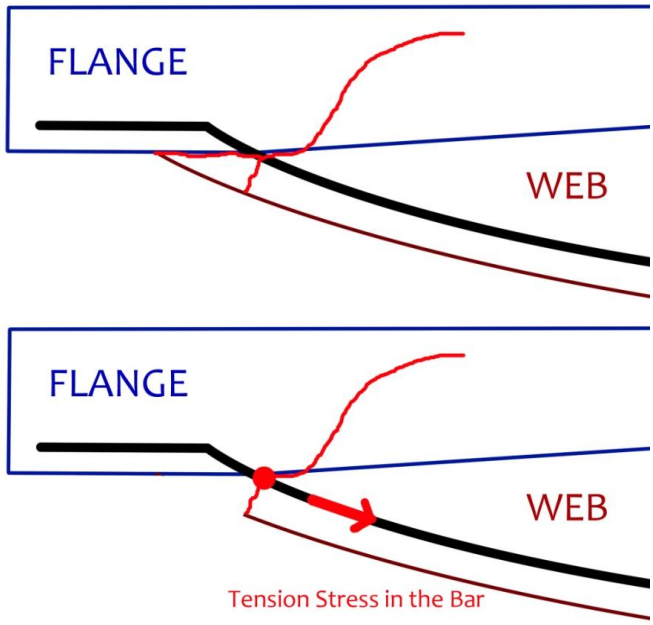

Figure 6-48: After the horizontal crack is fully developed the flange section loses stiffness and becomes more prone to the shear failure

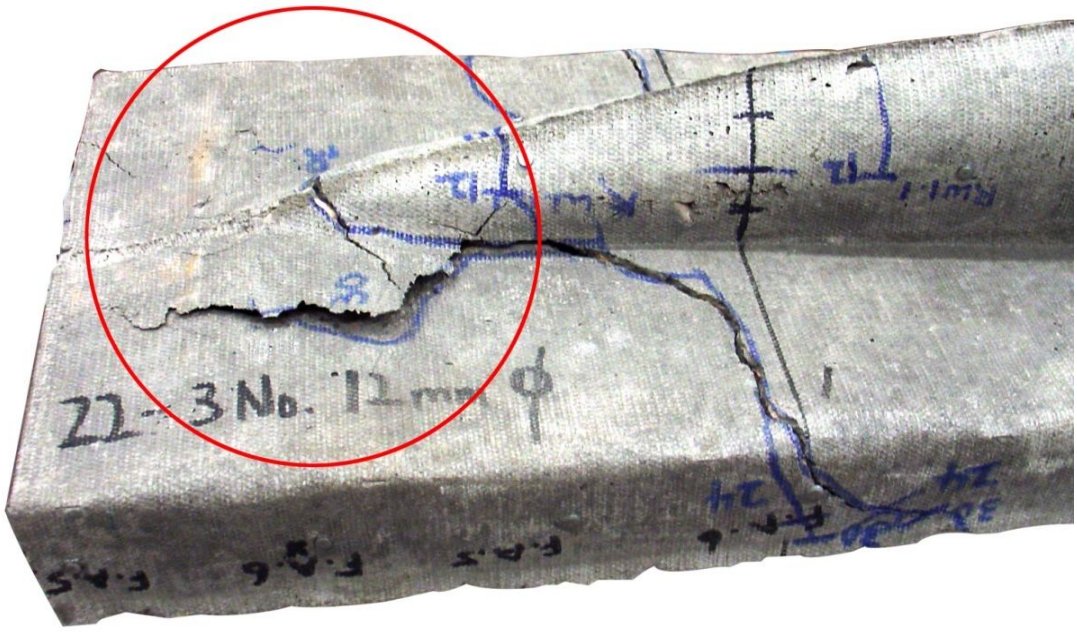

Figure 6-49: Crack showing the rebar pulling out the anchorage due to the separation of web and flange

6.5.3 Design Proposal – based on the results of 22SADF3no10mm and 22SADF3no12mm

The principal cause of shear failure of 22SADF3no12mm is the separation of the web and the flange of the section near the support. This separation is caused by the horizontal crack formed due to the combination of the horizontal shear stress and the dowel shear action induced at the interface of the web and the flange. Thus the objective is to reduce the stresses and to have the web and the flange as one working body. The simple solution is to increase the interface area to decrease the induced stress based on the simple rule of stress = force/area.

Thus it is proposed to change the narrow profile of the web towards the supports to spread out over the full width of the flange (Figure 6-50).

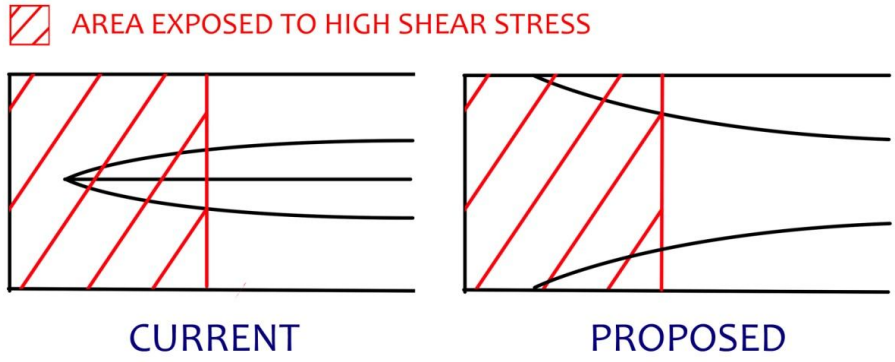

Figure 6-50: Comparing the current web design and the proposed web design

6.6 Design and Development 5: The Double-Concave Web

6.6.1 Concept design

The following picture shows the existing web design of the initial beams and the proposed design. As it is proposed in the above section the end of the web has been changed to spread out to cover the full width of the beam. Rest of the design is kept the same. This new design is applied to both 11DADF12mm and 22SADF3no12mm since both beams failed by the same failure mode (Figure 6-51).

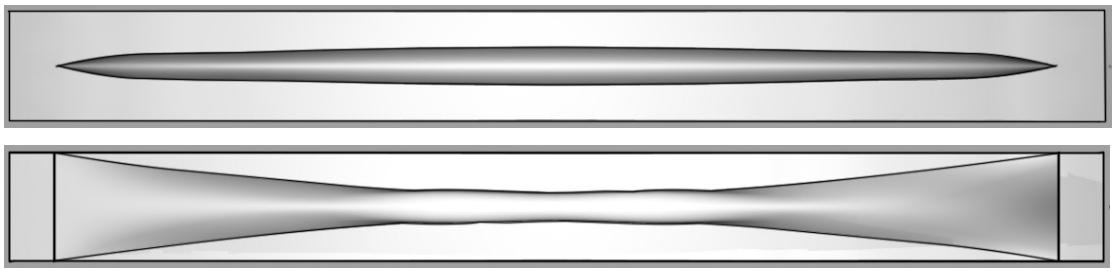

Figure 6-51: Top is the initial web plan and bottom is the modified double concave web

6.6.2 Discussion of Experiment Result

6.6.2.1 General Discussions

Design Development Number	Beam	Ultimate Load (kN)	Load increase from the initial design (%)	Failure Mode	Location (mm)
2	11DADF10mm	21.34	10.23	Rebar Yielding	Mid-Span
	22SADF10mm	23.83	40.18	Rebar Yielding	Mid-Span
3	11DADF12mm	26.00	21.84	Shear Tension	310mm~400mm from support
	22SADF12mm	33.90	42.26	Rebar Yielding	Mid-Span
4	22SADF 3no 10mm	32.00	0.00	Rebar Yielding	Mid-Span
	22SADF 3no 12mm	32.26	0.00	Shear Tension	310mm~400mm from support
5	11DADFWW12mm	35.60	36.92	Rebar Yielding	Mid-Span
	22SADFWW3no12mm	52.80	63.67	Rebar Yielding	Mid-Span

Table 6-6: Summary of Test Results of 11DADFWW12mm and 22SADFWW3no12mm

The ultimate loads of both beams have been increased. The load of 11DADFWW12mm has been increased by 37% from 11DADF12mm, and the load of 22SADFWW3no12mm has been increased by 48% from 22SADF3no12mm.
Again no sign of concrete crushing is found near the anchorage area despite the high applied loads. The following calculation is carried out for the purposes of comparison. The same Strut-Tie model is used for the analysis;

The reaction of 11DADFWW12mm
= (35600N + 351.69N + (125.37N*2))/2 = 18101.3N
The reaction of 22SADFWW3no12mm
= (52800N + 351.69N + (125.37N*2))/2 = 26701.22N

The total compressive force applied by the anchorages to the concrete (thus the total resistance force applied by concrete) at the failure load is,

For 11DADFWW12mm
18101.3/ tan 11 = 93123.12 N
For 22SADFWW3no12mm
26701.22/ tan 22 = 66087.84 N

Total surface area of anchorages of which the concrete is compressed by is,

For 11DADFWW12mm

((200-20)*10) *2 = 3600 mm^2

For 22SADFWW3no12mm

((200-20)*10) = 1800 mm^2

Thus, the total axial compressive stress applied to concrete by the anchorages is,

For 11DADFWW12mm

93123.12/3600 = $\underline{25.87\ N/mm^2}$

For 22SADFWW3no12mm

66087.84/1800 = $\underline{36.72\ N/mm^2}$

From the concrete cube test results, average compression strength of concrete is obtained;

For 11DADFWW12mm,

39.7N/mm^2 * 0.8 = $\underline{31.76N/mm^2}$; which is the equivalent cylinder strength.

Thus the capacity is about 23% greater than the applied stress.

For 22SADFWW3no12mm

41.3N/mm^2 * 0.8 = $\underline{33.04N/mm^2}$; which is the equivalent cylinder strength.

Thus the capacity is about 10% less than the applied stress.

The calculation shows that for 11DADFWW12mm the applied compression anchorage stress was less than the concrete capacity; however for 22SADFWW3no12mm the concrete could sustain the high applied uni-axial stress owing to its high tri-axial compression capacity with the great thickness of the flange.

6.6.2.2. Bending Tension (rebar yielding) Failure of 11DADFWW12mm and 22SADFWW3no12mm

The beams showed vertical cracks at mid-span (Figure 6-52), which opened up wider than any other cracks in the beam at the collapse load suggests that they have failed due to the rebar yielding.

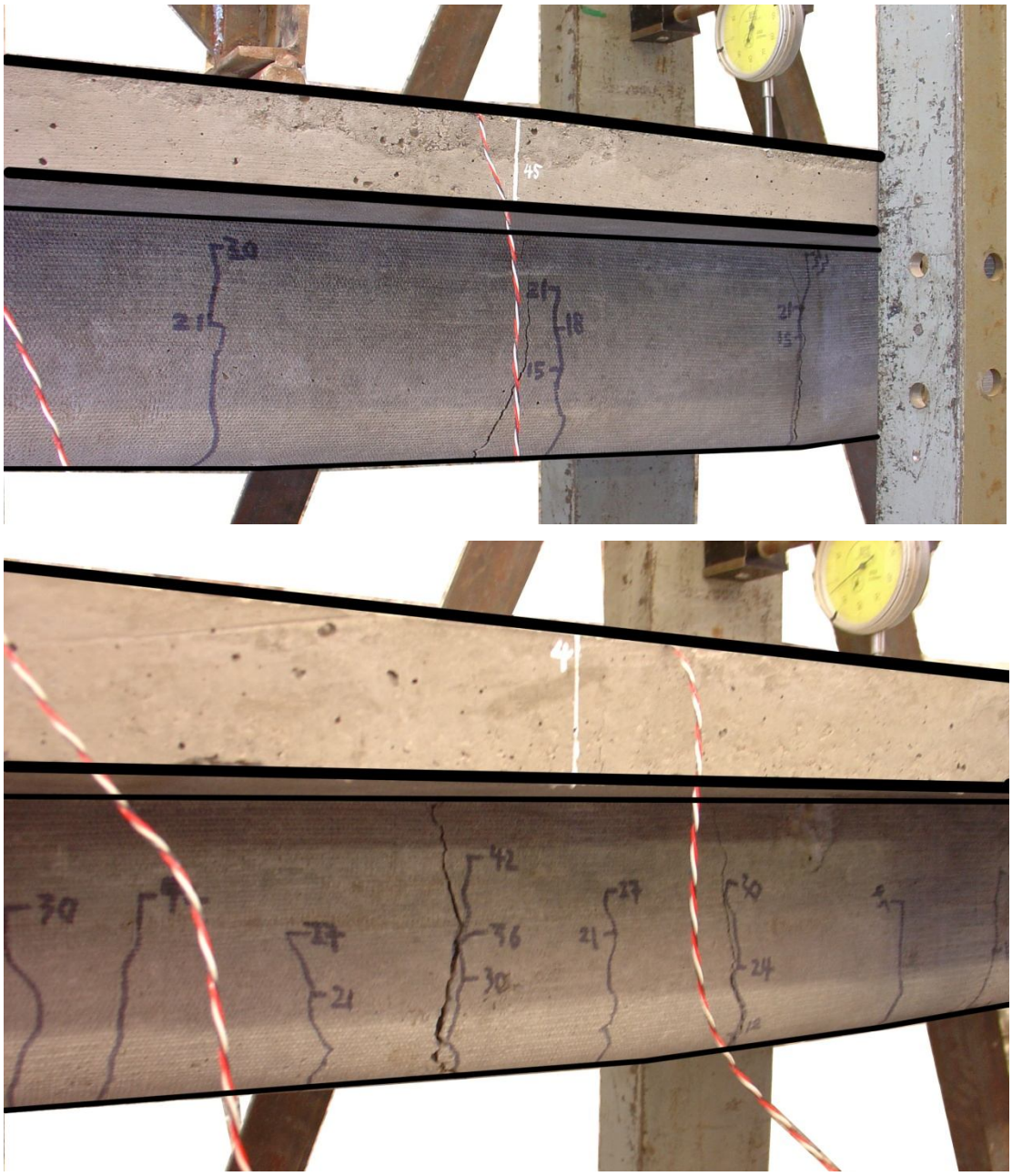

Figure 6-52: Showing Bending Cracks near the Mid-Span of 11DADFWW12mm (top) and 22SADFWW3no12mm (bottom)

The following graphs (Figure 6-53 and 6-54) show the tensile strains of the rebar at given sections. In both graphs the rebar strains have reached the yield strain (at 1860mm for 11DADFWW12mm, and at 1240mm for 22SADFWW3no.12mm).

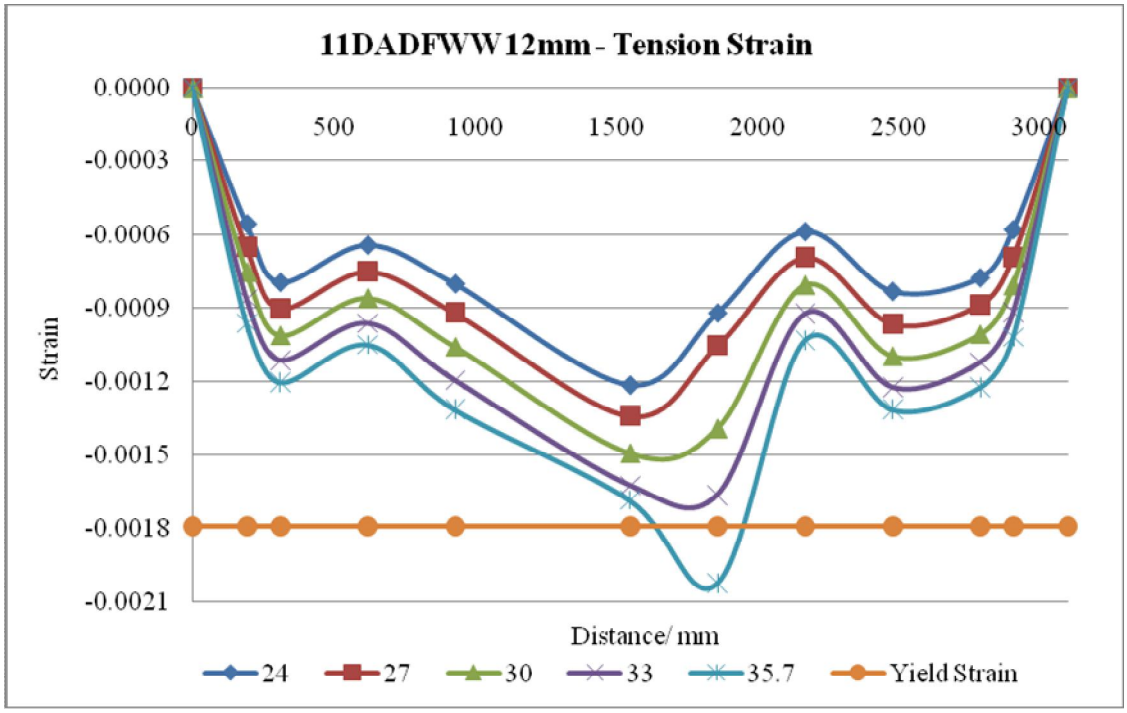

Figure 6-53: Rebar tension strain of 11DADFWW12mm

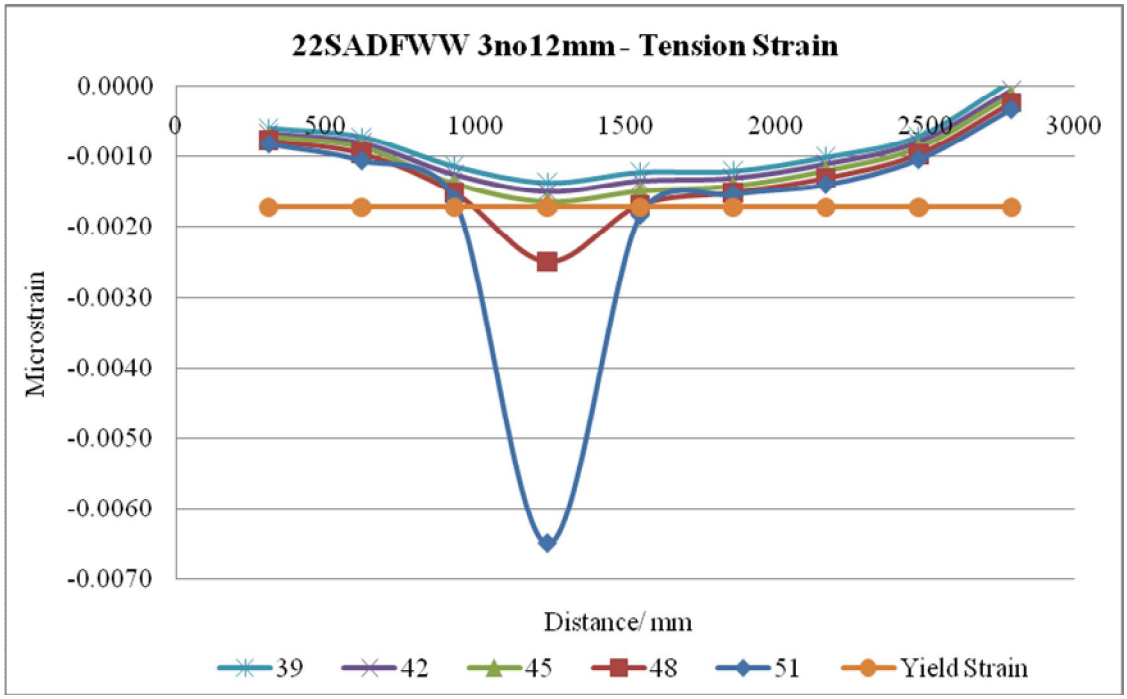

Figure 6-54: Rebar tension strain of 22SADFWW3no12mm

The following graphs (Figure 6-55 and 6-56) compare the moment capacities with the applied moments of the sections and the applied moments for the beams.

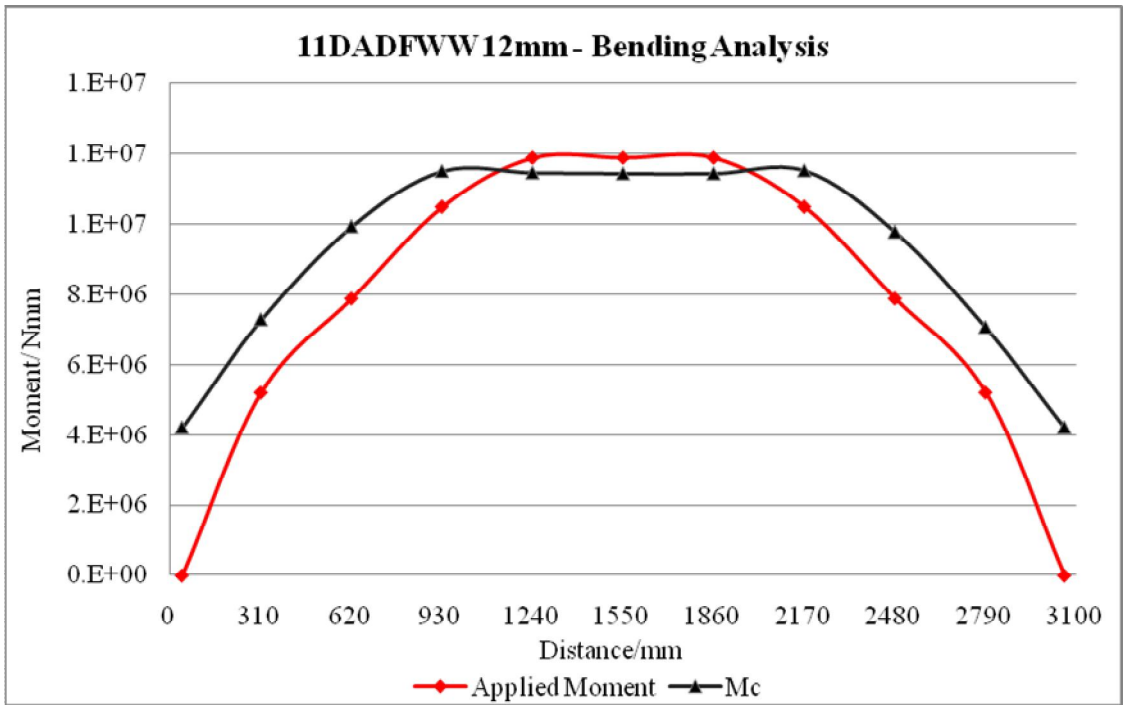

Figure 6-55: Bending graph for 11DADFWW12mm

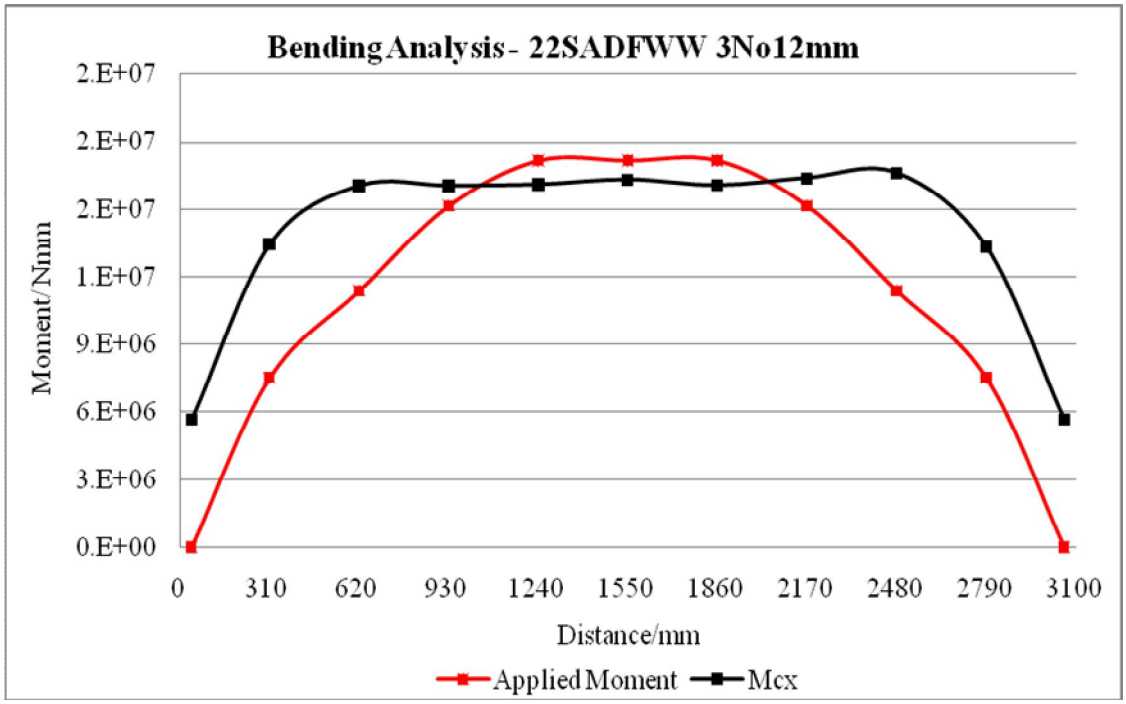

Figure 6-56: Bending graph for 22SADFWW3no12mm

The above results show that the rebars at the mid-span have yielded.

6.7 Summary and Conclusion

This chapter presented the designs and development process of the fabric formed beams. The process includes the modification of designs based on the evaluations of test results, the development of concept design, and analysis of the experiment results.

Through the development of the beams the effects of the following variables have been studied:

- Flange Depth
- Web Geometry
- The amount of Tension Reinforcement (Steel Ratio)
- Number of Anchorage
- The Effect of Compression Steel Mesh

After each design and development stage each of the above variables were modified to improve the beam's structural performance. In the consideration of which all the structural variables are studied and adapted in the forms of 11DADFWW12mm and 22SADFWW3no12mm, the forms have become the final forms of the study.

It should be stated that throughout the development in general only one beam is tested for each type. Normally at least three beams should be tested for each type to prove the consistency in its performance and data. However, there have been some restrictions to the use of laboratory which also pressurized on the timeline of the research. Yet, the results of the consecutive beam tests confirm the soundness of design improvement and development; for example the significant increase of the ultimate load and the desired failure mode of the last beams.

Based on the test results of the beams in respect of the above variables the following conclusions are drawn:

1. The results of 11DA10mm shows that the addition of the transverse bars at anchorage has improved the distribution of the anchorage compression stress, and reduced the stress exerted on the surrounding concrete. This effect increased the load capacity of the beam.
2. The result of 22SA10mm shows that the increase of rebar angle has reduced the horizontal compressive force at the anchorage, and reduced the stress exerted on the surrounding concrete. This effect increased the load capacity of the beam.

3. The result of 11DA-WS10mm shows that the absence of compression steel mesh caused the premature shear compression failure of the section near support. In contrast 11DA10mm which has the compression steel mesh could sustain much higher shear stress. The results show that the shear capacity of the section is increased as the compression capacity of the section is increased. This result also agrees with the Compression Force Path theory, that the shear stress in the reinforced concrete section is sustained by the un-cracked concrete within the region of compression force path in the beam.
4. The result of 22SADF10mm in comparison with the results of 22SA10mm shows that the increasing thickness of the flange (thus increasing the effective depth) can increase the shear capacity of the section.
5. Both 22SA10mm and 22SADF12mm had shear tension failure. The ultimate load of 22SADF12mm is twice the ultimate load of 22SA10mm, and the effective depth of the section (in this case same as the flange depth of the section) of 22SADF12mm is also twice the depth of 22SA10mm. This comparison implies that the shear capacity of section is proportional to the effective depth of the section.
6. The results for 11DADF12mm show that the shear failure of the section is mainly initiated by the formation of the longitudinal bond failure crack incurred along the line of the reinforcement. The formation of the crack makes the flange more prone to rotate about the un-cracked section which gradually leads to a ductile shear failure.
7. Based on the results of the following beams it is found that the increase of the steel content does not increase the shear capacity of the section.
    - 22SADF12mm
    - 22SADF3no10mm
    - 22SADF3no12mm
8. 22SADF3no12mm also failed by shear near support due to the rotation of the separated flange about the un-cracked section, as it was seen for 11DADF12mm. Thus the web profile of the beams was changed to give increased contact area between the flange and the web. The modification has successfully prevented the premature shear failure of the beams, and increased the ultimate loads. Both 22SADFWW3no12mm and 11DADFWW12mm failed at the mid-span by the rebar yielding.

9. The shear failure of reinforced concrete beam occurs in a sudden and brittle manner without prior warning to the collapse. Thus engineers' take this into consideration and design the beams for steel yielding at the position of maximum bending moment (the mid-span), which occurs in a ductile failure with sufficient warnings prior to its ultimate collapse. This is generally achieved with 'under-reinforced sections', which means that the section is designed so that the reinforcement in the section yields before the concrete reaches the crushing point. However, this type of failure can be also achieved by manipulating the form using the fabric formwork. When the final two beams (the ones with wide web) were built, the width of the web at the mid-section was noticeably reduced as the mid-span brace of the formwork was pressing against the fresh concrete. This reduced width could be more easily observed from the following plan diagram.

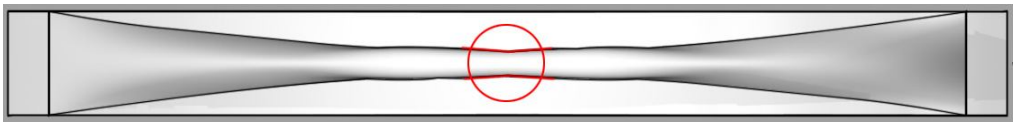

Figure 6-57: Plan drawing of 22SADFWW3No12mm showing the reduced width of web at the mid-span

The reduced width results the reduction in the cross-sectional area and increased the stress generated in the section. Thus this effect made the section more vulnerable to the formation of tension bending crack. Once the tension crack is formed the second moment of area of the section is reduced. This will make the steel at the section more vulnerable for further straining in tension in comparison with the uncracked sections. It must be stated that such idea requires further investigation, and the idea is discussed for its potential application.

In closing of this chapter there is an interesting fact to mention in regard with the final forms. Around the time when the construction of the two beams was completed the author had a chance to hear about Harry Seidler, an Australian architect. Seidler's buildings have won many awards and he was also awarded with Gold Medal of the Royal Institute of British Architects (RIBA). The interest here is the so-called 'ribbon beam' and its form that he used in his buildings.

In the Harry Seidler Offices and Apartments (1973-94, in Sydney) and Hong Kong Club building (1980-84, in Hong Kong Central) interesting beams can be found. The

general shape of the beams surprisingly similar to the last version of fabric formed beams. These appear to have been constructed using conventional formwork. The ribbon beams' web has sharp edges possibly due to the rigid formworks, and the shapes of the curves seem more controlled. Meanwhile the fabric formed beams do not have the sharp edges in the web, and there are more free curves surrounding the body since the shapes are formed by natural sag of the fabric due to the weight of the fresh concrete. Despite these differences both types of beam seem to suggest same philosophy. His beams are exposed to view and the forms are architectural as well as structural. It is useful to know that beams with a similar form are in use and the structural quality has been tested throughout the time. With fabric formwork technology future beams of similar types could be constructed with a lot less cost and effort.

Figure 6-58: Street façade of original building and two additions (Harry Seidler Offices and Apartments; Photo by Eric Sierins) (Harry Seidler and Associates)

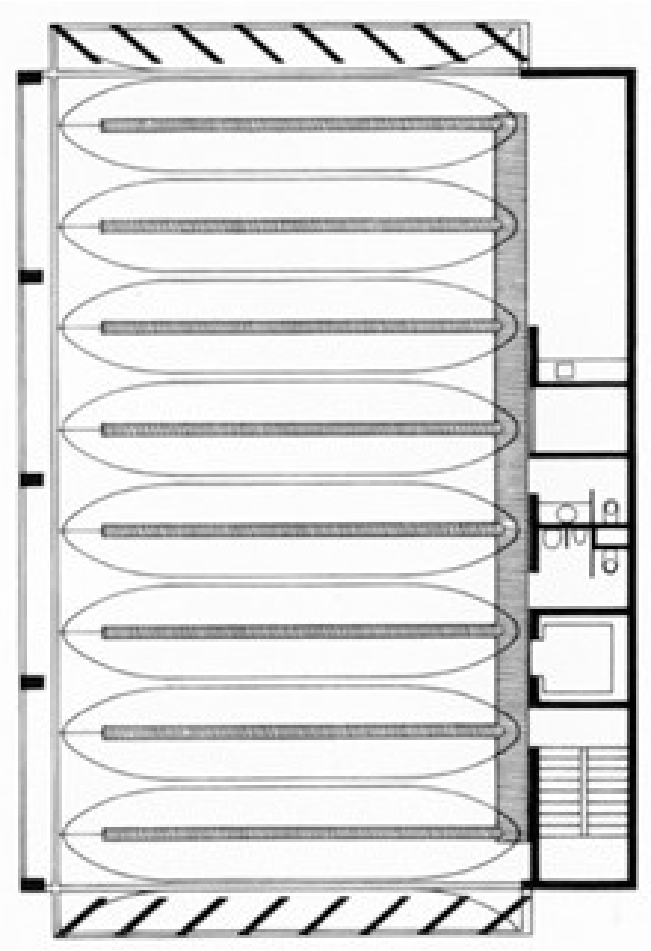

Figure 6-59: Structural plan of original building with T-beams (Harry Seidler Offices and Apartments, Photo by Harry Seidler & Associates) (Harry Seidler and Associates)

Figure 6-60: Mezzanine office with view of city and harbour bridge (Harry Seidler Offices and Apartments, Photo by Max Dupain) (Harry Seidler and Associates)

Figure 6-61: Garden lounge with Helen Frankenthaler tapestry (Hong Kong Club building; photo by John Gollings) (Harry Seidler and Associates)

Chapter 7: Formwork Design and Construction

7.1 Introduction

This chapter illustrates the construction process of the fabric formwork beams. The construction methods have been modified through the evolution of the beam designs, and thus three different formwork types and their construction procedures are illustrated.

The first approach consists of timber soffit formwork for the flange and fabric formwork for the web. The web profile is defined with plywood pieces cut into the curved shape. Also the fabric formwork is centered using two additional centring braces. This formwork is then slightly modified when the flange design of the beam is changed to adapt the parabolic shape. In order to construct such a form of the flange simply additional plywood elements are added to the existing formwork.

The third version of formwork is designed to adapt the new wide web profile, and the soffit profiles were cut in the inverse shape. Also the plywood pieces that were used to define the web profile were removed, reducing the number of plywood components. Instead, the fabric is premeasured to the required geometry and fixed on to the soffit formwork. The fabric is allowed to sag naturally under the concrete's self-weight. Also the reinforcement bars are no longer suspended in the air by a string, but it is directly placed onto the fabric using wood spacers. Also the formwork elements are cut into smaller pieces, in doing so there is less chance of damage during the assembly and striping operations. It is important to note that the complexity of the beam's form actually increased but the construction process has become simpler and efficient with the less construction materials. The following pages will illustrate the construction processes in more detail with the relevant pictures.

7.2 Formwork Type 1

Formwork Type 1 has been constructed for the following beams:

- 11DA – WS 10mm
- 11DA 10mm
- 22SA 10mm

7.3 Construction Process – Type 1

1. The steel support is assembled.
2. Timber table pieces are assembled and placed on the steel support.

Figure 7-1: The steel support (left) and the timber table on the steel support

3. The fabric is cut to the approximate size with extra length at the top. Then it is folded into half.
4. Timber pieces of the web profile are cut.
5. The timber web profile is fixed onto the folded fabric.
6. The fabric is then pushed up into the timber table, and fixed using staples.

Figure 7-2: The timber web profile is fixed onto the fabric formwork

7. Centering braces are attached to the bottom of the timber table to hold the timber web profile at the centre.

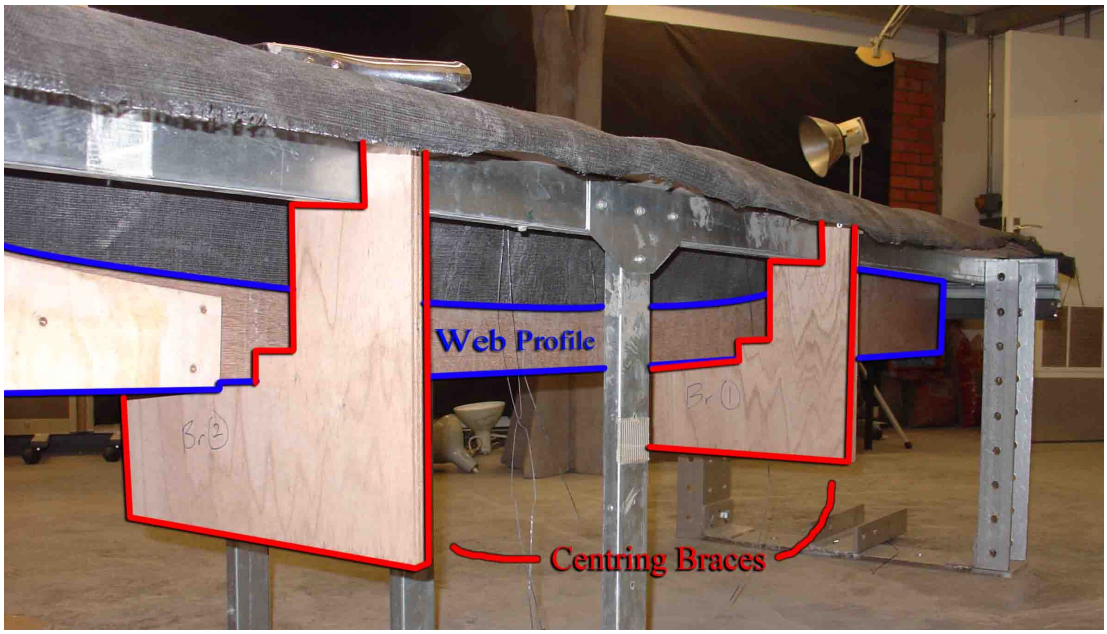

Figure 7-3: Showing the braces holding the web profile at the centre of the formwork

8. Fabric is then stretched and stapled. Most of the wrinkles on the fabric need to be eliminated. Canvas straining pliers are used to stretch fabric.
9. Using the perpendicular ruler, the each end of the 320mm long width of flange section is marked on the table. Using the chalk-o-matric the inner lines of the flange section are drawn on the fabric. (Figure 7-4)
10. A timber frame for the flange section is set on the table. The width of 320mm is constantly checked at several different places.
11. Reinforcement is curved into the web profile.
12. The ends of the reinforcement are then bent by heating.
13. The finished reinforcement bars are welded together.
14. The anchorages are then prepared and welded to the reinforcements. The bent section of the reinforcements is 45mm long, the diameter of each anchorage is 10mm, and thus this leaved the rear cover length of (80mm-45mm-10mm =) 25mm.
15. The reinforcement is then placed in the formwork, it is suspend from wire at midspan to ensure the correct effective depth.

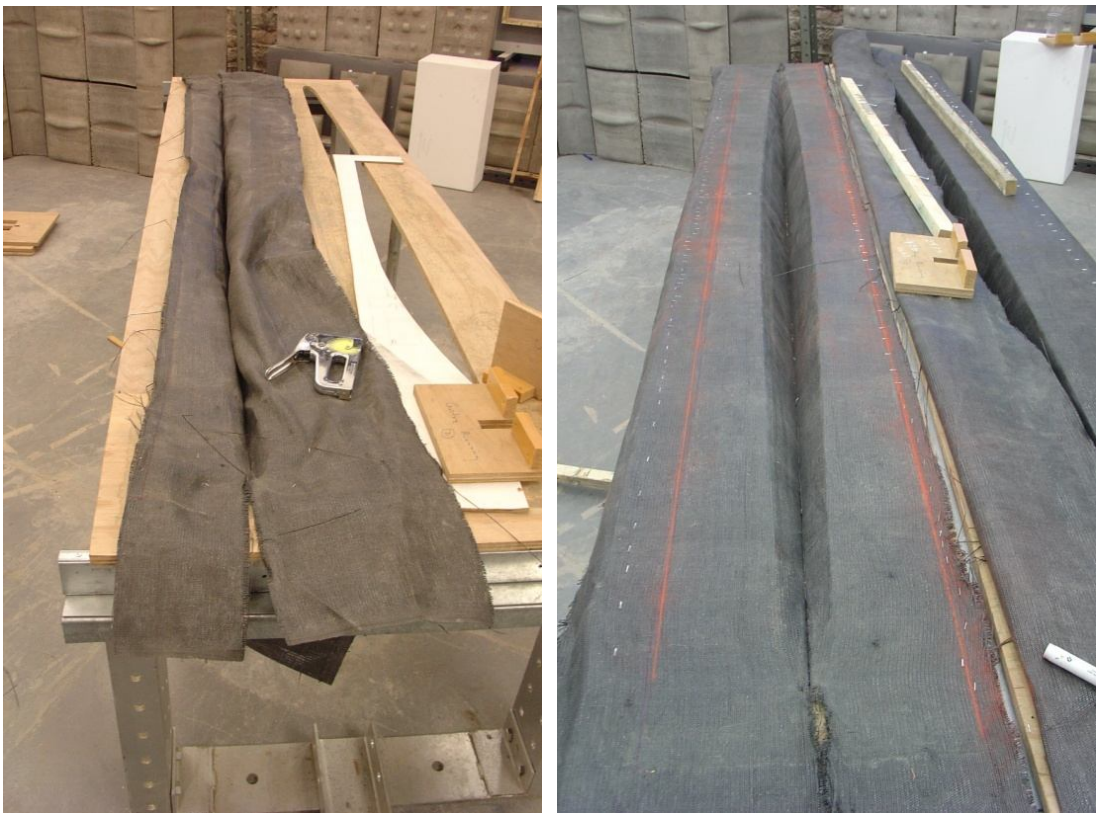

Figure 7-4: Fabric is stapled on to the table and flange width is marked using the chalk-o-matric

Figure 7-5: Curved reinforcements

Figure 7-6: Curved reinforcements

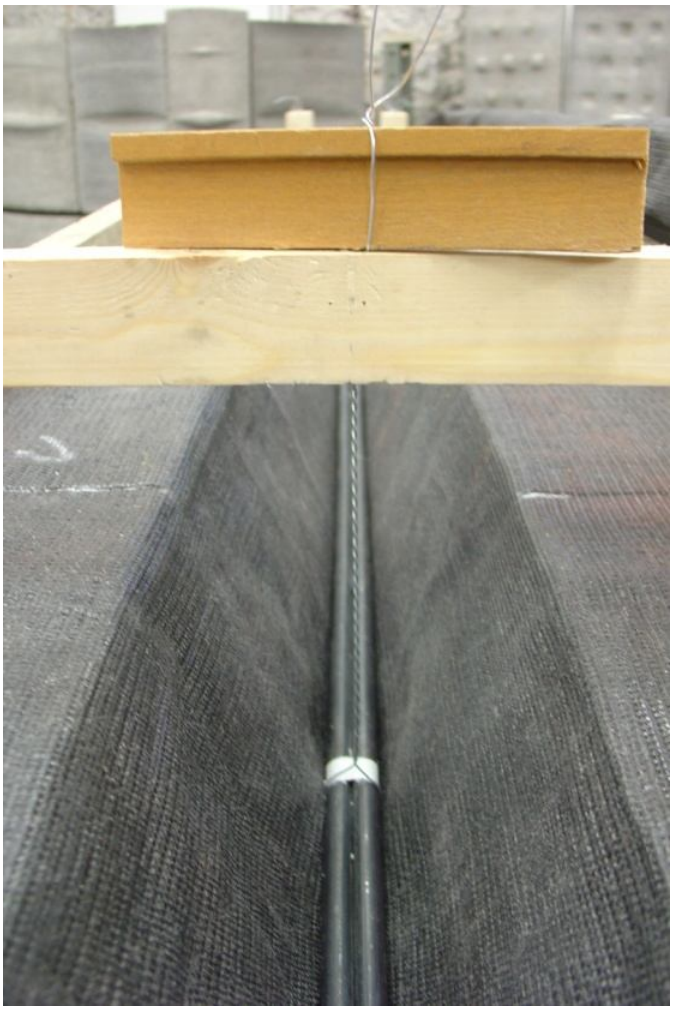

Figure 7-7: The reinforcement is held at correct effective depth using steel wire

16. The anchorages are supported at the average height of 17mm above the top of the plywood formwork. Above the anchorages there are timber blocks that are attached to the flange formwork frame. Long screws are put through these timber blocks and provide the anchorages downward forces. It is better to mark the points on the top of the anchorages where the screws will come in contact, or the screws possibly will slip aside. Then metal strings will go around the bottom of the anchorages, come back up through the timber blocks and tied at the top of the screws. This will provides upward forces to the anchorages which will balance out with the downward forces from the screws to keep the anchorages in the intended depth. It is important to leave a sufficient gap above the anchorages to allow for effective cover. The timber blocks below are then removed.

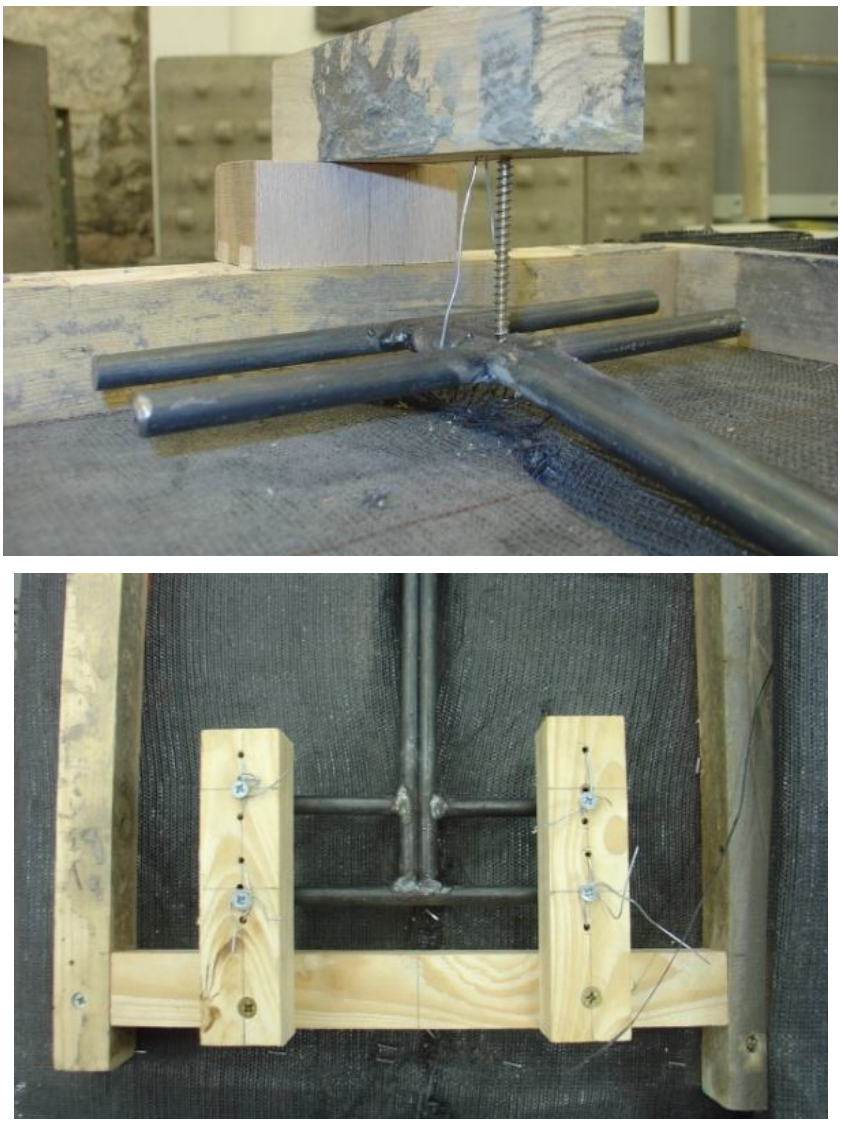

Figure 7-8: Use of timber blocks to support reinforcement at ancrhoage

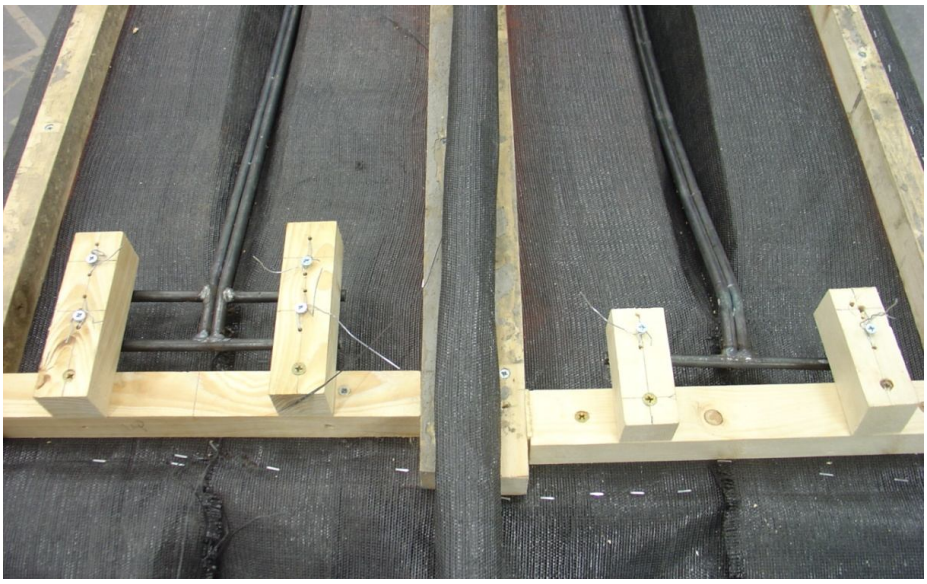

Figure 7-9: The reinforcements and anchorages are held in the right positions

17. After the reinforcement is placed, it is checked that there is enough space to place the concrete. If the space between the reinforcements and the fabric is too narrow, then the reinforcements are lifted up using the mid-span metal string support until sufficient space is secured at both sides of the reinforcements.
18. Position of the reinforcements in the formwork is determined by measuring the depth from the top of the formwork at 19 different sections.
19. The timber supports for the lifting hooks are then placed on top of the timber frame of flange.
20. Steel compression mesh is premeasured and cut into the right lengths and widths.
21. A final check is made.
22. Concrete is mixed using the Portland cement, aggregates and water only. No additives are included in the mix. Firstly the mixer is started and the aggregates are poured into the rotating mixer using the measuring boxes. Wait for 30 seconds for them to thoroughly mix. Then add the cement using the measuring box to the mixer. Wait for another 30 second. Water is then added using the measuring cylinder. Based on the eye judgement make sure that the mix is not too watery, if so do not add any more water to the mix. If the mix contains too much water the mix starts to spill off the mixer and this should be avoided. The amount of water added is then recorded.

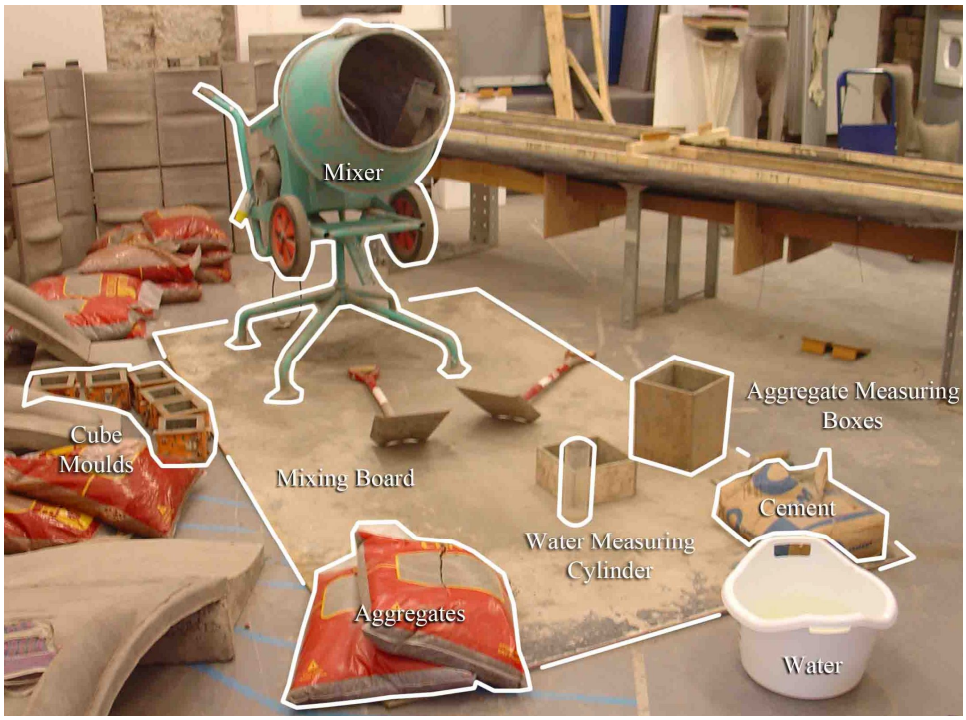

Figure 7-10: A set up for concrete mixing

23. The fresh concrete is poured only in the web section first. The concrete is carefully placed around the reinforcement, and then the wire holding the bars is removed. The hooks are constantly adjusted to be in the right position in the process of pouring the concrete.
24. When concrete is poured up to the top level of web the supports for the hooks are removed. The centre string support is also cut and removed.
25. More concrete is poured in to the formwork. This time the concrete is filled up to about half way of the flange depth.
26. Steel mesh is put onto the poured concrete. Unnecessary bits of the mesh are cut off to fit inside the formwork
27. The concrete is placed to the top of the formwork. Again extra care is needed in distributing concrete evenly around the anchorage area.
28. At last finish the process by floating the top surface of the beam.

Figure 7-11: Beam casting

Figure 7-12: Cast beam, turned before fabric is peeled off

Figure 7-13: Cast beam

7.4 Formwork Type 2

Formwork Type 2 has been constructed for the following beams:

- 11DADF 10mm
- 11DADF 12mm
- 22SADF 10mm
- 22SADF 12mm
- 22SADF 3no. 10mm
- 22SADF 3no. 12mm

7.5 Construction Process – Type 2

Not the entire process will be illustrated as aspects were the same as Type 1 formwork, but only the modifications made to the formwork will be discussed.

At this point the new design of beam has the flange adopting the parabolic curve to increase the thickness at the supports and hence enhance its capacity against the shear. Thus the additional plywood sheets are put on top of the existing soffit members and curved to the required profile. The plywood sheets are curved on top of timber blocks varying in depths and glued to the blocks to stay in the shape.

Figure 7-14: Showing the additional plywood sheets and the MDF slopes at one end

The plywood sheets were too thick to run for the entire length, thus MDF sheets were

cut into three slopes are placed and another thin MDF sheet is placed on top of the slopes to complete the curve.

Figure 7-15: MDF sheet forming curved flange

Forming curved flange all the pieces are fixed waterproof varnish is applied (Figure 7-16), and finally the fabric is stretched and stapled onto the soffit formwork (Figure 7-17).

Figure 7-16: Showing the complete timber soffit formwork

Fabric is then stretched over the soffit formwork. The fabric is stretched at every 50mm point, and the direction of pull constantly perpendicular to the span of the beam.

Figure 7-17: Showing the soffit formwork with the fabric on.

At last the flange formwork pieces are put up and the rebars are placed in the formwork. The following processes are identical to type 1.

Figure 7-18: The completed formwork

7.6 Formwork Type 3

Formwork Type 3 has been constructed for the following beams:

- 11DADFWW 12mm
- 22SADFWW 3no. 12mm

7.7 Construction Process – Type 3

Type 3 formwork is designed to cast the beams with wider web towards the ends. Thus the existing soffit formwork is required to change completely. Please refer to the following picture showing the type 3 soffit formwork (Figure 7-19).

Figure 7-19: the type 3 soffit formwork

Figure 7-20: Fabric is laid over the soffit formwork and fabric stretched over and stapled on top of the soffit formwork

In type 3 the timber pieces defining the web curve have been removed. Instead, the perimeters of the web are predetermined at sections and they are marked on the fabric. The part of fabric that is marked is dropped into the void of the soffit formwork and the rest of the fabric is stapled down. When the fabric is securely fixed the rebar is placed on to the fabric. The rebar is no longer suspended at the mid-span from a wire but sits on a spacer, directly placed on the fabric. Thus it is the weight of rebar that stretches the fabric downward. There are nine spacers in total placed at 310mm intervals throughout the beam. The main function is to ensure enough concrete to go around the reinforcement but also it is devised to hold the rebar at the centre line of the web. Please look at the following picture (7-21).

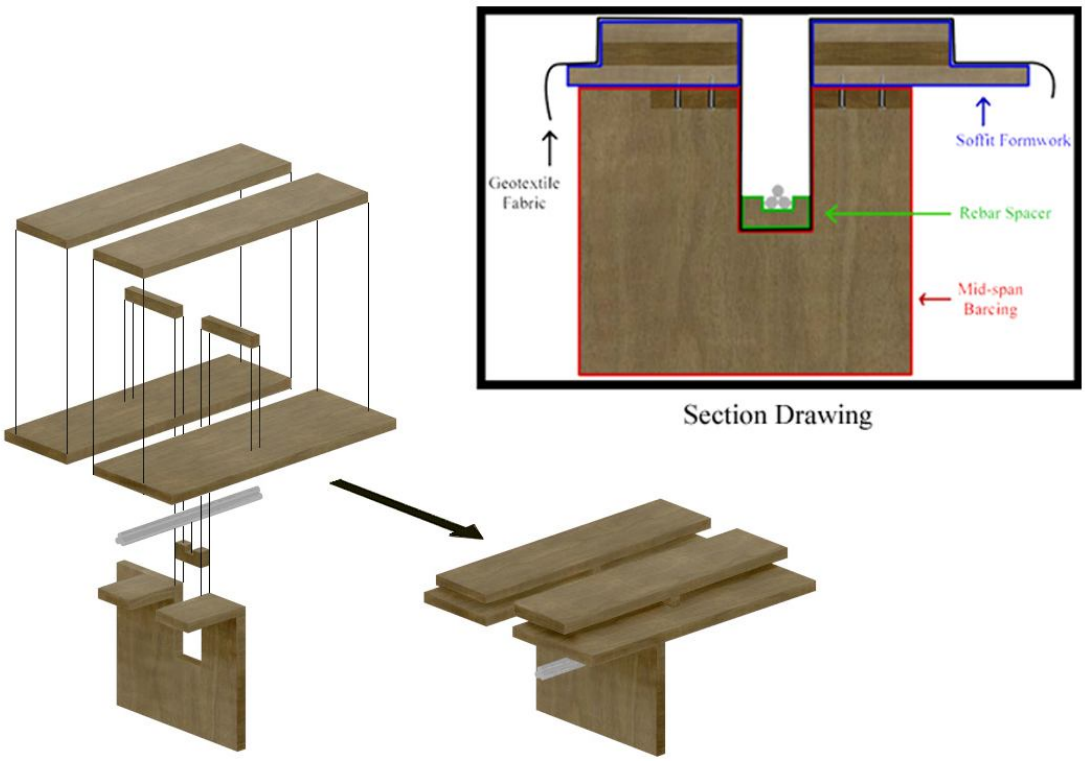

Figure 7-21: Showing the bracing system at the mid-span

The picture shows the bracing system at the mid-span of the beam. The purpose of the bracing is to increase the overall strength and stability of the formwork, but it is also holds the spacer in the centre and prevent from the lateral movement which might incur during the concrete pouring process.

Later on the formwork development, the soffit elements are cut into smaller components (Figure 7-22). From the earlier assembly and stripping processes there were a number of cases where the formwork elements were damaged that either repair or replacement of them was required. The damage was mainly due to the large size of some of the elements, and during the construction process the excessive

bending of the elements was incurred. Reducing the size of the elements is to prevent this unnecessary damage from occurring. Also smaller components are easy to handle and more ideal to store when they are not in use.

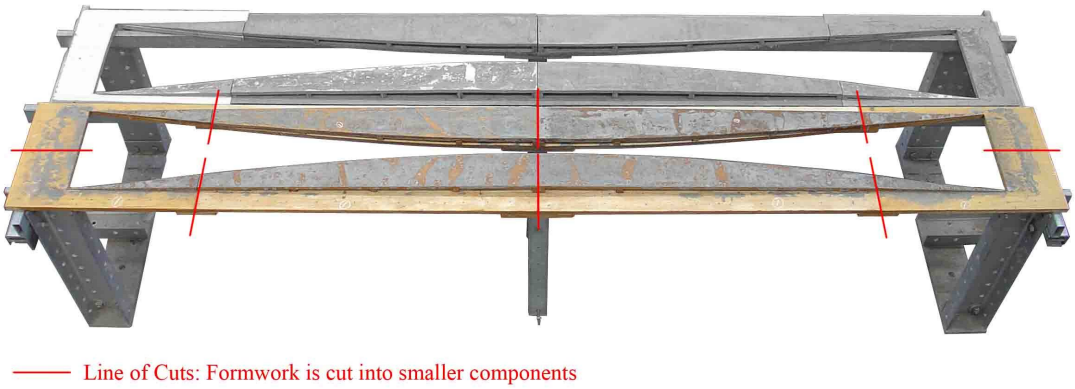

Figure 7-22: Showing the lines where the formwork is cut into smaller components

7.8 Measuring the Beams

The beams' dimensions are measured after minimum two days of curing. The measured dimensions are compared between beams and the consistency of the forms could be checked. The dimensions of the flange are straight forward to measure due to its rather simple form. In case of the web, the form varies along different axes and more work is required to record the dimensions. It is the width and the depth of the web that are to be measured. Both varies depends on the location, and thus the beam is marked at nine sections and the dimensions are taken from them. For the width of the sections, each web is divided vertically into smaller sections with equal distances between them and the widths are measured at the smaller sections. The widths are measured using a metal caliper (Figure 7-23).

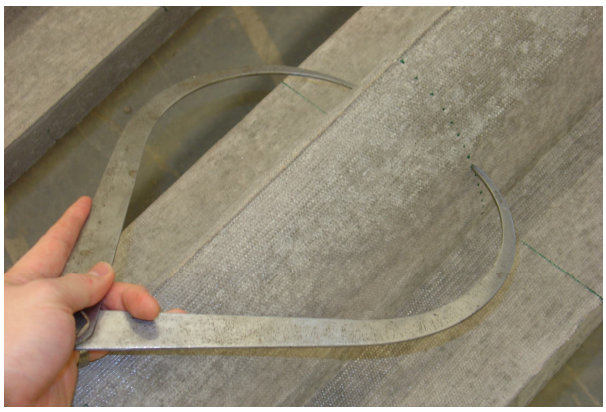

Figure 7-23: Measuring width of web at different vertical locations

The height (or the depth) of the web could not be measured accurately only with the available tools and a device was developed to measure the web.

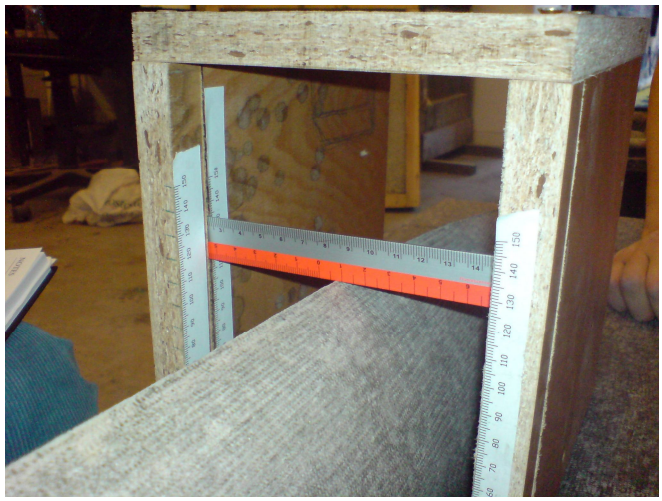

Figure 7-24: Measuring the height of the web

There are two rulers vertically standing on both sides of the web, perpendicularly to the base (Figure 7-24). The divisions of the rulers are checked to be at the same vertical points. A narrow metal ruler is placed on the peak point of the web section. Now the metal ruler crosses the two vertical rulers and the readings are taken at the crossing points. When the readings taken at the vertical rulers do not match, the metal ruler is adjusted about the peak point until its ends are crossing at the same values, which is the height of the web.

The comparison of the beams' geometry shows that there is a good consistency between the web heights. It is generally the timber profiles are used in the formwork to prevent the vertical sagging of the fabric, however, in the case of the final two beams the formwork did not include the timber profiles the web heights varies slightly yet within the acceptable range as there was not significant elongation in the geotextile fabric.

The widths of the web, however, tend to vary more between the beams (and between the sections) as the fabric has more freedom to deform laterally as the concrete gets poured. This lateral deformation is not a significant issue in engineering point of view, and even in the visual sense the surface grooves formed by the varying widths is only noticeable in a close distance. However from the point of view of construction accuracy that the type of fabric used in the formwork did not significantly vary the geometry of the beam from what was initially intended.

With the dimensions measured the cross section of each section of the beams are drawn, and they are used for the calculation of sections' structural properties.

In addition, the areas of the sections are compared to see the variation throughout the beam's span. The following Figure 7-25 compares the cross-section areas of

11DADFWW12mm, which has one of the latest forms developed.

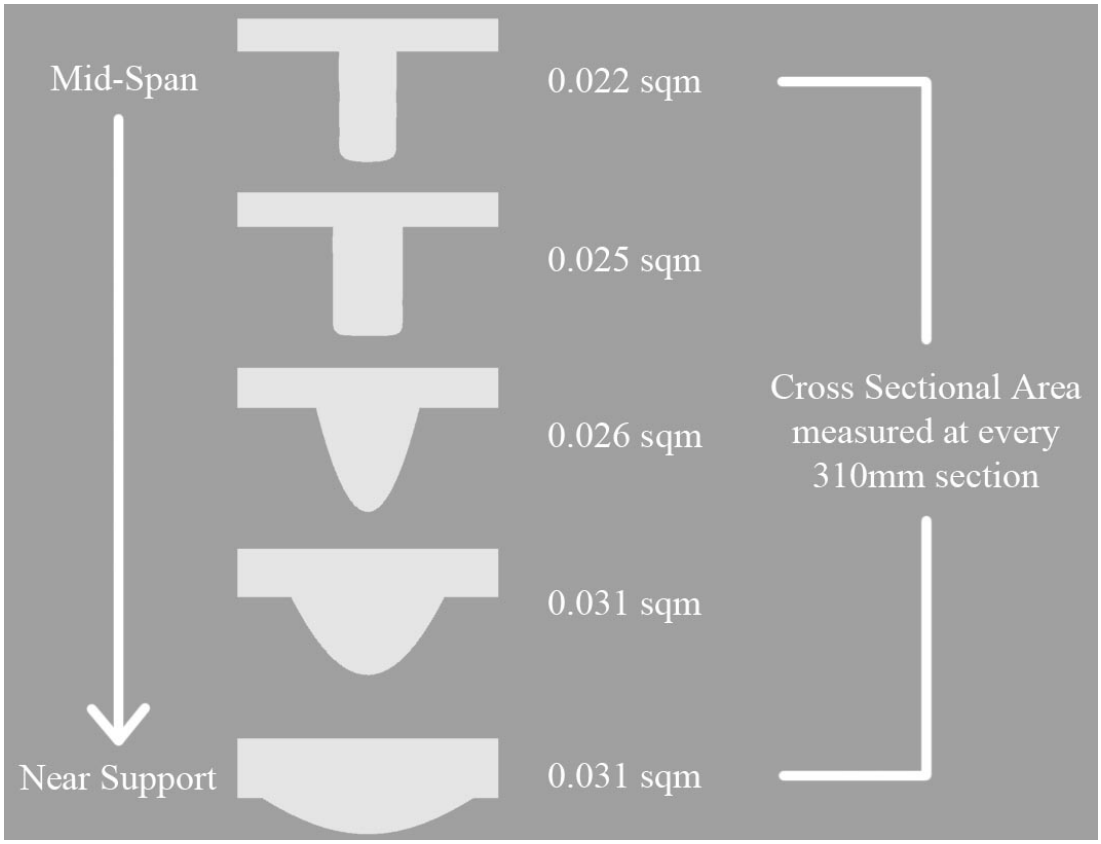

Figure 7-25: Comparison of different cross-sections along the span of beam for 11DADFWW12mm.

The figure shows how the mass is redistributed along the span of the beam. At the mid-span the mass is distributed more vertically to maximize its bending capacity, and towards the support more mass is located in the compression flange to maximize the shear capacity. In terms of the cross sectional area, the mid-span has the smallest area, and the section near the span has the largest area (increased by 41% from the mid-span section). In the mid-span section the bending moment is the most dominant and it is resisted by concrete and steel. In the sections closer to the support the shear is more dominant over the bending moment, and shear is mainly resisted by the concrete and thus for this reason the mass of concrete is increased in the sections.

Chapter 8: Reinforced Concrete Beam Design Theory and Analysis Methods

8.1 Introduction

The aim of this chapter is to present the current theories of reinforced concrete beam and the analysis methods. There is extensive range of literature about reinforced concrete beam and only those aspects that are particularly relevant to the fabric formed beams are presented in this chapter, with the intention to assess their applications in the design of fabric formed beams.

8.2 Reinforced Concrete Beam Design

In general beam design requires to be checked against the following failure criteria:

- Ultimate Limit State: Moment
- Ultimate Limit State: Shear
- Serviceability Limit State: Deflection

Since reinforced concrete consists of two materials; concrete and steel, it is important to understand the characteristics of both materials and to balance their behaviour to achieve the desired failure mode. In normal circumstances beams are designed to fail by the yielding of steel at point of maximum applied bending moment, the mid-span of simply supported beam for example. If steel yields before concrete fails in compression such beam is said to be under-reinforced and it fails in a ductile manner. Such failures are accompanied by large deflections and clearly visible vertical flexure cracks giving sufficient warning prior to the ultimate collapse. If the beam fails by crushing of the compression zone prior top steel yielding then the beam is said to be over-reinforced and failure tends to be less ductile with less warning, often sudden. Thus codes of practice and design procedures are devised to avoid such failure. In the following section the RC beam design theory and method for the above failure criteria are explained in more detail including the design method of the British Standard Code of Practice BS 8110[5]. There is an intention to compare the behavior of fabric formed beams with the existing code procedure and it would be possible to repeat such a comparison with other codes.

5 The British Standard BS 8110-1:1997, "Structural Use of Concrete – Part 1: Code of practice for design and construction", BSI 2002

8.2.1 Ultimate Limit State Moment

The ultimate bending capacity of a beam section is normally referred to the tension capacity of the section,beam should be designed as under-reinforced beam with the purpose to avoid the brittle compression failure of concrete above. Thus the ultimate moment capacity of a section, M_{ult} is expressed as,

$$M_{ult} = A_s * f_y * z \text{.....Equation 8-1}$$

Where,

A_s = Area of Steel (mm),

f_y = Yield strength of Steel (N/mm^2),

z = Lever Arm (mm)

The lever arm, z is defined as the distance between the centre of the action of compression force in the concrete and the tension force in the steel. The position of the concrete compression force is at the centroid of the compression stress block. A stress block draws simply the stress-strain relationship of concrete in compression, where the stress and strain is zero at the neutral axis position. Often standardized and simplified stress blocks are used for design for the practical reason, and the following is some of the stress blocks in the current methods (KONG, F. K. and Evans, R. H., 2001):

1. Hognestad *et al* stress block; is defined with the characteristic ratios, k_1 and k_2, and the ultimate strain of the concrete varies with its compression strength, not like the current British design codes (American codes also) which assume the ultimate strain to be a definite value, 0.0035. k_1 is the characteristic ratio of the maximum compressive stress to average compressive stress and k_2 is the ratio of the centroid of the stress block to the neutral axis depth. Please see the following Figure 8-1.

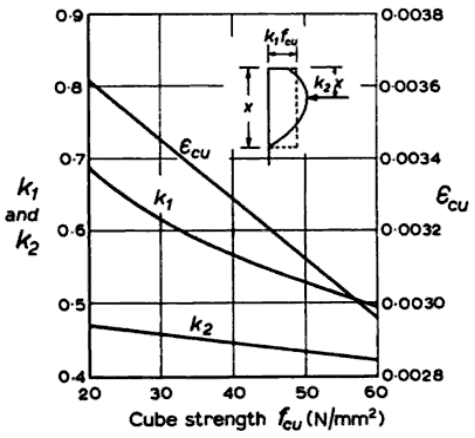

Figure 8-1: Characteristics of Hognestad *et al.*'s stress block (KONG, F. K. and Evans, R. H., 2001)

2. Whitney's equivalent rectangular stress block is a modified stress block replacing the actual stress block. The modified stress block's capacity is reduced by multiplying 0.85 to the cylinder strength (for the Hognestad stress block this ratio varies with the cube strength of the concrete), and the neutral axis depth of the block, x is also reduced to x_w, which is found from the condition of equilibrium using the equation shown below:

$$M_{ult} = A_s f_y (d - x_w/2) \quad \text{.....Equation 8-2}$$

or

$$M_{ult} = 0.85 f'_c \, b x_w (d - x_w/2) \quad \text{.....Equation 8-3}$$

Where,

M_{ult} = the ultimate moment/ Nmm

A_s = Area of reinforcement/ mm^2

f_y = Yield strength of steel may be taken as the stress corresponding to a strain of 0.004.

f'_c = cylinder strength/ Nmm^{-2}

b = width/ mm

x_w = depth of the stress block which is limited to 0.536d/ mm

d = effective depth/ mm

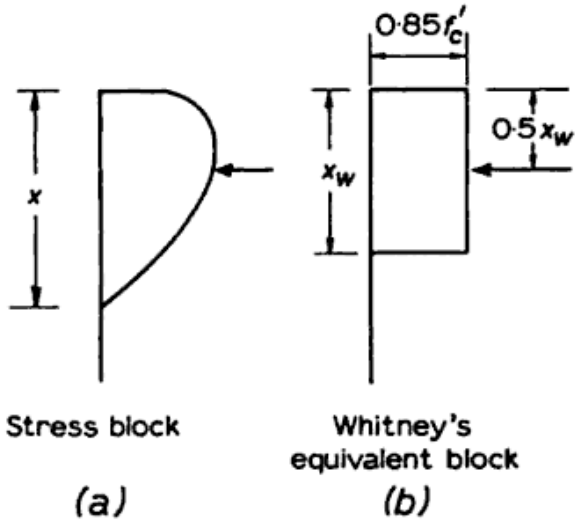

Figure 8-2: Whitney's equivalent rectangular stress block (KONG, F. K. and Evans, R. H., 2001)

3. BS 8110 stress block is also derived from a idealized strain stress relationship of concrete with the following modifications (KONG, F. K. and Evans, R. H., 2001):
    - Concrete partial safety factor of 1.5 is applied.
    - Ultimate concrete strain is taken as 0.0035

- The parabolic part of the curve ends at where strain = $\sqrt{f_{cu}}/5000$.

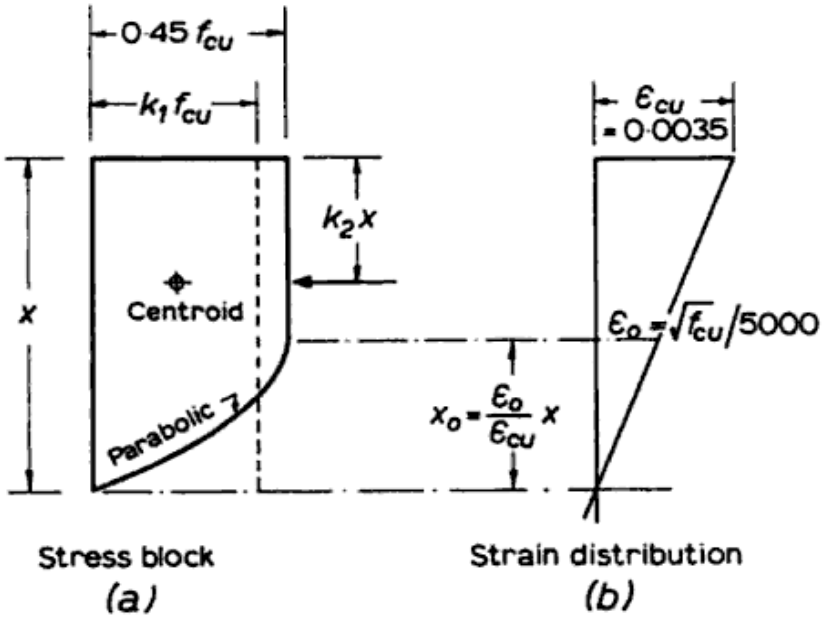

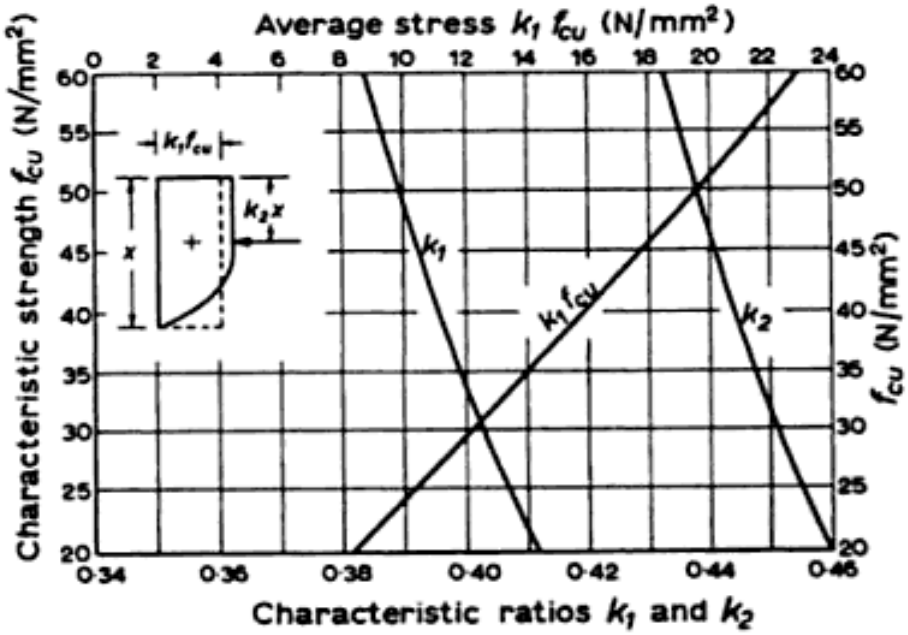

Figure 8-3: Characteristics of BS8110 stress block – Ultimate Limit State (KONG, F. K. and Evans, R. H., 2001)

4. The BS 8110 simplified rectangular stress block is further simplified from the above stress block, and assumes that the moment of resistance may be determined from a simple rectangular stress block with the concrete capacity of $0.45f_{cu}$ and with stress block depth of $0.9x$. Please note that 0.45 already includes the partial safety factor[6].

6 Partial Safety Factor is applied to the material strength to underestimate the capacity. It is to ensure that 95% of times the actual strength of the material is stronger than the design strength. Thus for the

Any of these stress blocks can be used for the reinforced concrete design purpose, however in this thesis the stress-strain relationship of concrete defined by the following equation[7] is used. This is because it depicts the curve (Figure 8-4) that reflects the actual stress-strain curve of concrete more closely in comparison with the other simplified stress blocks.

$$Fc = 1.8fc' * \left\{ \frac{\frac{\varepsilon}{\varepsilon o}}{1 + \left(\frac{\varepsilon}{\varepsilon o}\right)^2} \right\}$$ .....Equation 8-4

Where,

ε = strain

$\varepsilon o = 1.71 f_c / E_c$

f_c' = concrete cylinder strength

E_c = modulus of elasticity of concrete, which is equal to $4750\sqrt{f_c'}$

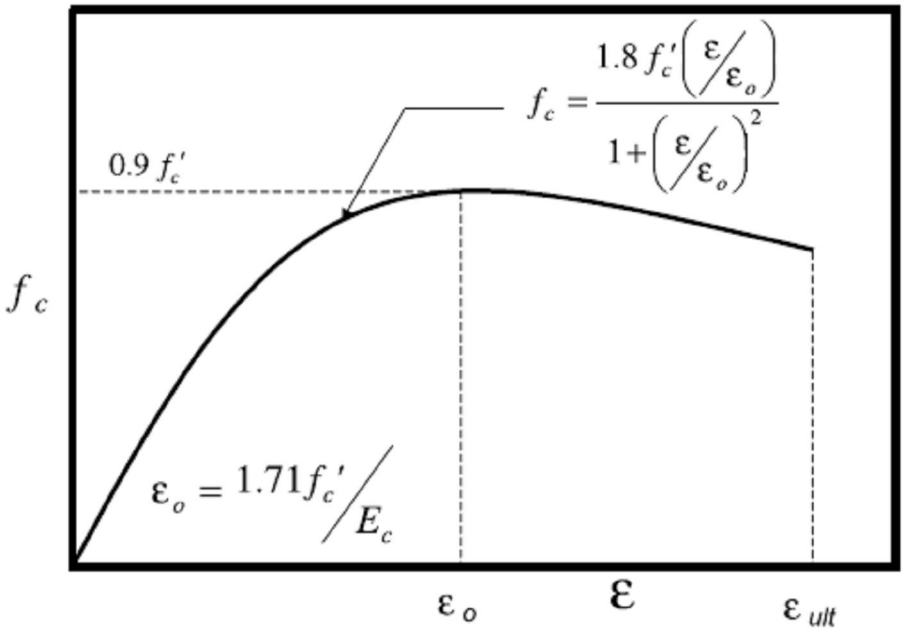

Figure 8-4: Stress-Strain relationship of concrete (NEWHOOK, J., Ghali, A., Tadros, G., 2002)

For stress-strain relationship of steel the following graph is used (Figure 8-5). The relationship is given in the British Standard Code of Practice BS8110.

---

research purpose the partial safety factor should be ignored, and the actual strength and the behavior must be used.

7 MacGregor, J.G. 1997. 'Reinforced concrete, mechanics and design'. Prentice Hall, Upper Saddle River, N.J. :mentioned in paper 'Concrete flexural members reinforced with fiber reinforced polymer: design for cracking and deformability' by John Newhook, Amin Ghali, and Gamil Tadros. Can. J. Civ. Eng. Vol. 29, 2002

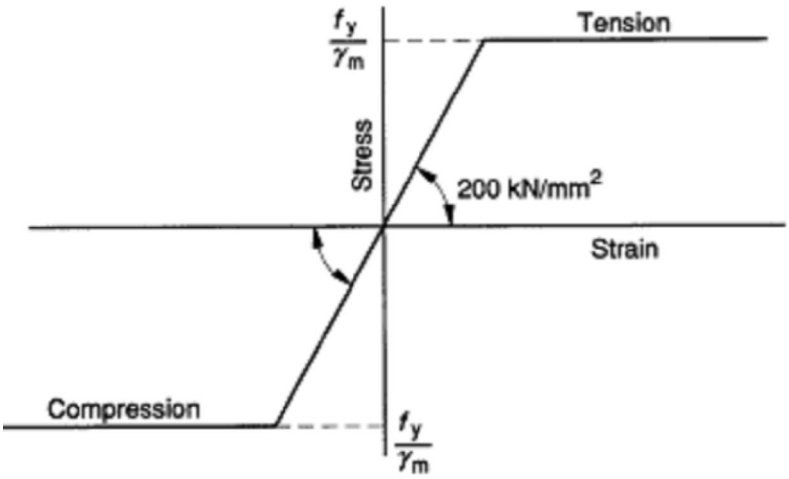

Figure 8-5: Stress-strain relationship of steel[8]

The neutral axis, *x* of a section is found from the following computation:

1. Compression strain at the extreme fibre of concrete is assumed.
2. Neutral axis of the section is assumed as 0.5**d*.
3. Using the stress block compressive force of concrete is calculated.
4. Based on strain compatibility strain in the reinforcement bar is calculated.
5. Tension force in the bar is calculated based on its stress-strain relationship.
6. If the compression force and the tension force are equal, the assumed neutral axis value is kept, otherwise change the neutral axis value and repeat the process from stage 3.

Alternatively, the neutral axis can be found from the following equation (GHALI, A. and Favre, G., 1994) (Equation 8-5),

$$x = \frac{-b + \sqrt{b^2 - 4ac}}{2a} \quad \text{.....Equation 8-5}$$

Where (please refer to the Figure 8-6),

$$a = \frac{bw}{2}$$

$$b = hf(b - bw) + ans * Ans + aps * Aps + (ans - 1)A'ns$$

$$c = -\frac{1}{2}hf^2 * (b - bw) - ans * Ans * dns - aps * Aps * dps - (ans - 1)A'ns * d'ns$$

ans = modular ratio of reinforcement and;

aps = modular ratio of prestressed steel

8 British Standard BS8110 – 1: 1997 Structural Use of Concrete – Part 1: Code of practice for design and construction

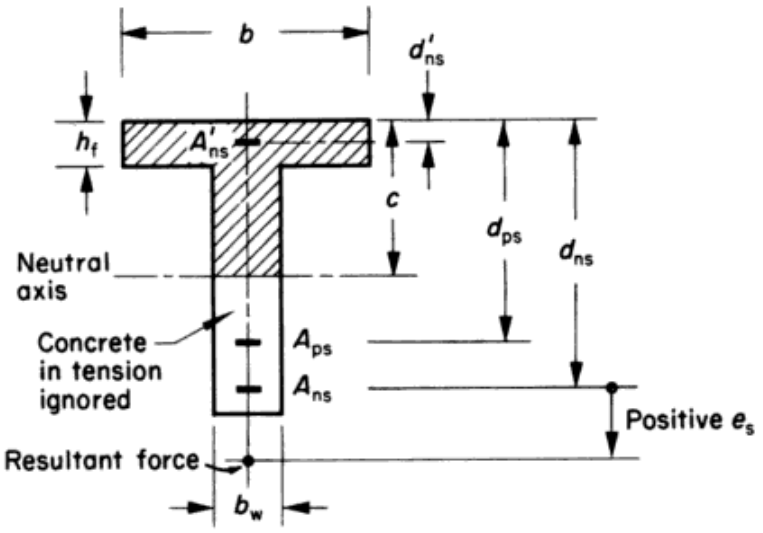

Figure 8-6: Definitions of Symbols

In case of singly reinforced concrete section, A'_{ns} (Compression reinforcement) and A_{ps} (prestressed steel) equal to zero.

8.2.2 Ultimate Limit State Shear

Shear failure occurs in reinforced concrete beams due to the formation of diagonal shear cracked normally initiated by vertical bending cracks. However it is very difficult to calculate the exact stress and the location of the stress that causes the formation of the diagonal crack. This is mainly because of the complex stress condition of the section in combination of shear and flexure stresses, and that reinforced concrete is a composite, non-homogeneous, and non-isotropic materials.

In general there are two types of failure modes of shear failure; 1) shear-tension failure and 2) shear-compression failure. Shear tension failure occurs from the excessive opening of the inclined crack results in the loss of bond between the concrete and the reinforcement. This eventually can proceed to anchorage failure. Shear compression failure is when the concrete at the tip of the inclined crack crushes due to high compression stress.

A reinforced concrete beam resists the shear through the three possible mechanisms (KOTSOVOS, M. D. and Pavlovic, M. N., 1999):

- Shear in compression zone: Compressive stress provided by the un-cracked concrete at the tip of the inclined crack. When the concrete fails the beam is said to have failed by shear compression.

- Aggregate interlock: the interlocking of the aggregates over the crack interface provides the resistance against the shear. It is believed that aggregate interlock take the major role in resisting the shear.
- Dowel action from longitudinal reinforcement: Some of the shear resistance is provided through the shear deformation of the reinforcement sitting in the line of shear crack.

The shear stress causing the inclined crack results from a combination of vertical shear stress and longitudinal bending stress, which is often, referred as principal stress.

Horizontal Shear Stress, $f = \frac{VQ}{Ib}$ ……..…Equation 8-6

Vertical Shear Stress, $v = \frac{V}{bd}$ .....Equation 8-7

Principal Stress = $\frac{f}{2} \pm \sqrt{\left(\frac{f}{2}\right)^2 + v^2}$ ……..Equation 8-8

Where,

V = Vertical Shear Force,

Q = First moment of area,

I = Second moment of Area,

b = Width of the section at horizontal layer under consideration

d = Effective depth

When the principal stress exceeds the ultimate tension strength of the concrete a diagonal crack is formed. The strength of un-reinforced concrete in pure shear is known to be in the range of 10 ~ 20% of the compressive strength, however concrete is rarely subjected to pure shear condition and actual tensile strength is lower than shear strength.

However it often very difficult to accurately predict the shear failure of a reinforced concrete beams because the failure is not just simply related to the 'shear strength' or the 'tensile strength' of the concrete. Shear failure is due to the combination of bending and shear behaviour of the section, and thus it is also difficult to predict at which location the particular combination would result the highest stress. There have been extensive works carried by researchers looking into the ways to accurately

describe the mechanisms, and to predict the shear failure. There are some methods based on numerical analysis that accurately predicted the shear failure of experimental beams, yet the broader applications of such methods are still in question. This does not imply that the current methods are not appropriate for designing reinforced concrete beams. The methods have been found to be satisfactory in normal design situations. Yet amid the current use of these methods one should still bear in mind about the level of accuracy of the methods in reflecting the real behaviour of the structure.

According to the British Standard Code of Practice, BS8110: Structural Use of Concrete, a reinforced concrete section is designed based on the design shear stress in the section and the design shear stress of concrete.

The design shear stress in the section, v is defined by,

$$v = \frac{V}{b_v d} \quad \text{.....Equation 8-9}$$

Where, V is design shear force due to the ultimate loads, b_v is breadth of the section (for a flanged beam this should be taken as the average width of the rib below the flange), and d is the effective depth. The code limits the stress by $0.8\sqrt{f_{cu}}$ or 5 N/mm^2 whichever is lesser, and the limits already include the factor of safety of 1.25.

The design shear stress of the concrete, v_c, is defined in the following table,

Table 3.8 — Values of v_c design concrete shear stress

$\frac{100A_s}{b_v d}$	Effective depth mm							
	125	150	175	200	225	250	300	400
	N/mm²	N/mm²	N/mm²	N/mm²	N/mm²	N/mm²	N/mm²	N/mm²
≤ 0.15	0.45	0.43	0.41	0.40	0.39	0.38	0.36	0.34
0.25	0.53	0.51	0.49	0.47	0.46	0.45	0.43	0.40
0.50	0.67	0.64	0.62	0.60	0.58	0.56	0.54	0.50
0.75	0.77	0.73	0.71	0.68	0.66	0.65	0.62	0.57
1.00	0.84	0.81	0.78	0.75	0.73	0.71	0.68	0.63
1.50	0.97	0.92	0.89	0.86	0.83	0.81	0.78	0.72
2.00	1.06	1.02	0.98	0.95	0.92	0.89	0.86	0.80
≥ 3.00	1.22	1.16	1.12	1.08	1.05	1.02	0.98	0.91

NOTE 1 Allowance has been made in these figures for a γ_m of 1.25.

NOTE 2 The values in the table are derived from the expression:

$0.79\{100A_s/(b_v d)\}^{1/3} (400/d)^{1/4}/\gamma_m$

where

$\frac{100A_s}{b_v d}$ should not be taken as greater than 3;

$\left(\frac{400}{d}\right)^{\frac{1}{4}}$ should not be taken as less than 0.67 for members without shear reinforcement;

$\left(\frac{400}{d}\right)^{\frac{1}{4}}$ should not be taken as less than 1 for members with shear reinforcement providing a design shear resistance of ≥ 0.4 N/mm².

For characteristic concrete strengths greater than 25 N/mm², the values in this table may be multiplied by $(f_{cu}/25)^{1/3}$. The value of f_{cu} should not be taken as greater than 40.

Figure 8-7: Table 3.8 of BS8110-design concrete shear stress values

Note 2 in the table (Figure 8-7) gives the expression from which the values in the table are calculated from, and it must be noted that the values (, which are the design shear stress values) increase as the area of steel reinforcement increases. The code recommends the addition of shear reinforcement according to the following criteria:

Table 3.7 — Form and area of shear reinforcement in beams

Value of v N/mm²	Form of shear reinforcement to be provided	Area of shear reinforcement to be provided
Less than $0.5v_c$ throughout the beam	See NOTE 1	—
$0.5v_c < v < (v_c + 0.4)$	Minimum links for whole length of beam	$A_{sv} \geq 0.4 b_v s_v / 0.95 f_{yv}$ (see NOTE 2)
$(v_c + 0.4) < v < 0.8\sqrt{f_{cu}}$ or 5 N/mm²	Links or links combined with bent-up bars. Not more than 50 % of the shear resistance provided by the steel may be in the form of bent-up bars (see NOTE 3)	Where links only provided: $A_{sv} \geq b_v s_v (v - v_c)/0.95 f_{yv}$ Where links and bent-up bars provided: see **3.4.5.6**

NOTE 1 While minimum links should be provided in all beams of structural importance, it will be satisfactory to omit them in members of minor structural importance such as lintels or where the maximum design shear stress is less than half v_c.

NOTE 2 Minimum links provide a design shear resistance of 0.4 N/mm².

NOTE 3 See 3.4.5.5 for guidance on spacing of links and bent-up bars.

Figure 8-8: Table 3.7 of BS8110-provision of shear reinforcement

One of the most recent approaches in predicting the shear failure (diagonal tension failure) of reinforced concrete beam can be found in the book, '*Ultimate limit-state design of concrete structures – A new approach*' (KOTSOVOS, M. D. and Pavlovic,

M. N., 1999) It states that the shear failure of a beam can be predicted from the corresponding moment using the following equation (Equation 8-10; for more detail information about the equation please refer to section 2.3.2 in chapter 2).

$$M_{cx} = 0.875a_{vx}d\{0.342b_1 + 0.3M_{fx}/d^2 * \sqrt{(z/a_{vx})}\} * \sqrt[4]{(16.66/\rho_w f_y)} \ldots \text{Equation 8-10}$$

It is 'a slightly modified (more conservative) version of an empirically derived formula for a beam's shear capacity, the latter already being adopted by the British code of practice for the fire-resistance design of concrete structure' (KOTSOVOS, M. D. and Pavlovic, M. N., 1999). The equation adapts the concept of the compressive force path theory and "the stress conditions within the compressive force path that cause 'shear' failure" (KOTSOVOS, M. D. and Pavlovic, M. N., 1999). The method also presents the results which show that the design method with the application of the above equation could closely predicts the load carrying capacity of the beams, especially for the case of T-beams.

8.2.3 Deflection

There are a number of methods to calculate deflection of a reinforced concrete beam. Most methods require the second moment of area of sections to be uniform throughout the length of the beam. For the beam with varying I values (which is the case of this research), the Moment-Area theorem can be used in the deflection calculation.

Finding the Second Moment of Area

For a reinforced concrete section the 'transformed section' is used to calculate the second moment of area.

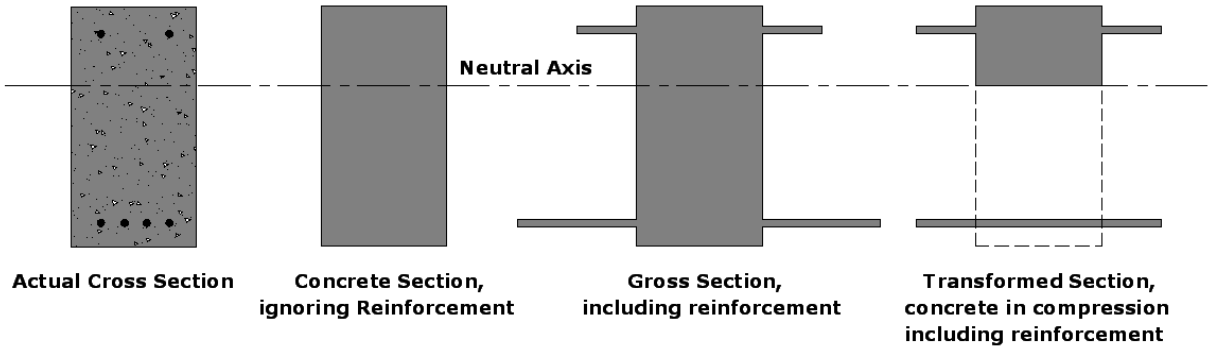

Figure 8-9: Transformed Section Theory

As the above diagrams indicate there are two transformed section types; un-cracked section and cracked section. The equivalent of steel section is defined as $n*A_s$, where n is the modular ratio which is defined by E_s/E_c. E_s and E_c are the elastic modulus of steel and concrete respectively. Once the neutral axis is known the second moment of area can be found using the below equation for un-cracked section (SCHODECK, D. L., 2004);

$$I_x = \int y^2 \, dA \quad \text{.....Equation 8-11}$$

Where,

I_x = the second moment of area of the section about the neutral axis x

dA = an elemental area

y = the perpendicular distance from the axis x to the element dA

For cracked section, the parallel axes theorem is used to calculate the second moment of area. The parallel axes theorem is described briefly below (SCHODECK, D. L., 2004):

$$I_x = I_c + Ad^2 \quad \text{.....Equation 8-12}$$

Where,

I_x = the second moment of area of the section about the axis x

I_c = the second moment of area of element about its centre of gravity

A = the area of the element

d = distance from the centre of gravity of the element to the neutral axis x of the section

Thus for the T-section where the neutral axis lies in the flange, the above two equations (Equation 8-11 and 8-12) can be combined into;

$$I_x = bx^3/3 + nA_s (d-x)^2 \quad \text{.....Equation 8-13}$$

Where,

b = the width of flange

n = modular ratio

A_s = area of reinforcement

x = neutral axis of the section

and for the T-section with the neutral axis in the flange, the two equations (Equation 8-12 and 8-13) can be combined into,

$$I_x = b*(h_f^3/12) + A_{cc}*(h_f/2+(x-h_f))^2 + b_w*(x-h_f)^3/3 + nA_s(d-x)^2 \ldots \text{Equation 8-14}$$

Where,

h_f = flange height

A_{cc} = area of concrete in compression below flange

x = neutral axis

b_w = width of the web

It should be noted that the second moment of area from the above equation assumes a fully cracked section. If a deflection at a certain load is sought it would be more accurate to use the effective second moment of area, I_{eff}, which considers the concrete tension stiffening effect (which describes the concrete's tension carrying capacity after cracking, and this contributes to the post-cracking stiffness of the member). However only the maximum deflection limit needs to be checked in normal design process and, from the assumption that the section is fully cracked would give more conservative value than when the effect of concrete in tension is taken into account. Thus in this research I_x is used in the deflection analysis.

Moment-Area Theorem (Curvature-Area Theorem) (HIBBELER, R. C., 2008)

This is a very powerful method for calculating the deflection of a beam with varying section depth (hence varying the second moment of area) using the M/EI diagram. For a beam with uniform section the shape of the M/EI diagram is exactly same is the bending moment diagram of the beam. The method is developed by Mohr and the theory is based on the moment-curvature relationship of the Euler-Bernoulli Theory of Bending.

$$1/R = M/EI \ldots\ldots\ldots\ldots\ldots\ldots \text{Equation 8-15}$$

Where,

R = radius of curvature

M = moment

I = the second moment of area

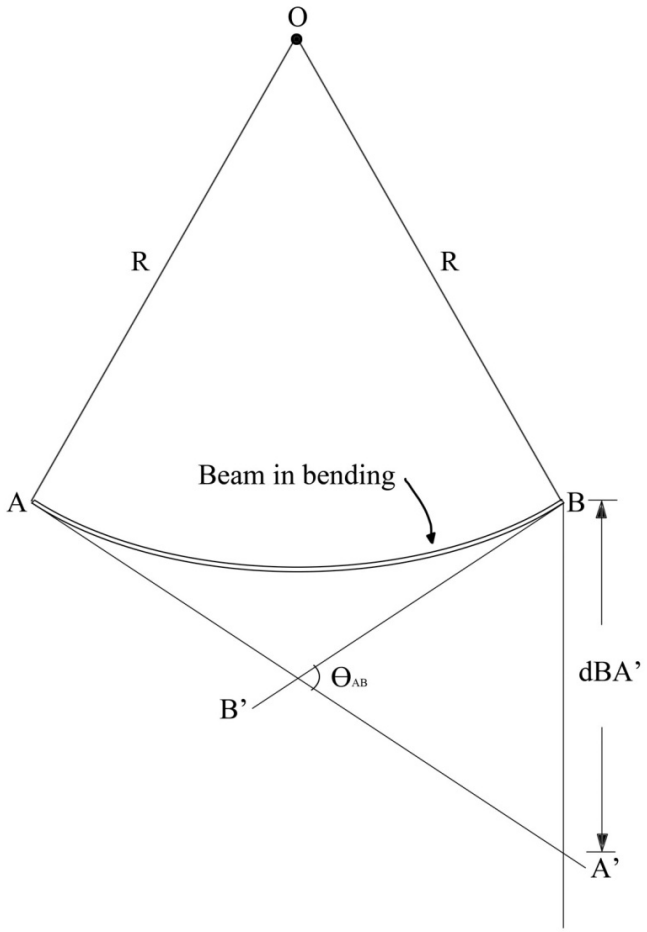

Figure 8-10: Beam in bending

The above diagram (Figure 8-10) shows a beam in bending;

- AA' is a tangent line to the point A, and BB' is a tangent line to the point B.
- Θ_{AB} is change in slope from A to B.
- dBA' is the vertical intercept and it the distance from B to the tangent line AA' which crosses at A'.

According to the Mohr's First Theorem;

'the change in slope between point A and B equals the area of the M/EI diagram between these two points'

and the Mohr's Second Theorem says that;

'dBA' equals the moment of M/EI diagram between point A and B calculated about point B, where dBA' is to be determined'

Thus in case to find the central deflection of a beam, simply the position of A should be moved to the mid-span, and the moment of M/EI between in A (at mid-span) and B (at the support) is calculated about B.

The procedure to calculate the central deflection of a beam by using the moment area theorem is as follow;

1. The beam is divided in to a number of sections.
2. Applied moments at certain locations of beam are calculated.
3. Second moment of area of each section calculated.
4. M/EI (= 1/r) for each section is calculated and plotted on a graph.
5. Area of each segment is calculated.
6. Each area is multiplied by the distance from the centroid of the segment to the support (point B).
7. The central deflection is found by adding up all the values found in step 5.

The above procedure is automated using the Microsoft Excel. The example can be found in the Appendix CD.

Chapter 9: Structural Analysis and Design Methods of the Beams

9.1 Introduction

This chapter includes the structural analysis of the fabric formed beams. The theoretical methods adopted for the following analysis are all included and pre-discussed in the chapter 8, 'RC beam analysis theory and methods'.

The structural analysis is carried out on the following criteria, and the purpose of each analysis is described in the following sections:

- Anchorage Stress
- Bending
- Shear
- Mid-span Deflection

Anchorage Stress Analysis

The initial beams, 11SA10mm and 11SA12mm demonstrated a weakness in the anchorage zone. Thus it is important to be able to predict the section's capacity against the applied anchorage stress, and design the section correctly to sustain the stress. Thus the analysis compares the concrete capacity of the section with the applied anchorage stress calculated from the Strut-and-Tie model. Based on the comparison the analysis makes an attempt to understand the structural behavior around the anchorage in more detail. In subsequent beams the anchorage failure was avoided by modifying the reinforcement and the form of the beam.

Ultimate Limit State Moment Analysis

This analysis examines whether the bending capacities of the fabric formed beams can be predicted (and so the ultimate load of the beam corresponding to bending can be determined) using the current theoretical methods. The neutral axis values of the sections used in the analysis are obtained in two ways (; using the formula for T-section, the compression and tension force compatibility method (computation using Python included in Appendix), or extracted from the graph of experimental compression and tension strain readings), and the moment capacities calculated from these neutral axis values are also compared with the applied moment. As long as it can be confirmed that the current structural

theories can accurately predict the bending capacities of the section, it demonstrates that they can be designed in accordance with the BS 8110:1997.

Ultimate Limit State Shear Analysis

The purpose of this analysis is to examine whether a shear failure of the beam can be predicted using the known theoretical methods; including the formula stated in the book by Kotsovos and Pavlovic (KOTSOVOS, M. D. and Pavlovic, M. N., 1999) and the BS 8110 shear check.

It is difficult to fully understand and accurately predict the beams' true behaviour in shear. Thus the main goal is not to find the theory or analytical methods that would accurately predict the shear failure load and the location of the failure, but to make certain confirmations in regard with the possible structural results of a fabric formed beams, which are designed in accordance with the above widely accepted methods and put to use. Thus the theoretical results are compared with the experimental results, and their relationships are evaluated. As long as the designs from the methods are more conservative than the experimental results it is considered as satisfactory.

Serviceability Limit State Deflection Analysis

The nature of this analysis is similar to that of the shear analysis. It is sought to find a stable relationship between the theoretical results and the experimental results which can possibly be adopted in the in the future design methods.

9.2 Anchorage Stress Analysis

11SA10mm and 11SA12mm failed by the crushing of concrete around the anchorage zone. Initially it was considered that the failure of the above beams is due to the high uni-axial compression stress of the anchorage exceeding the compression capacity of the adjacent concrete. A simple Strut-and-Tie model was used to calculate the applied anchorage compressive force.

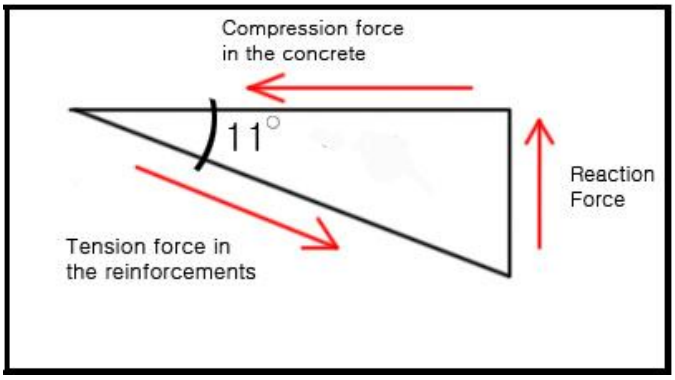

Figure 9-1: Strut-and-Tie Model

The following table (Table 9-2) and compares the anchorage compression stress induced in each beam with the concrete compression strength. Please note that as it was mentioned in the chapter 6, the values of the anchorage compression stress are rough estimations for the actual stress, and the purpose of this comparison is for the preliminary guidance only.

Beam	Reaction Force/ N	No. of Anchorage	Rebar Angle	Total Surface Area of Anchorage/ mm2
11SA10mm	5666	1	11	1800
11SA12mm	4961	1	11	1760
11DA10mm	9981	2	11	3600
11DADF10mm	10971	2	11	3600
11DADF12mm	13301	2	11	3520
11DADFWW12mm	18101	2	11	3520
22SA10mm	8801	1	22	1800
22SADF10mm	12216	1	22	1800
22SADF12mm	17251	1	22	1760
22SADF3no10mm	16301	1	22	1800
22SADF3no12mm	16431	1	22	1760
22SADFWW3no12mm	26701	1	22	1760

Table 9-1: Anchorage Bearing Stress and Compression Strength of Concrete

Beam	Compressive Stress Under Anchorage/ Nmm-2	Cylinder Strength/ Nmm-2	Ratio: Applied Stress/ Cylinder Strength
11SA10mm	**16.19**	**21.76**	**0.74**
11SA12mm	**14.50**	**16.24**	**0.89**
11DA10mm	14.26	31.68	0.45
11DADF10mm	15.68	26.16	0.60
11DADF12mm	19.44	23.15	0.84
11DADFWW12mm	26.46	31.76	0.83
22SA10mm	12.10	30.90	0.39
22SADF10mm	16.80	21.96	0.76
22SADF12mm	**24.26**	**21.42**	**1.13**
22SADF3no10mm	22.41	23.15	0.97
22SADF3no12mm	23.11	26.16	0.88
22SADFWW3no12mm	**37.55**	**33.04**	**1.14**

Table 9-2: Anchorage Bearing Stress and Compression Strength of Concrete

The cube strengths are converted to the cylinder strengths with the multiplication factor of 0.8 (KONG, F. K. and Evans, R. H., 2001).

The table 9-1 and 9-2 show that increasing the angle of the rebar, and increasing the number of anchorages have reduced the compressive stress of anchorage (11DA10mm and 22SA10mm).

In the table 9-2 the concrete cylinder strengths of 11SA10mm and 11SA12mm have not been reached by the anchorage compressive stress calculated by the strut-tie model, yet the test results show that both beams have failed at the anchorage zone. The table 9-2 also shows that for 22SADF12mm and 22SADFWW3no12mm the applied anchorage compression stressed have exceeded the cylinder strengths by 13% and 14% respectively, however the experimental test results show that there have been no signs of failure around the anchorage zone.

The first possible explanation on how the sections could sustain greater loads than the known uni-axial concrete compression capacities is in relation to the tri-axial stress state of the concrete; when concrete in a structure is compressed by a localised stress it undergoes lateral expansion. However this lateral expansion is resisted by the adjacent concrete (if there is sufficient surrounding concrete) and this provides the confining pressure which as result the concrete compression capacity to increase. Please refer to the following statement:

'...a small confining stress of the order of 0.1f_c (where f_c is the uniaxial cylinder compressive strength of concrete) leads to an increase of the compressive strength in the orthogonal direction by more than 50%.' (KOTSOVOS, M. D. and Pavlovic, M. N., 1999)

Thus based on the above statement it can be explained that even though the anchorage compression stress has exceeded the uni-axial compression strength of the concrete, yet it has not exceeded the increased compression strength of concrete in tri-axial condition.

The additional view is that the failure of concrete around the anchorage zone (which was the case for 11SA10mm and 11SA12mm) was not actually due to the compression failure of the concrete, but due to the transverse tension stress incurred in the concrete adjacent to the axis of anchorage compression stress. In this view the sections did not fail by crushing of concrete, but failed by splitting of concrete. Due to concrete's weak tensile capacity before the applied stress reaches the compressive strength of the concrete it fails by transverse tensile stress. This also explains the failures of the beams despite the compressive strengths concrete were stronger than the applied stresses from the anchorage.

The bearing stress problems typically occur at the anchorage of pre-stressed concrete construction resulting from insufficient transverse reinforcement. Please look at the following diagrams (Figure 9-2 and 9-3)

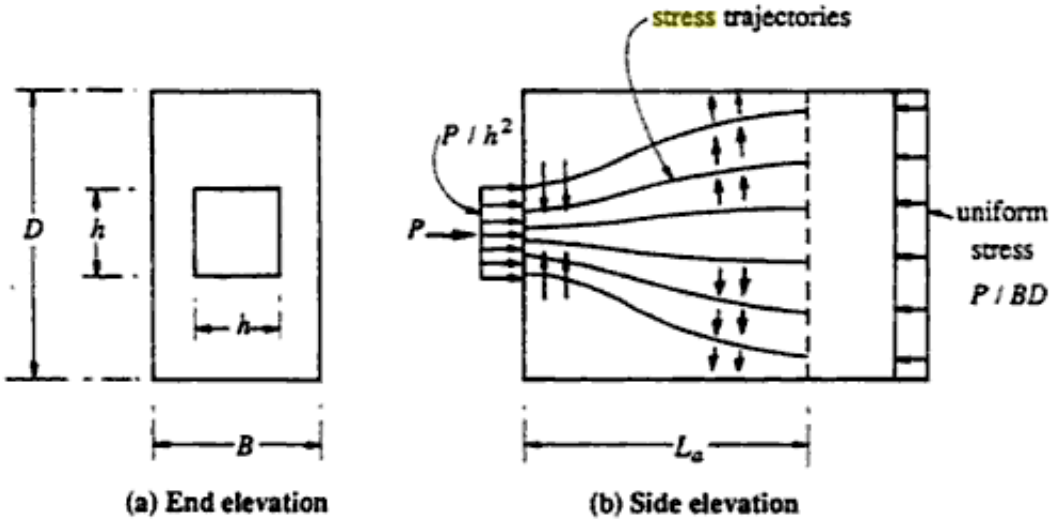

Figure 9-2: Diagrammatic stress trajectories for a centrally placed anchorage (GILBER, R. I., and Nickleborough, N. C., 2002)

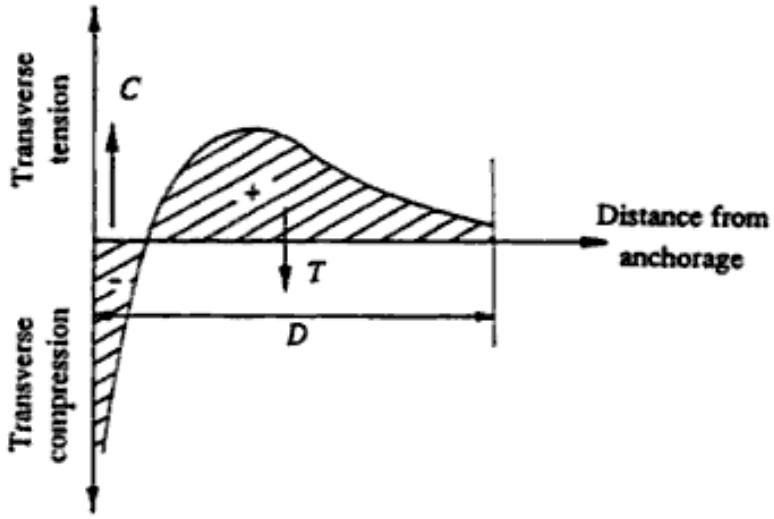

Figure 9-3: Distribution of transverse stress behind single central anchorage (GILBER, R. I., and Nickleborough, N. C., 2002)

The figures illustrate that high transverse compression stress is induced immediately behind the anchorage, and as the distance moves away the compression stress rapidly changes to transverse tension stress. In case of the fabric formed beams the anchorage is a round steel bar and the contact surface between the rebar and the concrete is in very thin line, it is considered that very large splitting tension stress has induced immediately behind the anchorage (Figure 9-4). Thus it seems that the concrete of the anchorage zone is failed by splitting of the concrete section due to this tension stress.

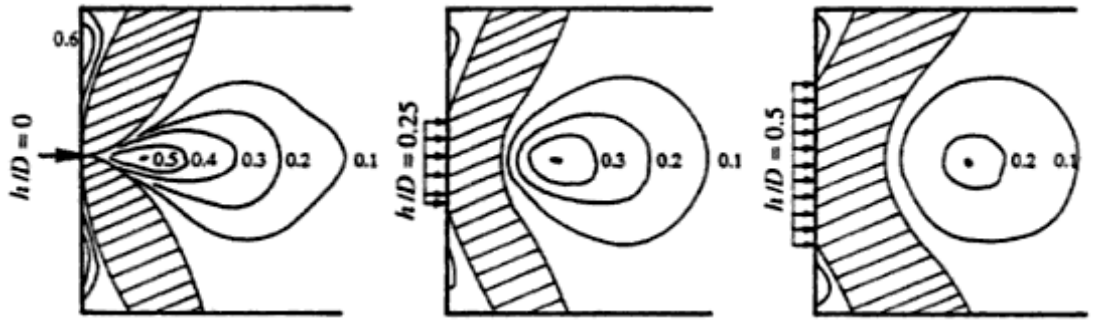

Figure 9-4: Stress isobars of transverse stress distribution for central anchorage of various sizes; the shaded areas are in compression (GILBER, R. I., and Nickleborough, N. C., 2002)

In the later beams with the thicker flange depth of 80mm, the anchorage is not located at the centre of the section but it is located closer to the bottom of the flange, and this result in eccentrically applied compression stress. Please refer to the following diagram (Figure 9-5)

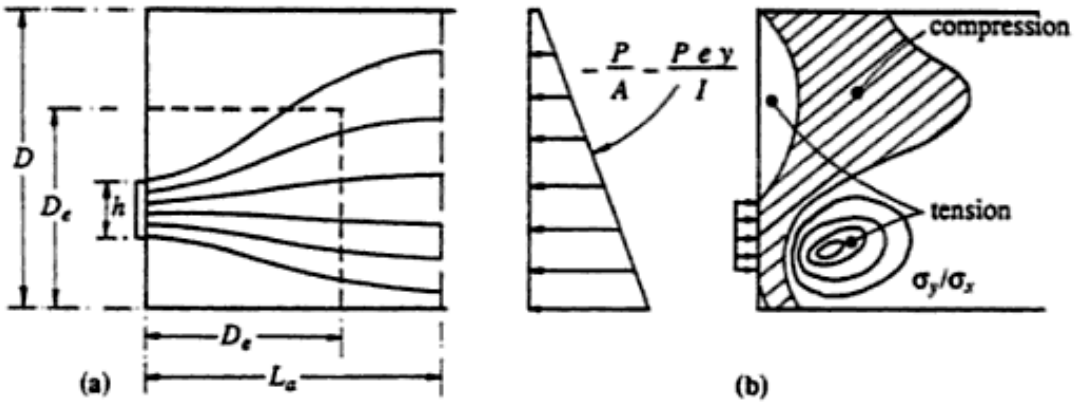

Figure 9-5: Diagrammatic stress trajectories and isobars for an eccentric anchorage (GILBER, R. I., and Nickleborough, N. C., 2002)

The above diagram is slightly modified for the anchorage with very small *h* value, which is the case of the fabric formed beams, and the stress distribution is predicted as follow (Figure 9-6)

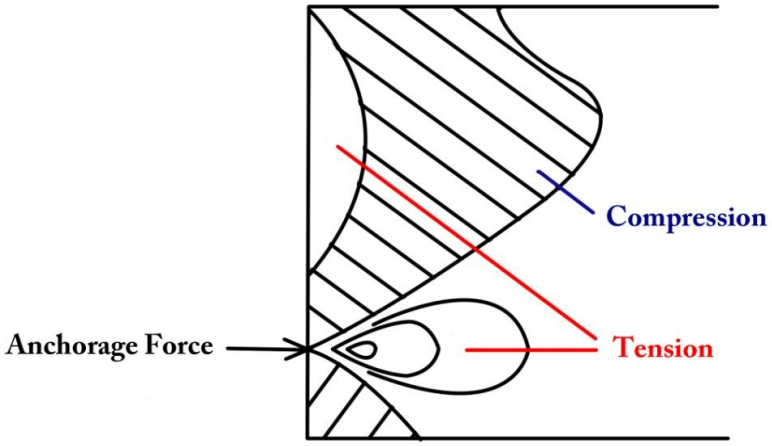

Figure 9-6: Re-interpretation of the isobars for an eccentric anchorage

In the above case the transverse tension stress is covered by the large compression stress region from above and by the relatively small region from the below, which will be companied by further compression stress incurred by the reaction force from the support. Thus it is considered that these surrounding compression stresses have prevented the section from failing by the splitting of the concrete.

There are other factors affecting the stress condition inside the concrete

The stress distribution around the anchorage is further explored using the finite element models using the software called Abaqus CAE, and the results will be discussed in the later chapter (Chapter 10).

In summary the analysis shows that the failure around the anchorage zone can be

avoid by reducing the compressive stress applied by the anchorage (more anchorage and increase rebar angle) and/or by increasing the thickness (or the surrounding concrete) of the flange to work against the splitting stress of concrete.

9.3 Ultimate Limit State Bending Analysis

This section examines the use of the current reinforced concrete bending theory for the design of fabric formed beams.

The bending capacity of the section is calculated based on the basic moment capacity expression stated below:

$$M_c = F_T * z \quad \text{.....Equation 9-1}$$

Where,

M_c = the moment capacity based on the reinforcement tension strength (Nmm or kNm)

F_T = the ultimate tension force the reinforcement (N or kN)

z = lever arm (mm)

The compression force, F_C, and the lever arm, z depend of the stress-strain distribution (curve) of the concrete section. For more information please refer to Chapter 8.

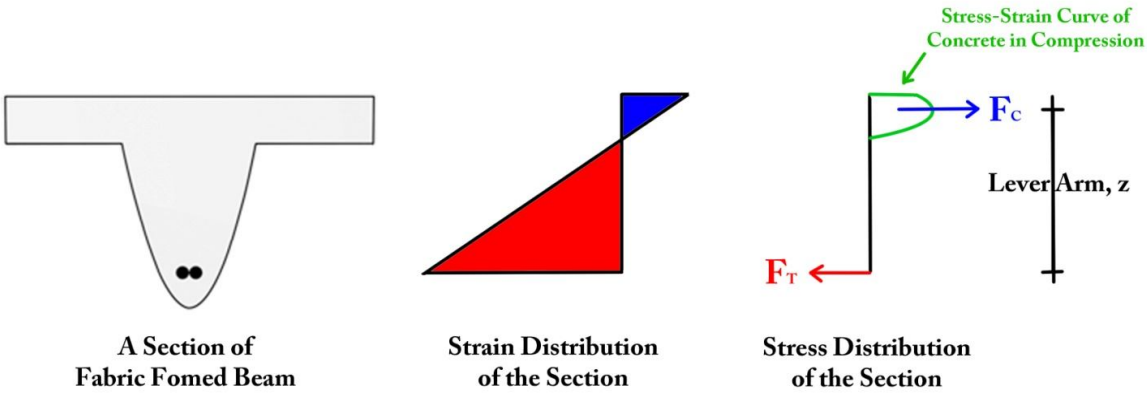

Figure 9-7: Strain and Stress Distribution of Reinforced Concrete Section

Table 9.3 compares the calculated moment capacities of the experimental moments at failure. The ratios of Mc/Ma show very good accuracy of the predicted capacities. In the most cases the sections could take 1% ~ 11% more moment than predicted, and for just two cases the predicted values are overestimated by up to 5%.

The results show that the current reinforced concrete bending theory and the method of calculating the bending capacity of reinforced concrete section can accurately predict the bending capacities of fabric formed sections.

Beam	Theoretical Moment Capacity, Mc/ kNm	Applied Failure Moment, Ma/ kNm	Ratio Ma/Mc
11DA10mm	2.85	2.69	0.95
11DADF10mm	8.38	8.44	1.01
11DADFWW12mm	11.43	11.87	1.04
22SADF10mm	7.79	8.63	1.11
22SADF12mm	11.06	12.19	1.10
22SADF3no10mm	11.65	11.52	0.99
22SADFWW3no12mm	16.31	17.17	1.05

Table 9-3: Comparing Theoretical and Experimental Moment

9.4 Ultimate Limit State Shear Analysis

This section examines the use of the following expression in predicting the shear failure of the fabric formed beams. The expression (Equation 9-3) is derived based on the experimental results (BOBROWSKI, J., 1982), (BOBROWSKI, J. and Bardhan-Roy, B. K., 1969), and further modified to a more conservative version (KOTSOVOS, M. D. and Lefas, I. D., 1990).

$$M_c = 0.875sd\{0.342b_1 + 0.3(M_f/d^2)*\sqrt{(z/s)}\}*\sqrt[4]{(16.66/\rho_w f_y)} \quad \text{.....Equation 9-3}$$

where,

M_c = the moment corresponding to 'shear' failure (Nmm)

s = is the distance of the cross-section where M_c is calculated measured from the support closest to it:

- $s = a_v$; for the case of two-point loading (i.e. the shear span); (single-point loading can be viewed as a special case of two coincident point loads)
- $s = 2d$; for the case of uniformly-distributed loading (including any case where more than two point loads are uniformly distributed along the beam span)

M_f = the flexural capacity (Nmm)

z = lever arm (mm)

d = the effective depth (mm)

$\rho_w = As/(b_o d)$

f_y = the characteristic strength of the tension steel (N/mm2)

b_1 = min (b_o + 2b_s, b_o+2d_s);

(it should be noted that for a rectangular cross-section of width b, b_1 = b.)

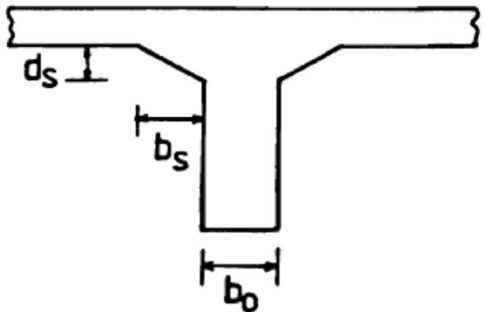

Figure 9-8: Definition of b_o, b_s, d_s

In case of fabric formed beams, the definition of b_o is not clear. Thus b_o is considered to be 0, and thus b_1 is lesser of 2b_s and 2d_s. The definition of b_s and d_s for the fabric formed beams' sections is shown below.

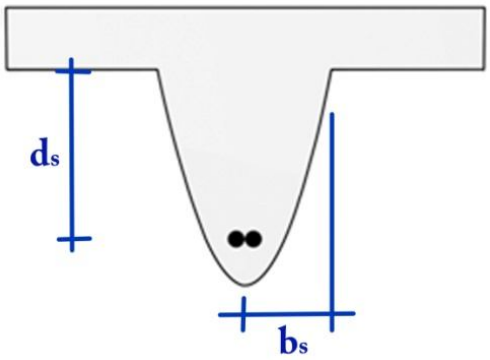

Figure 9-9: Definition of b_s and d_s

Another thing to note is the steel ratio, which is defined in the above section as, ρ_w = As/(b_od). It is discussed that b_o is considered as 0, which is not applicable for the calculation of steel ratio. However as the definition of the steel ratio is' the steel area to the web area of concrete to the effective length'[9], the equation could be written as, ρ_w = As/($b_s d_s$); the equation assumes that the web area is twice the area of the triangle calculated by 0.5* d_s * b_s.

It must be mentioned that in reality the web area towards the support where the high

9 *"...The formula applies for beams with the same cross section throughout their span. However, it may be applicable to beams such as yours, if you establish the relationship between Mcx and Vcx at various cross sections by replacing in the formula each time the cross-sectional characteristics and flexural capacity of the cross section considered. As steel ratio, rho w, I have always used the steel area to the web area of concrete to the effective depth…."*
Extracted from the e-mail received from Professor Kotsovos on the 13th of February, 2009 at 15:14:53.

shear stress presents is very small, and thus the effect of which any slight differences in the calculation of web area has on the overall result of the shear calculation is negligible. Hence the above discussion regarding the web area is more to find the correct interpretation of the definitions for the case of fabric formed beam than to increase the accuracy of the calculation.

For the beams that failed by shear, the failed location has been near the 310mm section, except for 22SA10mm which the failed section located at about 130mm from the support. Also the shear crack exists over certain length, thus it is not easy to say exactly at which location the failure took place. Thus the shear capacities of certain sections are calculated and the sections in between are estimated.
In the most cases the formula has underestimated the shear capacities of the sections. Table 9-4 compares the applied moment with the section capacity taken at 310mm location from the end of flange since it is where the most shear failure occurs, except for 22SA10mm which had shear failure at 130mm location from the support.

Beam	Moment Applied, Ma	Mcx (Kotsovos)	Ma/Mcx
11DA10mm	2.69 kNm	1.28 kNm	2.11
11DADF10mm	3.40 kNm	2.06 kNm	1.65
11DADF12mm	**4.03 kNm**	**2.87 kNm**	**1.44**
11DADFWW12mm	5.21 kNm	8.71 kNm	0.60
22SA10mm	**1.14 kNm**	**1.15 kNm**	**0.99**
22SADF10mm	3.79 kNm	3.61 kNm	1.05
22SADF12mm	5.35 kNm	4.22 kNm	1.27
22SADF3no10mm	5.05 kNm	4.57 kNm	1.11
22SADF3no12mm	**5.05 kNm**	**4.66 kNm**	**1.08**
22SADFWW3no12mm	7.53 kNm	12.13 kNm	0.62

Table 9-4: Comparing the applied moment and the moment capacity of the critical section corresponding to the shear failure. The highlighted beams are failed by shear.

For the beams 22SA10mm and 22SADF3no12mm, which failed by shear near the 310mm section, the predictions are very close and the discrepancies are only 1% and 8% respectively. However for 11DADF12mm, which also failed by shear the section could take about 44% more than predicted value. In design point of view it is safer to underestimate the shear capacity of the beams, and thus it is shown that using the expression to design the fabric formed beam sections will give satisfactory result.

It is interesting to note that the results of 22SADF3no10mm and 22SADF3no12mm show that the shear capacity of the sections have not increased despite the 44% increase in the total reinforcement area. This shows that the shear capacity of the

fabric formed section is not related to the amount of steel in the section, which is suggested by the Kotsovos and Lefas' expression.

In addition to this, the above test results are showing that the shear capacity of the section is mainly related to the effective depth of the section, and the efficient structural form about the section which enhances the distribution of the induced stresses.

The explanation for the large discrepancy between the predicted value and the experimental result in case of 11DADF12mm is yet to be investigated. However the paper by Bobrowski and Bardhan-Roy (BOBROWSKI, J. and Bardhan-Roy, B. K., 1969) indicates that a shear resistance of a reinforced concrete section can be substantially increased by the having a 'haunch' or 'fillet' of the web.

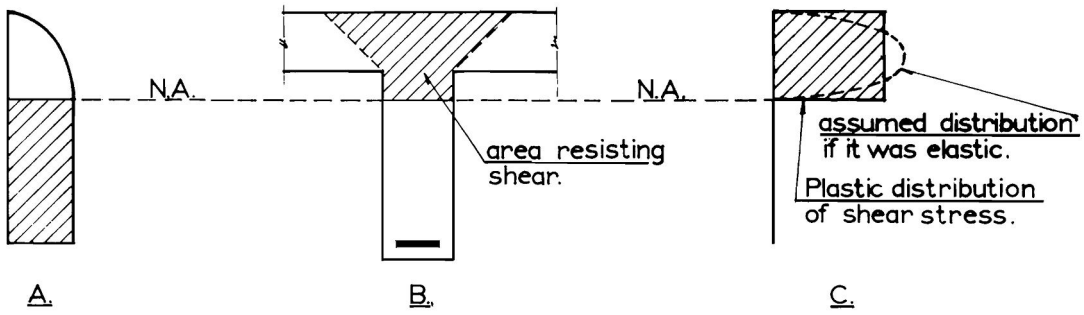

Fig 19 Shear stress distribution in a RC T beam. (A, B, C)

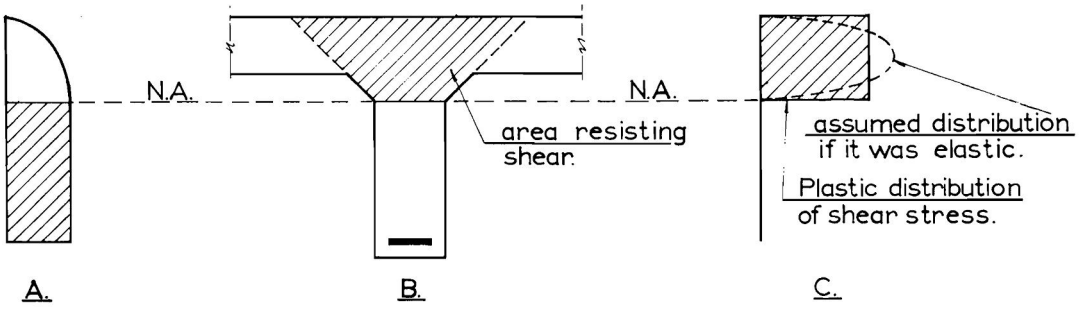

Fig 20 Shear stress distribution in a RC T beam with (A, B, C) haunch.

Figure 9-10: Effect of Hunch of the Web in Shear Resistance (BOBROWSKI, J. and Bardhan-Roy, B. K., 1969)

As the above diagrams suggest the shear stress could be distributed over a larger area by having the haunch. In case of the fabric formed beam sections, this area is maximised due to the unique cross-section shape of the web. However, it must be noted that the haunch will make the significant increase in the shear capacity when the neutral axis is below the flange. If the neutral axis is in the flange, which is the case for the last beams with wide web with the neutral axis around 32mm and 43mm

point from the top, then the haunch does not take any shear stress.

The following table summarizes the results of shear design checks of the fabric formed beams in accordance with the British Code BS8110 method. In the most cases the BS 8110 method suggest that sections only require the minimum shear links. For 22SADF12mm and 22SADF3no10mm the methods suggest including shear links, and from the test results the beams did not fail by the shear however the sections shear capacities were almost reached. For 22SA10mm the code suggests that the section only requires the minimum links, and the experiment showed that the beam failed by shear. For the beams, 11DADF12mm and 22SADF3no12mm the code suggests including the shear links and the test results also showed that the beams failed in shear.

Beam	v	vc	vc + 0.4	0.8√fcu	Shear Links Requirement
11DA10mm	2.45	2.15	2.55	5.03	Min. Links
11DADF10mm	1.94	2.64	3.04	4.57	Min. Links
11DADF12mm	**2.23**	**1.72**	**2.12**	**4.30**	**Design Shear Links**
11DADFWW12mm	0.64	1.67	2.07	5.04	Min. Links
22SA10mm	**0.76**	**3.46**	**3.86**	**4.97**	**Min. Links**
22SADF10mm	1.62	1.94	2.34	4.19	Min. Links
22SADF12mm	2.37	1.59	1.99	4.14	Design Shear Links
22SADF3no10mm	2.47	1.68	2.08	4.57	Design Shear Links
22SADF3no12mm	**2.22**	**1.64**	**2.04**	**4.30**	**Design Shear Links**
22SADFWW3no12mm	0.76	1.62	2.02	5.14	Min. Links

Value of v N/mm²	Form of shear reinforcement to be provided	Area of shear reinforcement to be provided
Less than $0.5v_c$ throughout the beam	See NOTE 1	—
$0.5v_c < v < (v_c + 0.4)$	Minimum links for whole length of beam	$A_{sv} \geq 0.4b_v s_v / 0.95f_{yv}$ (see NOTE 2)
$(v_c + 0.4) < v < 0.8\sqrt{f_{cu}}$ or 5 N/mm²	Links or links combined with bent-up bars. Not more than 50 % of the shear resistance provided by the steel may be in the form of bent-up bars (see NOTE 3)	Where links only provided: $A_{sv} \geq b_v s_v (v - v_c)/0.95f_{yv}$ Where links and bent-up bars provided: see 3.4.5.6

NOTE 1 While minimum links should be provided in all beams of structural importance, it will be satisfactory to omit them in members of minor structural importance such as lintels or where the maximum design shear stress is less than half v_c.

NOTE 2 Minimum links provide a design shear resistance of 0.4 N/mm².

NOTE 3 See 3.4.5.5 for guidance on spacing of links and bent-up bars.

Table 9-5: Shear reinforcement requirement guidance according to the BS8110 (the above table is directly extracted from the reference[5])

Based on the above table it can be summarized that the code does not accurately predict the shear requirement of fabric formed beams. Though in general it can be

accepted that when the code suggests the beam to have the minimum amount of shear links the shear capacity of the fabric formed beam section is sufficient to resist the design shear stress; and when the code indicates that the design shear links are required, then the section's effective depth should be increased, or actually add the shear links.

9.5 Serviceability Limit Deflection Analysis

This section checks the central deflection of the beams under the service load with the deflection limit (Span/250) suggested by the British Standard Code of Practice BS8110. The limit is suggested to avoid any cracking and vibration that would cause the structure to become unserviceable (REYNOLDS, C. E., Steedman, J. C., and Threlefall, A. J., 2008). Also the experimental deflection values are compared with the theoretical values calculated with the Moment-Curvature Method. Due to the varying geometry of the beam along the span, the Moment-Curvature relationship has to be found at the every given section, and the vertical deflection owing to the bending of each section is calculated. The vertical displacements of all the sections are summed up to give the central deflections of the beams.

The following Table 9-6 shows the experimental deflections of the beam at the service loads. The service load of the beams are calculated by dividing the ultimate loads by 1.6; based on the code BS8110.

Beam	Service Load/ kN	Empirical Deflection/ mm	Ratio of Deflection to Span/250
11DA10mm	12.1	9.74	0.81
11DADF10mm	13.69	14.15	**1.17**
11DADF12mm	16.25	11.4	0.94
11DADFWW12mm	22.25	12.1	1.00
22SA10mm	10.63	8.19	0.68
22SADF10mm	14.89	8.78	0.73
22SADF12mm	21.19	10.89	0.90
22SADF3no10mm	20	11.34	0.94
22SADF3no12mm	20.16	8.52	0.71
22SADFWW3no12mm	33	13.6	**1.13**

Table 9-6: Experimental Deflection and the limit by BS8110

The span of the beams is 3020mm, and the BS8110 recommends the deflection limit under service load to be Span/250 = 12.08mm. The most of the beams satisfied this criterion except 11DADF10mm and 22SADFWW3no12mm, which exceed the limit by 17% and 13% respectively.

The following (Table 9-7) compares the experimental deflection values with the theoretical deflection values, which are calculated with the Moment-Curvature method.

Beam	Service Load/ kN	Theoretical Deflection/ mm	Experimental Deflection/ mm	Ratio: Experimental/ Theoretical
11DA10mm	12.10	9.84	9.74	0.99
11DADF10mm	13.69	11.37	14.15	1.24
11DADF12mm	16.25	7.01	11.40	1.63
11DADFWW12mm	22.25	8.20	12.10	1.48
22SA10mm	10.63	9.20	8.19	0.89
22SADF10mm	14.89	9.47	8.78	0.93
22SADF12mm	21.19	8.13	10.89	1.34
22SADF3no10mm	20.00	7.41	11.34	1.53
22SADF3no12mm	20.16	5.62	8.52	1.52
22SADFWW3no12mm	33.00	10.63	13.60	1.28

Table 9-7: Comparing the theoretical and experimental deflection values

The results show that for the most of the beams the theoretical values underestimate the actual deflections of the beam in the range of 24% ~ 63% (2.76mm ~ 4.4mm).
In the overall pattern, the discrepancy between the theoretical and the experimental values increases as the service load increases; however it has actually decreased when the geometry of the web changed. For example, from 11DADF12mm to 11DADFWW12mm the service load increased by 37%, but the discrepancy in the deflection values decreased by 15% (From 63% to 48%). Also from 22SADF3no12mm to 22SADFWW3no12mm the load increase is 64% but the discrepancy in the deflection is decreased by 24% (From 52% to 28%). Such reductions could be due to the increase in the second moment of area of the sections near the supports. However it could also be argued that the second moment of area of the cracked sections is not affected by the web geometry when the neutral axis actually lies in the flange. Yet the results show that development of the web geometry has increased the overall stiffness of the beam.

In the graphs the empirical deflection curves show the non-linear behaviour of the beam in contrast to the theoretical deflection curves, and it is because in theory it assumes that the stress-strain relationship of concrete is constant, yet in the actual beam it is non-linear, therefore the load-deflection relationship is non-linear.

Another aspect about the discrepancy between the theoretical and experimental deflection values is that it is greater for the beam with the shear crack formed near supports. Please refer to the following Figure 9-11.

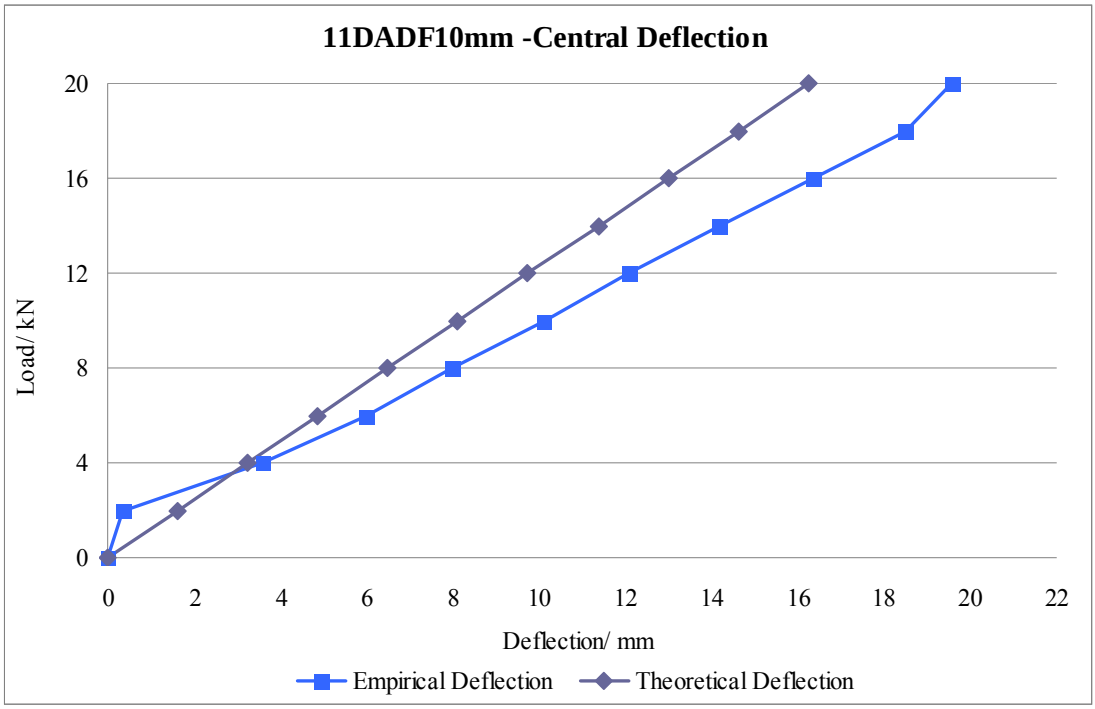

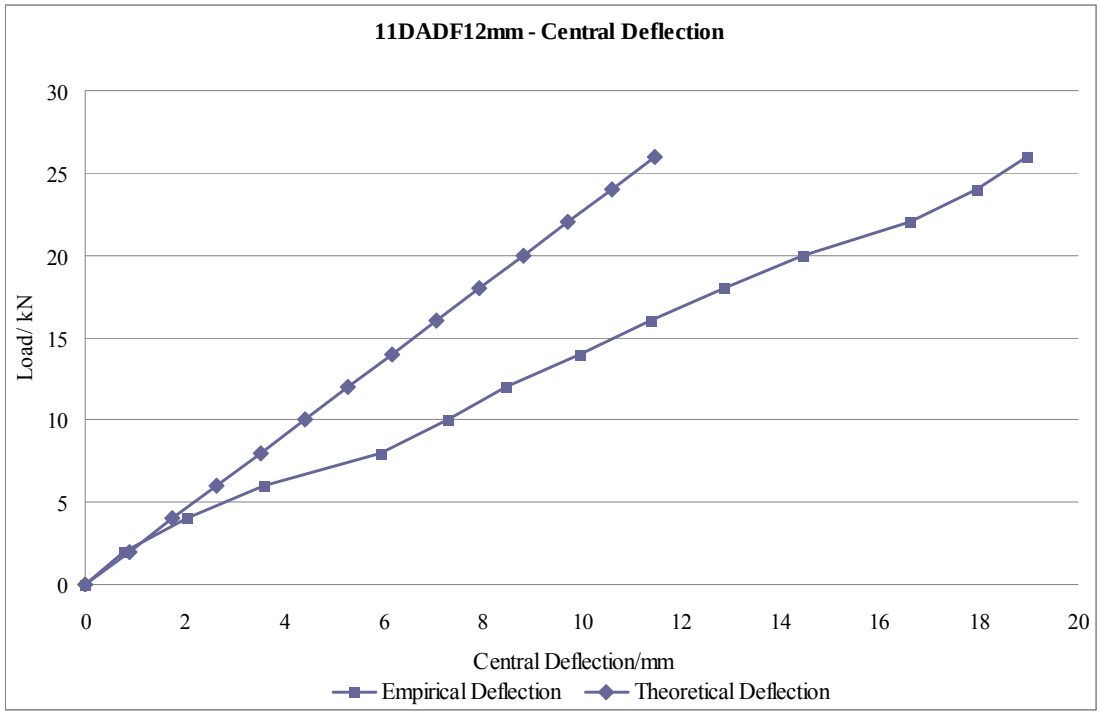

Figure 9-11: Deflection graphs of 11DADF10mm and 11DADF12mm

The graphs show compare the theoretical and experimental deflections of 11DADF10mm and 11DADF12mm, which failed by mid-span rebar yielding and shear respectively. In the graph of 11DADF12mm the separation between the two curves are clearer. The same can be seen from the comparison of the following Figure 9-12.

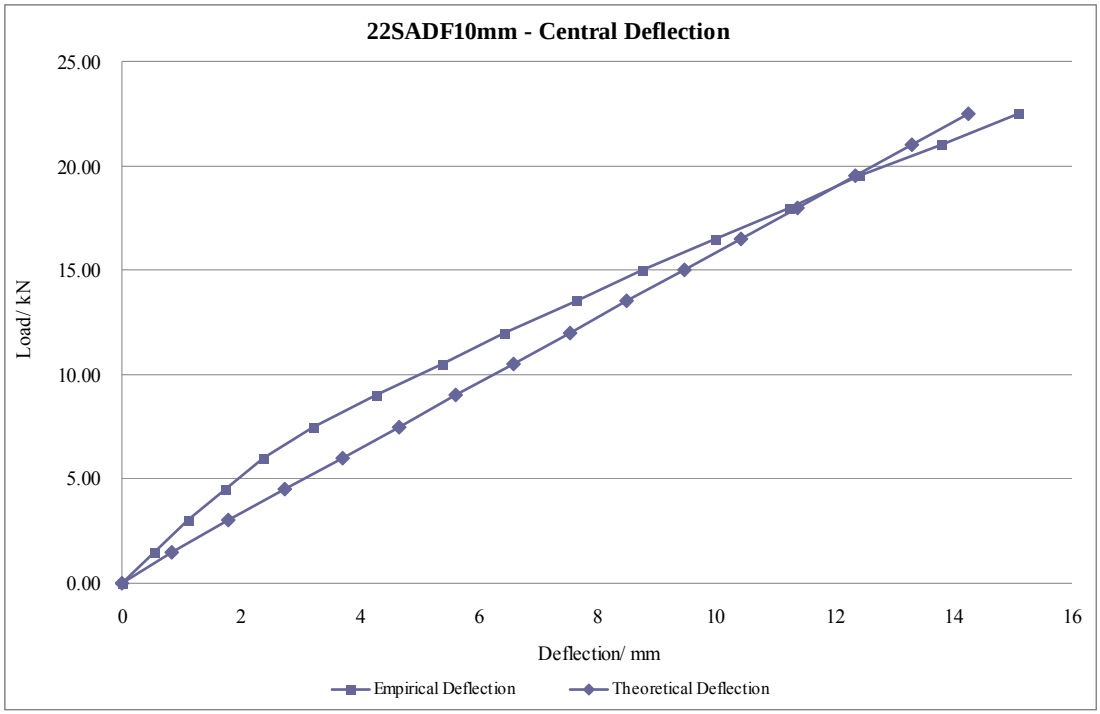

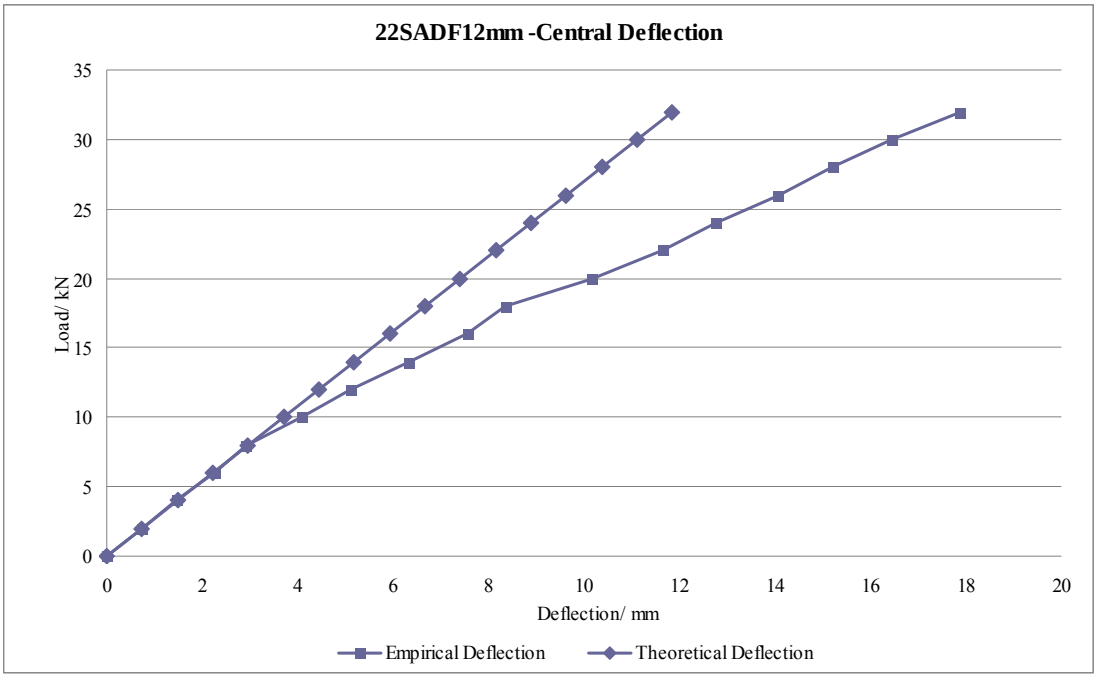

Figure 9-12: Deflection graphs of 22SADF10mm and 22SADF12mm

Again the separation of the theoretical and experimental values is greater in the graph of 22SADF12mm than in the graph of 22SADF10mm. Both beams failed by yielding of the rebar at the mid-span, but clear shear crack were present at the sections of 22SADF12mm.

Thus in addition to the common view that the non-linear behaviour of the beam is due to the progressive development of cracking, non-linear behaviour of concrete, and the contribution of tension stiffening, the large discrepancies between the values

may possibly be either as a result of the shear cracks near support. The theoretical deflection of the beam is calculated based on the moment-curvature relationship of the sections. Thus the calculation does not consider the deflection corresponding to the opening of diagonal shear cracks. As the shear cracks are far from the mid-span of the beam, even the small opening of crack can cause additional deflections at the mid-span.

It is already discussed in the strain analysis that, for the beams failed by shear the great compression strain is measured at the top of the shear crack. This means there is a large vertical deflection occurs at the section with the shear crack. Thus it can be said that the large part of the central deflection of the beam owes to the section with the shear crack.

However the above view still requires further investigation.

9.6 Summary and Conclusions

Anchorage Compression Stress Analysis

The analysis used simple Strut-and-Tie model to compare the anchorage compression stress with the uni-axial compression capacity of the concrete. The comparison shows that the applied compression stress of anchorage has exceeded the concrete compression capacity of 22SADF12mm and 22SADFWW3no12mm. The test results showed no sign of concrete failure in those beams. Based on the above observation the following points have been discussed:

1. The above comparison is made with the uni-axial compression capacity of concrete, and the concrete in the beams is likely to be exposed to tri-axial stress condition. When the confining pressure is applied to concrete in the tri-axial condition, even the small magnitude of pressure can increase the compression capacity of the concrete by a significant amount. Thus the sections could sustain more stress than the uni-axial compression capacity.
2. The other aspect is that, the main factor that causes the failure of the section is due to the splitting failure of concrete by the anchorage compression stress. The splitting failure is caused by the transverse tensile stress induced at perpendicular to the anchorage compression. Especially in the thinner flange (which is the case of 11SA10mm and 11SA12mm) where there is lack of surrounding concrete to provide sufficient confining pressure the tensile failure of concrete is more likely to occur..

   As the flange depth increases and the anchorage is located eccentrically from the centre, and the induced transverse compressive stress is formed over wider concrete region, which surrounds the transverse tensile stress region. This confinement from the compressive stress region prevents the section from developing the tensile stress to split the concrete.

Ultimate Limit State Bending

This analysis shows that the bending capacities of the fabric formed sections can be accurately calculated using the current theories.

This implies that the application of the current BS8110 for design the fabric formed beams for bending is also acceptable.

The moment capacities of the sections are calculated with the neutral axis of sections found from the force compatibility theory, and with the lever arm calculated based on

the concrete stress block depicted by the given expression (NEWHOOK, J., Ghali, A., Tadros, G., 2002).

Ultimate Limit State Shear Analysis

This section examined the application of expression modified by Kotsovos and Lefas (KOTSOVOS, M. D. and Lefas, I. D., 1990) in designing the fabric formed beam for shear.

In general the expression underestimates the shear capacity of the sections. In case of 11DADF12mm, it could take about 44% more the moment which corresponds to the shear failure than the predicted value. There are also cases when the accurately predicted the shear failure of the section with the discrepancies of 1% and 8%.

The analysis results also show that the major contributors to the shear capacity of the fabric formed sections are a) the effective depth of the rebar, and b) the overall efficiency of the section's structural form. The results show that the increase of steel content does not increase the shear capacity of the section.

The test results are also compared with the BS 8110:1997 method. Based on the results it is concluded that thecode does not accurately predict the shear requirement of fabric formed beams, though in general it can be accepted that when the code suggests the beam to have the minimum amount of shear links the shear capacity of the fabric formed beam section seems sufficient to resist the design shear stress; and when the code indicates that the design shear links are required, then the section's effective depth should be increased, or actually add the shear links.

At the end of the analysis it is felt that more extensive investigation is required around the shear behaviour of fabric formed beams to be able to predict the shear capacity more accurately. It is important since the failure related to shear is often catastrophic, though the shear failure of the fabric formed beams occurs in a ductile manner with sufficient warning prior to the ultimate collapse.

Serviceability Limit State Deflection Analysis

The most of the beams satisfied the BS8110's Span/250 deflection limit under the service load condition, though 11DADF10mm and 22SADFWW3no12mm exceeded the limit by 17% and 13% respectively.

The comparisons between the theoretical and experimental deflection values shoe that the theoretical values underestimate the beams' deflections by 24% ~ 63% (2.76mm ~ 4.4mm).

The degree of discrepancy between the theoretical and experimental values generally increases with the applied loads, however, the change of web geometry in the final beams (11DADFWW12mm and 22SADFWW3no12mm) has changed this pattern and the discrepancies were lower than expected.

Design Method for Fabric Formed Beam

The following information is prepared in case one would decide to design the fabric formed beam. The main purpose of the information is to point out the key design aspects of fabric formed beam which the designer should consider during the design check. It must be noted that such design and construction are only acceptable for experiment purpose in laboratory or similar environment.

- Anchorage zone design: More extensive studies are required to establish more precise design method for the anchorage zone, however at the current state of research the design should consider the following aspects, which are related to the anchorage failure of fabric formed beam:
    - Number of Anchorage
    - The angle of rebar
    - The depth of flange and location of the rebar(surrounding concrete and eccentricity of rebar from the mid-depth of the flange)

  And the following check should be satisfied:

  1. The depth of concrete at both above and below of the anchorage should be more than 1.5 of the depth of the anchorage.

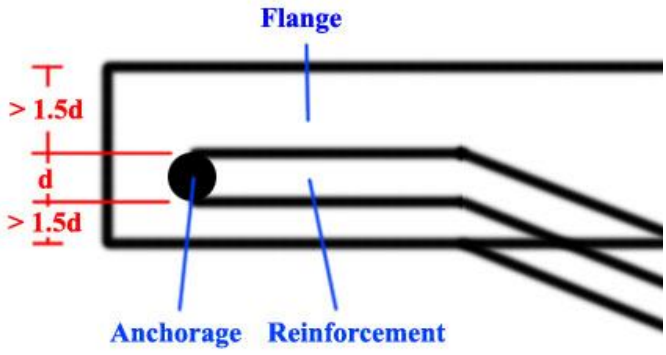

Figure 9-13: Minimum depth of surrounding concrete

  2. Using the simple strut-tie model, the design compressive stress by the anchorage should be less than 70% of the concrete cylinder strength. This could be achieved by either varying the number of anchorage or

by increasing the rebar angle.

- Shear Design: The study shows that for the beams which failed by shear (diagonal tension failure), the Kotsovos equation gives relatively accurate prediction. It must be considered that shear failure is most vulnerable at the location where the rebar enters from the flange to the web.

  The British Standard BS8110 is not recommended for the shear design check of the fabric formed beam.
- Bending Design: The study shows that the current bending theory for the design of reinforced concrete beam is sufficient, and it is confident that the current British Standard BS8110 with the simplified stress block can be used for the design check of the fabric formed beam of bending.
- Deflection: Again further studies are required to find more accurate method to predict the central deflection of the fabric formed beam.

  If the moment-area method is used it should be noted that the actual deflection could be in maximum about 63% more that the predicted value.

Chapter 10: Finite Element Model (FEM) Analysis (with Abaqus CAE Ver. 6.8-1)

10.1 Introduction

The aim of the finite element analysis is to provide broader understanding on the structural behaviour of fabric formed beams. A series of modifications were made to the design of the beams to improve the structural performance. This chapter studies and compares the effect of these modifications by using finite element analysis to examine the impact of these changes and validate other than experimentally the improvements.

This chapter presents the finite element model analysis for the following aspects of the beams:

1. Stress distribution analysis of the anchorage zone: The failure around the anchorage zone is still in question. Thus more detailed analysis is required to study the stress conditions in the concrete around the anchorage. The analysis studies the bearing compressive stress and transverse tensile stress generated in the concrete of the anchorage zone. From the results the possible causes of the failure of 11SA10mm and 11SA12mm are explored and how the beams with thicker flange avoided such failure is further discussed.
2. Analysis of the stress distribution within the final form of the beam: The overall efficiency of the forms requires clearer picture with respect to the distribution of the induced stresses. Thus the analysis examines the stress distribution in the beams and discusses how the forms of the final beams, 11DADFWW12mm and 22SADFWW3no12mm could avoid the shear failure that was evident for the tests of 11DADF12mm and 22SADF3no12mm.

The finite element models used for the analysis are designed to reflect the real-time conditions as close as possible including the behaviour of the materials, however, there are some inevitable difficulties faced during the modelling process and in such cases the most realistic solutions are sought. The following summarizes the characteristics of the models:

1. on the geometry
   - A simplified rectangular section is used for the steel anchorage and reinforcement. It is not practical to use circular section due to the

complications in defining the mesh and the interaction property, especially at the connection point of rebar and anchorage. Where the circular sectioned models are used, these generally were ill-conditioned with many warning and error messages regarding unstable and inaccurate calculation results.

2. on the material properties
    - For steel the simple linear elastic behaviour is considered up to the point of the yield strength. After the yield strength the material is designed not to take any more stress and elongate indefinitely.
    - For concrete the same compression stress-strain relationship, which is mentioned in the theoretical analysis is used (Chapter 8), and also the concrete in the model adapts the effect of damaged elastic stiffness (please refer to the graph below). The effective uni-axial cohesion stress after formation of cracks can be calculated using the equation below (Equation 10-1);

$$\bar{\sigma}_c = \frac{\sigma_c}{(1-d_c)} = E_0(\varepsilon_c - \tilde{\varepsilon}_c^{pl}).$$ .....Equation 10-1

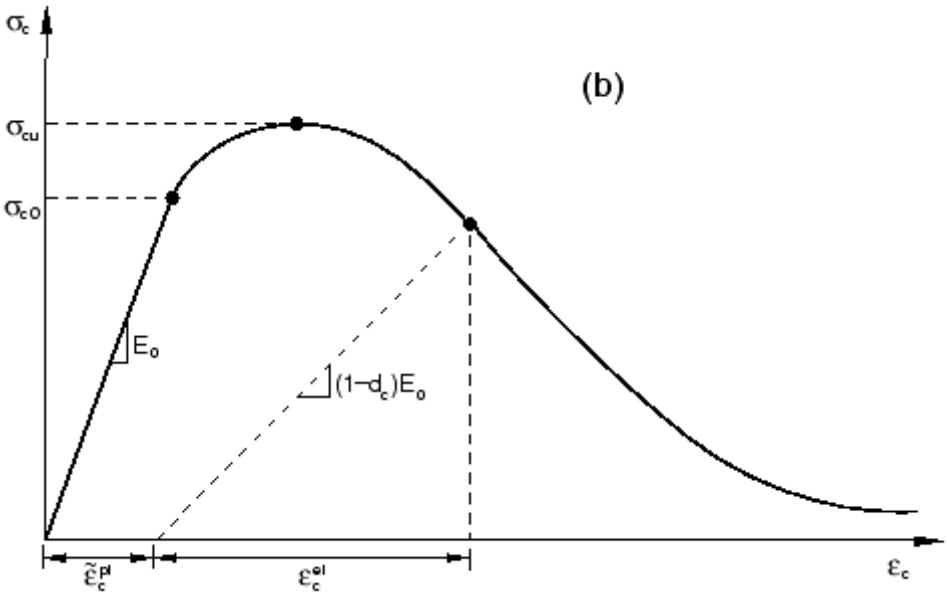

Figure 10-1: Behaviour of concrete in uniaxial compression[10]

- For the concrete behaviour in tension the yield stress can be either assumed as 9% of the cube compression strength, or it could be

10 Abaqus Theory Manual, 4.5.3 A cracking model for concrete and other brittle materials, Tension softening models.

estimated from the following relationship (FEDERATION INTERNATIONALE DU BETON) (Equation 10-2):

$$F_{ctm} = f_{ctmo} * \ln (1 + f_{cm} / f_{cmo}) \ldots\ldots\ldots\ldots \text{Equation 10-2}$$

Where:

f_{ctm} = mean axial tensile strength [Mpa]

f_{ctmo} = 2.12 Mpa

f_{cm} = mean compressive strength [Mpa]

f_{cmo} = 10 Mpa

Two ways have been considered to define the tension behaviour. One is using the fracture energy of the material which can be assumed from the following statement[11];

Typical values of G_f^I range from 40 N/m (0.22 lb/in) for a typical construction concrete (with a compressive strength of approximately 20 MPa, 2850 lb/in^2) to 120 N/m (0.67 lb/in) for a high strength concrete (with a compressive strength of approximately 40 MPa, 5700 lb/in^2).

Or from the following equation (Equation 10-3):

$$G_F = G_{Fo} (f_{cm} / f_{cmo})^{0.7} \ldots\ldots\ldots\ldots\ldots \text{Equation 10-3}$$

Where:

G_F = fracture energy [N/mm]

G_{Fo} = base value of fracture energy which depends on maximum aggregate size d_{max} as given in the table below which is extracted from the reference;

d_{max}	[mm]	8	16	32
G_{Fo}	[N/mm]	0.025	0.03	0.058

Table 10-1: Effect of maximum aggregate size d_{max} on the base value of fracture energy G_{Fo}

The other is to use the following post-failure stress-strain curve (Figure 10-2).

11 Abaqus Theory Manual, 4.5.3 A cracking model for concrete and other brittle materials, Tension softening models.

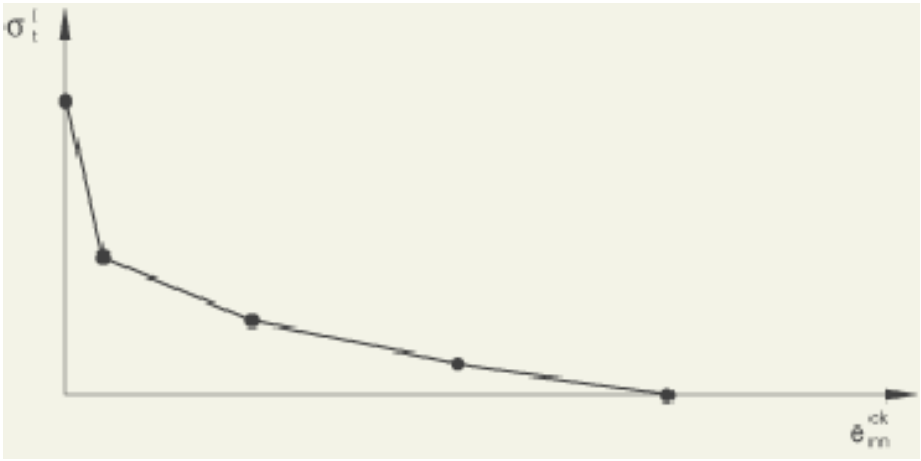

Figure 10-2: Post-failure stress-strain curve of concrete

The strain at failure of concrete is typically known as 0.0001, and it is assumed that the stress reaches zero at the strain of 0.001. Though later it is discovered that if the tension stiffening is too little it causes local failure of concrete which makes the model unstable. Thus, the initially defined stress-strain model is later modified to eliminate this problem and complete the analysis process successfully.

The following are definitions (Equation 10-4 and 10-5) of the physical properties of concrete used in the analysis (CHO, J., Cho, N., Kim, N., and Choun, Y., 2000) (WANG, T., and Hsu, T. T. C., 2001):

$E_c = 15{,}305\ N/mm^2$

Cracking stress of concrete,

$$f_{ck} = 0.339\ \sqrt{0.8 * f_{cu}} \quad \text{.....Equation 10-4}$$

and the tensile stress and strain relationship of concrete after cracking,

$$\sigma_t = f_{ck} * (e_{cr} / e_t)^{0.4} \quad \text{.....Equation 10-5}$$

where,

f_{cu} = concrete cube strength of the actual beam

σ_t = concrete tensile stress

e_{cr} = concrete cracking strain = f_{ck} / E_c

e_t = concrete tensile strain

3. On the applied loads
    - The values of the applied loads in FEM analysis are same as the experimentally measured applied models.
    - The external loads are applied to the model in the same way as they were applied in the real beam.
    - No virtual loads are applied to the model, and thus any stresses induced inside the models are due to the applied external loads. For example, the only load applied to the anchorage model is the support reaction force, which is obtained from the test result.

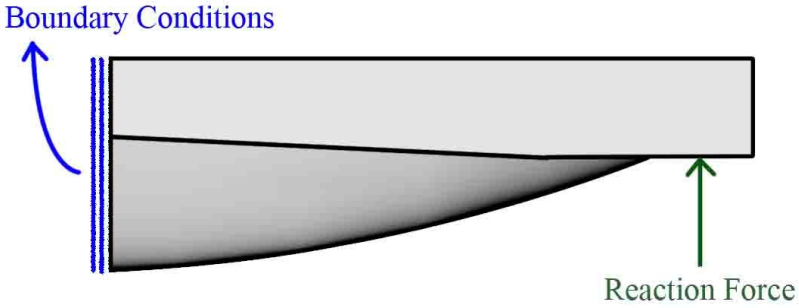

Figure 10-3: Diagram showing the example of only set of external force and boundary condition applied to an anchorage model.

It is not required to model the beams in full span, thus the models are only made to the appropriate length. Thus, the Anchorage models are only built to the point where the steel bar in the flange enters the web, as the length covers sufficient area of flange that is affected by the anchorage compression. Also the Beam models are built only to the mid-span, as the beam and the loads are in symmetry.
For the discussion of the analysis results, the stress distribution in the concrete and the steel is discussed separately in the sub-sections; A) Concrete, and B) Steel.

4. On the finite element model element type
    - Element type C3D4 (4-node linear tetrahedron) is used for both anchorage models (refer to section 10.2) and beam models (refer to section 10.3): Other element types were also considered such as hexahedral elements for more accurate result; however with hexahedral elements caused constant problems around the meshing of the contact area between concrete and steel.
    - The lack of accuracy of using C3D4 elements are due to the 'stiffness' of the elements, and thus fine mesh is used with increase number

elements. For instance, the largest seed global size used is 8mm and total element number is 27,669.

5. On the boundary conditions
    - As described above, the beams are symmetrical about the mid-span and thus they are modeled in half the length. Thus, for the beam models the following boundary conditions are applied at the mid-span cross-section:
        - XSYMM (U1 = UR2 = UR3 = 0); Displacement fixed along axis 1, Rotation fixed about axis 2 and axis 3 (refer to figure 10-4).
        - At the support the boundary condition is PINNED (U1 = U2 = U3 = 0); displacements are fixed in all axis.

    - For the anchorage model, the following boundary condition was applied at the cut cross-section:
        - ENCASTRE (U1 = U2 = U3 = UR1 = UR2 = UR3 = 0); Displacements and Rotations are fixed in all directions.

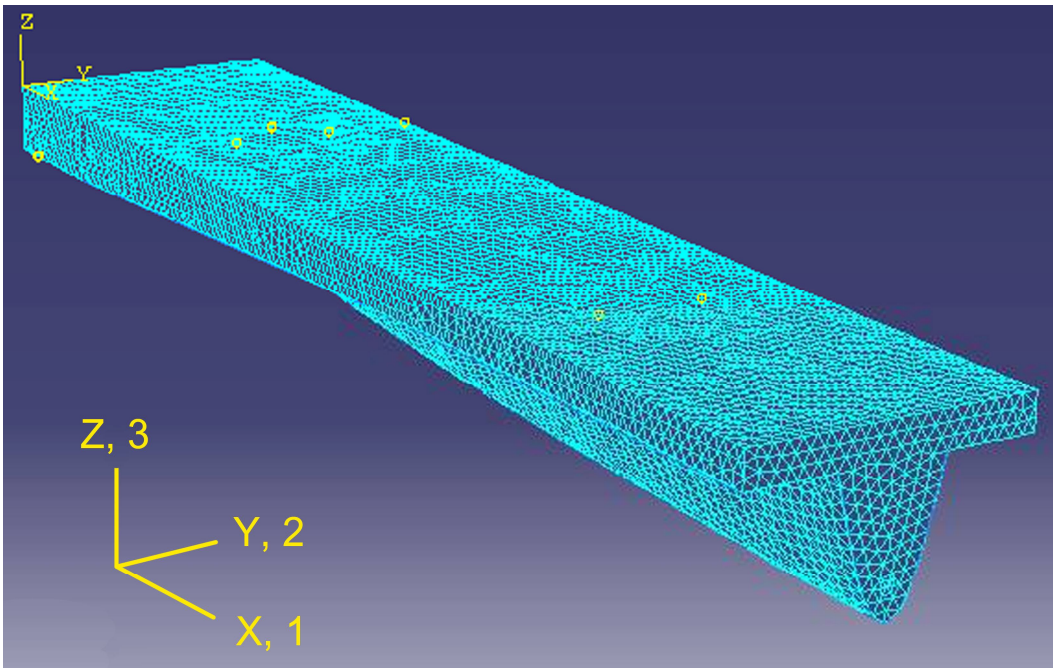

Figure 10-4: Diagrma showing the oreintation of the axis

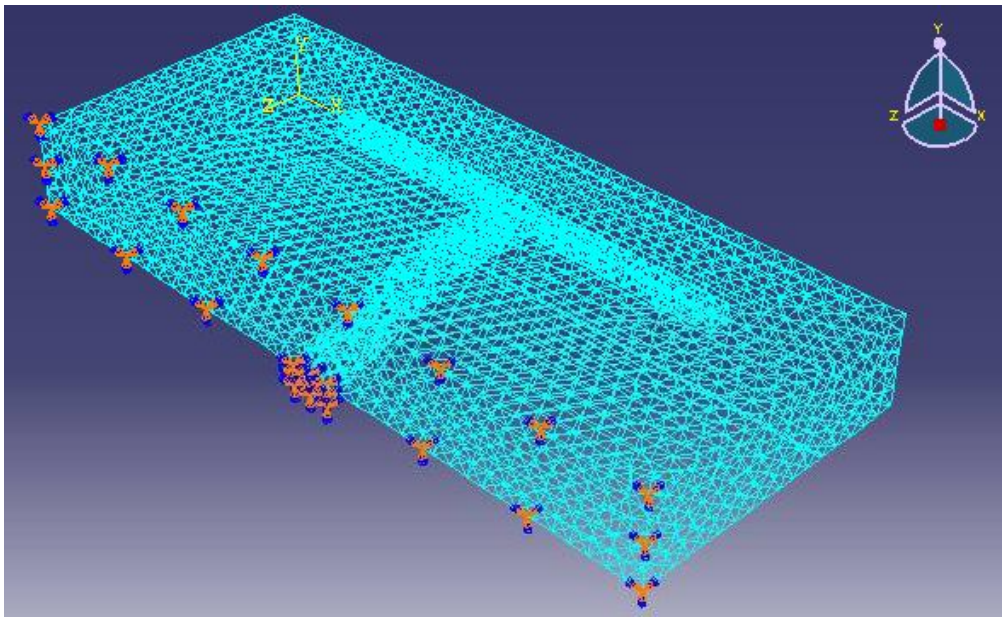

Figure 10-5: Diagrma showing the ENCASTRE boundary conditions of an anchorage model

10.2 Anchorage Models

11DA10mm and 22SA10mm were developed from 11SA10mm and 11SA12mm. The simple Strut-and-Tie model was used to analyse the concrete failure of 11SA10mm and 11SA12mm around the anchorage. The initial conclusion was that the excessive compression stress from the pulled in anchorage had caused the section to fail. Thus for 11DA10mm and 22SA10mm the design was modified to reduce this anchorage compression stress.

The test results of 11DA10mm and 22SA10mm showed that the modifications made around the anchorage prevented the concrete failure. The evidence is the increased ultimate loads of the beams, and the different collapse modes of the beams at the different locations (Figure 6-11).

However, the further analysis of the other following beams has lead to other possible explanations about the concrete failure in the anchorage zone. The following briefly summarizes the views on the failure:

- The initial conclusion in regard with the concrete compression failure of 11SA10mm and 11SA12mm was based on the uni-axial compression capacity of the concrete. However in the consideration that concrete inside the beam is the tri-axial stress condition, it is considered that the failure of section is not due to the uni-axial compression failure of concrete.
- But instead, the failure of the section seems to be closely linked with the transverse tensile stress, which is induced at perpendicular to the compression stress of anchorage. This view suggests that the section's failure is caused from the splitting of concrete.

  Such tensile behaviour of concrete in compression is also observed in the uni-axial cylinder compression. The following Figure 10-4 shows the development of the transverse strain, along with the development of axial compressive strain. The transverse tensile strain (and hence the transverse tensile stress) in the graph describes the lateral dilation of the cylinder under uni-axial compression. Such lateral dilation is restrained by the friction induced between the cylinder surface and the loading plate, however, such effect decreases towards the centre of the cylinder and thus the failure cracks formed near the centre of the cylinder are in vertical direction parallel to the applied compression stress, owing to the transverse tensile stress causing the concrete fail by splitting.

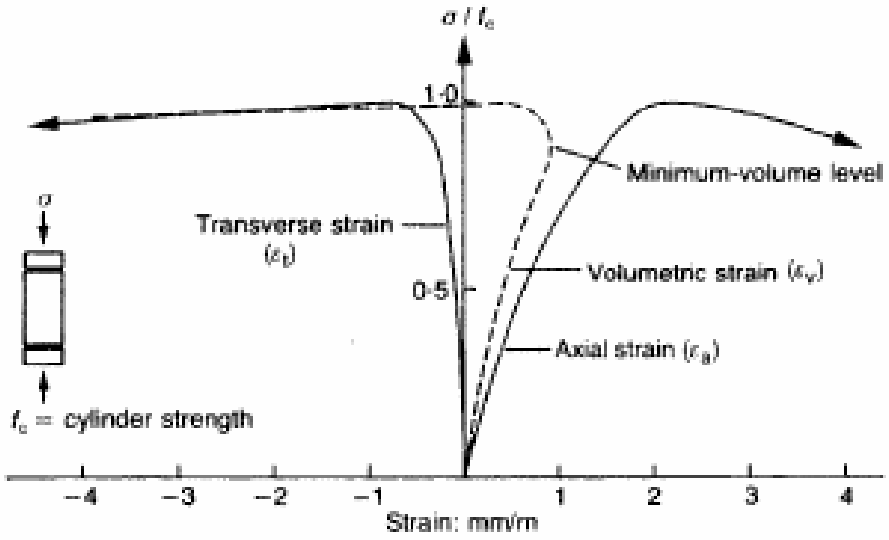

Figure 10-6: Experimental stress-strain curves for concrete in uniaxial compression (Figure and the description are extracted from the reference) (KOTSOVOS, M. D. and Pavlovic, M. N., 1999)

In addition to the above, as the height of the cylinder increases with respect to its width the compressive stress applied at the failure decreases since the specimen is more likely to fail by lateral splitting of concrete at the centre part (Figure 10-4).

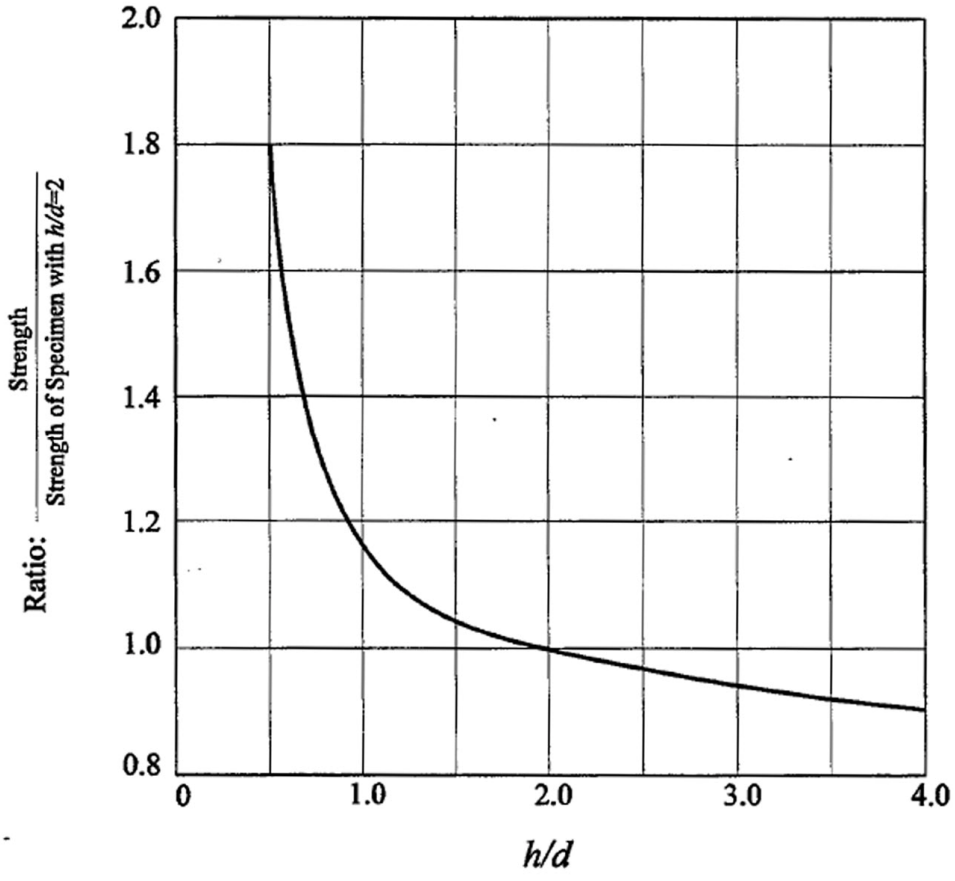

Figure 10-7: General relationship between height/diameter ratio and strength ratio (The figure and the description is extracted from the reference) (ELWELL, D. J., and Fu, G., 1995)

The tensile strength of concrete is much smaller than the compressive strength. Thus when a compressive stress is acting on the concrete it is more likely that the concrete fails by the transverse tensile stress before the concrete's compression capacity is reached.

Thus, the purpose of the following analysis of the anchorage area is to examine the above failure theories, and also to obtain further insights to the structural behaviour with the above aspects.

10.2.1 11SA10mm

The following is the finite element model analysis for 11SA10mm around the anchorage area. The dimensions, location of the boundary conditions and the uniformly distributed (UD) reaction force are identical for all the anchorage models, except the depth of the flange which is shown as 40mm in the below diagram (Figure 10-4), it changes to 80mm for the models of beams with deeper flange.

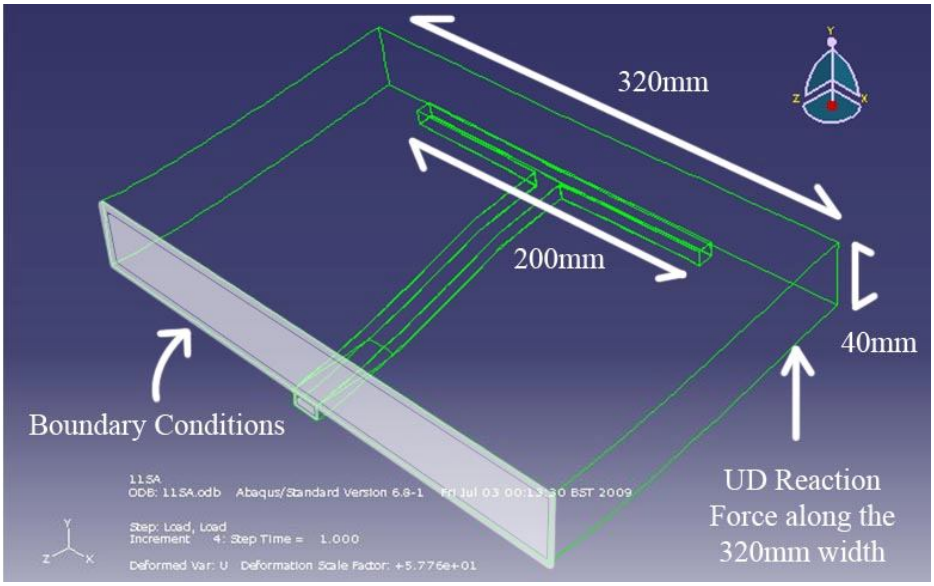

Figure 10-8: 11SA after deformation

A. 11SA10mm-Concrete

The concrete section is cut in the three principal planes to see the compression stress (S33-Stress in Z plane) distribution due to the anchorage.

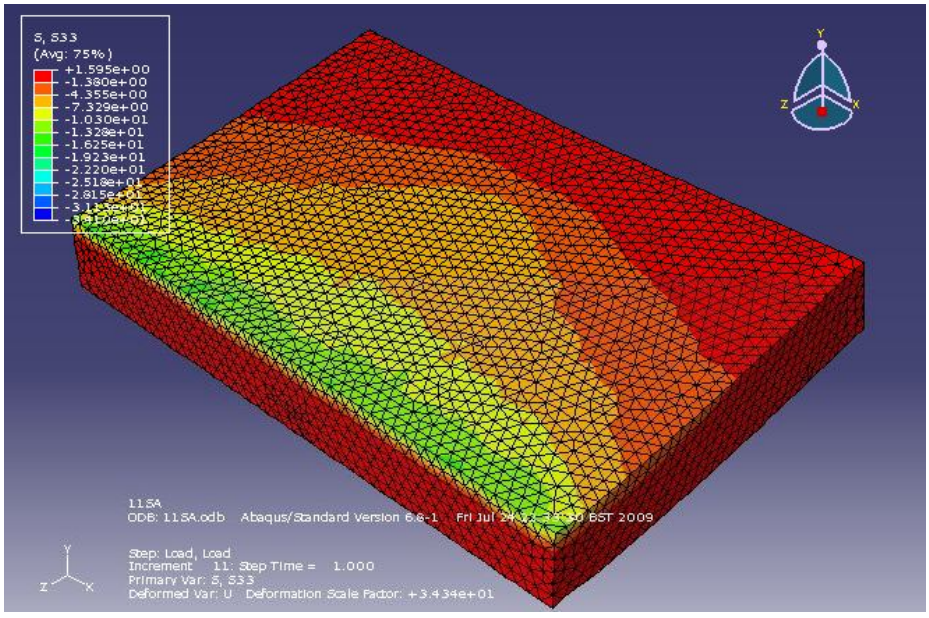

Figure 10-9: 11SA10mm - S33 stress contour of concrete after deformation

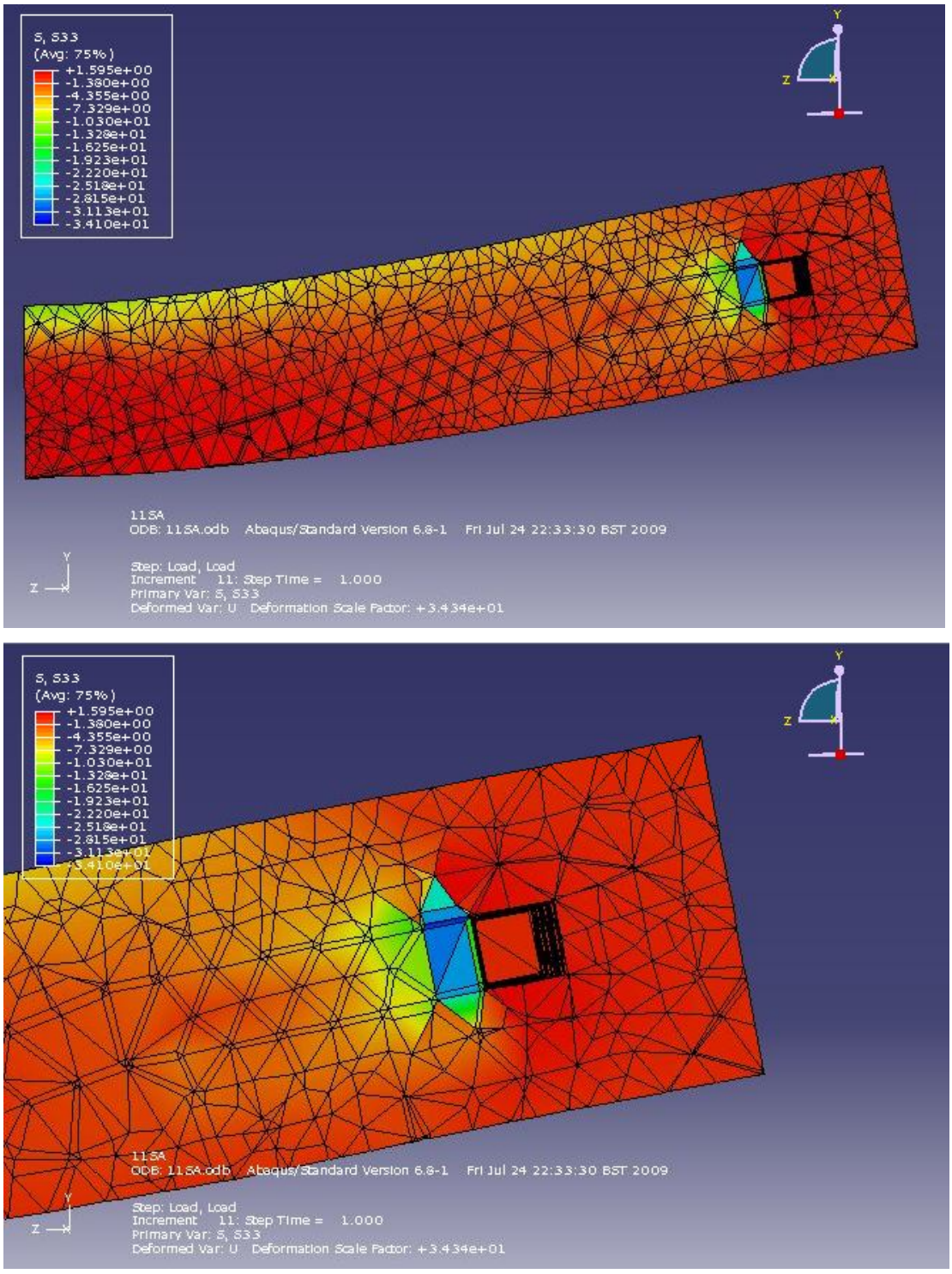

Figure 10-10: S33 stress in 11SA10mm-X –Plane Cut

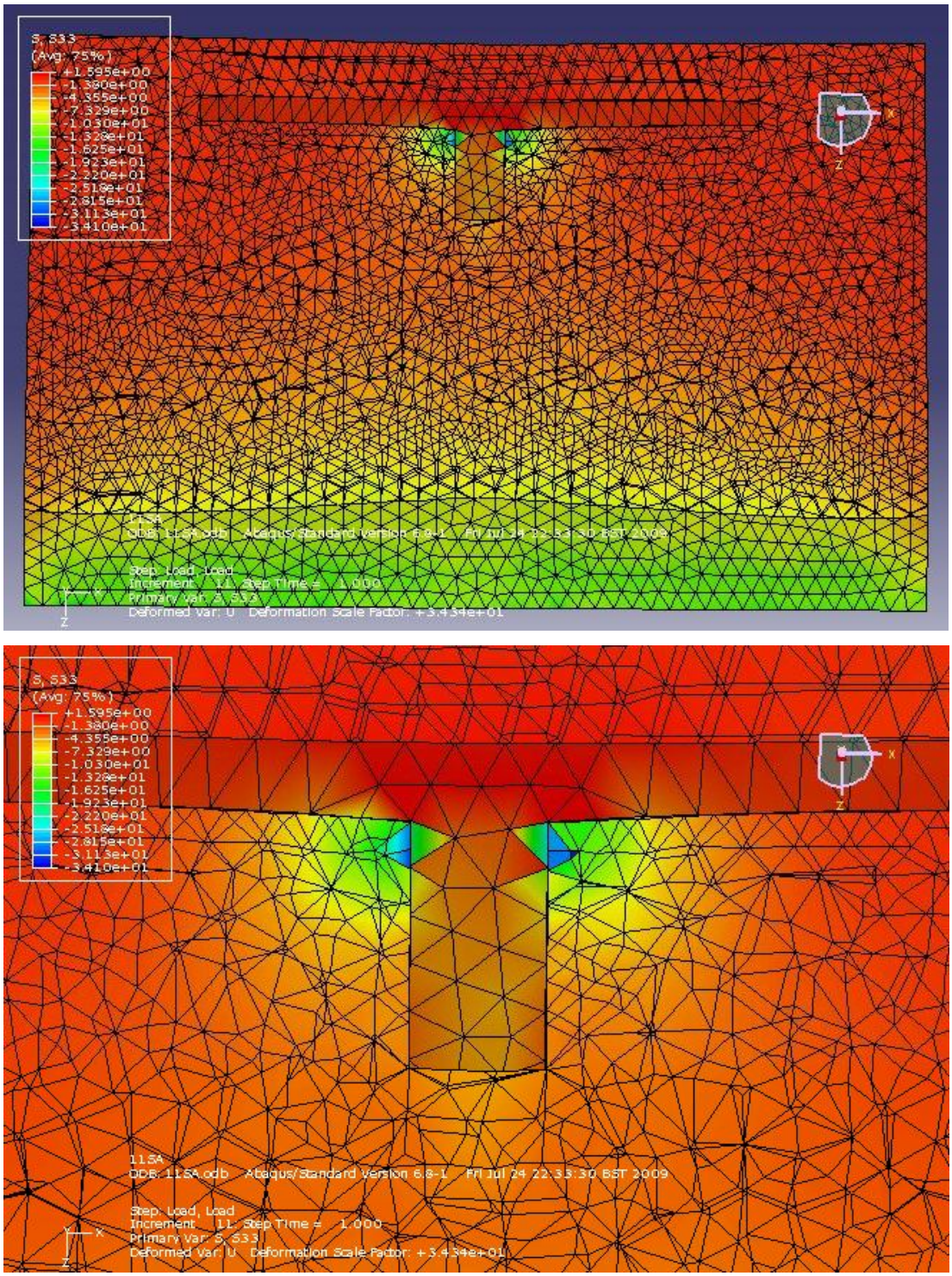

Figure 10-11: S33 stress in 11SA10mm-Y – Plane Cut

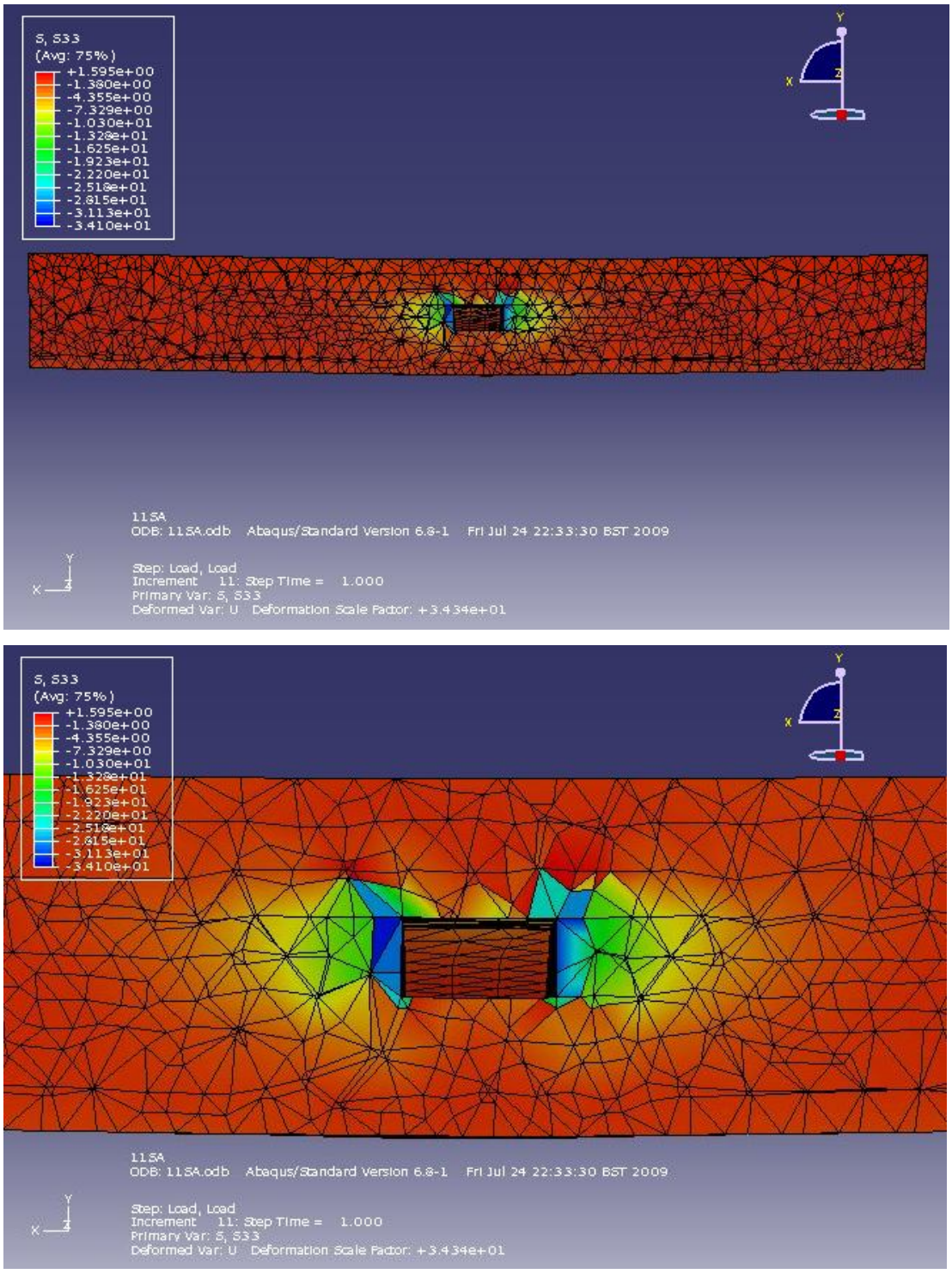

Figure 10-12: S33 stress in 11SA10mm-Z – Plane Cut

The following graph (Figure 10-11) shows the development of induced compression stress inside the concrete. Please note that the x-axis is plotted in Time. This is automatically set by the software and 0.00 is the time when the load is first applied and 1.00 is when all the load (which is set as the ultimate load of the beam) is applied. It can be interpreted as the percentage of the total load applied, and for example when time is 0.50, then it means 50% of the ultimate load is applied to the point.

The unit of the stress marked on the Y-axis is N/mm^2 (same for all the graphs mentioned in chapter 10).

The highest compression stress value (or the lowest in the graph since it is in the negative sign) is (-) 37.04 N/mm^2. The concrete cylinder strength is 21.45 N/mm^2. The applied stress is about 72.7% more than the concrete strength.

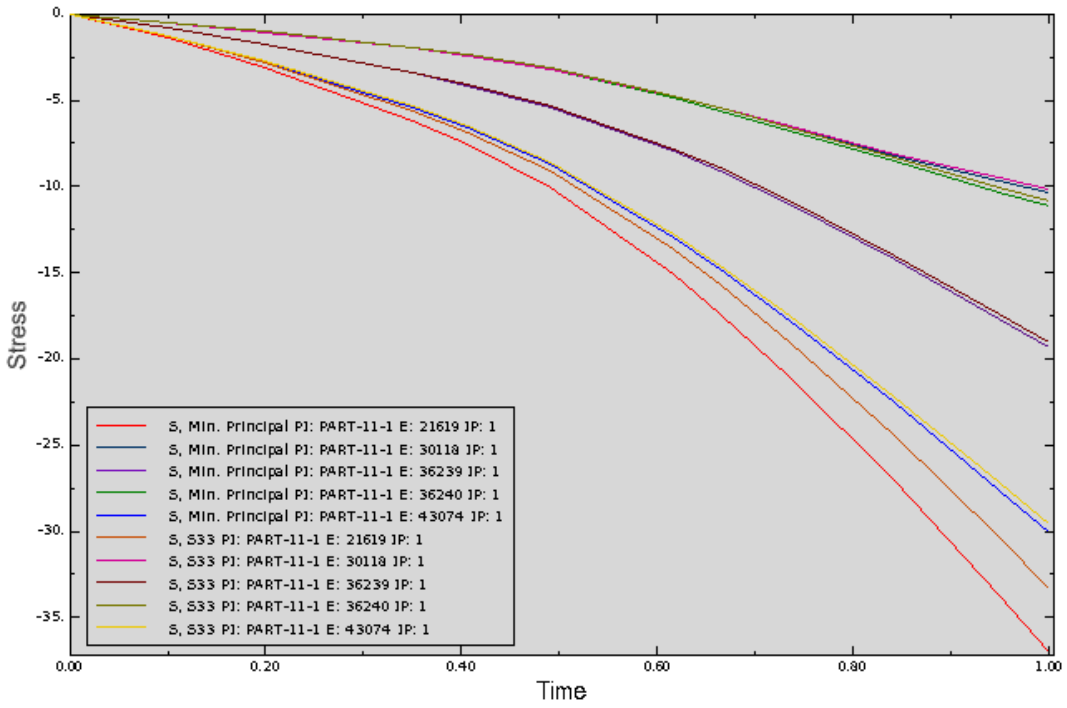

Figure 10-13: 11SA10mm Compression stress of selected concrete elements adjacent to the anchorage

The results show that the local concrete has possibly been crushed by the anchorage stress. However, the contour plot shows that the high compression stress is only affecting the local region, and does not affect over the full length of the anchorage. Even if the concrete in this region is crushed and the anchorage comes forth to press against the 'adjacent' concrete, there is no proof that this concrete will also be crushed and continues. If this is the case then the final location of the anchorage should have been found certain distance away from its original position, but it is seen from the tested beam that the anchorage remained where it was before.

In fact, when the local concrete is crushed the anchorage will deform to fit into the new space, and the compression stress would be distributed more efficiently and reduce the local magnitude of the compression stress in concrete. Thus, according to the contour plot the compression stress is not the sole cause of the large failure area of concrete that is cracked and pushed up, as it is seen from the experiment result. Instead it is more convincing to say that such failure is a result of the transverse tension stress which caused the upper layer of the concrete to split up.

Please look at the following transverse stress (S22, stress working in the vertical (Y-Y) direction in the figure) contour plot (Figure 10-12) of the model.

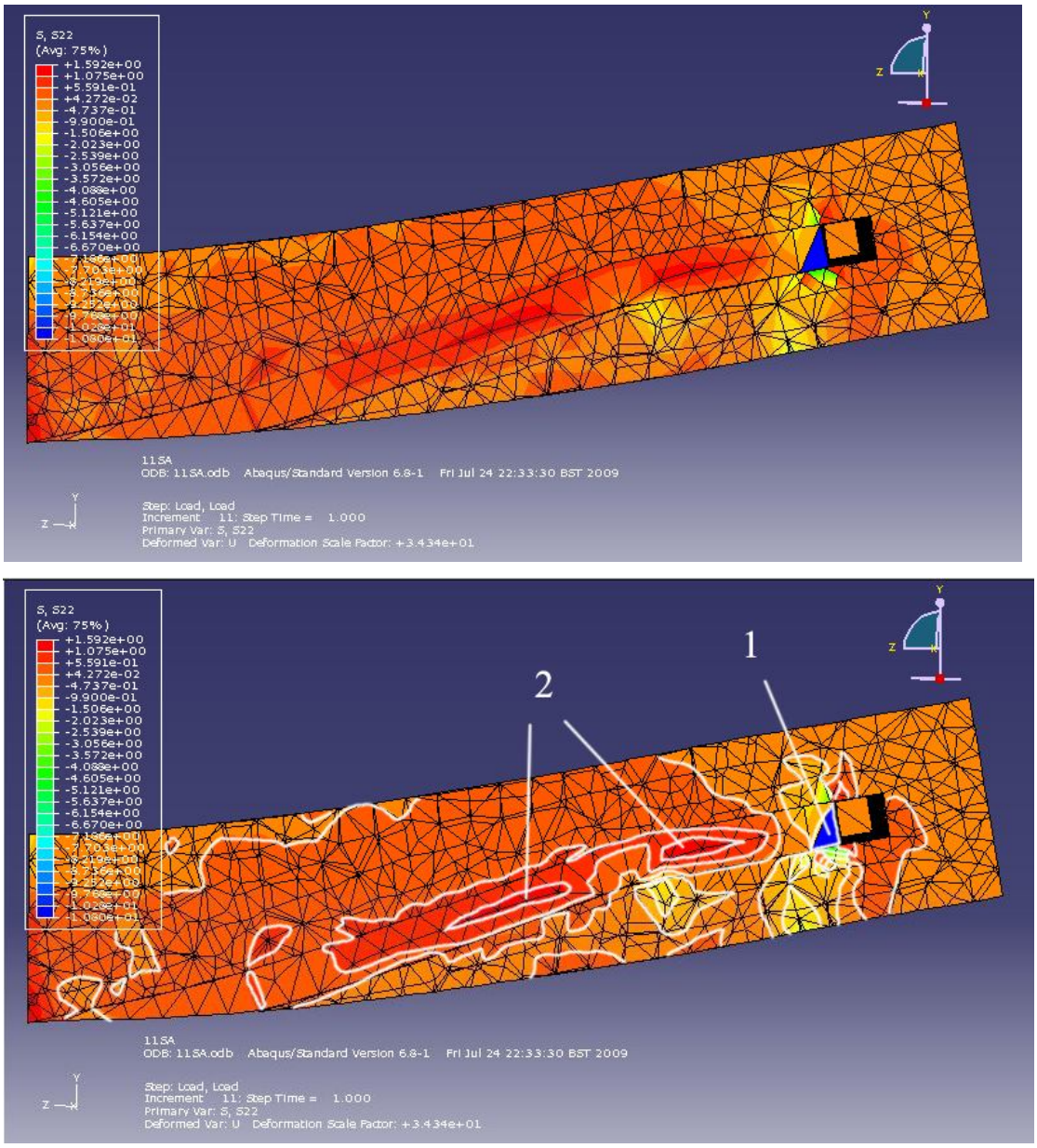

Figure 10-14: 11SA10mm – Transverse stress distribution contour

Figure 10-12 shows the maximum compressive stress immediately behind the anchorage (location 1) and the maximum tension stress at the location 2. The maximum compression stress is 10.8 N/mm^2, and the maximum tension stress is 1.57 N/mm^2. The estimated concrete crack stress is 1.58 N/mm^2 (please refer to the key note number 2 at the beginning of this chapter), which is very close to the induced stress. Also please note that the transverse tension stress affects the very top of the flange section. It seems this is the main reason for the concrete section has failed and the top layer has been separated and moved upwards.

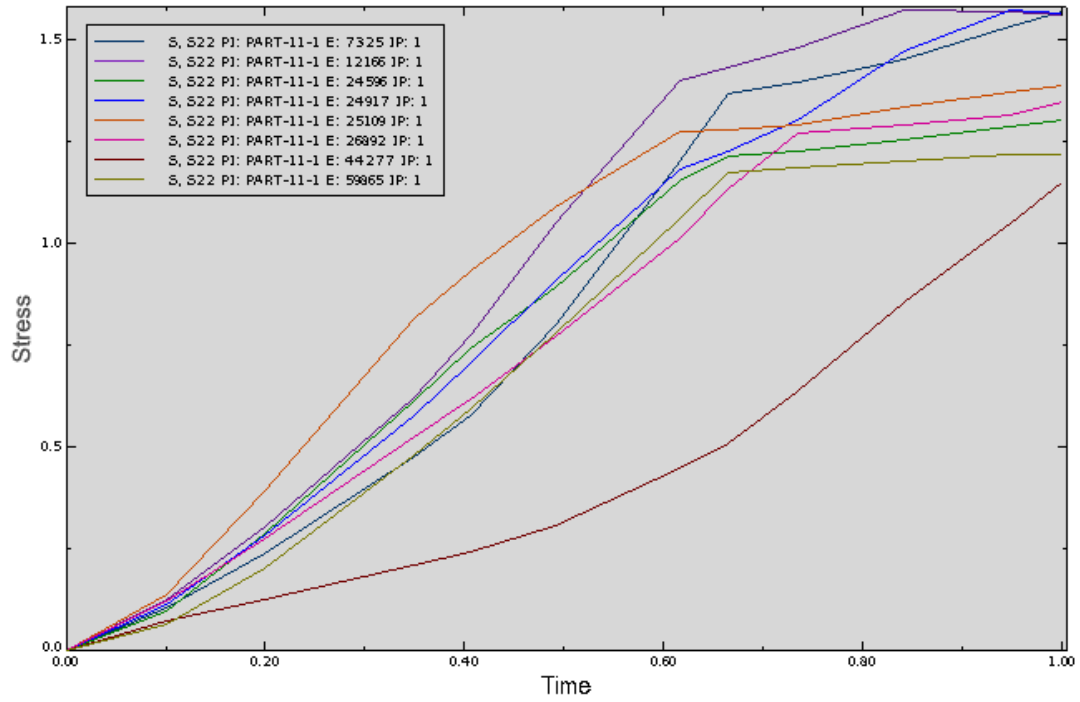

Figure 10-15: 11SA10mm – Transverse tension stress at location 2

B. 11SA10mm – Steel

Figure 10-14 is the von Mises stress contour plot of the steel in 11SA. The highest tension stresses are at the connection point of the rebar and the anchorage. The highest stress value is 164.95 N/mm^2 (Figure 10-15).

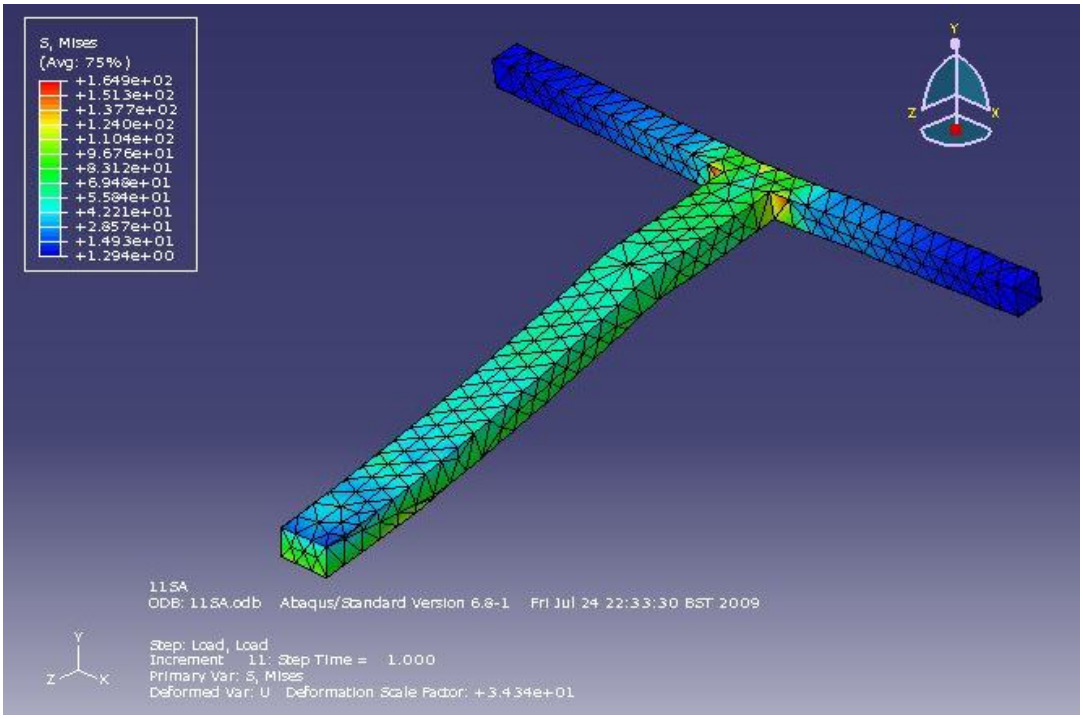

Figure 10-16: 11SA10mm steel section von Mises stress contour plot

The deformation of the steel suggests that the stress of the anchorage is concentrated

locally at the connection with the rebars.

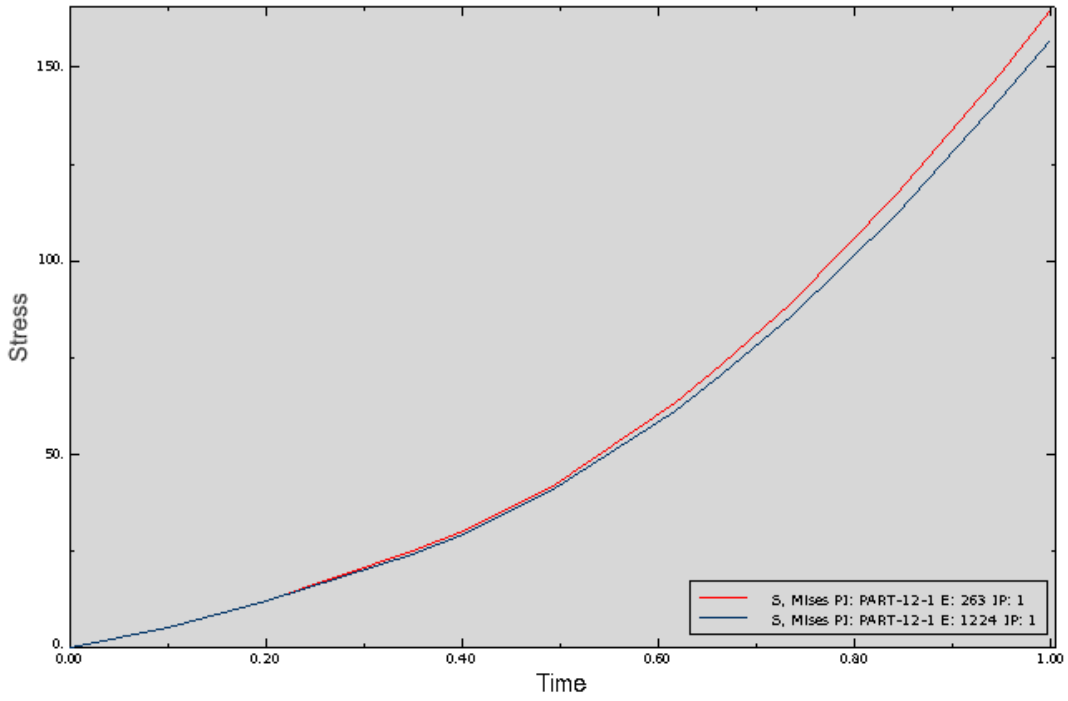

Figure 10-17: 11SA von Mises stress of selected steel elements at the connection region

10.2.2 11DA10mm

The following (Figure 10-16) is the finite element model analysis for 11DA10mm around the anchorage area.

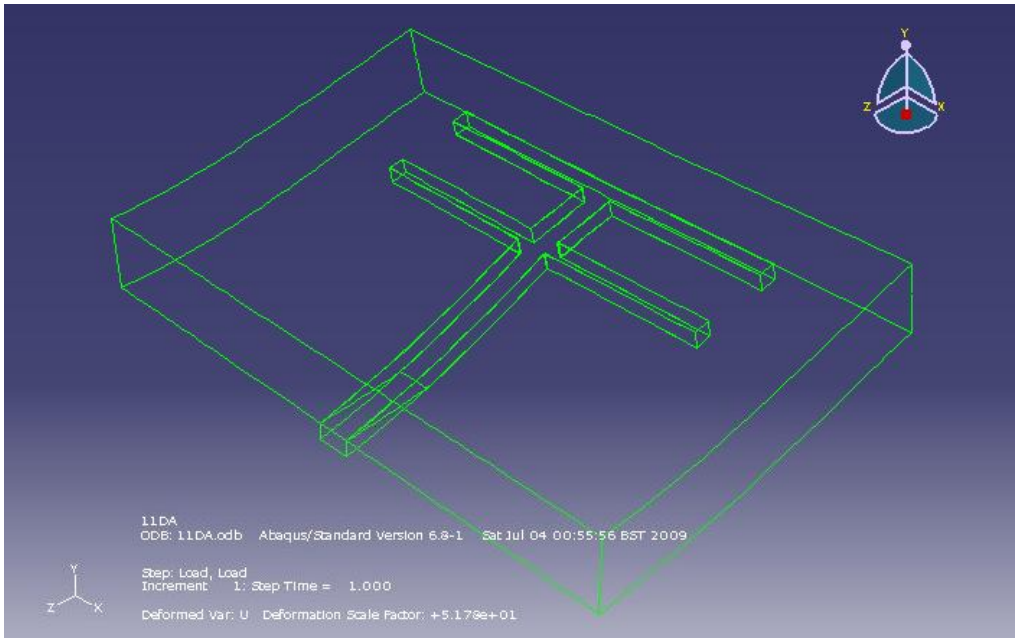

Figure 10-18: 11DA10mm after deformation

11DA10mm has double anchorage, developed to spread the compression stress over wider area, and avoid the failure of concrete.

A. 11DA10mm-Concrete

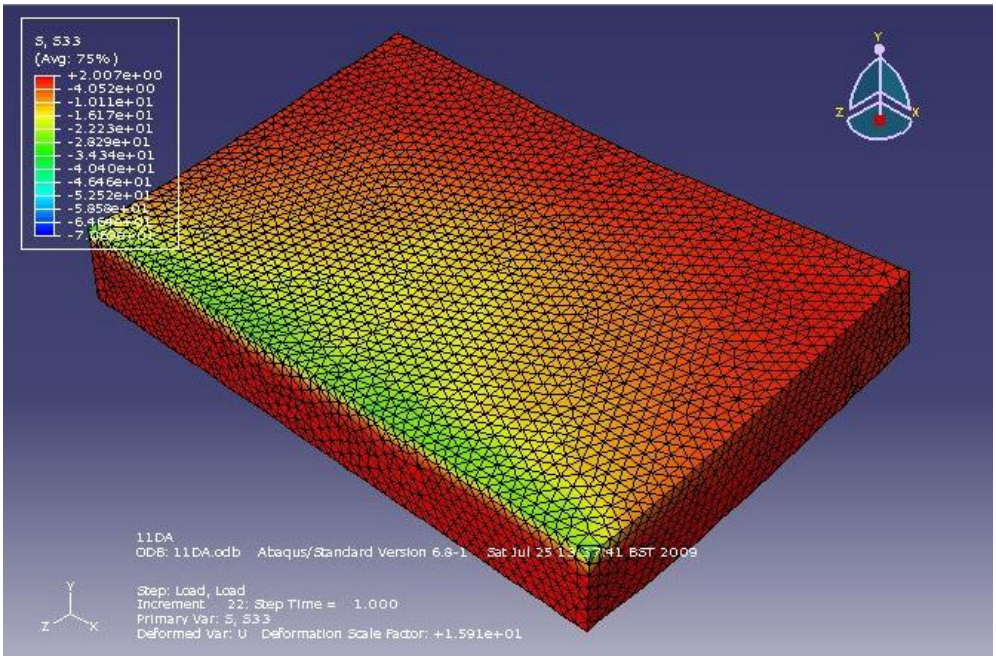

Figure 10-19: 11DA10mm - S33 stress contour of concrete after deformation

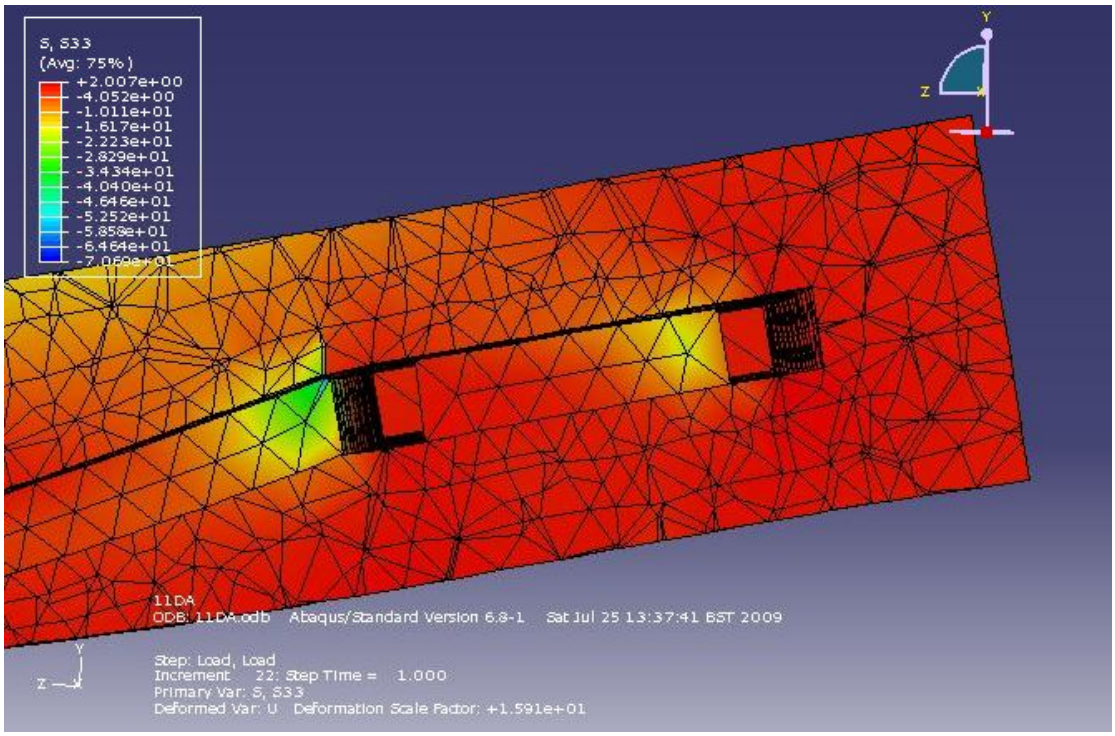

Figure 10-20: S33 stress in 11DA10mm-X-Plane Cut

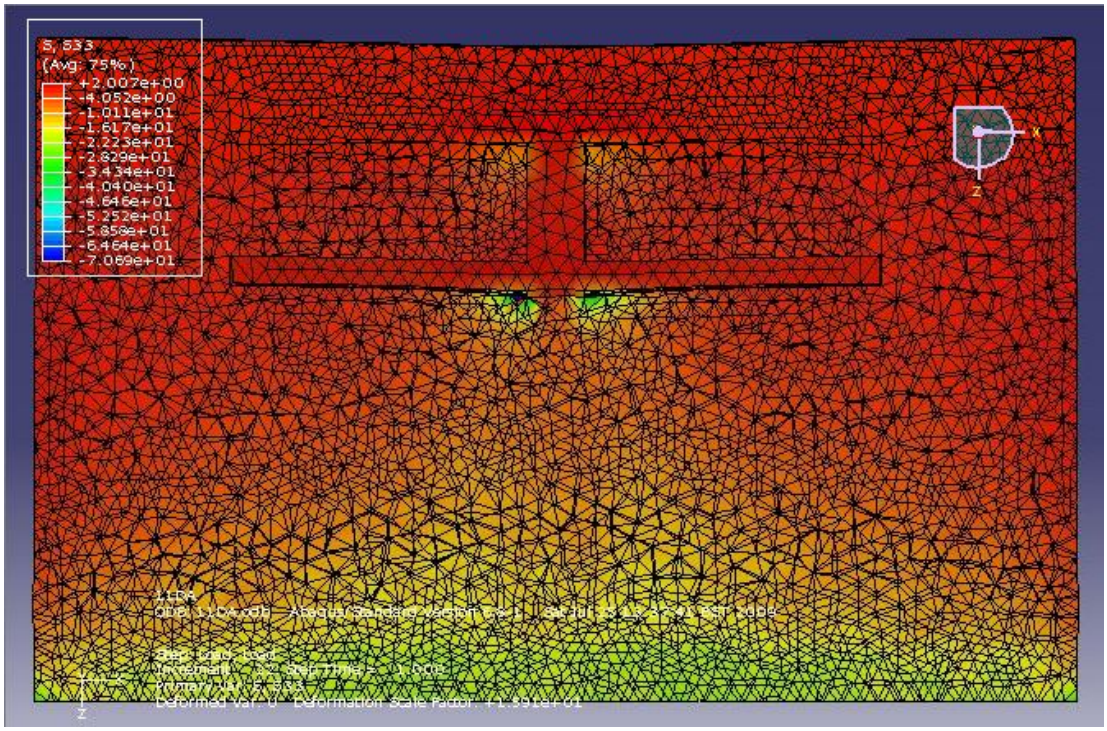

Figure 10-21: S33 stress in 11DA10mm -Y-Plane Cut

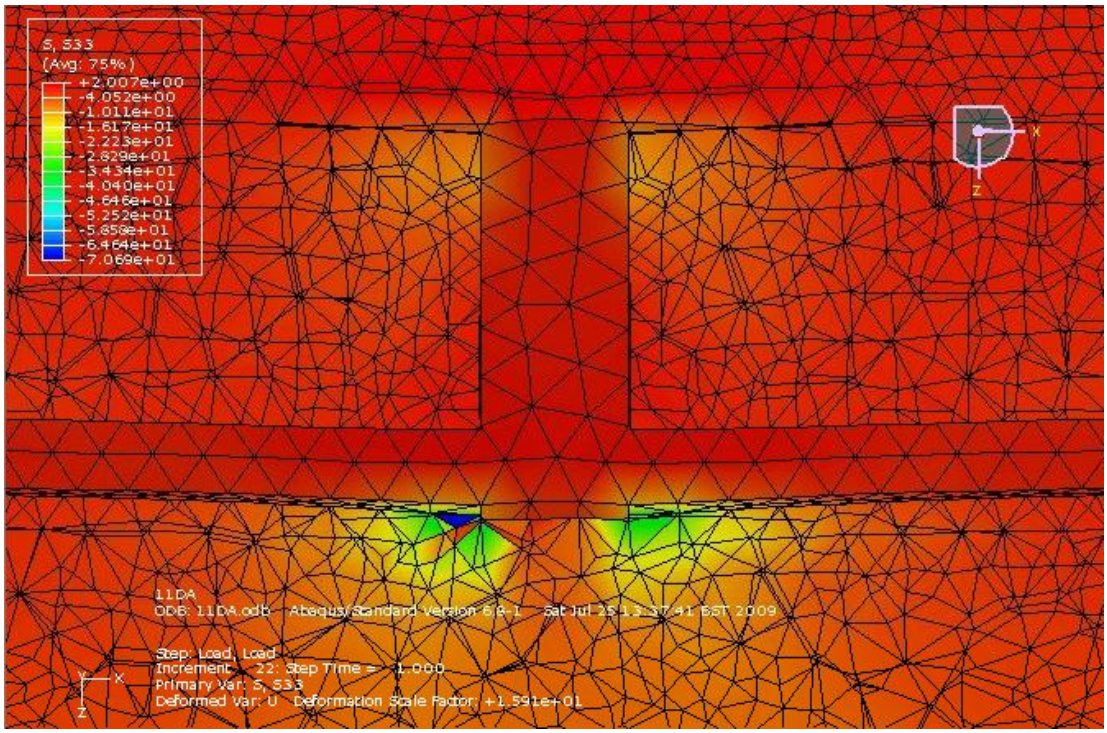

Figure 10-22: S33 stress in 11DA10mm -Y-Plane Cut in more detail

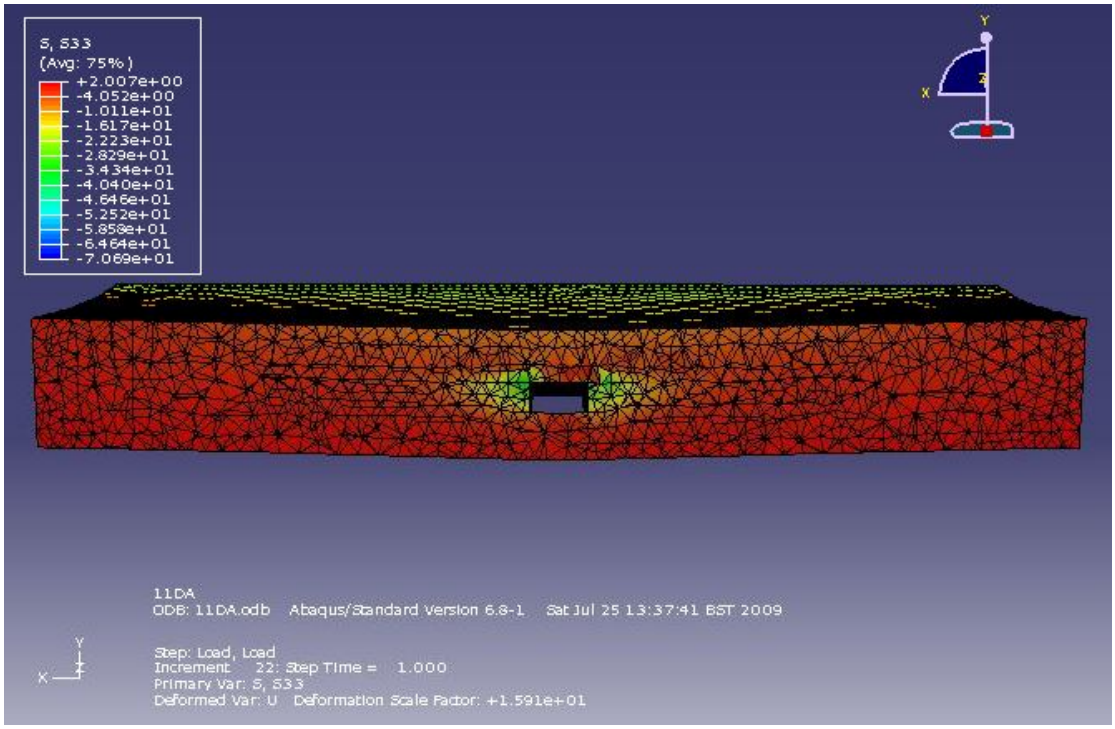

Figure 10-23: S33 stress in 11DA10mm- Z-Plane Cut, the inner anchorage area with higher stress

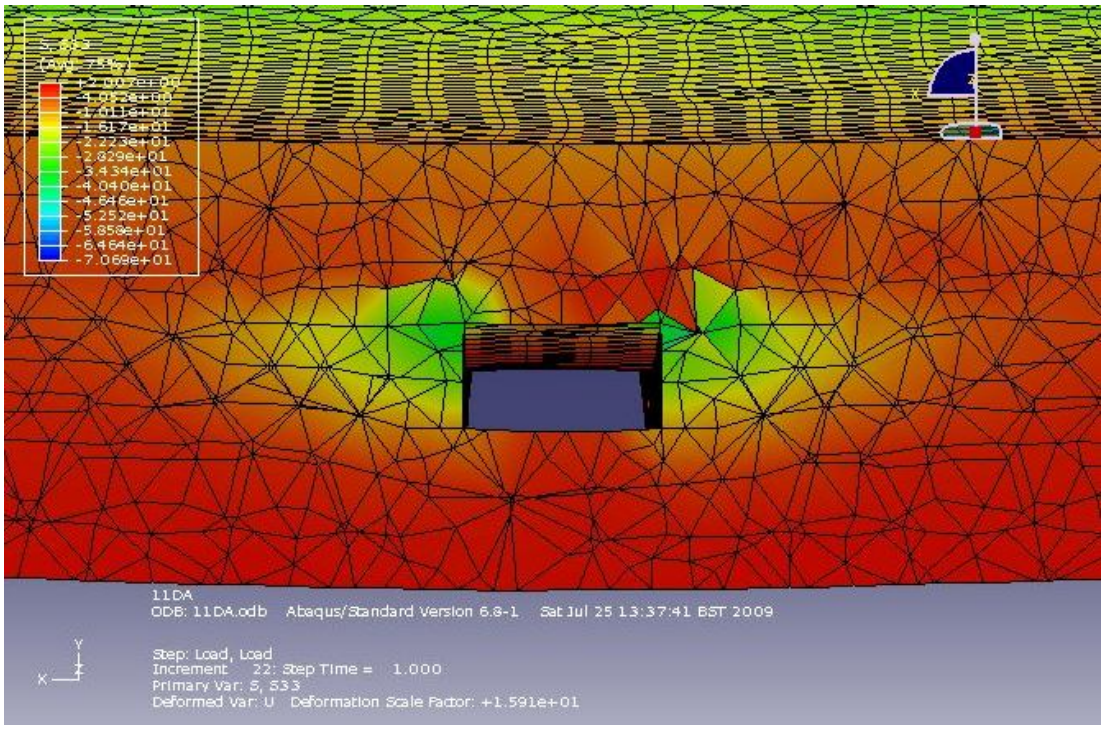

Figure 10-24: S33 stress in 11DA10mm -Z-Plane Cut, the inner anchorage area with higher stress in more detail

In the model the greatest compression stress value is 32.8 N/mm^2. The compressive strength of the concrete is 32.52 N/mm^2 and thus the uni-axial compression capacity of the concrete has been reached by the applied stress.

It is also noticed that some elements in the model shows higher compression stresses (the highest value was around 70 N/mm^2) (turquoise colour in Figure 10-23). However the elements of such high stresses are located near the edge of the rectangular rebar, and it is over very small area. It is thought that such a stress is owing to the rectangular shape of the model with sharp corners causing unusually high stress.

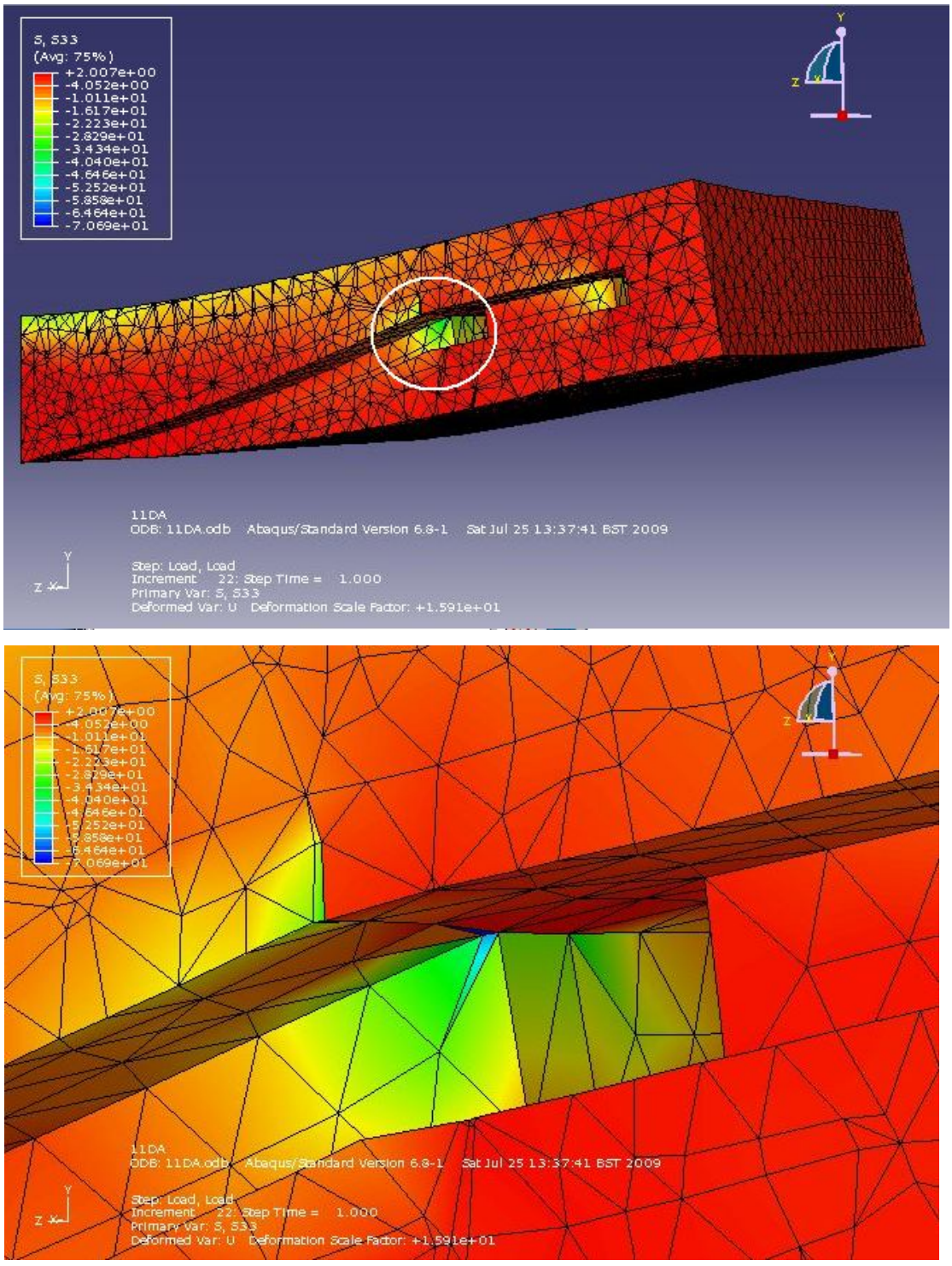

Figure 10-25: 11DA10mm-Showing the high stress points cause by rectangular steel section

The following contour plot (Figure 10-24) shows the distribution of transverse stress.

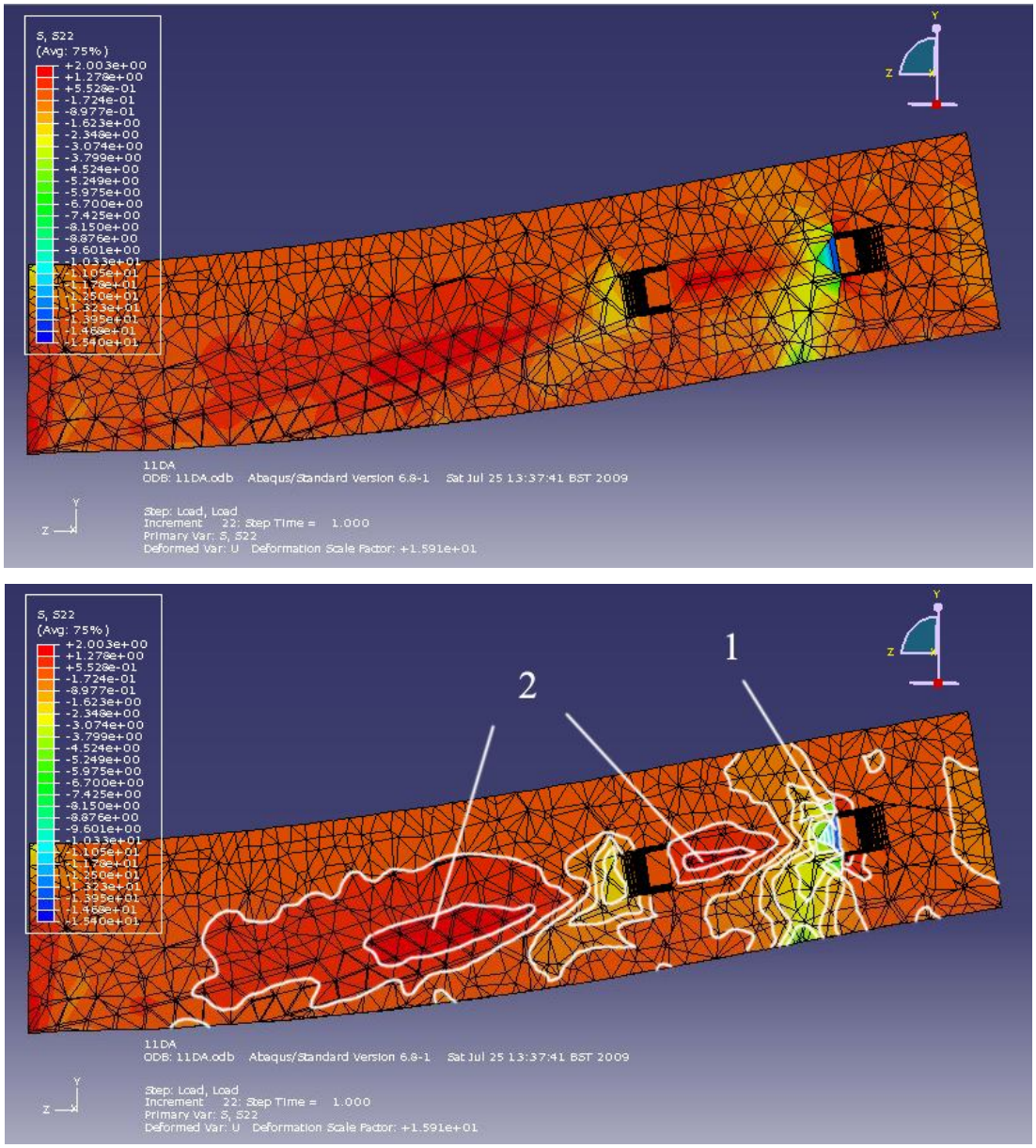

Figure 10-26: 11DA10mm – Transverse stress distribution contour

The above figure shows the greater transverse compression stress exists at the outer anchorage location than the inner anchorage. This is in contrast with the initially seen axial compression stress distribution, which was the greater around the inner anchorage.

The highest transverse compression and tension stress values are 13.69 N/mm^2 and 2.00 N/mm^2 respectively (Figure 10-25 and 10-26). The tensile capacity of concrete is 1.91 N/mm^2 and thus the section's capacity has been exceeded, yet the test result showed that the section did not show any sign of failure.

However, going back to the contour plot, in the upper part of the flange the

transverse tension stress is almost 0 N/mm^2. This is the difference when compared with the result of 11SA10mm, where the transverse tension stress spreads to the top of the flange.

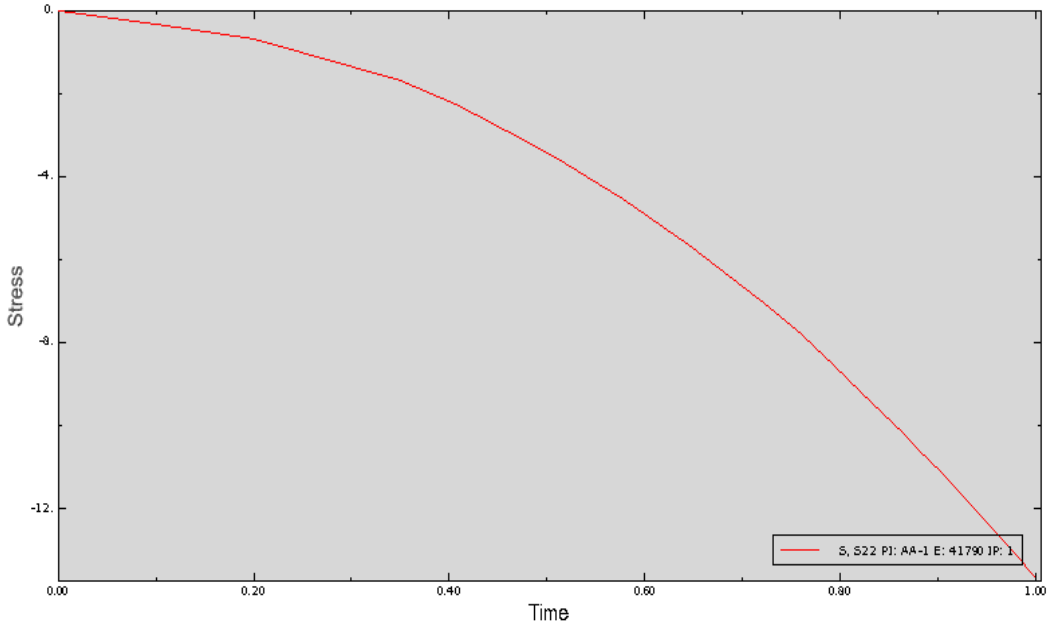

Figure 10-27: 11DA10mm – Transverse compression stress at location 1

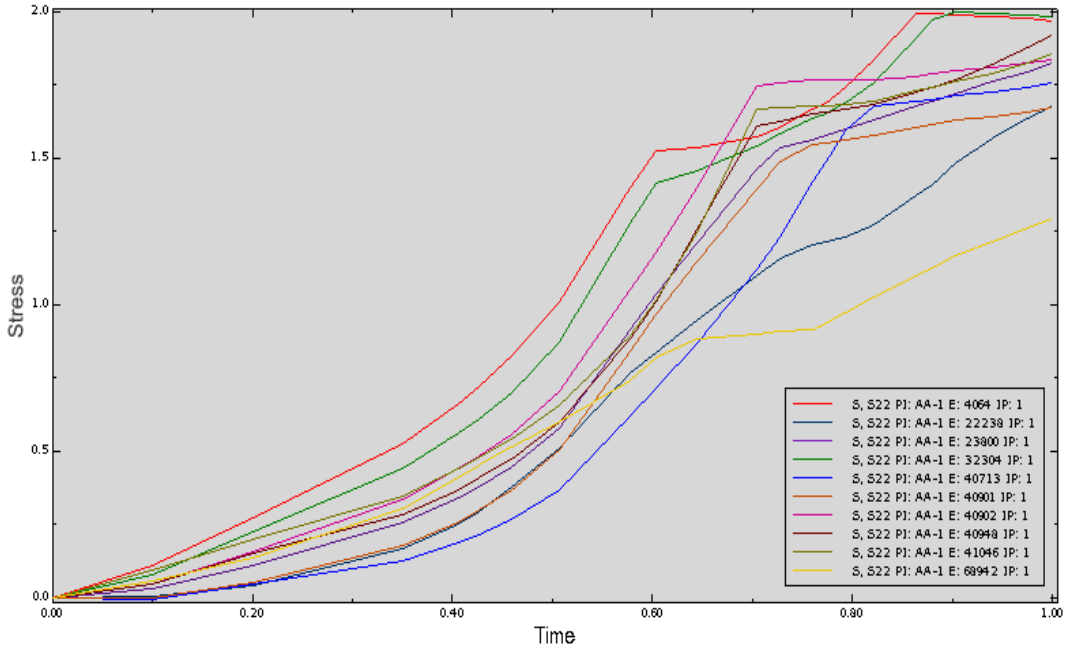

Figure 10-28: 11DA10mm – Transverse tension stress at location 2

B. 11DA10mm-Steel

Figure 10-27 is the von Mises stress contour plot of the steel in 11DA. In general

there are higher stresses near the inner anchorage than the outer anchorage. The values are 298.53 N/mm^2 at the inner anchorage and 201.34 N/mm^2 at the outer anchorage, the difference is 97.19 N/mm^2.

This result also shows the high stress concentration at the connections with the rebar.

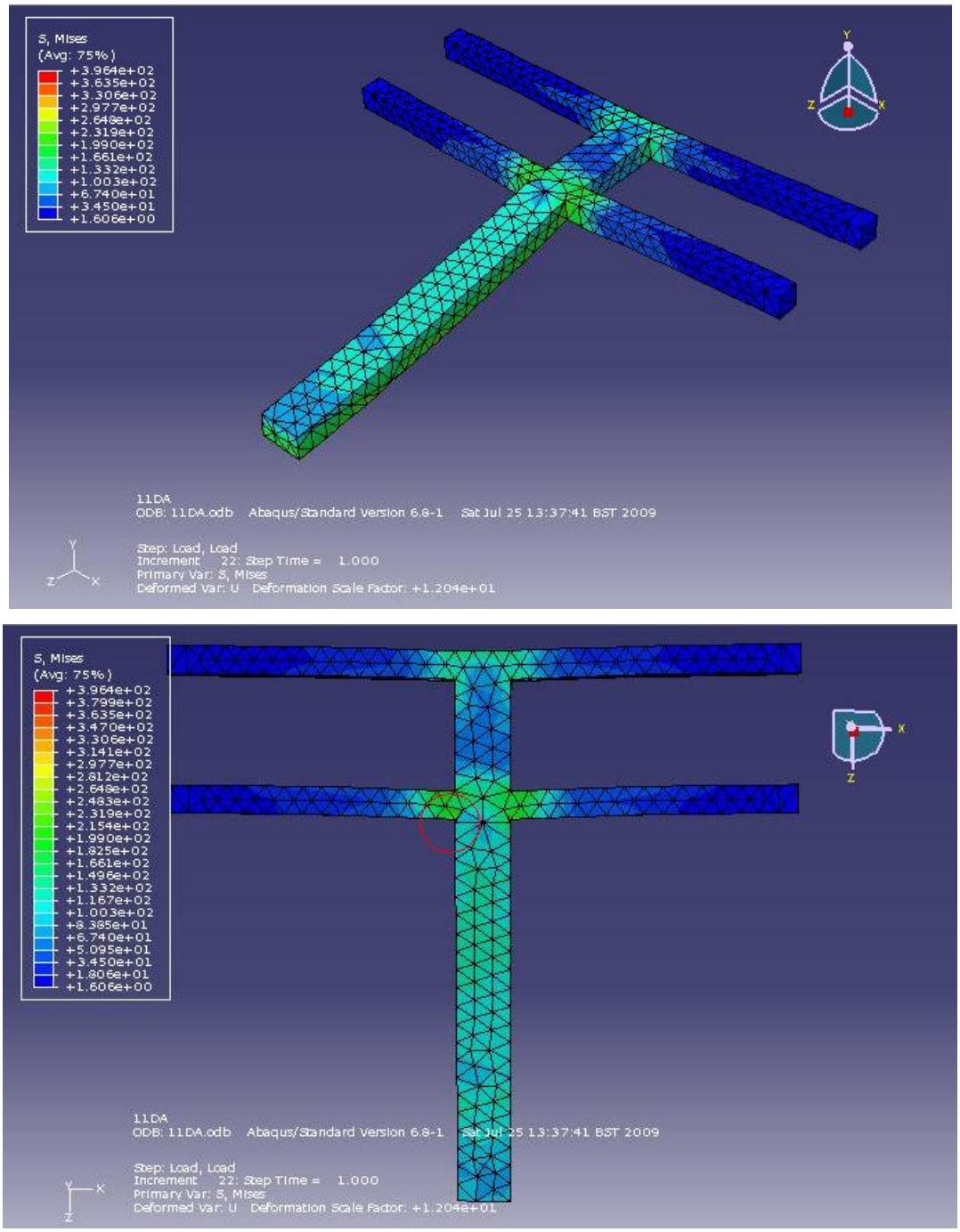

Figure 10-29: Steel section von Mises stress contour plot

10.2.3 22SA10mm

Figure 10-28 shows the finite element model analysis for 22SA10mm around the anchorage area.

Same as for 11DA10mm this beam is also proposed to decrease the anchorage compression stress. The difference is that 22SA10mm has a single anchorage but the angle of rebar is increased to 22º from 11°. By making the angle steeper there is less horizontal compression stress exerted to the concrete as well as in the steel bar.

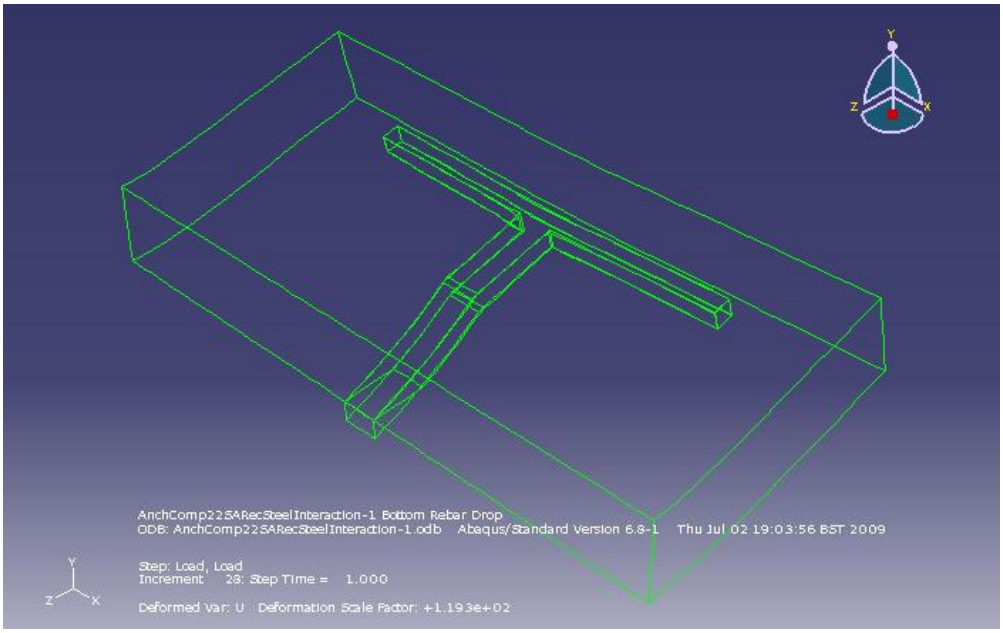

Figure 10-30: 22SA10mm after deformation

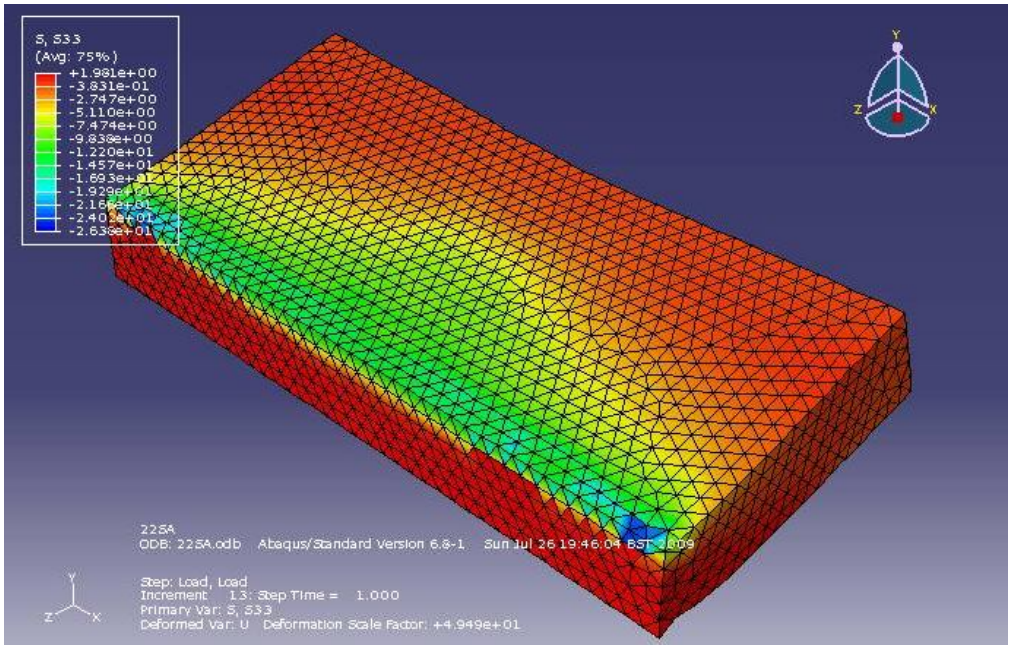

Figure 10-31: 22SA10mm - S33 stress contour of concrete after deformation

A. 22SA10mm-Concrete Part

The following figures (Figure 10-30 ~ Figure 10.33) show the axial compression stress contour of the concrete part of 22SA10mm.

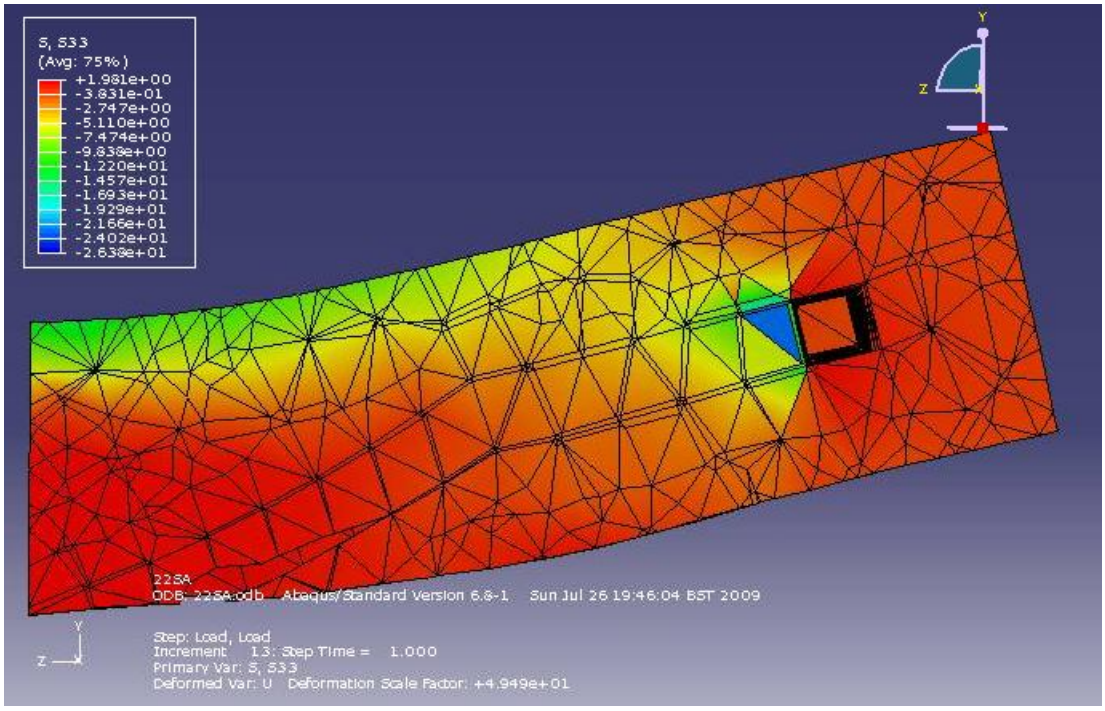

Figure 10-32: S33 stress contour in 22SA10mm X-Plane Cut

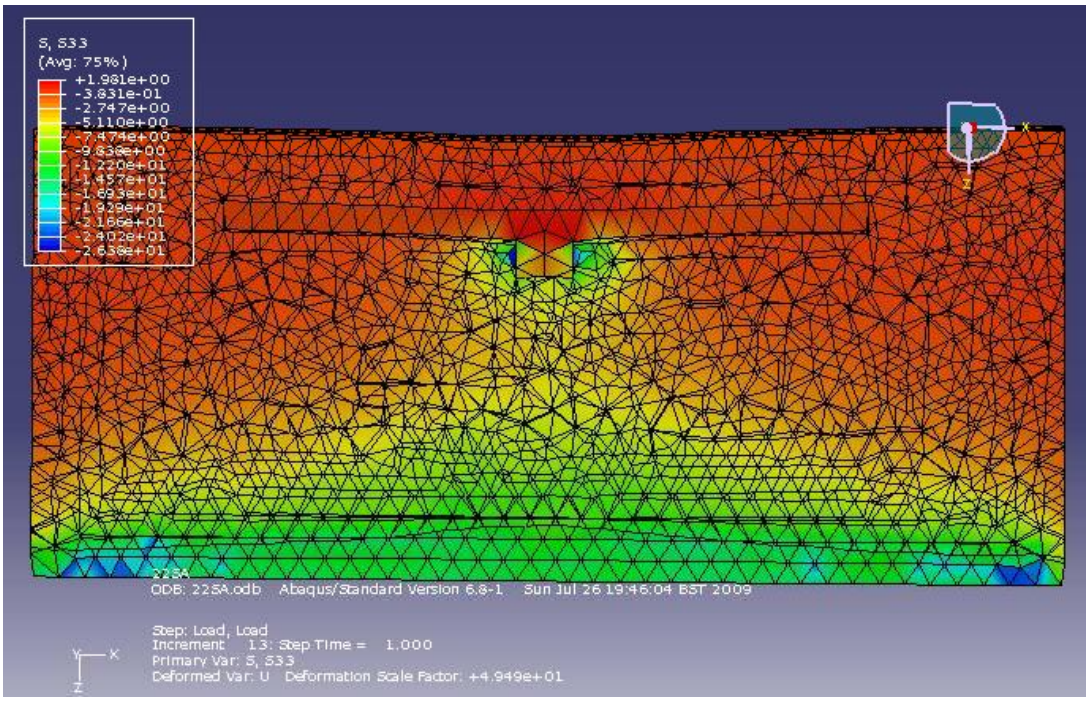

Figure 10-33: S33 stress contour in 22SA10mm X-Plane Cut

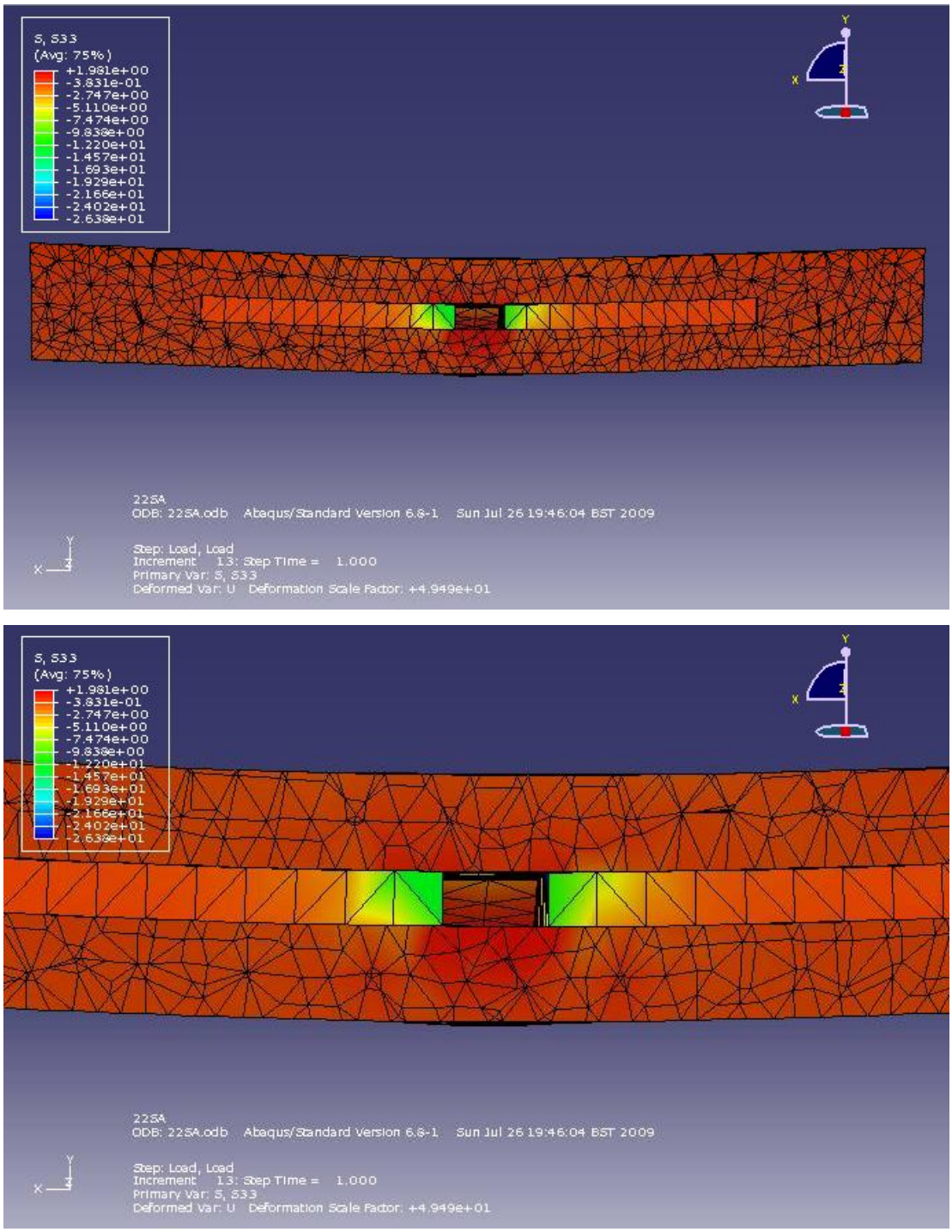

Figure 10-34: S33 stress contour in 22SA10mm Z-Plane Cut

The highest compression stress value is 12.86N/mm^2. The cylinder compression strength of 22SA10mm is 31.64N/mm^2. Thus based on these values the applied stress is not sufficient enough to crush the concrete.

The following Figure 10-33 shows the transverse stress distribution of the concrete.

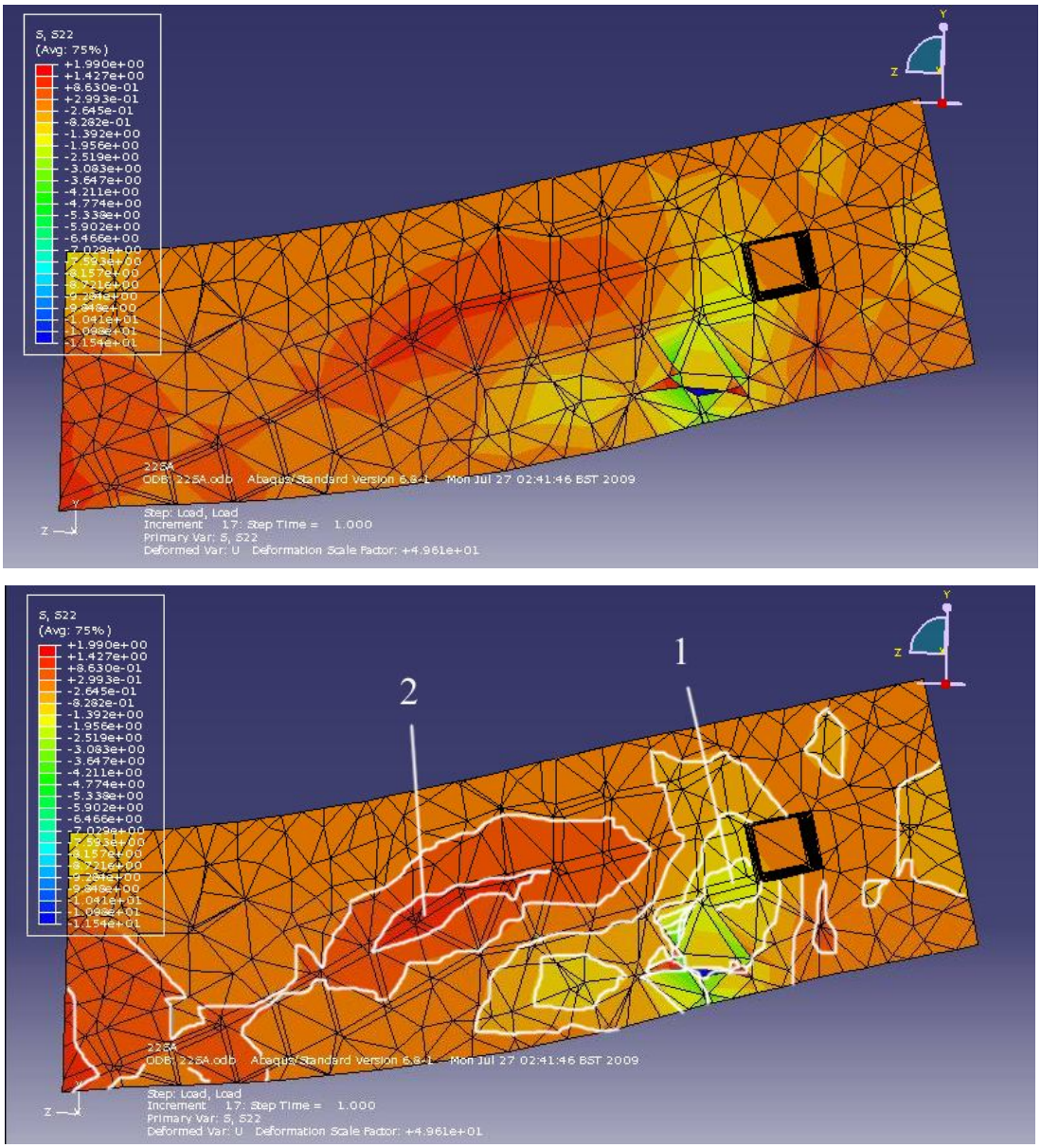

Figure 10-35: 22SA10mm – Transverse stress distribution contour

The maximum transverse tension stress measured at the location 2 is 1.63 N/mm^2 (Figure 10-34)

Again the top part of the flange is experiencing no transverse tension stress. This result makes the same point as for the result of 11DA10mm. Thus based on the results it can be said that, the section around the anchorage would not fail by the transverse tension stress as long as the affected area stays within the local region. Also there can be a possible explanation that the surrounding concrete is providing the confining stress against the transverse tension failure of the section.

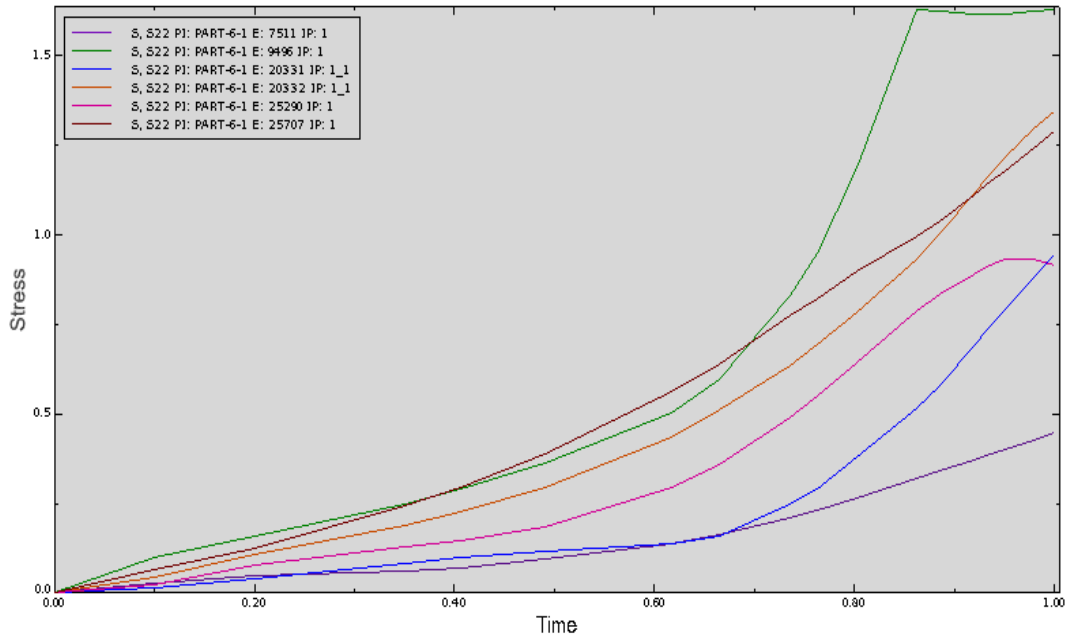

Figure 10-36: 22SA10mm – Transverse tension stress at location 2

B. 22SA10mm - Steel Part

The following plots (Figure 10-35 and 10-36) shows the von Mises stress distribution in steel. The stress values show that the rebar is not yielded in any location. The highest stress value is 208 N/mm^2, and interestingly the location is at the bottom side of the rebar at the point where it bends down.

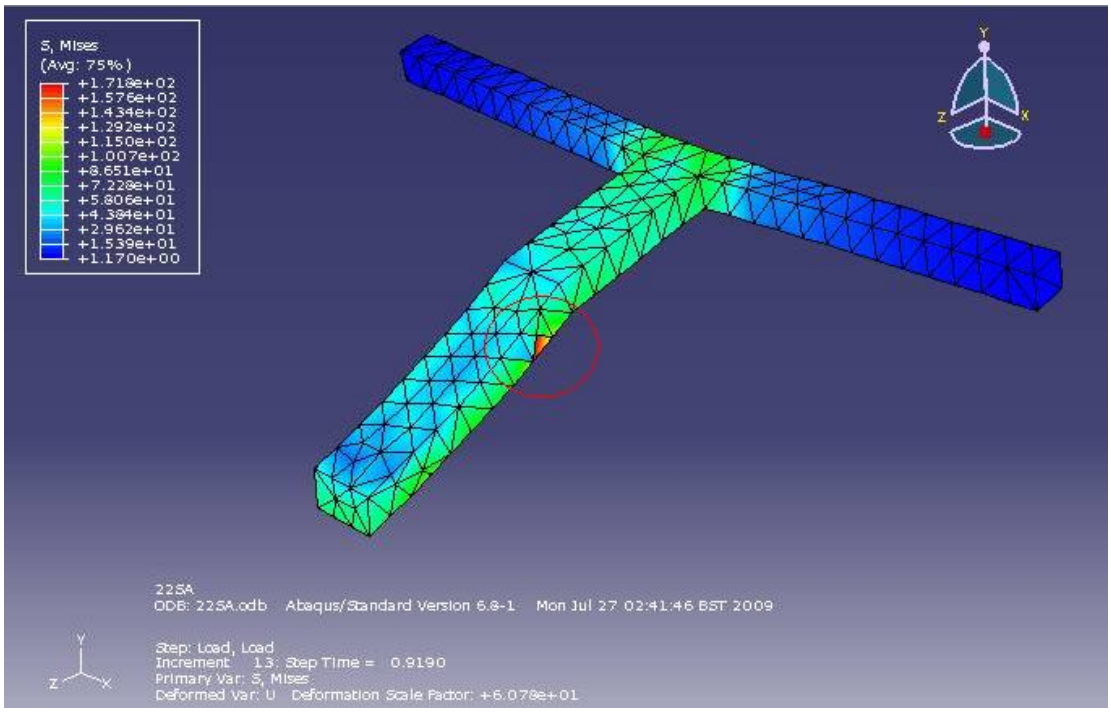

Figure 10-37: 22SA steel section von Mises stress contour plot

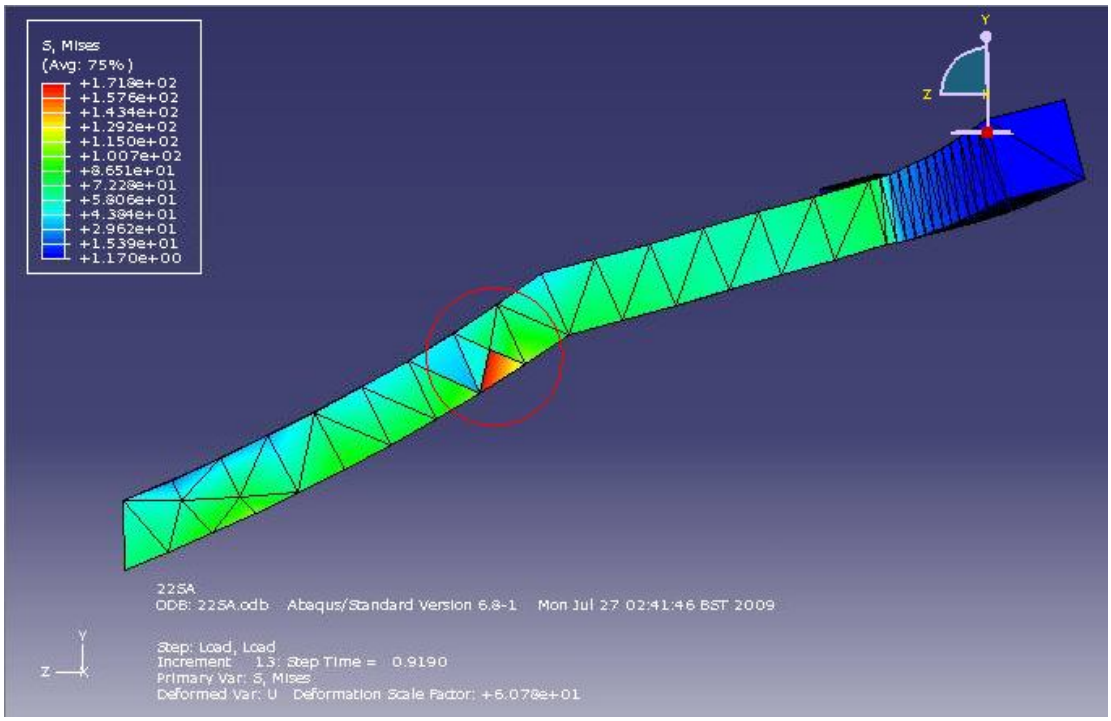

Figure 10-38: 22SA steel section von Mises stress contour plot

As the reaction force acting from the bottom near the anchorage, the horizontal part of the rebar is pushed up. As a result the rebar is forced to be straightened at the bent point. This generates such a high tension stress at the location.

10.2.4 11DADF 10mm and 22SADF 10mm

The following is the finite element model analysis for 11DADF10mm and 22SADF10mm around the anchorage area. The two beams represent the beams with thicker flange depth (80mm) near support, and the analysis of the beams is prepared to study the distribution of the transverse tension stress in the flange.

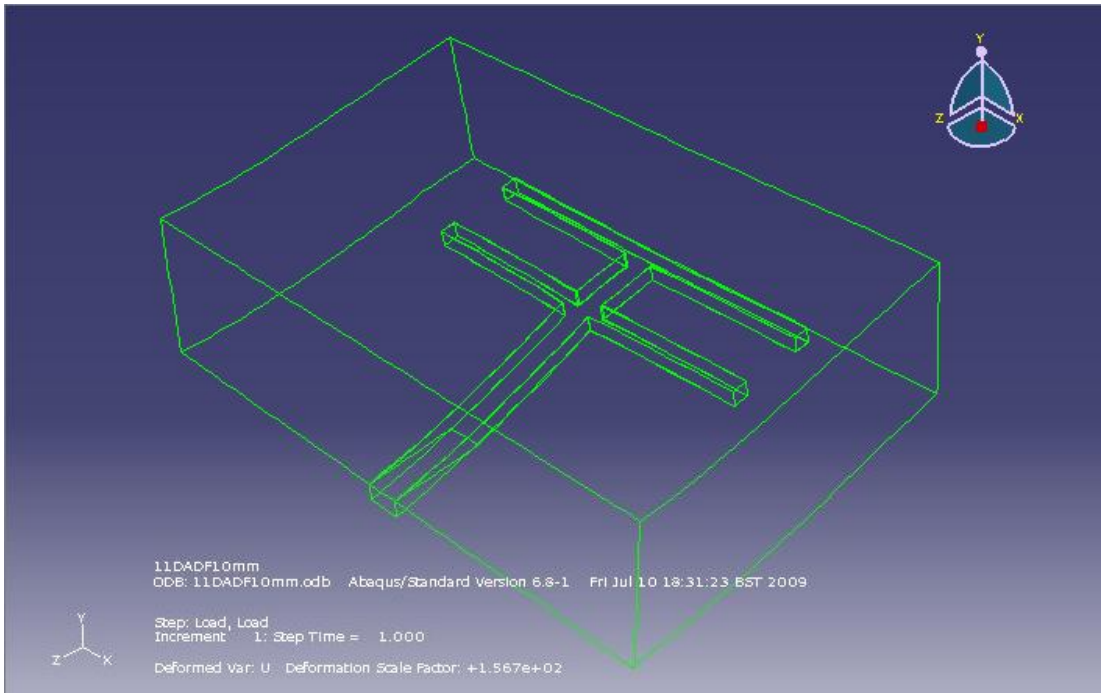

Figure 10-39: 11DADF10mm after deformation

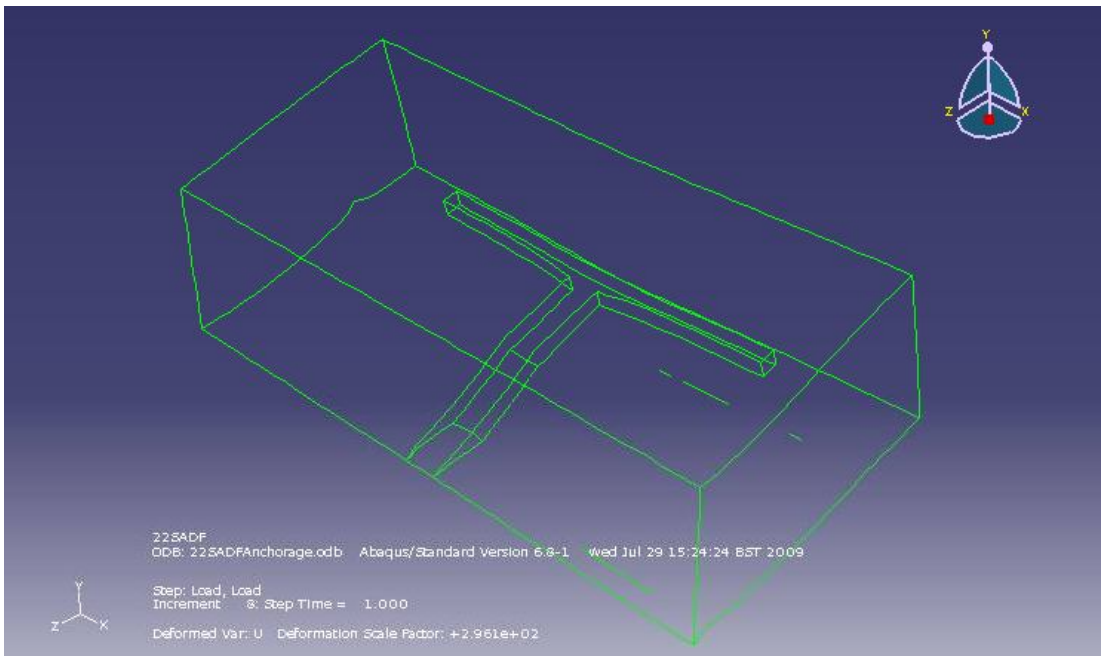

Figure 10-40: 22SADF10mm after deformation

A. Concrete

The applied loads are a lot greater than the earlier models, and the following FEM analysis shows that the axial compression stress has increased in the concrete around anchorage (Figure 10-39 and 10-40). Yet, the induced stresses are not as large as the uni-axial compression capacity of the sections. The maximum compression stresses are about 26 N/mm^2 for 11DADF10mm and 13.7 N/mm^2 for 22SADF10mm.

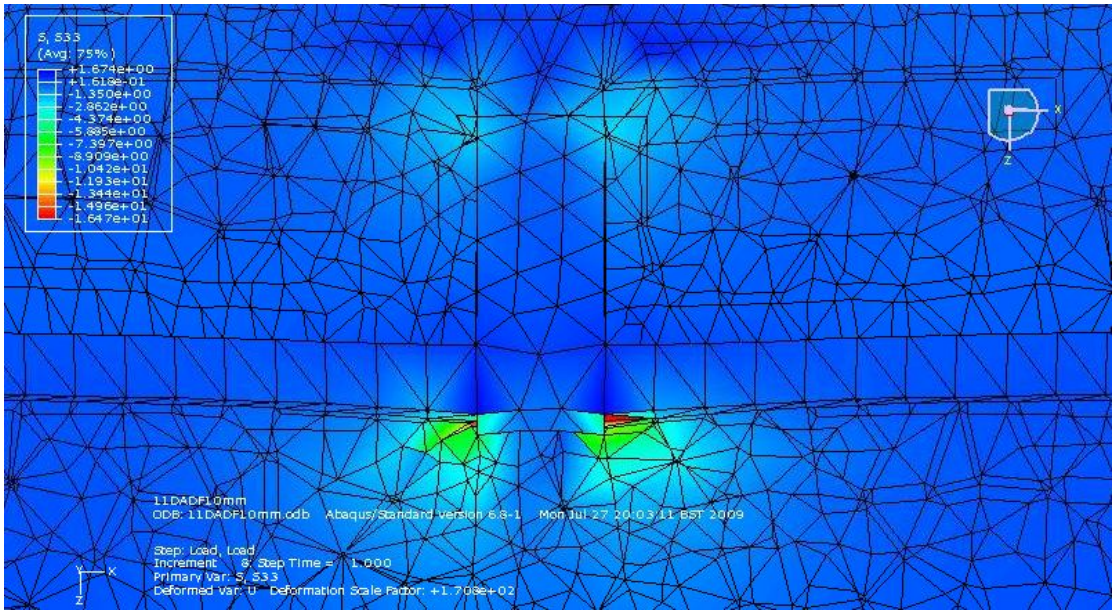

Figure 10-41: 11DADF10mm – S33 stress distribution contour plot at the ultimate load of 21kN

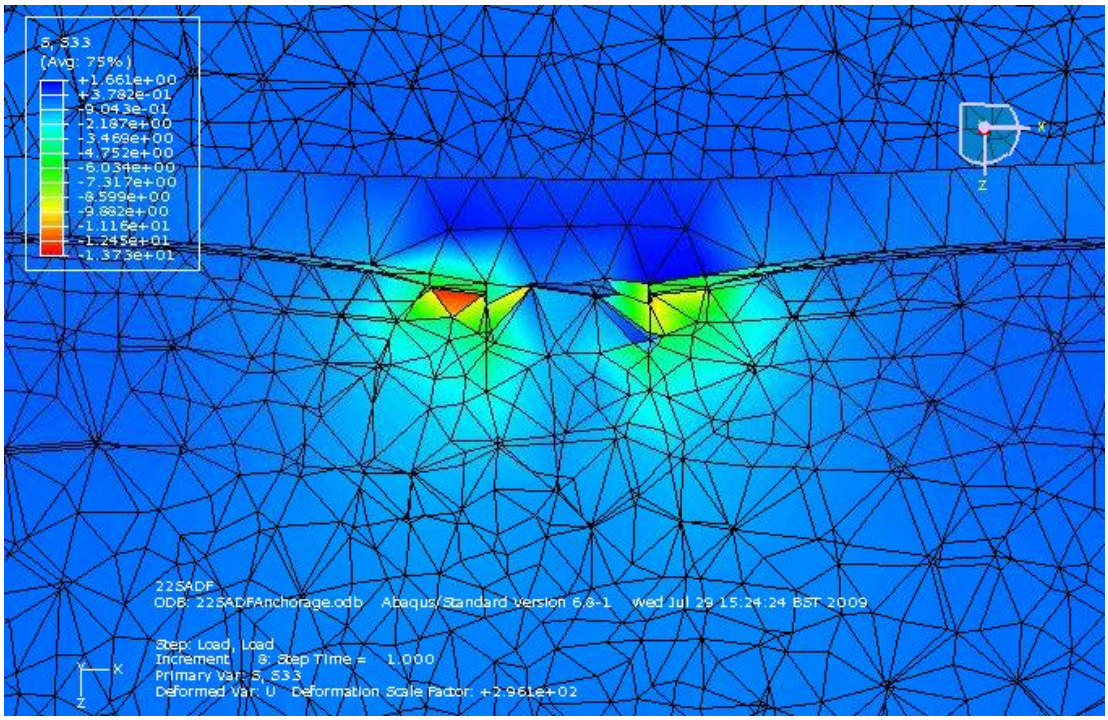

Figure 10-42: 22SADF10mm – S33 stress distribution contour plot at the ultimate load of 32kN

The following figures (Figure 10-41 and Figure 10.42) show the transverse tension

stress distribution in the concrete.

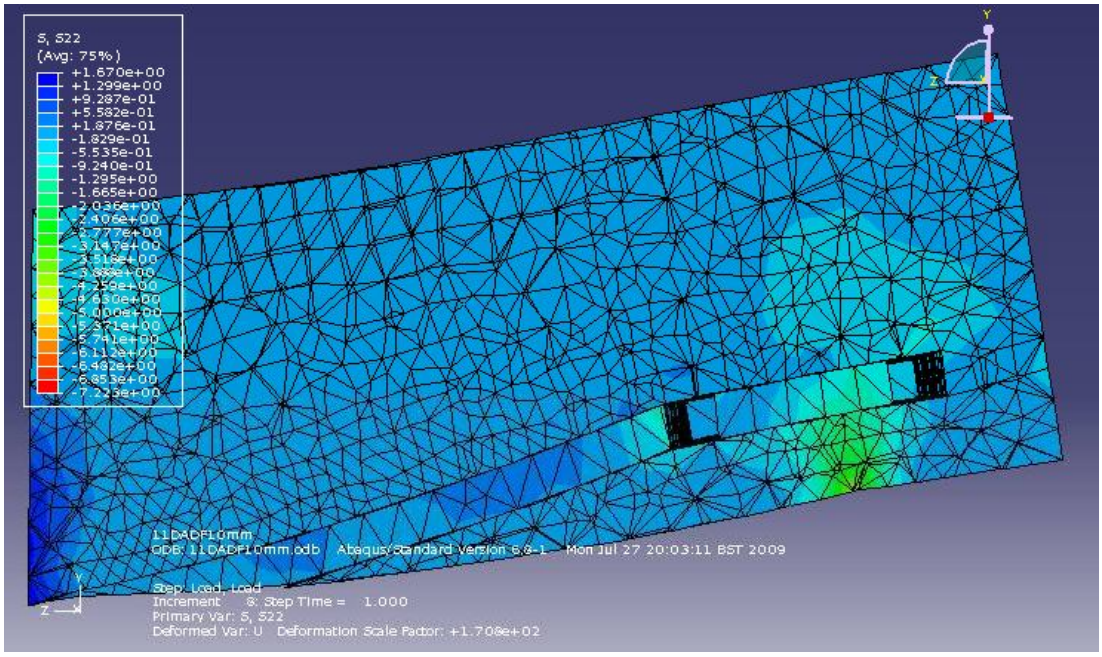

Figure 10-43: 11DADF10mm – Transverse stress distribution contour

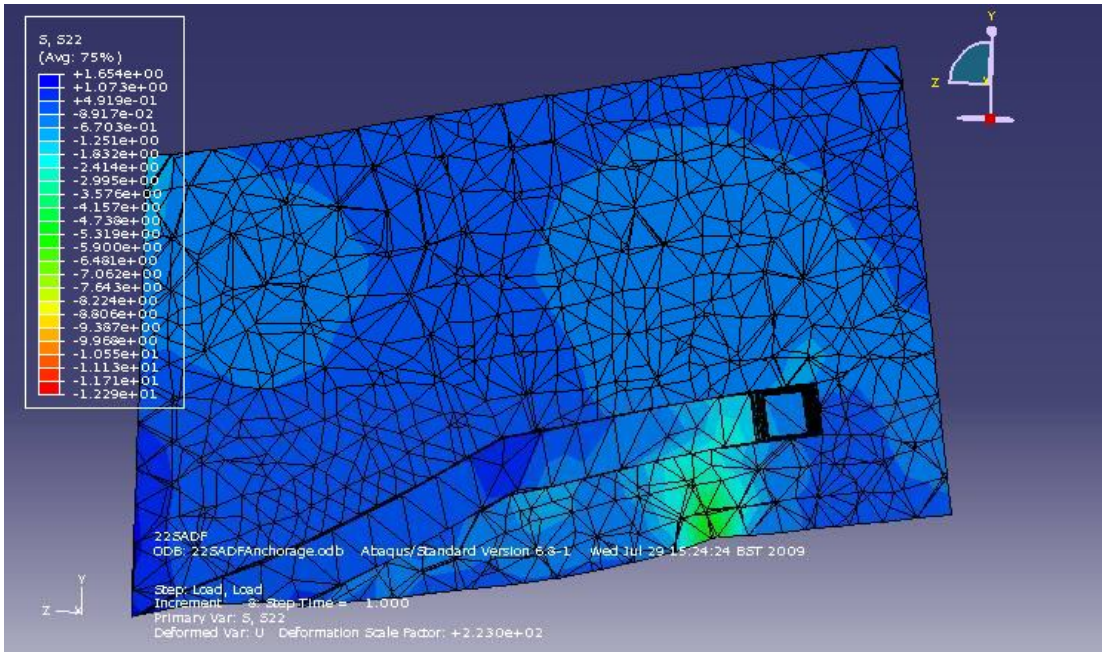

Figure 10-44: 22SADF10mm – Transverse stress distribution contour

The above figures show that the most of the concrete part is experiencing the compression stress and only small region is experiencing the tensions stress. Also the transverse tension stresses are very local and does not spread over large area. For both beams the magnitudes of the stress around the top part of the flange are in the range of (-0.183 ~ +0.188) N/mm^2 and (-0.089 ~ +0.491) N/mm^2 for 11DADF10mm

and 22SADF10mm respectively. The negative sign means for compression stress. Thus the result shows the decrease of the transverse tension stress area with the increase of the flange depth.

B. Steel

Again the highest von Mises stress is found at the connection point of the rebar and the in anchorage (inner anchorage in case of 11DADF10mm). The stress values are 117.11 N/mm^2 and 60.83 N/mm^2 for 11DADF10mm and 22SADF10mm respectively (Figure 10-43 and 10-44).

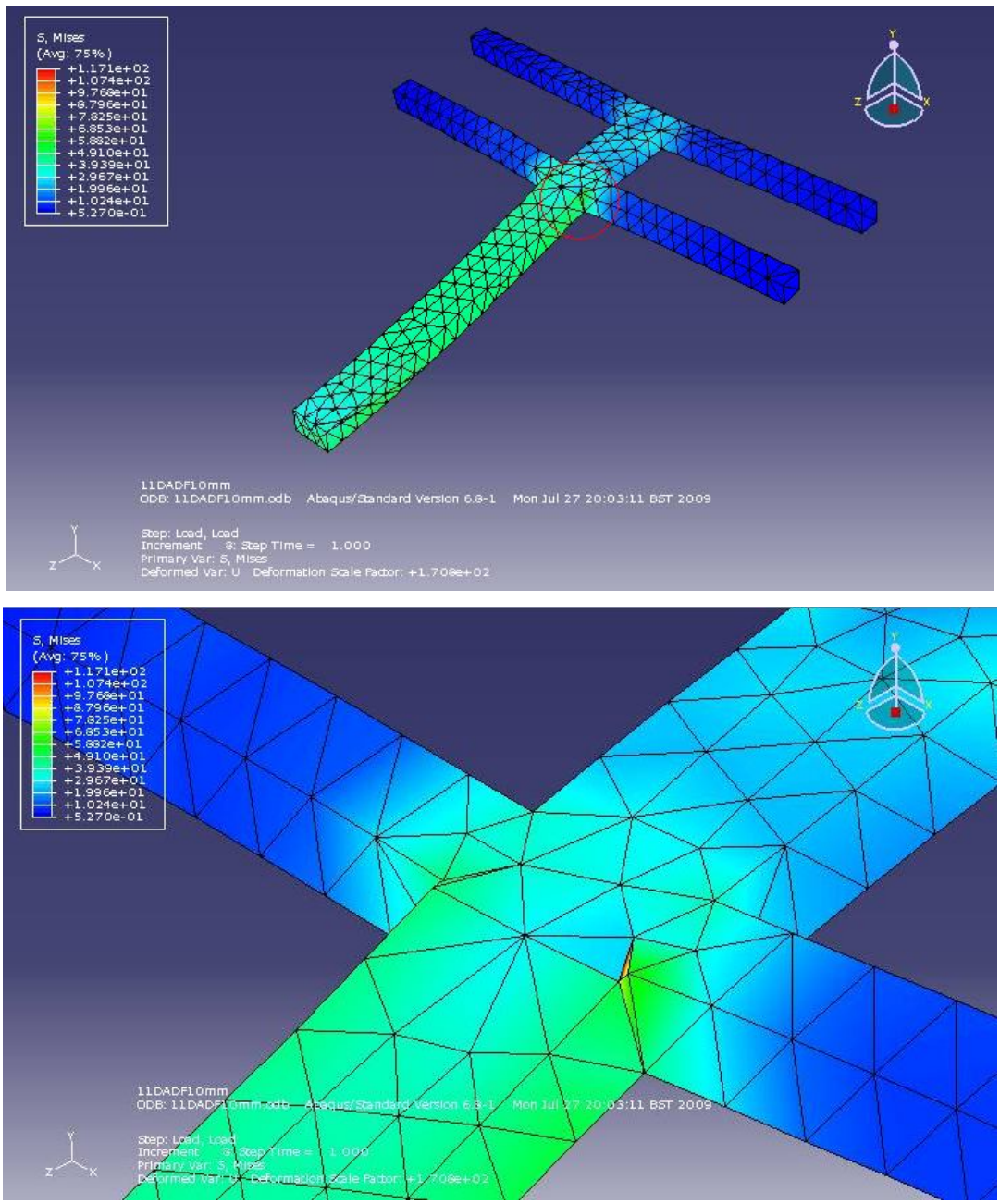

Figure 10-45: 11DADF10mm steel section von Mises stress contour plot

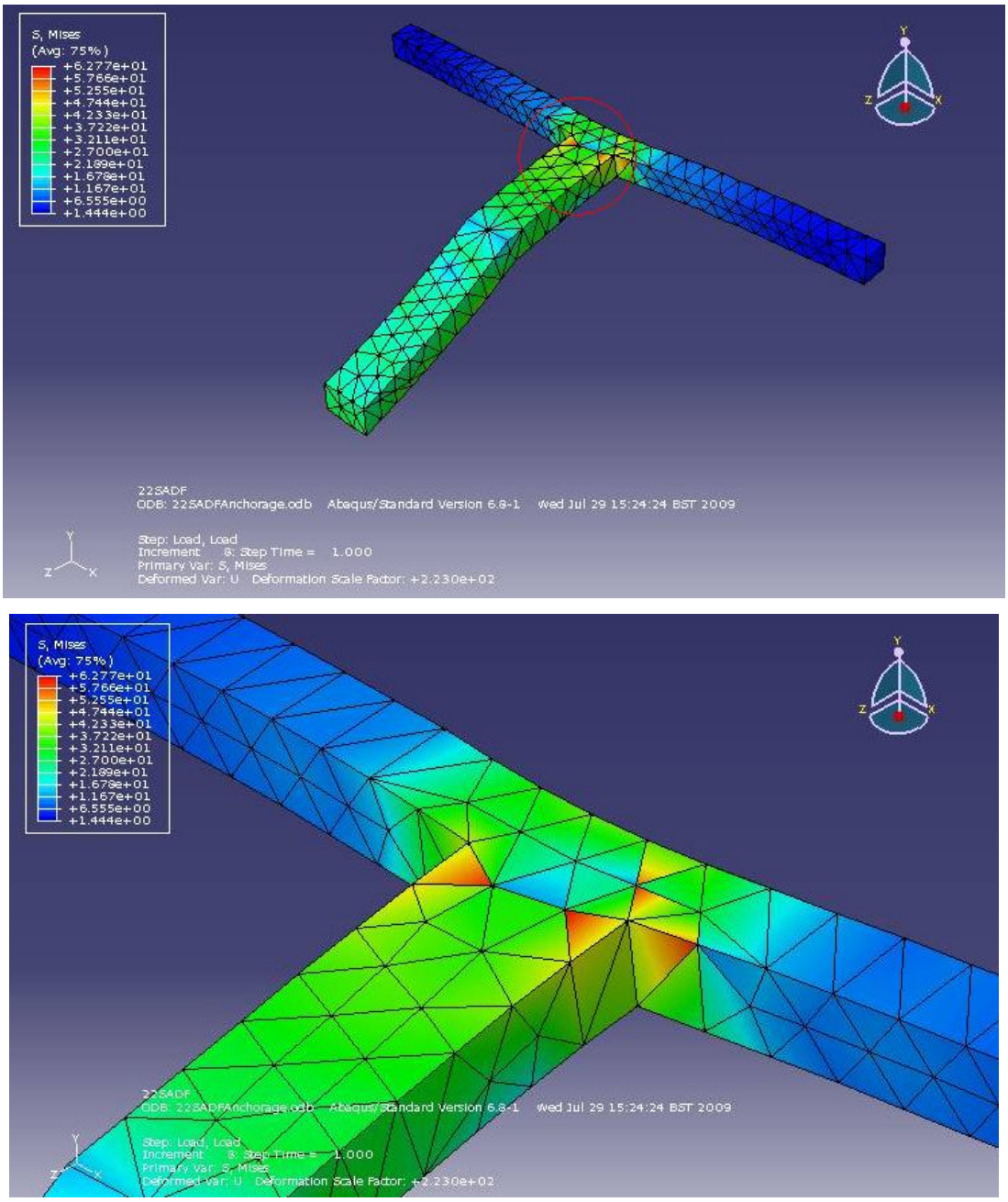

Figure 10-46: 22SADF10mm steel section von Mises stress contour plot

10.2.5 Summary and Conclusions of Anchorage Model Analysis

From the above anchorage FEM analysis the following conclusion has been drawn:

- For both 11DA10mm and 22SA10mm the applied compression stress from the pulled in anchorage is reduced, and the adjacent concrete has sustained the applied stress.
- The compression stress is not applied over the entire length of the anchorage as assumed in the initial theoretical calculation, but the stress is only concentrated over very limited region around the connection point of rebar and anchorage.
- It is found that the failure of 11SA10mm is not caused by the crushing of concrete due to the anchorage compression stress, but the transverse tension stress, which is affecting to the top of the flange. The affecting area of the transverse tension stress seems to be linked with the failure of the section.
- In case of 11DA10mm and 22SA10mm the transverse tension stress does not spread to the top of the flange, and as it was seen from the test results the section sustained the load, despite the induced tension stress reached the tension capacity of the concrete.
- In the beams with thicker flange the transverse tension stress is distributed over smaller area, and the most of the part is unaffected by the tension stress.

10.3 Section 2: Beam Models

The purpose of the analysis is to further examine the effect of the wider web on the shear behaviour of the beams. As the test results show, changing the geometry of the web has increased the ultimate loads of the beams considerably, and the beam failing near the mid-span due to the yielding of reinforcement. This result proves that the web's geometry has altered the way the overall stresses are distributed in section, and increased the shear capacity of the beam.

Thus the finite element models of the following beams are built, analysed, and compared to see the effect of the wider web.

The beams that are discussed in this part are:

- (11DADF12mm) VS (11DADFWW12mm)
- (22SADF3no12mm) VS (22SADFWW3no12mm)

10.3.1 Section 1: (22SADF3no12mm) VS (22SADFWW3no12mm)

10.3.1.1: 22SADF3no12mm

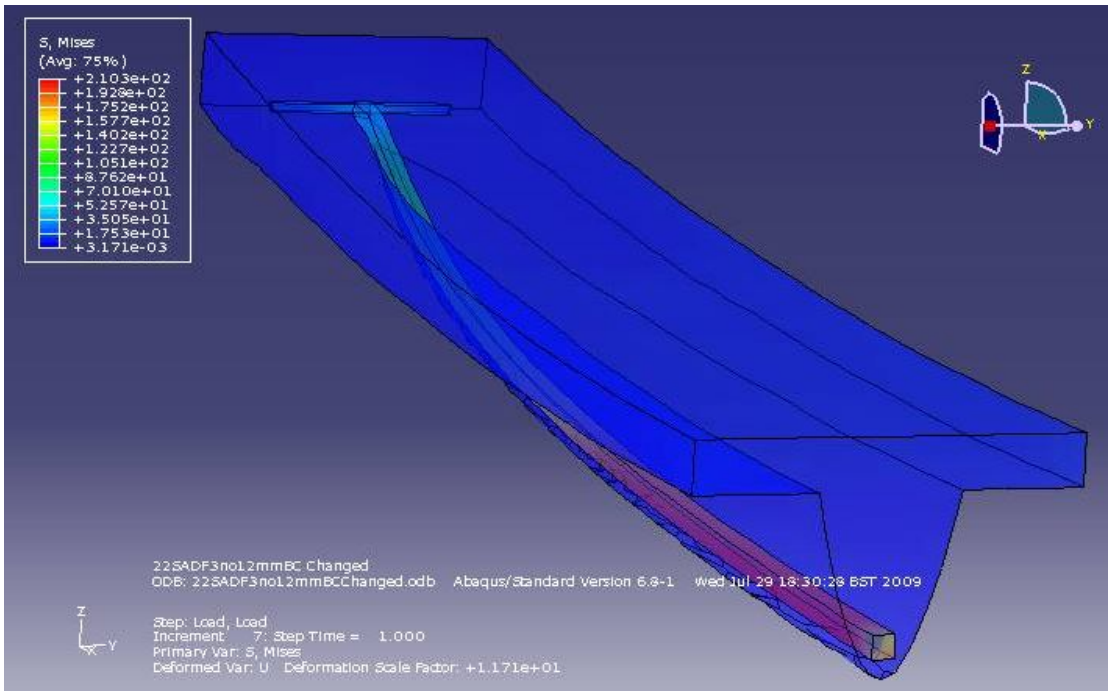

Figure 10-47: 22SADF3no12mm after deformation

A. Concrete - 22SADF3no12mm

The following Figure 10-46 shows the von Mises stress contour. A high stress point is observed at the circled location. Interestingly the location is where the diagonal tension failure occurred in the tested beam (Figure 10-47).

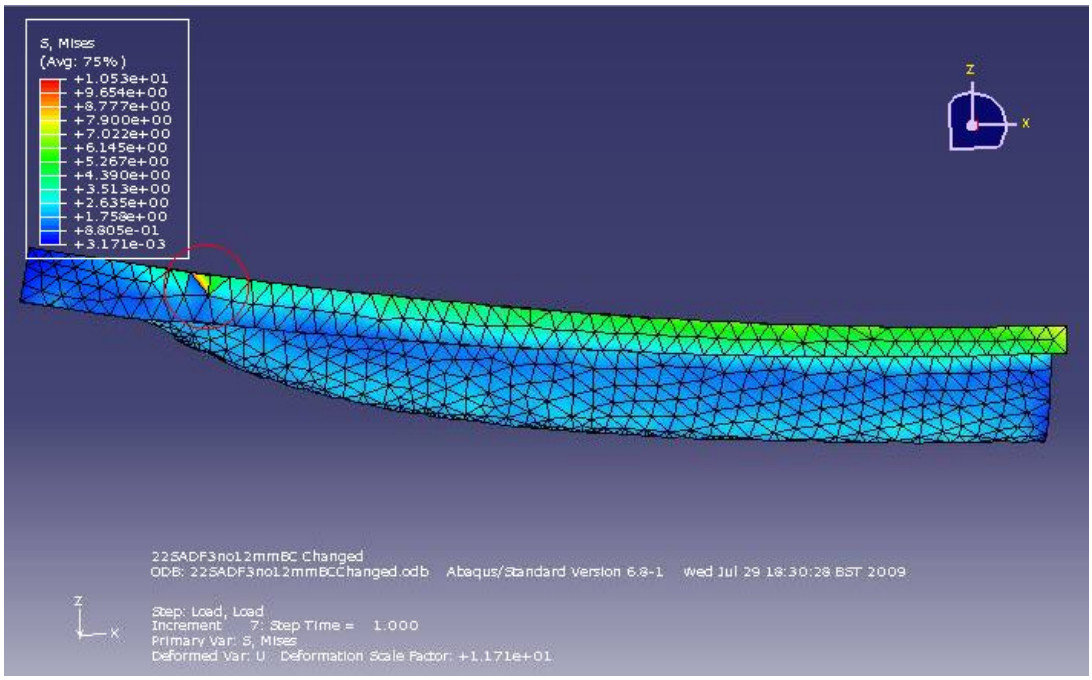

Figure 10-48: 22SADF3no12mm Mises stress contour

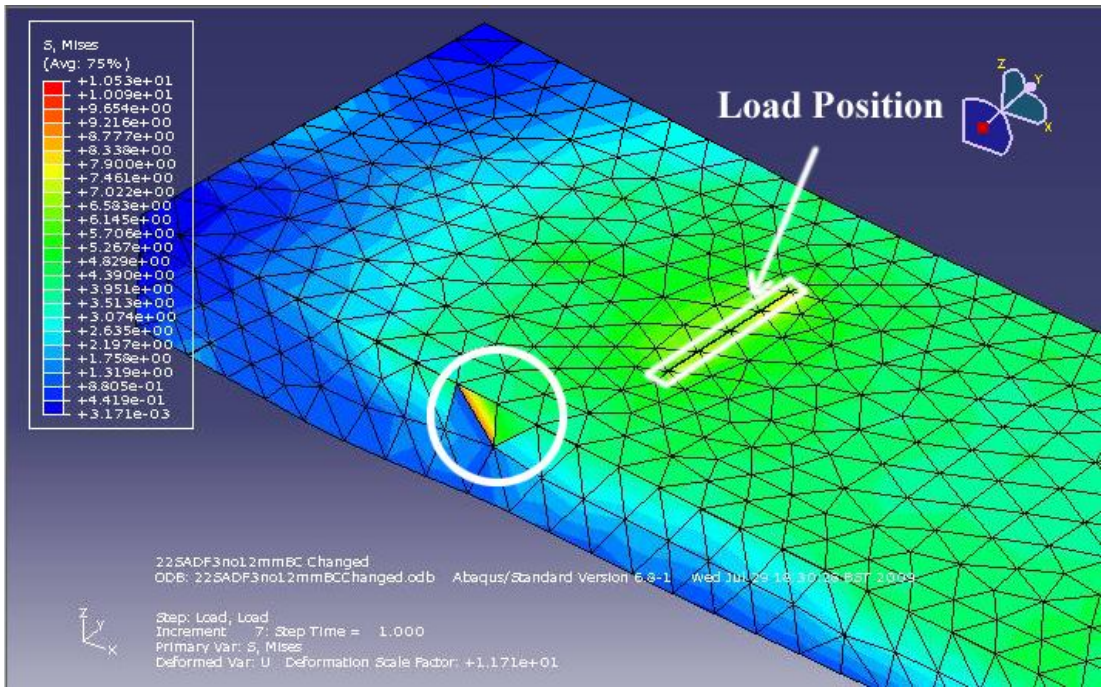

Figure 10-49: 22SADF3no12mm-Location of the applied load

The following principal stress contour (Figure 10-48) is plotted to examine the stress distribution around the web end. The figure shows high tension stress is concentrated around the end of the web. It is discussed in the earlier chapter that, such stress concentration initiates the cracks that causes the separation of the web and the flange which leads to the shear failure of the section.

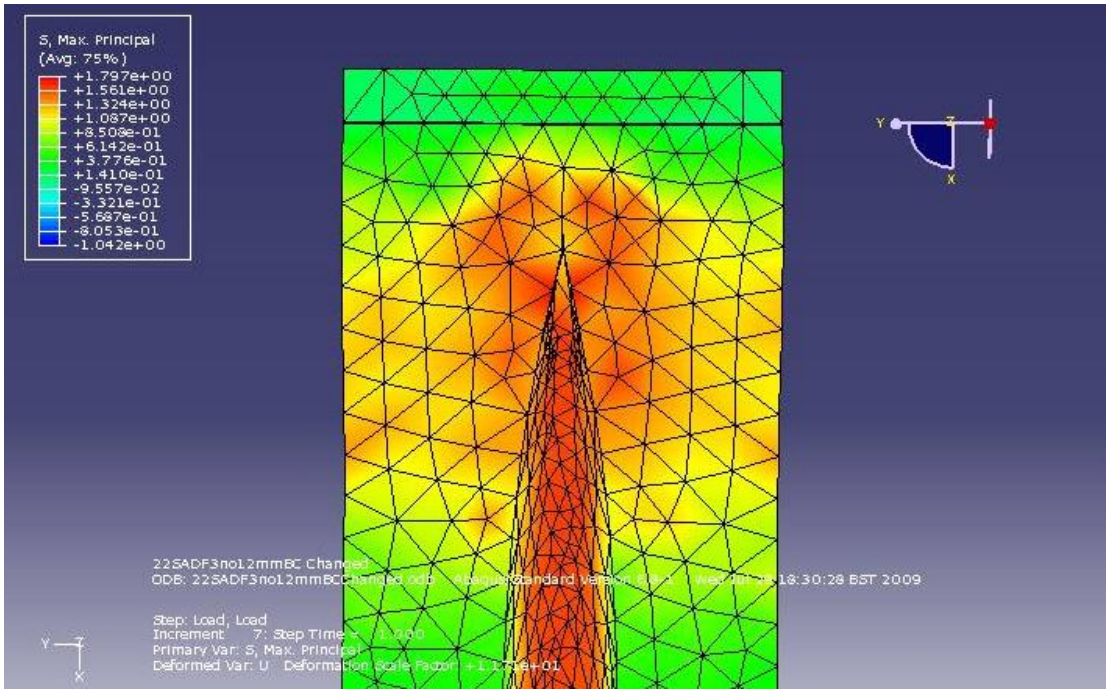

Figure 10-50: 22SADF3no12mm Maximum (tension) principal stress contour plot of the web end

The following figures show the distribution of the tensors around the web (Figure 10-49 and Figure 10-50). The short white lines represent the maximum principal tensors, and it can be seen that the most of them are pointing towards the end point of the web. This indicates the high concentration of tension stress acting in the direction of the end of the web.

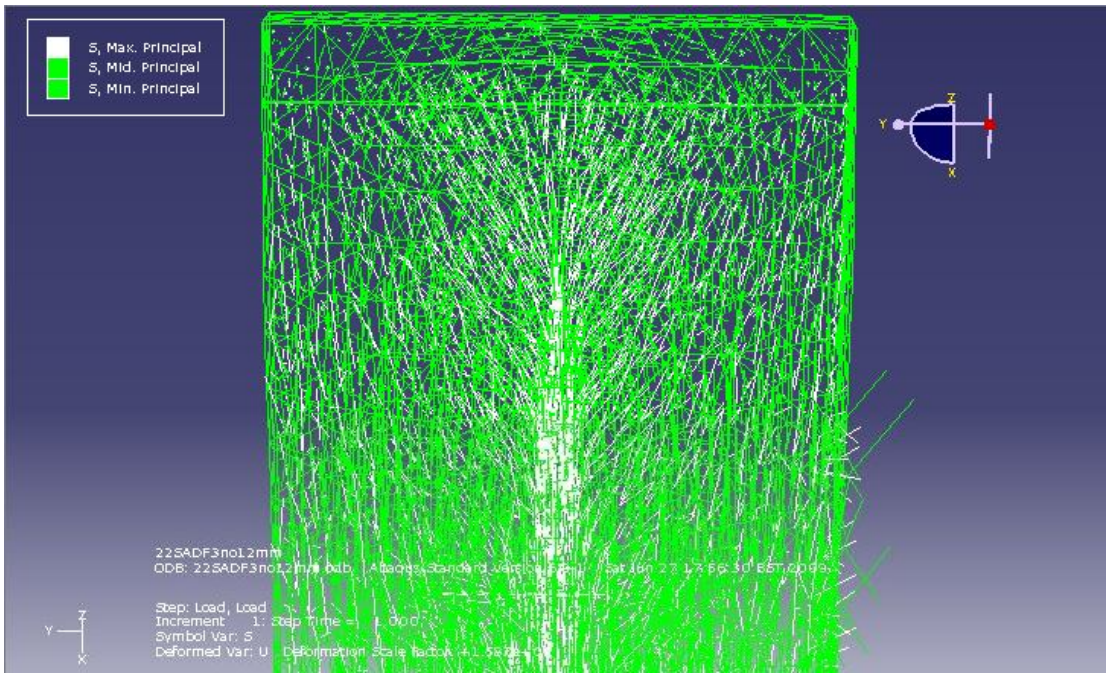

Figure 10-51: 22SADF3no12mm maximum principal tensors at the web end

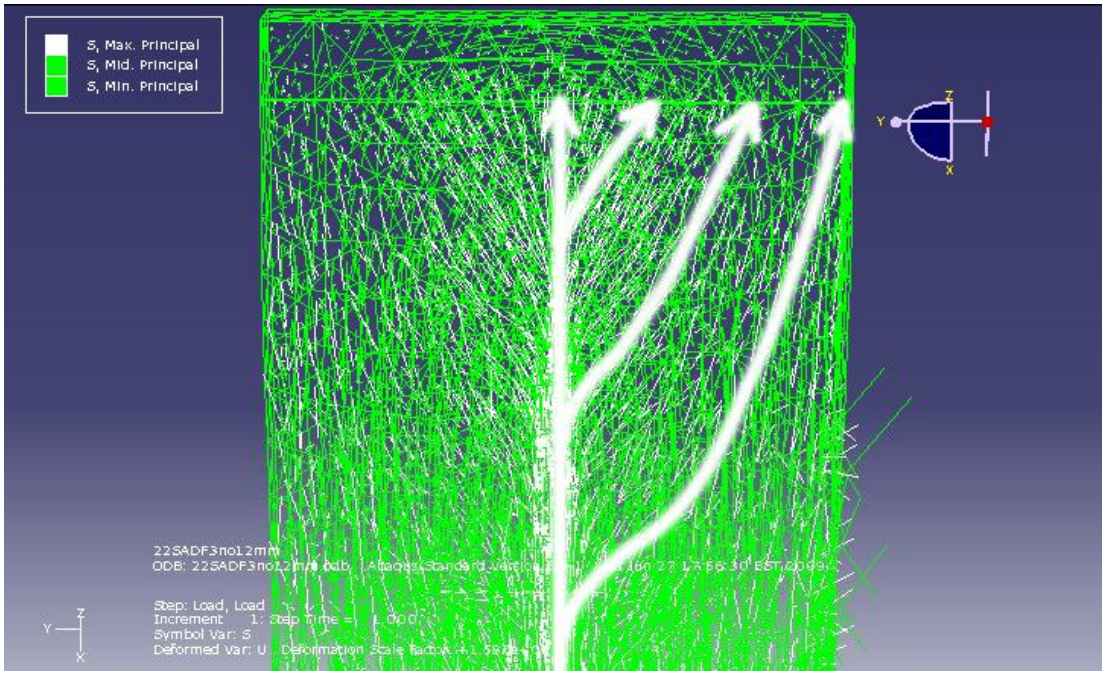

Figure 10-52: 22SADF3no12mm maximum principal tensors at the web end and their global orientations

B. Steel -22SADF3no12mm

The following Figure 10-51 shows the von Mises stress distribution in the steel section at the collapse load.

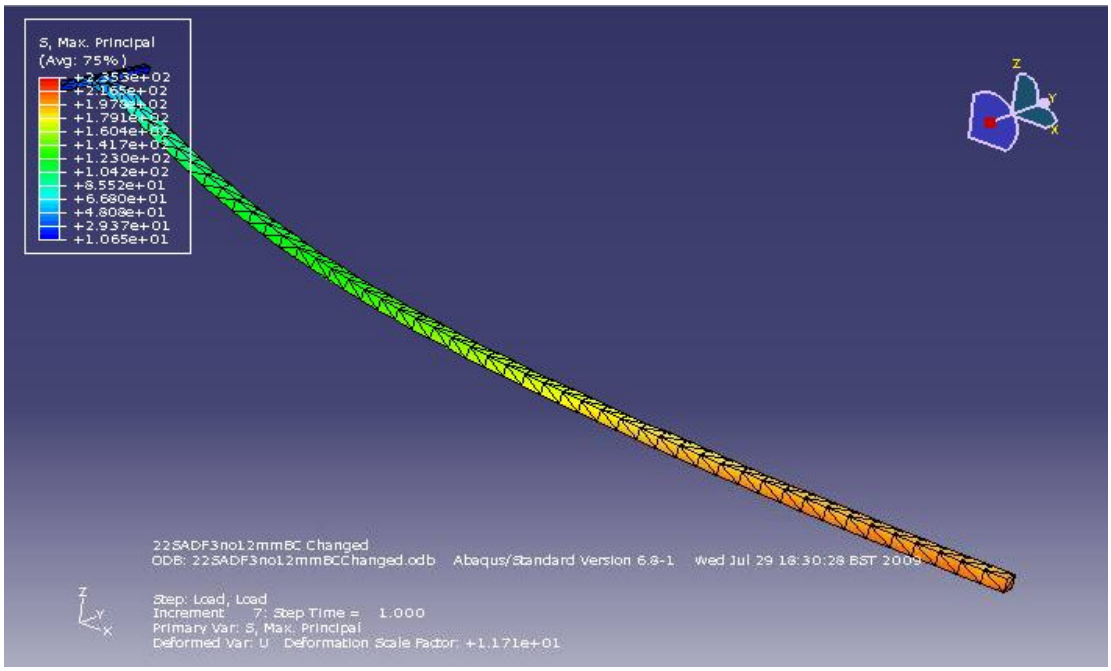

Figure 10-53: 22SADF3no12mm von Mises stress in the deformed steel section

The following graph (Figure 10-52) has been plotted to see the maximum tension stress incurred in the steel section. The highest stress value is 220.73 N/mm^2; 62% of the yield stress of the steel, 355N/mm^2.

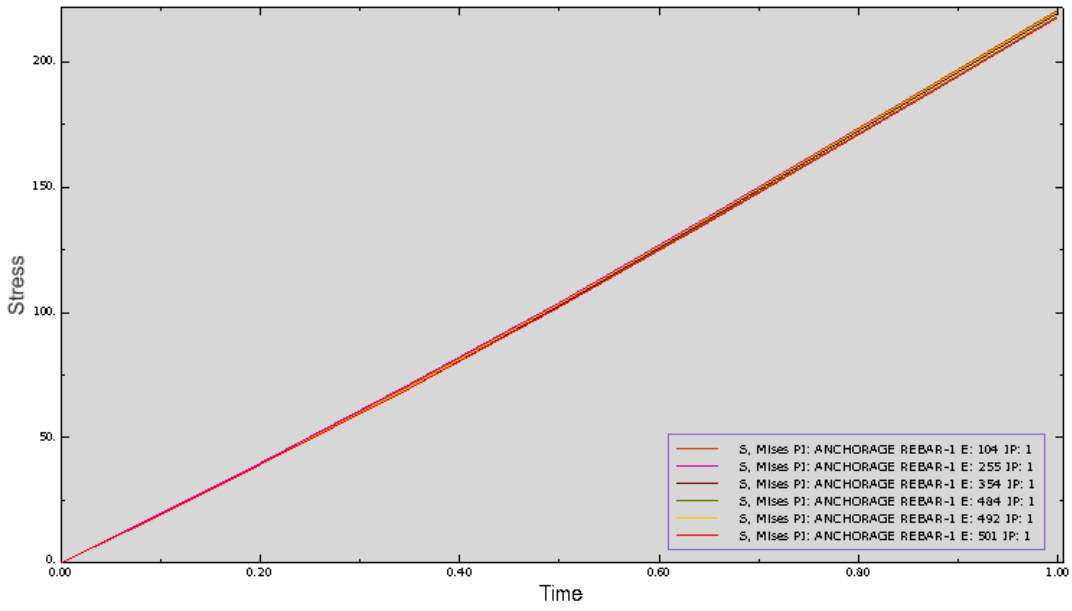

Figure 10-54: 22SADF3no12mm maximum tension stresses in the steel section

10.3.1.2: 22SADFWW3no12mm

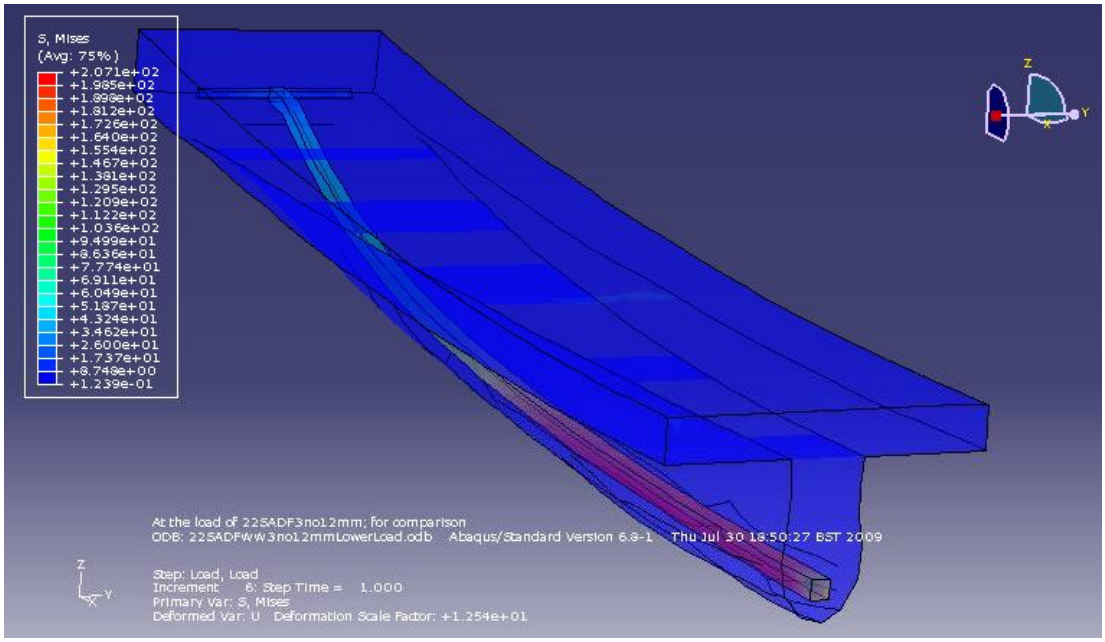

Figure 10-55: 22SADFWW3no12mm before deformation

A. Concrete-22SADFWW3no12mm

The following figures (Figure 10-54 ~ Figure 10-57) compare the stress distribution in the beams at the same applied loads. The first set of figures (Figure 10-54 and 10-55) show the maximum principal stress distribution at the cross-section of the beam, and the second set of figures show the maximum principal stress distribution over the web area.

The first set shows that 22SADF3no12mm with the pointy web is experiencing much greater tension stresses overall in comparison with 22SADFWW3no12mm with the wide web. Also towards the support, more part of the flange is exposed to greater tension stress in 22SADF3no12mm than 22SADFWW3no12mm.

The second set (Figure 10-56 and 10-57) shows that the maximum principal tension stress is affecting the web as well as the flange in 22SADF3no12mm, yet in the 22SADFWW3no12mm the stress is distributed over the web and hardly moved into the flange.

Set 1

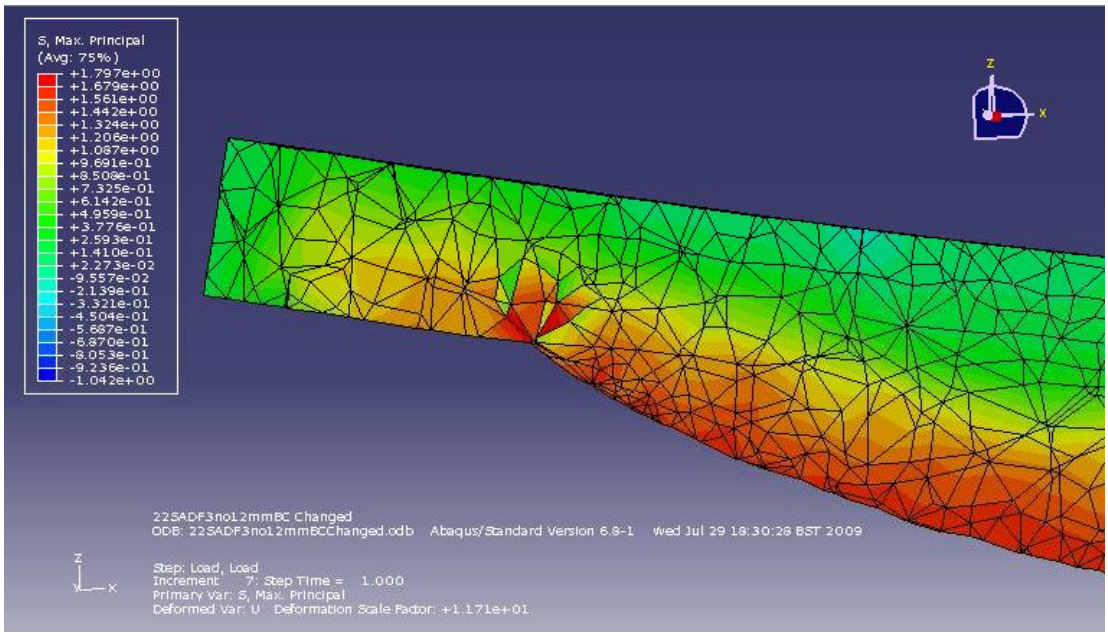

Figure 10-56: 22SADF3no12mm Maximum principal stress distribution at the cross section

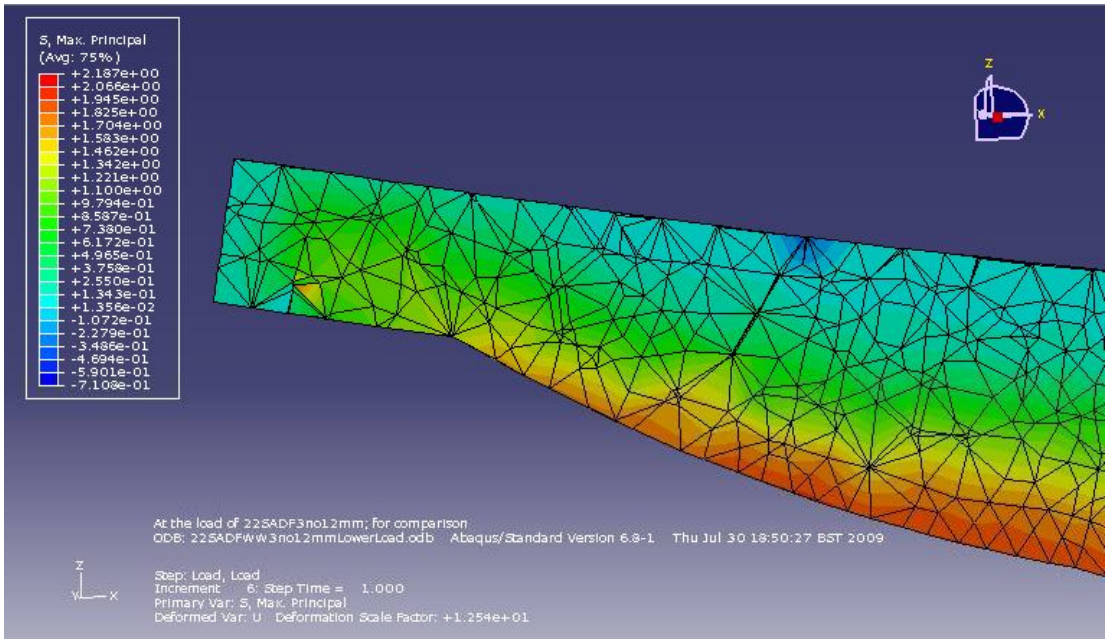

Figure 10-57: 22SADFWW3no12mm Maximum principal stress distribution at the cross section

Set 2

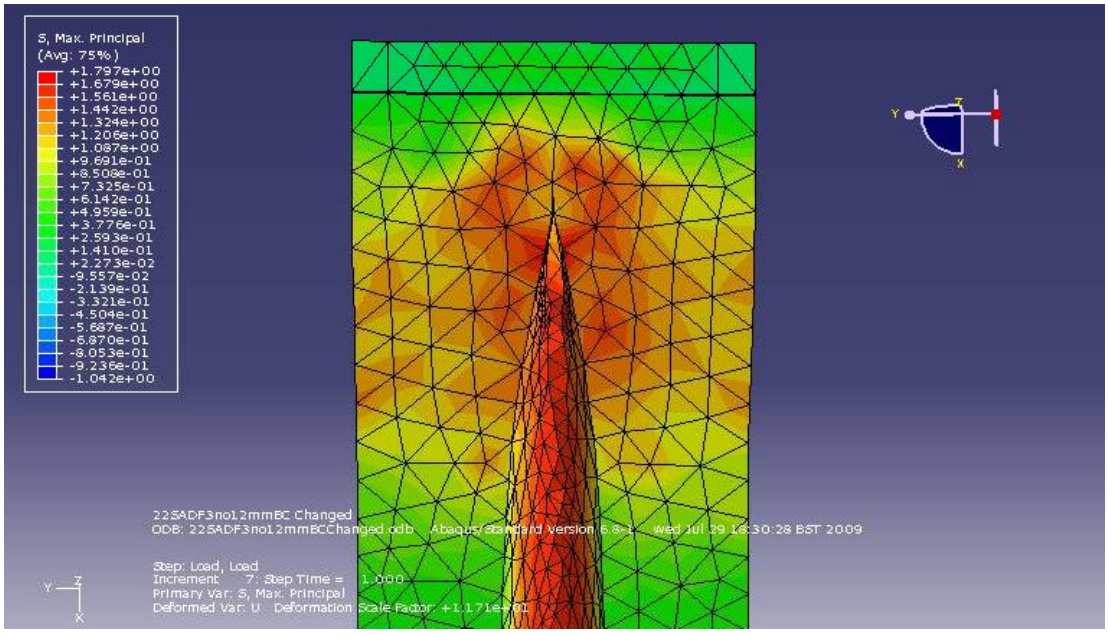

Figure 10-58: 22SADF3no12mm Maximum principal stress distribution over the web

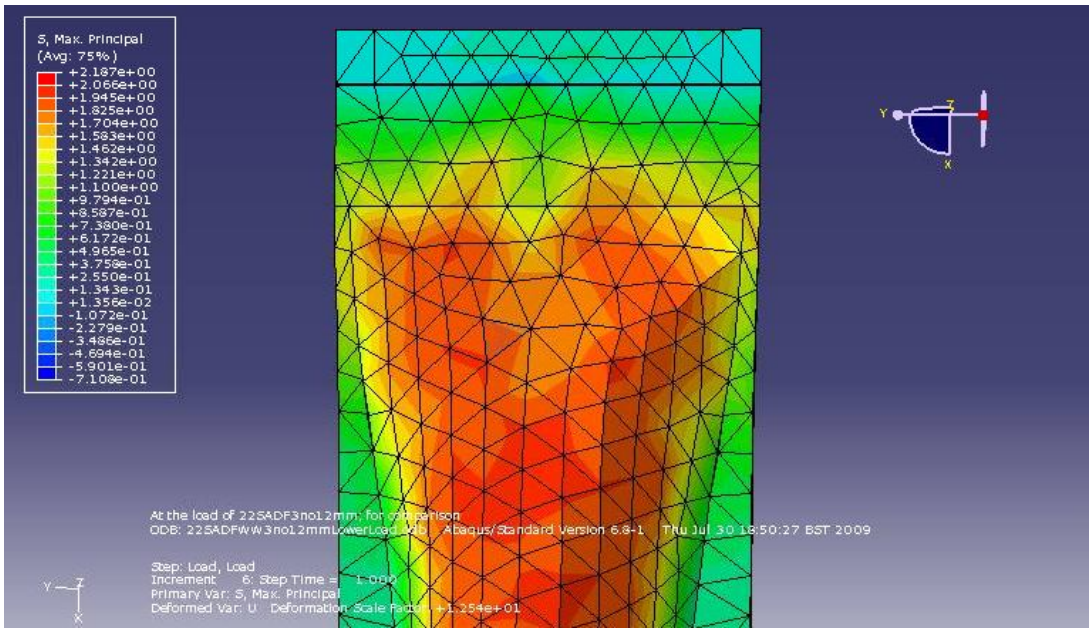

Figure 10-59: 22SADFWW3no12mm Maximum principal stress distribution over the web

The following diagrams (Figure 10-58) compare the distribution of the tensors in the beams. The figures show that in case of 22SADF3no12mm tensors are concentrated around the end of the web and also along the bottom line of the flange.

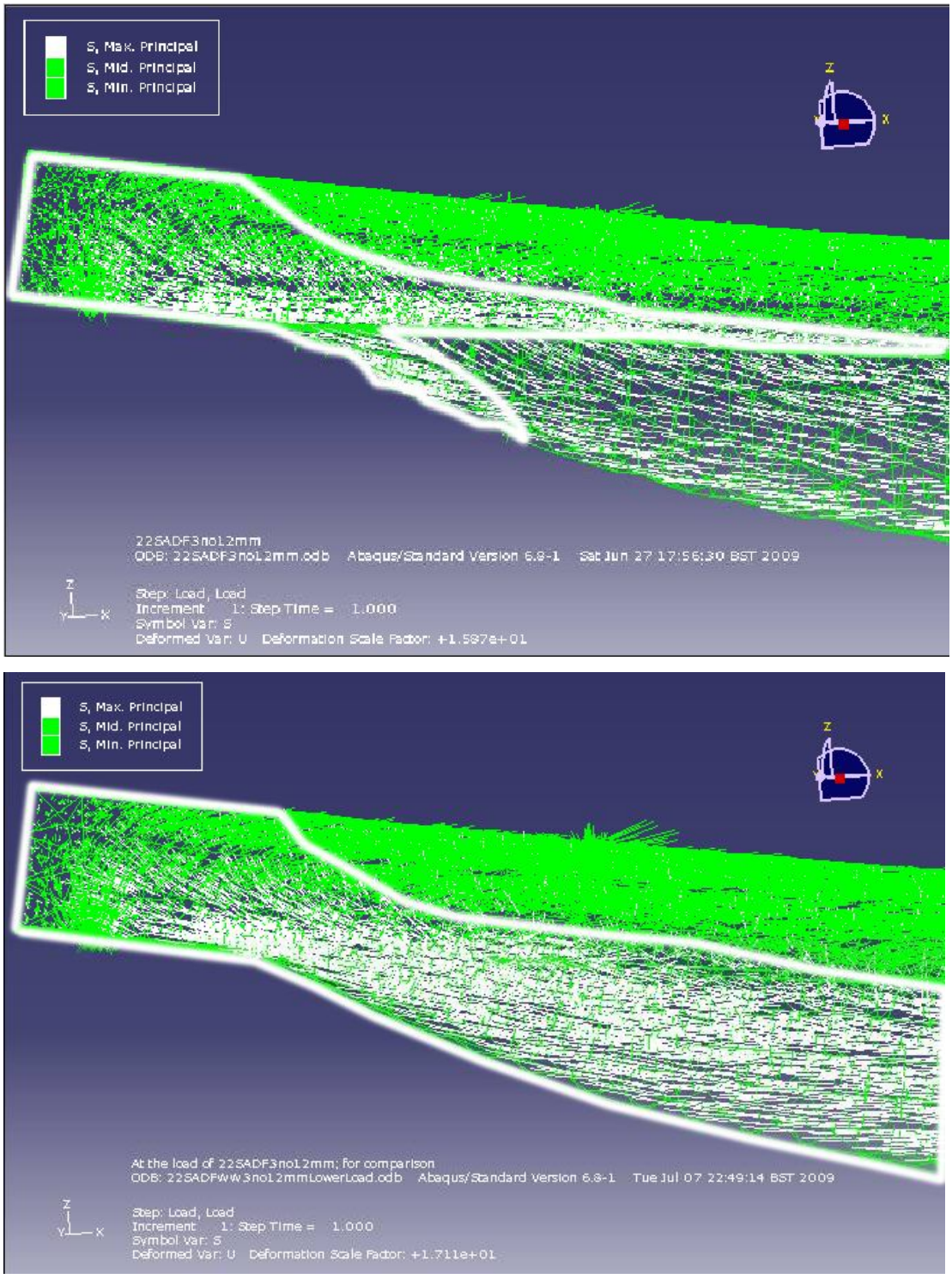

Figure 10-60: Maximum Principal Stress Tensor distribution for 22SADF3no12mm (Above) and 22SADFWW3no12mm (below)

Such uneven distribution of the stresses in 22SADF3no12mm seems caused the

cracks that separated the flange and the web, meanwhile, the more uniformly distributed stress in 22SADFWW3no12mm made the flange and the web to work as one unit.

The following diagrams (Figure 10-59) compare the global directions of the tensors in the beams. In 22SADF3no12mm there are more sudden changes in direction of the tensors over the web and the flange, and in 22SADFWW3no12mm the tensors are in more natural flow connecting between the flange and the web, and there is not any location where exceptionally high density of tensors is found.

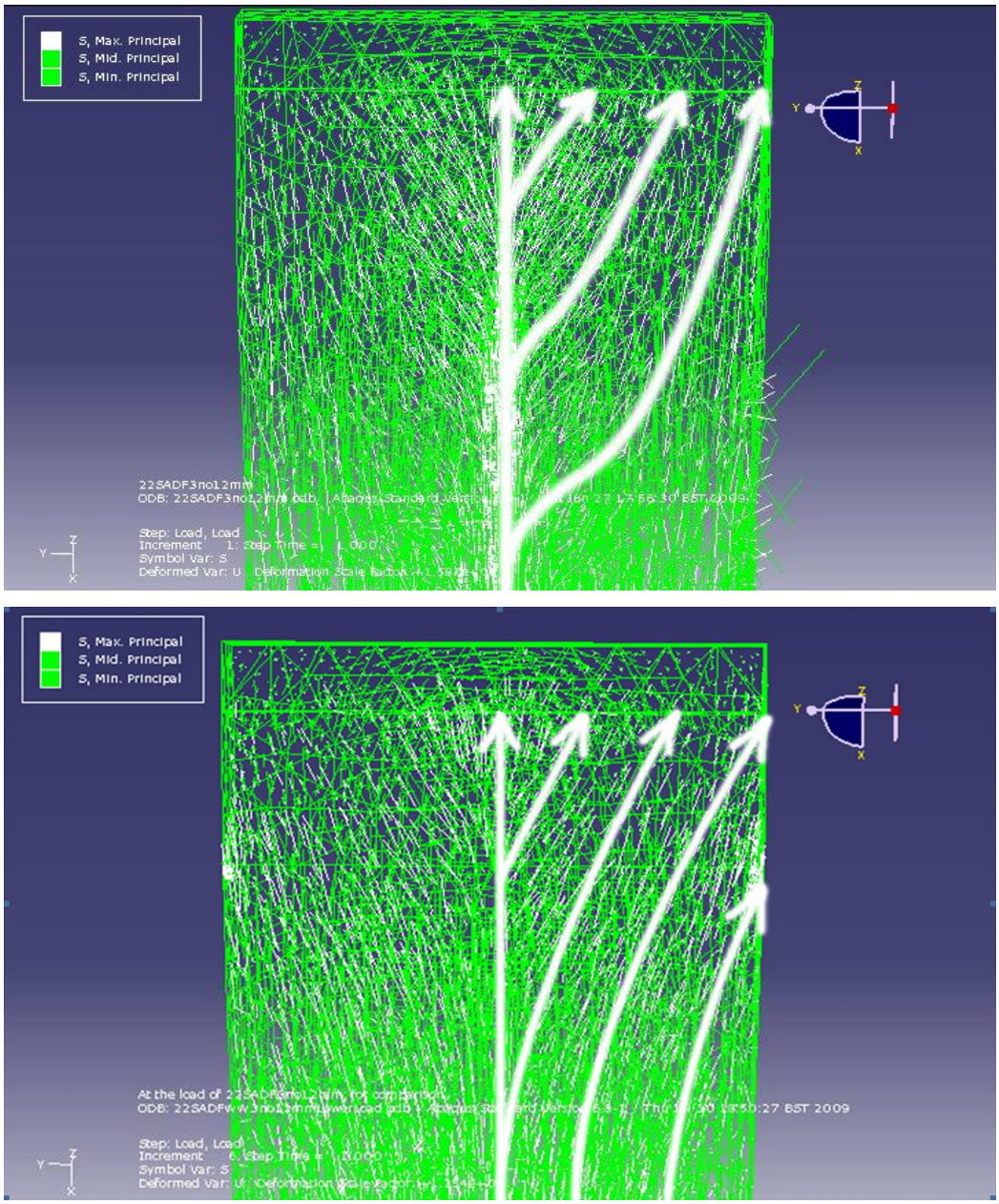

Figure 10-61: Global Direction of Maximum Principal Stress Tensor for 22SADF3no12mm (above) and 22SADFWW3no12mm (below)

B. Steel – 22SADFWW3no12mm

The following contour plot (Figure 10-60) and graph (Figure 10-61) show the von

Mises stress in the rebar at the collapse load of 52.8kN. The maximum stress is 342.58 N/mm^2, which is 96% of the yield stress of steel, 355 N/mm^2 (Figure 10-61). This shows the possible mid-span rebar yielding failure of the beam.

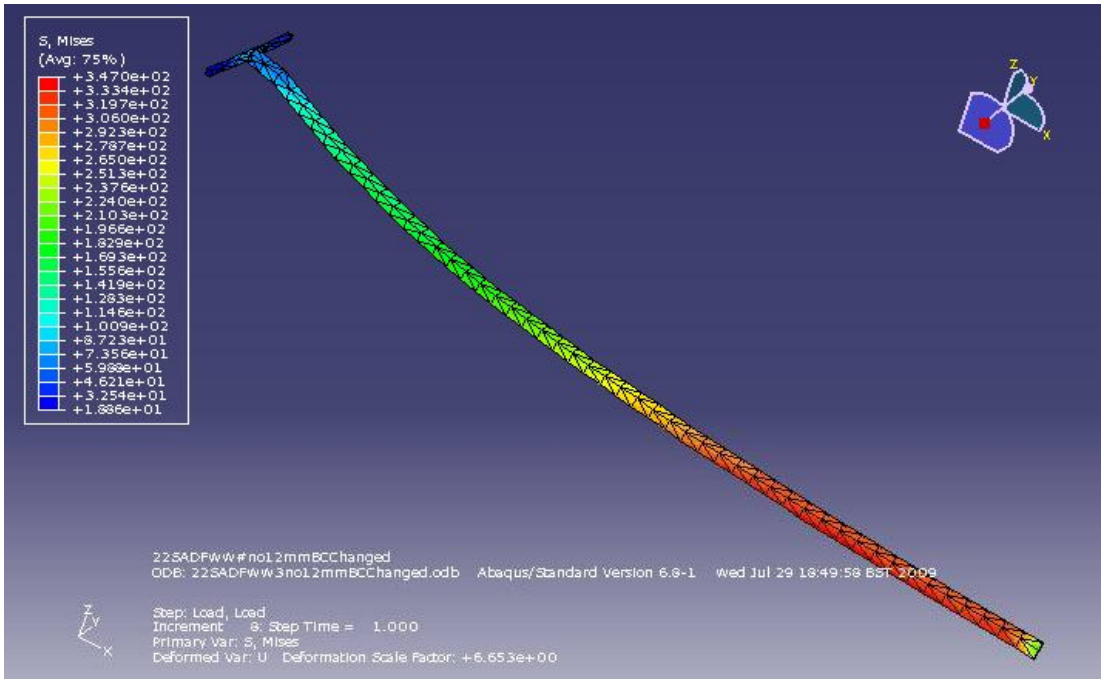

Figure 10-62: 22SADFWW3no12mm – Mises stress distribution in the rebar at collapse load

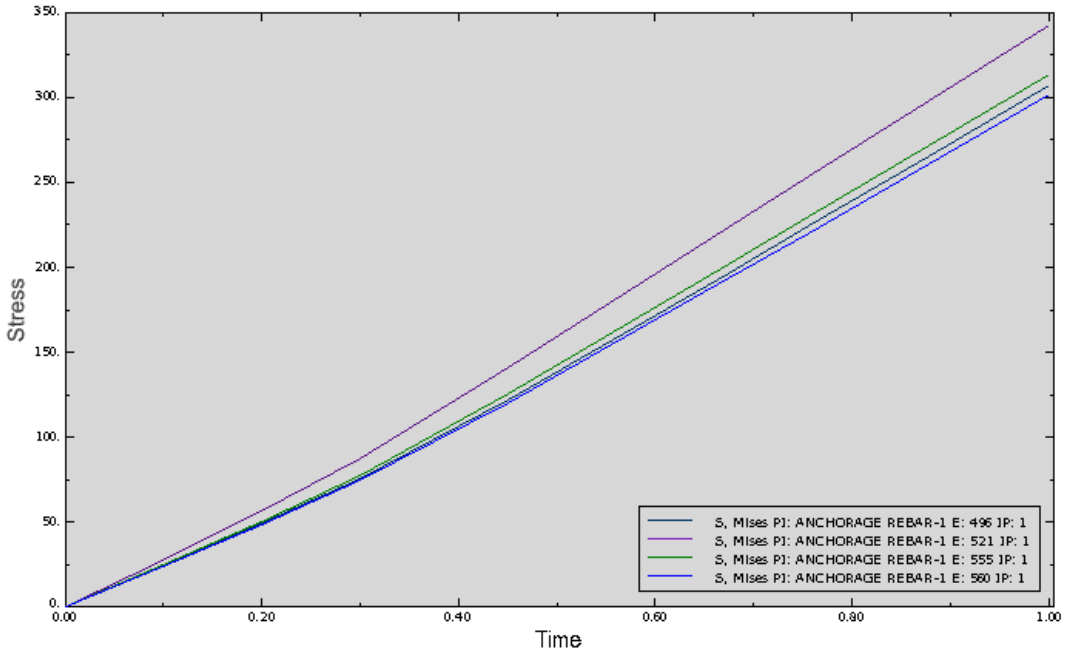

Figure 10-63: 22SADFWW3no12mm – Mises stress in the rebar at collapse load

10.3.2 Section 2: (11DADF12mm) VS (11DADFWW12mm)

10.3.2.1: 11DADF12mm

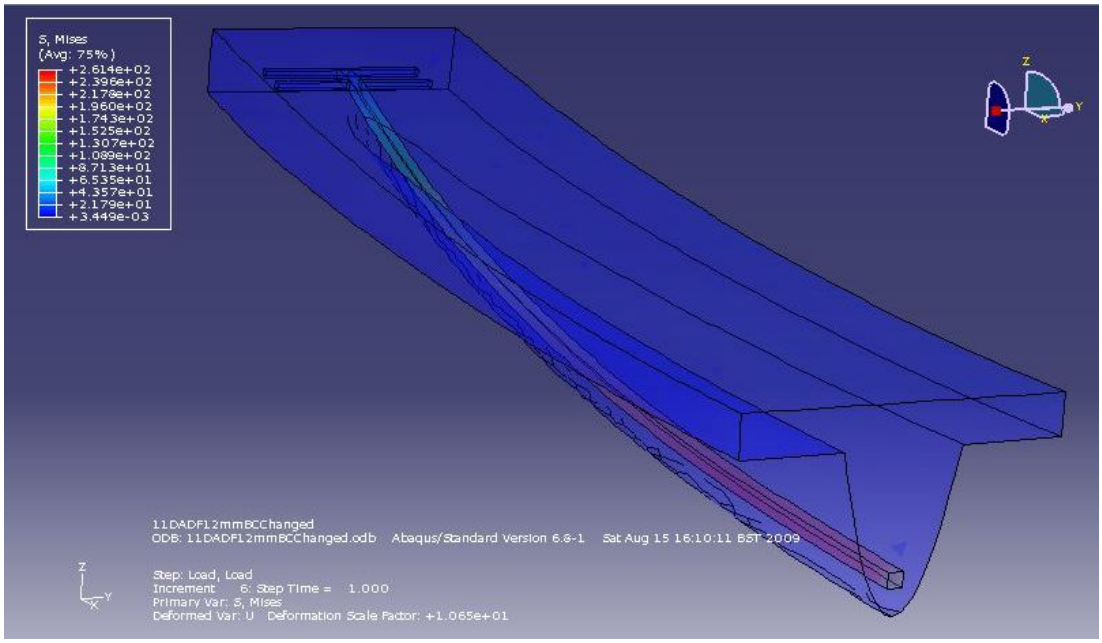

Figure 10-64: 11DADF12mm after deformation

A. Concrete -11DADF12mm

The following contour plot (Figure 10-63) show the maximum principal stress distribution of the beam. The plot show that highest tension stresses are distributed in the circled region.

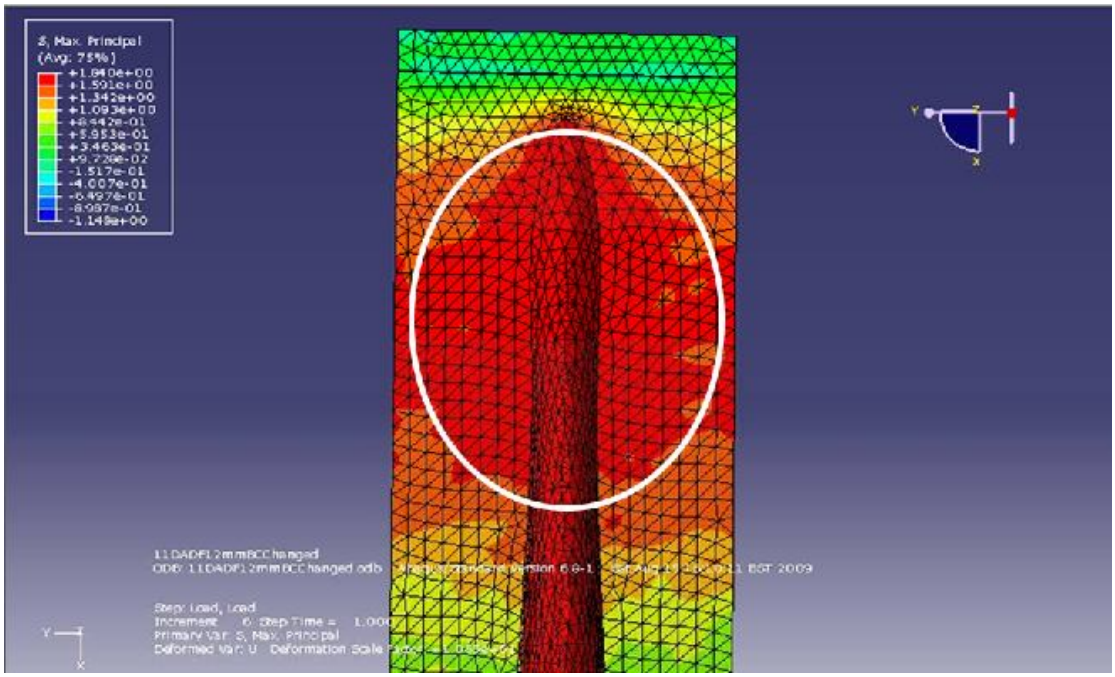

Figure 10-65: 11DADF12mm maximum principal stress distribution of web at 26kN

The following vertical section contour (Figure 10-64) are plotted to see the tension

stress distribution in the flange region. It can be seen that the tension stress exists up to the half depth of the flange. These stresses can cause diagonal tension crack and lead to shear failure of the beam.

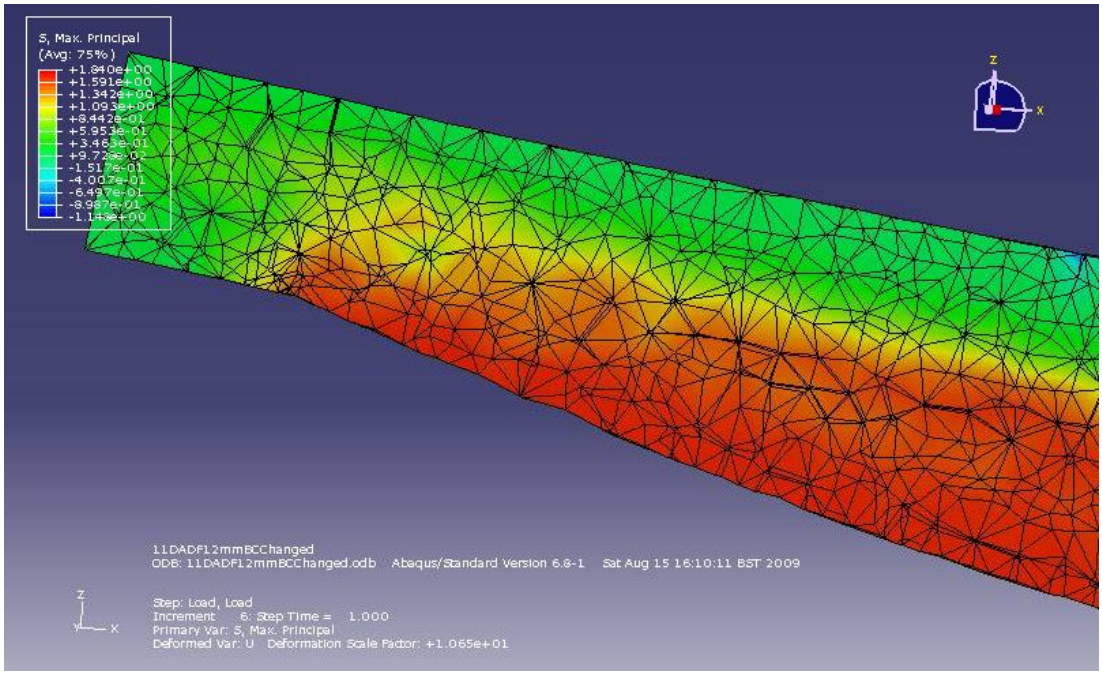

Figure 10-66: 11DADF12mm maximum principal stress distribution at the cross section

B. Steel -11DADF12mm

The following contour plot (Figure 10-65) shows the von Mises stress distribution of the steel in the beam at the failure load.

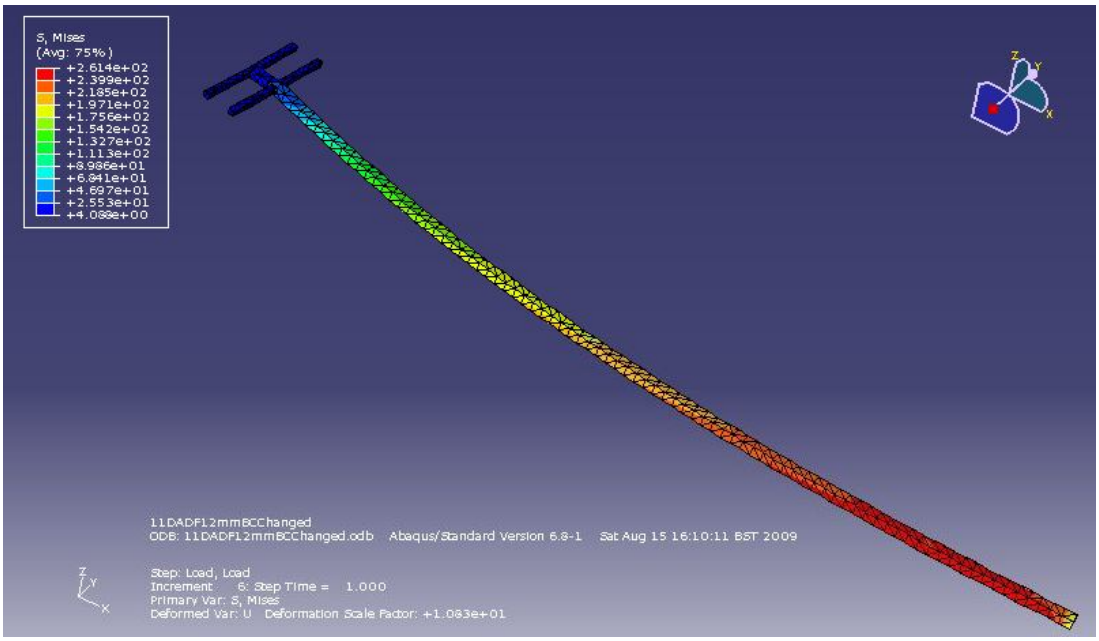

Figure 10-67: 11DADF12mm – Mises stress distribution in the rebar at collapse load

The highest stress of 261.4 N/mm^2 is located around the mid-span of the beam

(Figure 10-66). The yield strength of the steel is approximately 355 N/mm^2 and thus the steel has not yielded.

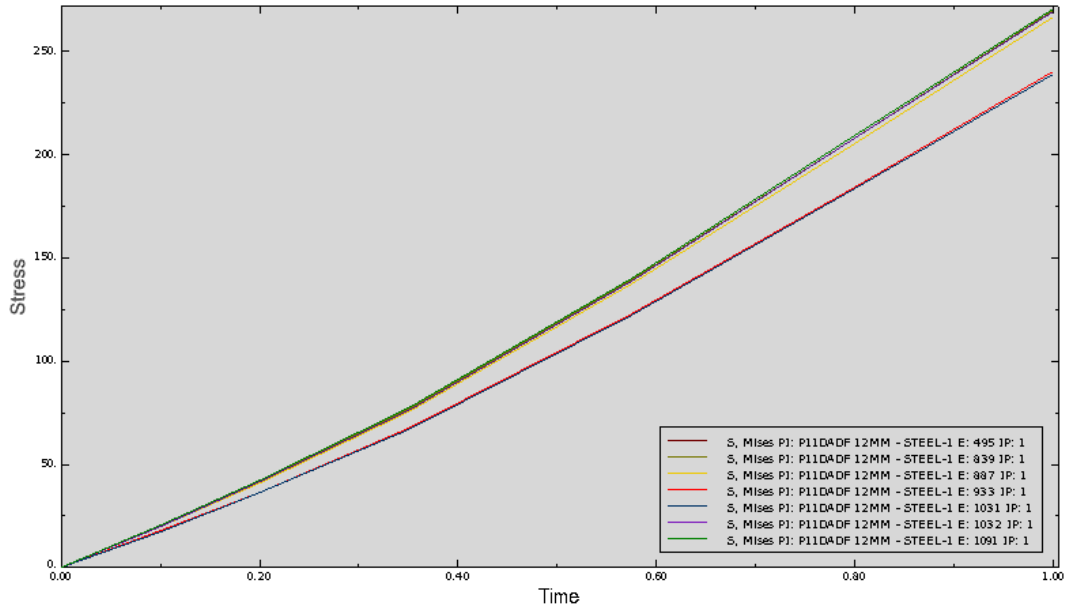

Figure 10-68: 11DADF12mm – Mises stress in the rebar at collapse load

10.3.2.2: 11DADFWW12mm

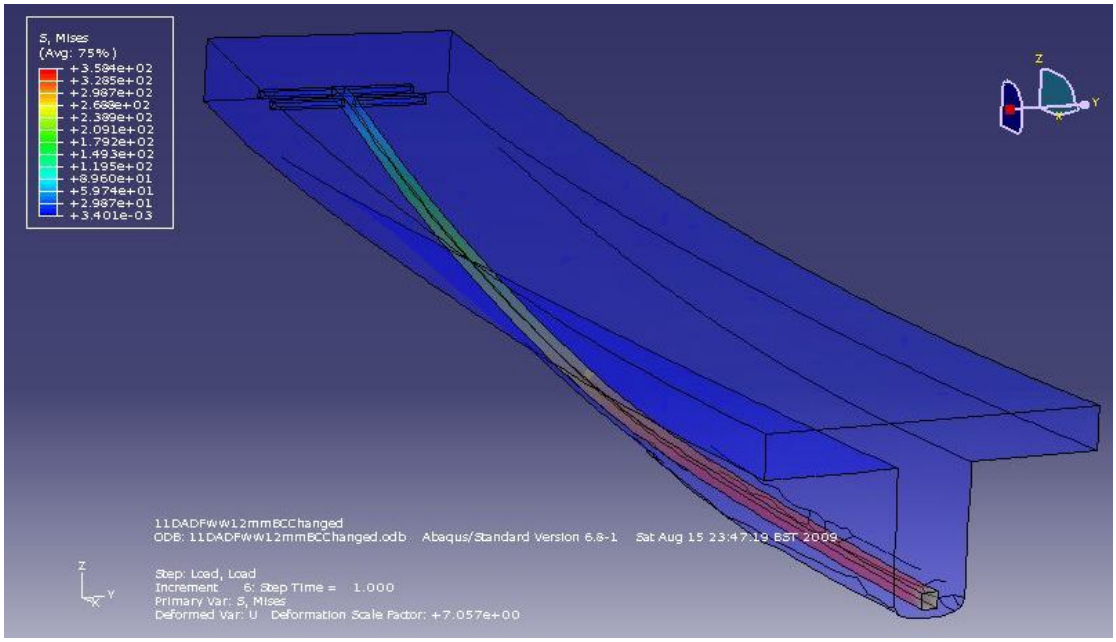

Figure 10-69: 11DADFWW12mm after deformation

A. Concrete -11DADFWW12mm

The following contour plot (Figure 10-68) shows the principle tensile stress distribution of the beam.

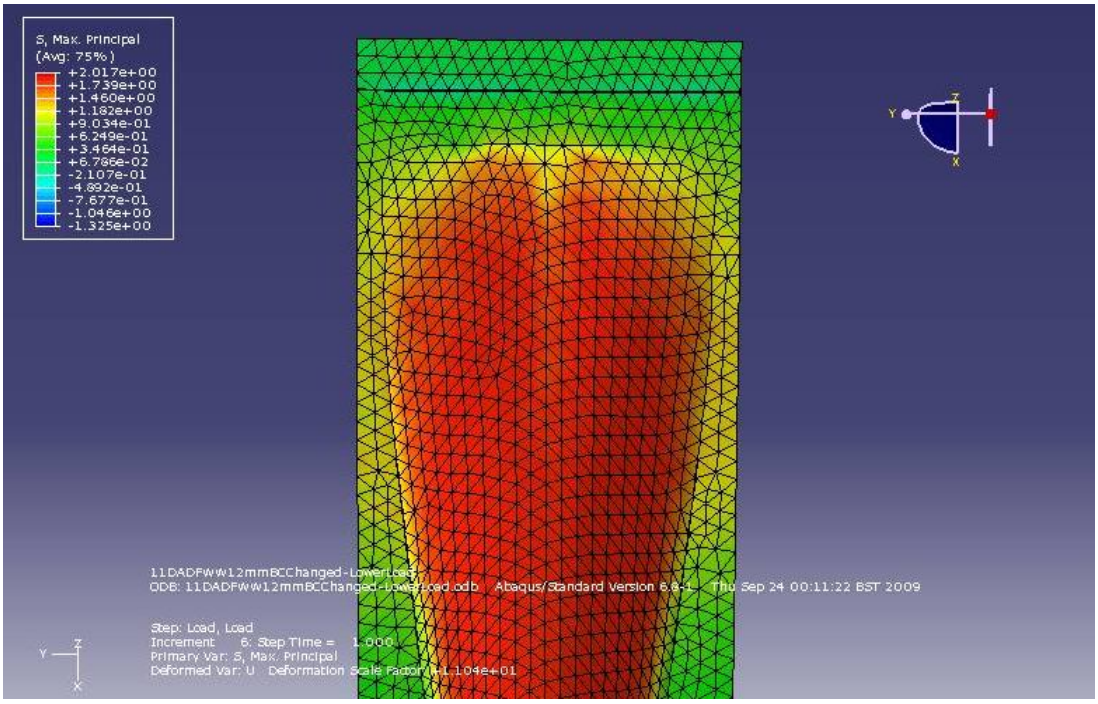

Figure 10-70: 1DADFWW12mm maximum principal tension stress distribution of web at 26kN

The above contour shows a uniform distribution of the tension stress over the web. Owing to this efficient distribution of the stress the area of the flange affected by the tension stress is a lot smaller than 11DADF12mm. This can be observed in the

contour plots shown below (Figure 10-69 and 10-70).

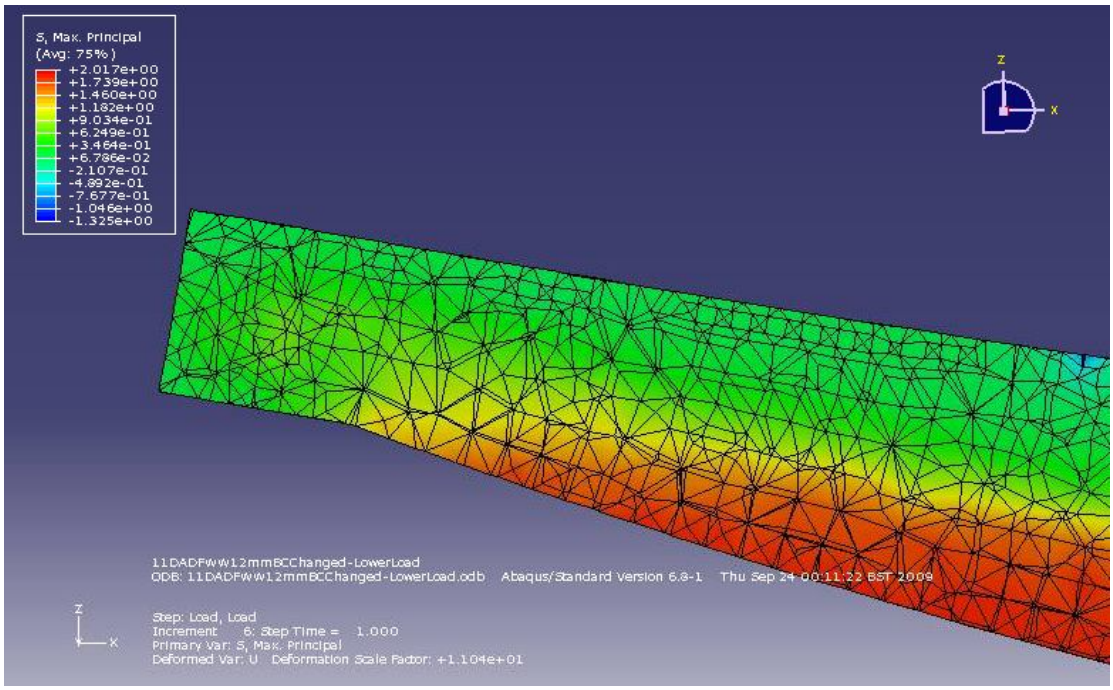

Figure 10-71: 1DADFWW12mm maximum principal tension stress distribution at the cross section

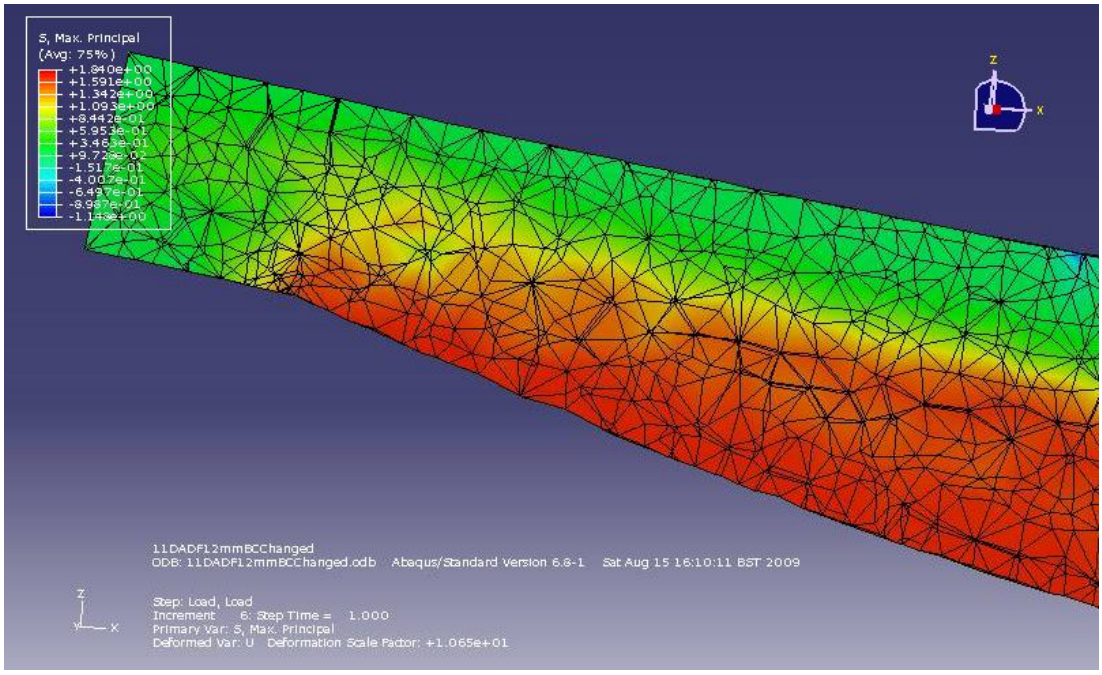

Figure 10-72: 11DADF12mm maximum principal tension stress distribution at the cross section

The above figures show that the maximum tension stress in 11DADF12mm is moving up into the flange higher than 11DADFWW12mm.

The following maximum principal tensor plots are prepared to compare the stress distribution in the beams further (Figure 10-71).

The plot of 11DADF12mm shows that there are great tensors concentrated along the bottom line of the flange and their orientations become more diagonal as they move

towards the top of the flange. However, the plot of 11DADFWW 12mm shows rather continuous distribution of the tensors between the flange and the web. Also the tensors do not reach into the flange as high as the tensors of 11DADF12mm, which means there is less change of causing diagonal tension crack in the flange.

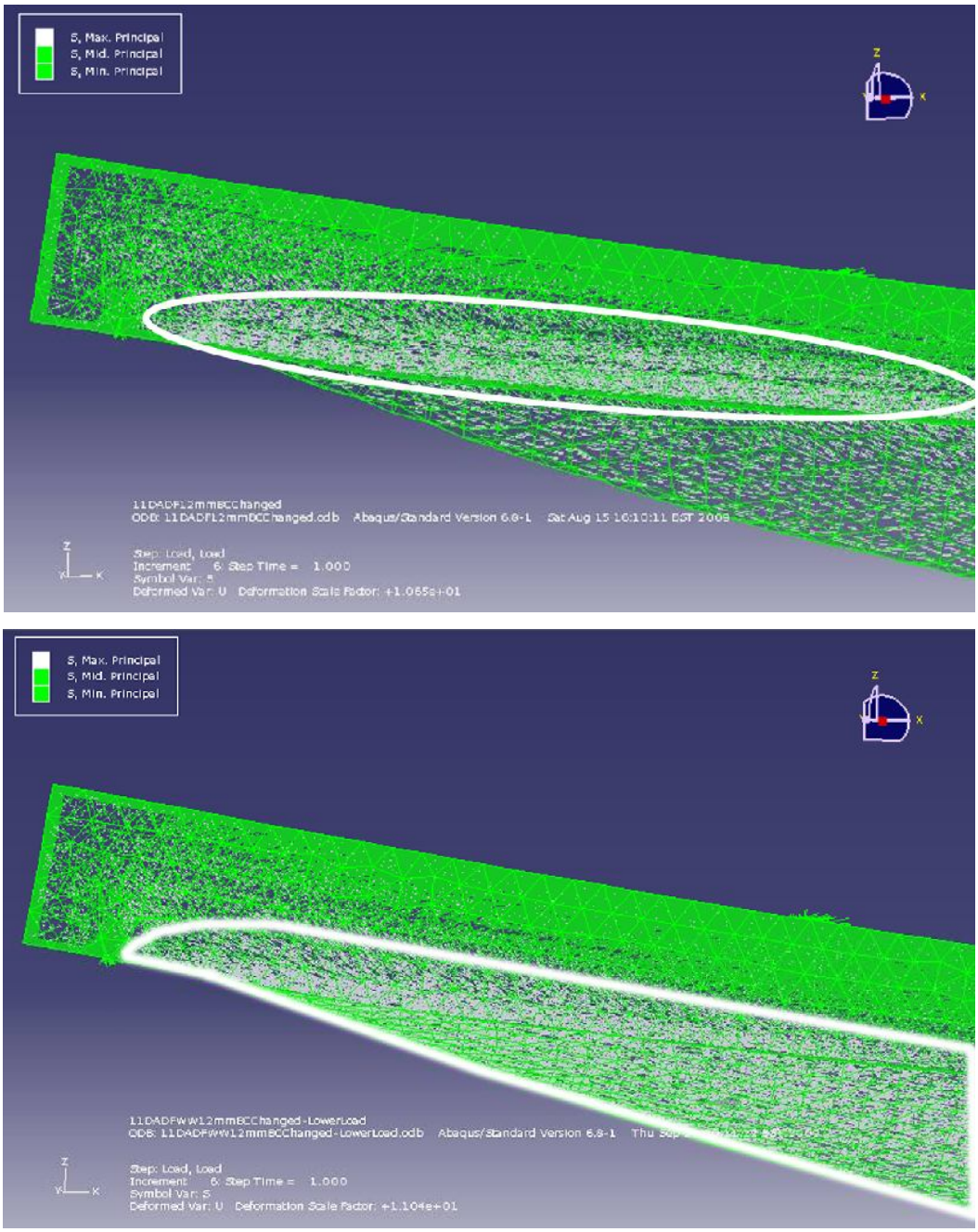

Figure 10-73: Maximum Principal Stress Tensor Plot for
11DADF12mm (Above) and 11DADFWW12mm (below)

B. Steel-11DADFWW12mm

The following von Mises stress contour plot (Figure 10-72) shows that the maximum stress of 377.1 N/mm^2 has been induced at the mid-span of the beam (Figure 10-73).

This shows that the beam is likely to be failed by bending tension failure of the beam.

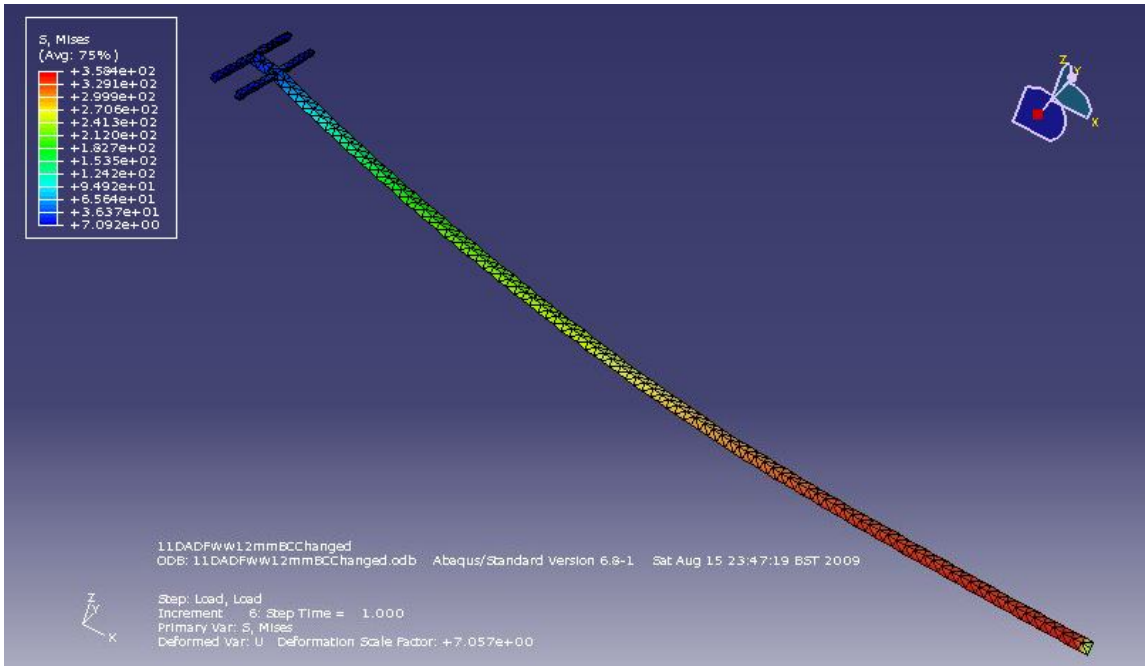

Figure 10-74: 11DADFWW12mm – Mises stress contour of steel at collapse load

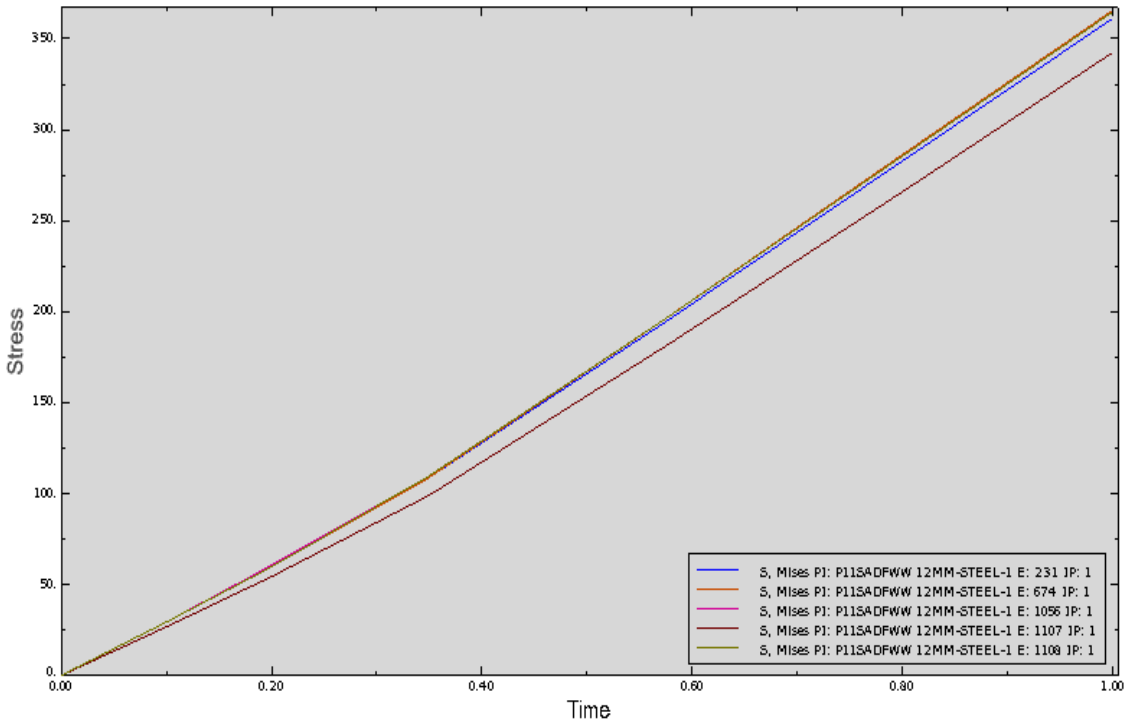

Figure 10-75: 11DADFWW12mm – Mises stress in the rebar at collapse load

10.3.3 Summary and Conclusions of Beam Models Analysis

Based on the FE models of the beams the following conclusions can be drawn:

- The pointed web gathers the principal tensile stresses over very small area, which results in higher stress level near the support than other locations of the beam.
- For the beam with pointed web, high concentration of tension stress is also observed along the bottom line of the flange, the intersection between the web and the flange. It was observed from the test that vertical bending crack as well as horizontal shear cracks developed at this location.
- The stress distribution in the wide web shows greater continuity and less disruption between the flange and the web, with lower stress concentration. Overall the beams with wider webs at the supports experience more gradual increase of stresses over the whole body.

Chapter 11: Embodied Energy Analysis

11.1 Introduction

The purpose of this chapter is to assess the construction efficiency of fabric formed beams by using the embodied energy analysis method. The total embodied energy required to construct the beam is calculated based on the 'Inventory of Carbon and Energy' (HAMMOND, G.), and the comparison is made with a virtual beam designed in accordance with the BS8110 method. It is important to see that the construction of such form-efficient beams is also economical and sustainable through the efficient construction method in comparison with conventional method of reinforced concrete beam.

For the purpose of this chapter 22SADFWW3no12mm is chosen for the analysis since the geometry and its fabric formwork system are at the latest development.

The virtual beam is designed in accordance with the BS 8110 based on the following design information:

- The virtual beam should be designed to satisfy the ultimate limit state criteria. The ultimate load of 22SADFWW3no12mm is 52.8kN. Thus this load is taken as the design load
- Design Moment = 18.65 kNm
- Design Shear = 26.4 kN
- The characteristic strength of reinforcing steel = 355 N/mm^2
- The experimental concrete cube strength = 41.3 N/mm^2
- Cover length = 20mm
- Span = 3020mm
- Bar size = 12mm
- Maximum Aggregate Size = 10mm
- Flange thickness = 40mm (as in 22SADFWW3no12mm)
- Flange width = 320mm (as in 22SADFWW3no12mm)
- Web width = 120mm (as in 22SADFWW3no12mm)
- Effective depth = 157mm (as in 22SADFWW3no12mm)

The embodied energy consumed for the construction of the form works is also calculated and compared between the two beams. For 22SADFWW3no12mm the fabric formwork is used for the calculation, and for the virtual T-beam a theoretical conventional timber formwork is constructed and the embodied energy is calculated.

In the embodied energy calculation the total volume of each material used is calculated. The volumes are then converted to the masses by multiplying the density of the materials. These values are then used to calculate the total embodied energy consumed.

11.2 T-Beam Design: BS 8110:1997

In summary the final design specification of the T-beam is as follow:

Flange width = 320mm

Flange depth = 40mm

Web width = 130m

Total depth = 200mm

Cover length = 20mm

Effective depth = 174mm

Tension reinforcement = 3 no. ø12mm

Shear link = ø 6mm @ 125mm centres; 25 links in total.

Based on the above design specification the amount of materials required is calculated as follow:

The total volume of concrete used = 104e6 mm^3.

The total volume of shear steel used = 0.31e6 mm^3.

Based on the Inventory of Carbon & Energy (HAMMOND, G., and Jones, C.) the total embodied energy consumed for the beam is calculated:

Embodied energy of coarse aggregate = 0.1 MJ/kg

Embodied energy of fine aggregate = 0.1 MJ/kg

Embodied energy of cement = 4.6 MJ/kg

Embodied energy of water = 0.0 MJ/kg

Embodied energy of steel = 24.60 MJ/kg

And the total energy consumed in the beam = 511.16MJ

Based on the design specification the following formwork has been designed.

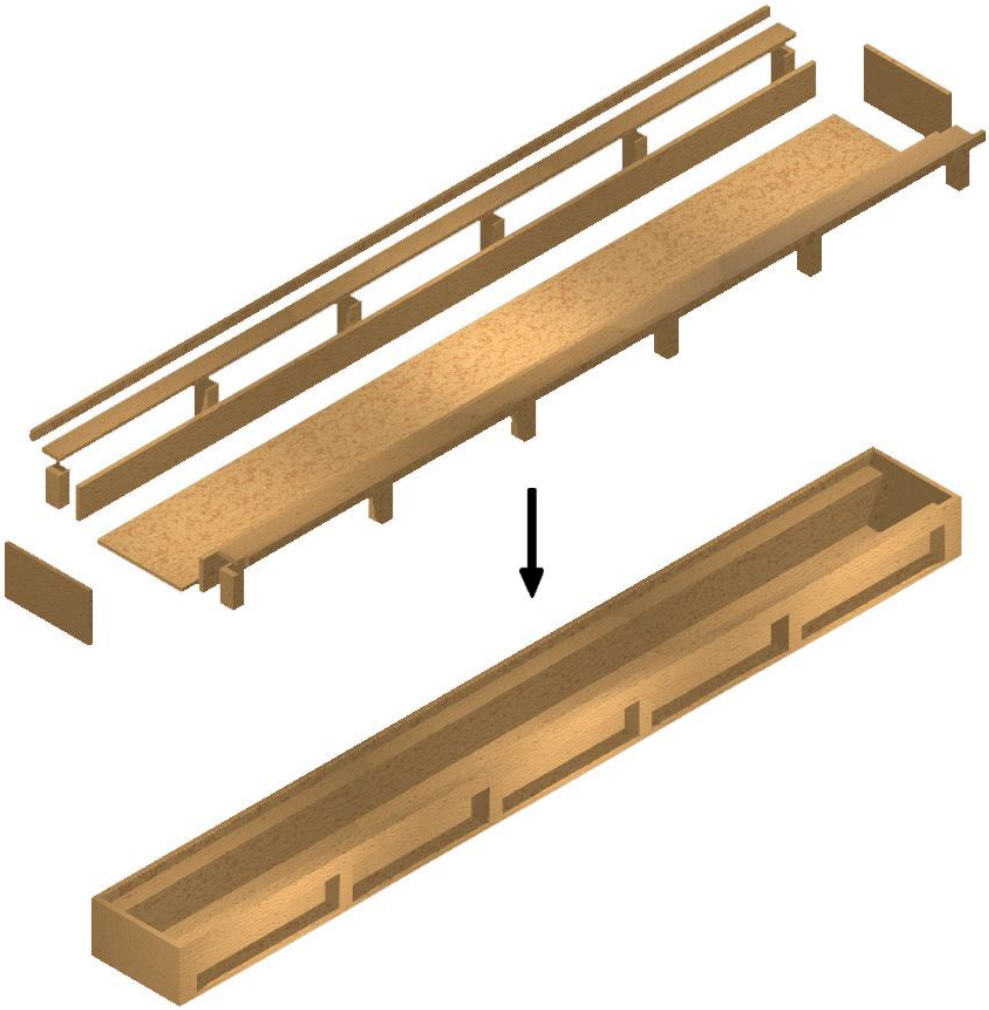

Figure 11-1: Formwork for the designed T-beam

The formwork consists of 19mm plywood sheet and softwood blocks in size of 50mm by 60mm by 127mm.

The total volume of plywood used = 32e6 mm^3

The total volume of softwood used = 5e6 mm^3

Embodied energy of plywood = 15.00 MJ/kg

Embodied energy of softwood = 7.40 MJ/kg

The total embodied energy consumed for the formwork construction of the T-beam = 352.2MJ.

11.3: 22SADFWW 3no12mm

The following is the design specification of the 22SADFWW 3no12mm:

Total length = 3100mm

Span = 3020mm

Flange width = 320mm

Flange depth = 40mm ~ 80mm

Web width = 70mm ~ 320mm

Total depth = 80mm ~ 185mm

Cover length = 20mm

Effective depth = 55mm ~ 156.93mm

Tension reinforcement = 3 no. ø12mm.

Shear link = none.

The total volume of concrete is obtained from the computer generated model of the beam: 91.89e6 mm^3.

The total volume of tension steel + anchorage used

= 3 * (6^2*π*(3070+200*2) = 1.18e6 mm^3.

Thus the total energy consumed in the beam is 403.67MJ

The following shows the embodied energy analysis of the fabric formwork.

The total volume of plywood used = 51.49e6 mm^3.

The following picture show the fabric used for the formwork. The actual fabric used for casting the beam was approximately 2.7e6 mm^2.

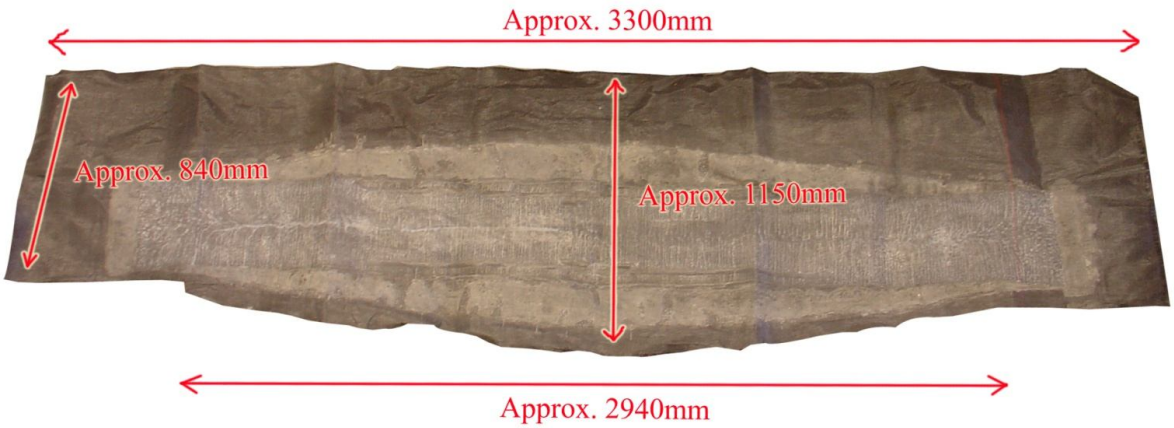

Figure 11-2: Size of the fabric used

Embodied energy of plywood = 15.00 MJ/kg

Embodied energy of polypropylene (used the value of 'orientated film' in the list of inventory) = 99.2 MJ/kg

Thus the total embodied energy consumed for the formwork construction of the fabric formwork is 572 MJ/kg

11.4 Summary and Conclusion

	Material	Fabric Formed Beam		RC T-Beam	
		Mass/	Embodied Energy/	Mass/	Embodied Energy/
Beam	Concrete	155.6	175.87	176	201.2
	Steel	9.26	227.8	12.6	309.96
Beam Total		164.86	403.67	188.6	511.16
Formwork	Plywood	36.04	540.6	22	330
	Softwood	0	0	3	22.2
	Fabric	0.32	38.69	0	0
Formwork Total		36.36	579.29	25	352.2
Construction Total		201.22	982.96	213.6	863.36

Table 11-1: Comparison of Beams

This chapter showed the break down of the beams and the formwork systems, and the materials used for the constructions of beams are interpreted in terms of the total embodied energy consumption.

The analysis shows that the total embodied energy consumer for the construction of the T- beam was 863MJ, and the total embodied energy of the construction of fabric formed beam was 983MJ. Based on these figures the construction of 22SADFWW3no12mm requires approximately 14% more embodied energy than of the T-beam. However, when only the embodied energy of the beam is considered the 22SADFWW3no12mm has 27% less embodied energy than the T-beam, which also has the potential to save further embodied energy during the transportation due to its lighter weight. Thus the result demonstrates the possible savings of the construction materials that is achieved with the fabric formwork technology and the efficient form for the beam.

Yet the analysis so far only deals with the embodied energy that is related to the construction of the beams. However, after the completion of the construction the building consumes energy throughout its life span. Such 'operational energy' takes a big part of the total embodied energy consumption throughout the building's life, and the energy is mainly used for the mechanical heating and cooling system, and also for the lighting as well (GRAHAM, P., 2003)

There are a number of cases where the thermal mass property of concrete flooring system is discussed for its possible use to reduce the cooling/heating energy consumption. Thermal mass can be referred to heat capacity of the material that is the ability to store heat in the body. For instance, during a hot summer day when the outdoor temperature is hot some of the indoor heat is absorbed and taken away by the thermal mass of concrete, and the heat is released back during the nighttime when the temperature is low. Thus the temperature fluctuation throughout the day is reduced and thus the use of additional mechanical cooling system is also reduced. The heat transfer between the concrete and the surrounding air is by a combination of radiation and natural convection (BARNARD, N., Concannon, P., Jaunzens, D., 2001), and the improved geometry and the increased surface area exposed are important factors for the effective heat transfer. The fabric formed beams have the soffit geometry with increased surface area in comparison with flat slab. Also it is considered that its unique form would enhance the natural convective flow of the air around the soffit in comparison with conventional T-beam.

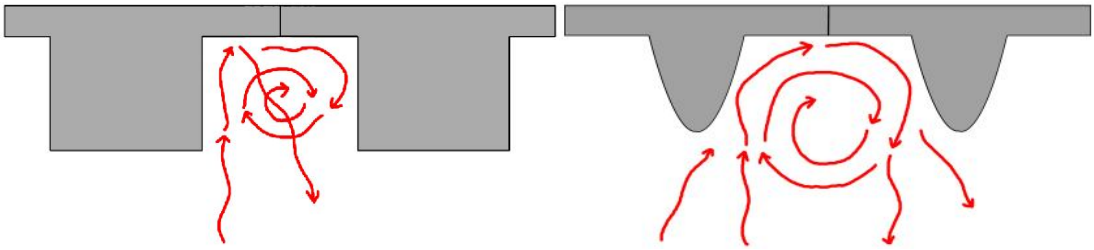

Figure 11-3: Comparing the air movement around the soffit of the beams

However such comparison requires detailed fluid dynamics analysis yet such work is beyond the scope of this research.

Chapter 12: Summary and Conclusions

This thesis presents the designs and the developments of fabric formed reinforced concrete beam into more optimized form. In total eleven different types of beams are designed, cast and tested and three different types of fabric formworks are developed and constructed. Through the structural analysis of the beams, the adaptation of the current reinforced concrete theories and the British code BS8110 are examined for the design of fabric formed. The structural analysis is carried out in the following criteria:

- Anchorage Stress
- Bending
- Shear
- Central Deflection

The finite element analysis is carried out using Abaqus CAE to gain comprehensive understanding of the structural behavior around the anchorage zone, and of the effect of the wider web against the shear stress.

The initial embodied energy of the latest fabric formed beam is estimated based on the Bath index, and it is compared with a T-beam designed in accordance with BS8110.

12.1 Conclusions

Based on the above studies the following conclusions could be drawn:

1. At sections where the diagonal tension crack is present, the compression strain at the top surface of the concrete is significantly high and much more responsive in comparison with the tension strain of the reinforcement. Thus the shear behaviour of the section is directly linked to the compression behaviour of the 'un-cracked' concrete.
2. Increasing the compression capacity of the concrete above the neutral axis can increase the shear capacity of the section
3. The experiment results show that the increasing the percentage of steel does not increase the shear resistance of the fabric formed beam.
4. The two main contributors to the shear capacity of fabric formed beam are 1) the effective depth of the section, and 2) the overall efficiency of the beam's form. (The experiment results show that by changing the shape of

the web the beam could avoid shear failure and the ultimate load is increased by 20.50kN)

5. The central deflections of the fabric formed beams are about 20% more than the predicted values using the Moment-Area theorem. However the discrepancies are a lot greater for the beams failed by shear (or experiencing a shear crack). This is because the Moment-Area theorem does not include the deflections owning to the shear cracks.
6. The shear capacities of the beams are underestimated in general cases using the modified expression by Kotsovos and Lefas, but in the cases where the beams failed by shear the expression rather accurately predicted the capacities.
7. The BS 8110:1997 method is also examined to predict the shear capacity of the sections. Based on the results it is concluded that the code does not accurately predict the shear requirement of fabric formed beams, though in general it can be accepted that when the code suggests the beam to have the minimum amount of shear links the shear capacity of the fabric formed beam section seems sufficient to resist the design shear stress; and when the code indicates that the design shear links are required, then the section's effective depth should be increased, or actually add the shear links.
8. The finite element analysis shows that the anchorage compression stress onto concrete does not spread over the full length of the anchorage as it was considered for the Strut-and-Tie model, but the stress is highly concentrated over the limited area near the connection point of the rebar and the anchorage.
9. The finite element analysis also shows the other possibility for the cause of Lee's (2005) beams failure. It shows that the failure might not be the compression failure of concrete, but due to the transverse tension stress induced by the anchorage compression stress.
10. In either way the concrete failure around the anchorage zone could be prevented by reducing the anchorage compression stress. The stress can be reduced either by adding more anchorage, or by increasing the rebar angle.
11. The principal tension stress tensor plots on the models show that, having the pointy web end can cause high concentration of stress and high

tension stress is formed along the bottom surface of flange. This causes diagonal tension crack in the flange which leads to shear failure of the beam. The wider web end can effectively reduce the stress and prevent any early formation of tension stress in the flange.

12. When the embodied energy of the fabric formed beam is compared with a T-beam designed in accordance with BS 8110:1997, about 40% less energy are consumed in the fabric formed beam.
13. When the formwork construction is included in the embodied energy calculation the fabric formed beam construction requires about 20% less energy than the T-beam construction. However, the figure can be dropped further by changing the type of fabric with less embodied energy; the fabric used in the calculation is geotextile fabric, which has exceptionally high embodied energy.

12.2 Future Research Proposals

In this research the roles of the constituent structural parts of fabric formed beams have been studied, and their specifications have been changed throughout the process to optimize the overall performance of the beam. The flange of the early beams was in simple slab form, and later it is curved into parabolic shape to resist against the shear more efficiently. The vertical profile was changed as the starting angle of the web is changed to 22°; otherwise the additional anchorage was added to reduce the anchorage compression stress. The latest beams' web profile is horizontally inverted from the earlier beams and have wider ends rather than pointy ends.

At the end of this development the author suggests possible further research in the following aspects:

1. The current reinforcement design has the horizontal bend at the ends. This is because initially the depth of flange was very shallow and if the reinforcement did not bend it would stick out of the flange. However with deeper flange depth such bend is not required and the reinforcement can have complete parabolic curve from the start to the end. This would make the construction process more convenient, and also the structural behaviour around the anchorage would be easier to understand.
2. Different fabric could be use for the formwork. The embodied energy consumption can be further reduced by changing the fabric to which consumes less embodied energy. Low energy consumption is one of the

merits in using fabric formwork and thus other materials should be explored to increase the effect.

3. It would be very interesting to investigate the effect of which fabric formed concrete has in reducing the energy consumption of mechanical service system in a building. It is considered that the unique shape of the beams can help to achieve better fluid movement in a room, which will improve the overall thermal mass effect of the beam. The investigation would involve rather complex fluid dynamics analysis, and according to the results the shape of the beams could modified.
4. Though the most of the beams satisfied the service limit state limit suggested by BS 8110, central deflection behaviour of the fabric formed beams requires further study. The prediction offset can be as large as 63% (4.4mm) and this level of accuracy should be improved. Also more simple method is required for the practical design process than the Moment-Area method.

List of Figures

Chapter 1: Introduction

Chapter 2: Literature Review

Chapter 6: Design and Development of the Fabric Formed Beams

Chapter 7: Formwork Design and Construction

Chapter 8: Reinforced Concrete Beam Design Theory and Analysis Methods

Chapter 11: Embodied Energy Analysis

Chapter 12: Summary and Conclusion

No Figures

List of Tables

Chapter 9: Structural Analysis and Design Methods of the Beams

Chapter 10: Finite Element Model (FEM) Analysis

Chapter 11: Embodied Energy Analysis

Chapter 12: Summary and Conclusion

No Table

References

1. ABU-HUSSEIN, M. M. and Al-Zaid, A. H. A. J. 1991. Deformational behaviour of reinforced concrete beams under service loading conditions. *Eng. Sic.*, pp.167-183.
2. ADDIS, B. 2007. *3000 Years of Design Engineering and Construction*. Phaidon Press Limited.
3. AL AWWADI GHAIB, M., Gorski, J. 2001. Mechanical properties of concrete cast in fabric formworks. *Cement and Concrete Research.*, pp.1459-1465.
4. AL-ZAID, R. Z., Abu-Hussein, M. M., and Al-Shaikh, A. H. 1991. Deformational behaviour of reinforced concrete beams under service loading conditions. *Eng. Sci.* **3**(2), pp.167-183.
5. *Arquitectura de casas: Casa en La Moraleja - Madrid*. [online]. [Accessed November 2010]. Available from World Wide Web: http://arquitecturadecasas.blogspot.com/2008/09/casa-en-la-moraleja-madrid.html
6. ARSLAN, G. 2008. Cracking shear strength of RC slender beams without stirrups. *Journal of Civil Engineering and Management*. **14**(3), pp.177-182.
7. ASHOUR, A. F. 2000. Shear capacity of reinforced concrete deep beams. *Journal of Structural Engineering*.
8. BAILISS, J. *Fabric-Formed Concrere Beams Design and Analysis, Masters Dissertation*. the University of Bath.
9. BARNARD, N. 1999. Making the most of thermal mass. *The Architect's Journal.*, pp.47-50.
10. BARNARD, N., Concannon, P., Jaunzens, D. 2001. *Modelling the performance of thermal mass*. BRE.
11. BAZANT, Z. P. and Yu, Q. 2005. Designing against size effect on shear strength of reinforced concrete beams without stirrup: I formulation. *Journal of Structural Engineering*.
12. *Betonu Biçimlendirmek*. [online]. [Accessed November 2010]. Available from World Wide Web: http://betonart2009.blogspot.com/2009/05/srads-ornekler-1.html
13. BEUKERS, A. and van Hinte, E. 2005. *Lightness*. 010 Publisher.
14. BHATT, P., Kader, M. A. 1998. Prediction of shear strength of reinforced concrete beams by nonlinear finite element analysis. *Computers and Structures.*, pp.139-155.
15. BOBROWSKI, J. and Bardhan-Roy, B. K. 1969. A method of calculating the ultimate strength of reinforced and prestressed concrete beams in combined flexure and shear. *The Structural Engineer*. **47**(5), pp.197-209.
16. BOBROWSKI, J. 1982. Origins of safety in concrete structures, PhD Thesis.
17. BURDET, O. L. 1990. *Analysis and design of anchorage zones in post-tensioned concrete bridges*.
18. CHANDLER, A., Pedreschi, R. (editied by). 2007. *Fabric Formwork*. London: RIBA Publishing.

19. CHANDLER, A. *Fabric Formwork: Case Study for the Knowledge Transfer Partnership, University of East London*.

20. CHILTON, J. 2000. *The Engineer's Contribution to Contemporary Architecture - Heinz Isler*. Thomas Telford Publishing, Thomas Telford Ltd.

21. CHO, J., Cho, N., Kim, N., and Choun, Y. 2000. Stress-strain relationship of concrete subjected to biaxial tension. *In*: *Transactions of the 17th International Conference on Structural Mechanics in Reactor Technology (SMiRT 17)*. Prague, pp.H03-02.

22. CHOI, C. K. and Cheung, S. H. 1996. Tension Stiffening mdoel for planar reinforced concrete member. *Computers & Structures*. **59**(1), pp.179-190.

23. CICEKLI, U., and Voyiadjis, G. Z., and Al-Rub, R. K. A. 2007. A plasticity adn anisotropic damage model for plain concrete. *International Journal of Plasticity*. **23**(27), pp.1874-1900.

24. COBB, Fiona. 2004. *Structural Engineer's Pocket Book*. Oxford: Elsevier Butterworth-Heinemann.

25. COLLINS, M. P., Mitchell, D., Adebar, P., and Vecchio, F. J. 1996. A general shear design method. *ACI Structural Journal*.

26. *Construction Techniques Fabriform Fabric Formed Concrete System*. [online]. [Accessed November 2010]. Available from World Wide Web: http://www.fabriform1.com/index.html

27. *Don & Low Woven and Nonwoven polypropylene industrial textiles*. [online]. [Accessed Novemebr 2010]. Available from World Wide Web: http://www.lotrak.com/

28. ELLIOTT, K. S. 2002. *Precast Concrete Structures*. Butterworth-Heinemann.

29. ELWELL, D. J., and Fu, G. 1995. *Compression Testing of Concrete: Cylinders vs Cubes*. Transportation Research and Development Bureau, New York State Department of Transportation.

30. *Environmental Design CIBSE Guide A*. 1999. London.

31. FABER, Colin. 1963. *The Shell Builder*. New York: Reinhold Publishing Corporation.

32. *Fab-Form Fabric-Formed Concrete*. [online]. [Accessed November 2010]. Available from World Wide Web: http://www.fab-form.com/

33. *Fabric Formed Concrete at Department of Architecture, the University of Edinburgh*. [online]. [Accessed November 2010]. Available from World Wide Web: http://www.fabricformedconcrete.ed.ac.uk/index.php

34. FEDERATION INTERNATIONALE DU BETON. *Structure Concrete*.

35. GHALI, A. and Favre, G. 1994. *Concrete Structures: stresses and deformations*. E&FN Spon.

36. GILBER, R. I., and Nickleborough, N. C. 2002. *Design of Prestressed Concrete*. Spon Press.

37. GRAHAM, P. 2003. *Building Ecology: First Principles for A Sustainable Built Environment*. Blackwell Science Ltd.

38. HAMMOND, G., and Jones, C. *Inventory of Carbon & Energy (ICE)*. Bath.

39. *Harry Seidler and Associates*. [online]. [Accessed November 2010]. Available from World Wide Web: http://www.seidler.net.au/

40. HIBBELER, R. C. 2008. *Structural Analysis*. Prentice Hall.

41. HIRSCH, T. J. 1962. Moudulus of elasticity of concrete as affected by elastic moduli of cement paste matrix and aggregate. *Proc. Amer. Conc. Inst.* **59**.

42. HOLZER, C. E., Garlock, M. E. M., and Prevost, J. H. 2008. Structural Optimization of Felix Candela's Chapel Lomas De Cuernavaca. *In*: *Fifth International Conference on Thin-Walled Structure*. Brisbane, Australia.

43. HSU, T. T. C. 1993. *Unified theory of rienforced concrete*. CRC Press, Inc.

44. IBELL, T., Darby, A., Denton, S. 2009. Fabric formwork for innovative concrete. *In*: *9th International Symposium on Fiber Reinforced Polymer Reinforcement for Concrete Structure*. Sydney, Australia.

45. ILLSTON, J. M. and Domone, P. L. J. (edited by). 2001. *Construction Materials: their nature and behaviour*. Spon Press.

46. ISONO, Yoshito. *Nicolas Janberg's Structurae [en]: Images: ID 87099*. [online]. [Accessed November 2010]. Available from World Wide Web: http://en.structurae.de/photos/index.cfm?JS=84993

47. KARA, I. F. and Dunbar, C. 2009. Effect of loading types and reinforcement ratio on an effective moment of inertia and deflection of a reinforced concrete beam. *Advances in Engineering Software*. **40**, pp.836-846.

48. KIM, D-Y, Kwak, H-G. 2001. Nonlinear analysis of RC shear walls considering tension-stiffening effect. *Computers and Structures*. **79**, pp.499-517.

49. KIM, J-K, Han, S. H., Song, Y. C. 2002. Effect of temperature and aging on the mechanical properties of concrete Part I. Experimental Results. *Cement and Concrete Research*. **32**, pp.1087-1094.

50. KONG, F. K. and Evans, R. H. 2001. *Reinforced and Prestressed Concrete*. Spon Press.

51. KOTSOVOS, M. D. 1979. Fracture processes of concrete under generalised stress states. *Materials and Structures (RILEM)*. **12**(72), pp.431-437.

52. KOTSOVOS, M. D., and Newman, J. B. 1981. Fracture mechanics and concrete behaviour. *Magazine of Concrete Research*. **33**(1), pp.103-112.

53. KOTSOVOS, M. D. 1982. A fundamental explanation of the behaviour of RC beams in flexure based on the properties of concrete under multiaxial stress. *Materials and Structures (RILEM)*. **15**(90), pp.529-537.

54. KOTSOVOS, M. D. 1983. Mechanisms of 'shear' failure. *Magazine of Concrete Research*. **35**(123), pp.99-106.

55. KOTSOVOS, M. D., Babrowski, J., Prof. Eibl, J. 1987. Behaviour of reinforced concrete T-beams in shear. *The Structural Engineer*. **65B**(1).

56. KOTSOVOS, M. D. and Lefas, I. D. 1990. Behaviour of reinforced concrete beams designed in compliance with the concept of the compressive force path. *ACI Structural Journal*. **87**(2), pp.127-139.

57. KOTSOVOS, M. D. and Pavlovic, M. N. 1999. *Ultimate limit-state design of concrete structures: A new approach*. London: Thomas Telford Ltd.

58. KOTSOVOS, G. M. and Kotosovos, M. D. 2008. Criteria for structural failure of

rc beams without transverse reinforcement. *The Structural Engineer*.

59. LAMBERTON, B., PRESIDENT, CONSTRUCTION TECHNIQUES INC. 1980. *Fabric forms for erosion control and pile jacketing*. The Aberdeen Group.
60. LEE, S. H. D. 2005. *The Structural Behaviour and Construction of Form-Active Structures using Fabric Cast Concrete*. Edinburgh: The University of Edinburgh.
61. LI, B. and Tran, C. T. N. 2008. Reinforced concrete beam analysis supplementing concrete contribution in truss models. *Engineering Structures*. **30**, pp.3285-3294.
62. LIEW, S. S., and Choo, E. L. 2004. Bending moment interpretation of structural element with measured deflection profile. *In*: *Malaysian Geotechnical Conference*. Sheraton Subang, Petaling Jaya, Malaysia.
63. MACGREGOR, J. G. 1997. *Reinforced concrete, mechanics and design*. Upper Saddle River, NJ: Prentice Hall.
64. MALONE, P. G. 1999. *Use of Permeable Formwork in Placing and Curing Concrete*. US Army Corps of Engineers.
65. MCLACHLAN, F., Pedreschi, R., Lee, S-H, Dhir et al. 2008. *Fabric Cast Concrete in Designing Concrete for the Visual Environment*. BRE Press.
66. MEYER, C. and Sheer, M. H. 2005. Do Concrete Shells Deserve Another Look? *Concrete International*., pp.43-50.
67. NATHER, A. 2005. Bone grafts and bone sustitutes: basic science and clinical applications. *World Scientific*.
68. NERVI, P. L. 1956. *Structures*. F. W. Dodge Corp.
69. NEVILLE, A. M., Brooks, J. J. 1987. *Concrete Technology*. Prentice Hall Publisher.
70. NEWHOOK, J., Ghali, A., Tadros, G. 2002. Concrete flexure members reinforced with fiber reinforced polymer: design for cracking and deformability. *Canadian Journal of Civil Engineering*. **29**, pp.125-134.
71. NIE, J., Xiao, Y. and Chen, L. 2004. Experimental studies on shear strength of steel-concret composite beams. *Journal of Structural Engineering*.
72. NORDENSON, G. (edited by). 2008. *Seven Structural Engineers The Felix Candela Lectures*. New York: The Museum of Modern Art (MoMA).
73. OZTEKIN, E. and Paul, S. and Husem, M. Determination of rectangular stress block parameters for high performance conrete. *Engineering Structures*. **25**, pp.371-376.
74. *P_Wall (2009)*. [online]. [Accessed November 2010]. Available from World Wide Web: http://matsysdesign.com/category/projects/p_wall2009/
75. *PERI Ltd. UK, Formwork, Scaffolding, Engineering*. [online]. [Accessed November 2010]. Available from World Wide Web: http://www.peri.ltd.uk/
76. PILLAI, S. U. and Menon, D. 2007. *Reinforced Concrete Design*. Tata McGraw-Hill Publishing Company Limited.
77. PRINCETON UNIVERSITY ART MUSEUM. *Manatiales Gallery*. [online]. [Accessed November 2010]. Available from World Wide Web: http://mcis2.princeton.edu/candela/ManantialesImages.html

78. PUNMIA, B. C. and Jain, A. K. 2007. *Limit State Design of Reinforced Concrete*. New Dehli: Laxmi Publications (P) Ltd.

79. REBEIZ, K. S. 1999. Shear strength prediction for concrete members. *Journal of Structural Engineering*., pp.301-308.

80. REBEIZ, K. S., Fente, J., and Frabizzio, M. A. 2001. Effect of variables on shear strength of concrete beams. *Journal of Materials in Civil Engineering*.

81. *Research Papers in Fabric Forming*. 2008. [online]. [Accessed November 2010]. Available from World Wide Web: http://www.fabricforming.org/research_papers.html

82. REYNOLDS, C. E., Steedman, J. C., and Threlefall, A. J. 2008. *Reynold's reinforced concrete designer's handbook*. Taylor & Francis.

83. ROTH, L. M. 1998. *Understanding Architecture Its Elements, History, and Meaning*. Harper Collins Publishers Inc.

84. ROWE, R. E. 1998. *The CEB (Comite Euro-International du Beton) - Its Nature and Work*.

85. RUSSO, G., Somma, G., and Mitri, D. 2005. Shear strength analysis and prediction for reinforced concrete beams without stirrups. *Journal of Structural Engineering*.

86. SATO, Y. and Tadokoro, T. and Ueda, T. 2004. Diagonal tensile failure mechanism of reinforced concrete beams. *Journal of Advanced Concrete Technology*. **2**(3), pp.327-341.

87. SCHLAICH, J. and Schafer, K. 1991. Design and detailing of structural concrete using strut-and-tie-models. *The Structural Engineer*. **69**(6).

88. SCHODECK, D. L. 2004. *Structures*. Pearson Prentice Hall.

89. SHACKLOCK, B. W. 1974. *Concrete constituents and mix proportions*. London: Cement and Concrete Association.

90. SHAVIV, E., Yezioro, A., Capeluto, I. G. 2001. Thermal mass and night ventilation as passive cooling design strategy. *Renewable Energy*. **24**, pp.445-452.

91. SIMULIA, DASSAULT SYSTÈMES. *Abaqus Theory Manual: 4.5.3 A cracking model for concrete and other brittle materials, Tension softening models*.

92. SIMULIA, DASSAULT SYSTÈMES. *Abaqus/ CAE Manual: 19.6.3 Concrete damaged plasticity*.

93. SRIKANTH, M., Kunmar, G. R. and Giri, S. 2007. Moment curvature of reinforced concrete beams using various confinement models and experimental validation. *Asian Journal of Civil Engineering (Building and Housing)*. **8**(3), pp.247-265.

94. STANDARD, The British. *BS 8110-2: 1985 Structural Use of Concrete - Part 1: Code of practive for design and construction*.

95. STRANMANDINOLI, R. S. B. and Rovere, H. L. L. 2008. An efficient tension-stiffening model for nonlinear analysis of reinforced concrete members. *Engineering Structures*. **30**, pp.2069-2080.

96. SULLIVAN, Mary Ann. *pantheoncrossection.jpg*. [online]. [Accessed November 2010]. Available from World Wide Web:

http://www.bluffton.edu/~sullivanm/romanpantheon/pantheoncrosssection.jpg

97. TEYCHENNE, D. C., Franklin, R. E., and Erntory, H. C. 1975. *Design of Normal Concrete Mixes*. London: HMSO.

98. *The 1st Concrete Industry Sustainability Performance Report*. The Concrete Centre, part of the Mineral Products Association, on behalf of the Concrete Industry Sustainable Construction Forum.

99. THE BRITISH STANDARD. *BS 1881 - 108:1983 Testing Concrete - Part 108: Method for making test cubes from fresh concrete*.

100. *The Centre for Architectural Structures and Technology*. [online]. [Accessed November 2010]. Available from World Wide Web: http://www.umanitoba.ca/cast_building/index.html

101. VECCHIO, F. J., and Collins, M. P. 1988. Predicting the response of reinforced concrete beams subjected to shear using modified compression field theory. *ACI Structural Journal*., pp.258-268.

102. WANG, T., and Hsu, T. T. C. 2001. Nonlinear finite element analysis of concrete structures using new constitutive models. *Computers and Structures*. **79**, pp.2781-2791.

103. WEST, M. 2006. Flexible fabric molds for precast trusses. *BFT International*. **72**.

104. WEST, M. *Construction - Research - Design - Invention, Elastic Behaviour in a Moist Environment*.

105. WEST, M. *Fabric-formed concrete columns for CASA DENT in Culebra Puerto Rico*.

106. WEST, M. *Fabric-formed concrete structures*. Winnipeg, Canada.

107. WHITNEY, Charles S. 1957. Ultimate shear strength of Reinforced Concrete Flat Slabs, Footings, Beams and Frame Members without shear reinforcement. *ACI Journal*. **29**(4), pp.265-298.

108. WHITTLE, R. 2008. *100 year of reinforced concrete frames building construction*.

109. WITTMANN, F. H. Crack formation and fracture energy of normal and high strength concrete. *Sadhana*. **27**(Part 4), pp.413-423.

110. YI, S-T, Kim, J-K, Oh, T-K. 2003. Effect of strength and age on the stress-strain curves of concrete specimens. *Cement and Concrete Research*. **33**, pp.1235-1244.

111. YIP, W. K. 1998. Generic form of stress-strain equations for concrete. *Cement and Concrete Research*. **28**(1), pp.33-39.

Appendix

The following information is included in the Appendix CD, which can be found at the last page of this thesis.

- Python script for the neutral axis calculation
- Vishay strain gauge application literature
    - CEA strain gauge data sheet
    - M-Bond AE-10 application process
    - M-Coat J application process
    - Soldering method for CEA strain gauge
    - Surface preparation procedure
- Abaqus CAE program files of all the anchorage and beam models